Surface Roughness Prediction When Milling With Square Inserts

Munoz-Escalona, Patricia

Award date:
2010

Awarding institution:
University of Bath

Surface Roughness Prediction when Face Milling with Square Inserts

Patricia Muñoz-Escalona

A thesis submitted for the degree of Doctor of Philosophy
University of Bath
Department of Mechanical Engineering

April 2010

Dedicated to
Julio, Stephan and Claudia

Summary

Surface quality is important in engineering and an important aspect of it is surface roughness since it plays an important role in wear resistance, ductility, tensile, and fatigue strength for machined parts. This research was undertaken in order to make a contribution to the field of knowledge related to surface roughness, tool wear and surface characterization during HSM.

In this study, an investigation involving mathematical, computational and experimental procedures has been undertaken, resulting in the development of a mathematical model (Fourier series), computational model (Artificial Neural Networks) and geometrical analysis model (recreation of the tool trail on the machined surface) for the prediction of surface roughness when face milling with square inserts.

The models are created using Mathcad and Matlab software systems and the experimental data was obtained by measuring the surface roughness using a non-contact white lamp instrument. The values of surface roughness were obtained using a wide range of cutting speed, feed per tooth and axial depth of cut when HSM aluminium alloy (Al 7075-T7351) with different values of tool nose radius (0.8 mm and 2.5 mm), where the Taguchi method was applied as the Design of Experiments.

The developed models can be used for similar combination of material workpiece and tool, when tool flank wear is not considered and are suitable for using any tool diameter with any number of teeth. The results show that the front cutting theoretical model based on geometrical analysis when considering the static tool runouts achieved the best performance with 98% accuracy in term of predicting the surface roughness when compared to a set of experiments select for this purpose. The model based on Feedforward Neural Network achieved an accuracy of almost 97% and the mathematical model based on the Fourier series achieved an accuracy of almost 90%. In addition, when using the Pareto ANOVA Diagram, the results show that, the tool nose radius has an influence of 69.80% on the surface roughness, followed by the cutting speed and feed per tooth with a contribution of almost 15% each. The axial depth of cut has a negligible influence on the surface roughness.

Extra experiments involving HSM of 416 martensitic stainless steel show that, in general, the abrasion tool wear mechanisms were present under all the studied conditions. Finally, it must be highlighted that these materials, 416 martensitic stainless steel and aluminium Al 7075-T7351, were selected for this research study due to their widespread use in the manufacturing of valve parts and structural parts in the oil, automotive and aerospace industries, respectively.

Acknowledgement

This research work has been possible thanks to the support I have received from many people within the Department of Mechanical Engineering of the University of Bath.

Special gratitude is given to my supervisor, Professor Paul G. Maropoulos for his support, suggestions and friendship. To Professor Stephen Newman, Andrew Green, Rob Pepler, Guy Brace, Vijay Rajput, Chris Bowen, Jason Matthews and Patrick Keogh, whose support throughout this work are sincerely recognized.

I would also like to say thank you to my sponsor Schlumberger Faculty for the Future Foundation, for their support and their financial help along these years, with special thanks to Dr. Larry Schwartz and Johana Dunlop.

Finally, I would like to give special thanks to Julio, Stephan and Claudia for the endless support and the words of encouragement during these last years.

Contents

Notations

ANN:	Artificial Neural Network
ASTM:	American Society of Testing Material
Al:	Aluminium (%)
ap:	Axial depth of cut (mm)
C:	Carbon (%)
° C:	Unit of temperature, Celsius
Cr:	Chromium (%)
Ct:	Chip thickness (mm)
Cw:	Chip width (mm)
D:	Distance from the machined surface towards the centre of the specimen (mm)
$Ø_{TOOL}$:	Tool diameter (mm)
EDX:	Electro Dispersive X-Ray
EM:	Error Module (%)
EM_P:	Error Module between predicted and experimental values (%)
EM_T:	Error Module between trained and experimental values (%)
EM_V:	Error Module between validated and experimental values (%)
° F:	Unit of temperature, Fahrenheit
fz:	Feed per tooth (mm/rev*tooth)
FFNN:	Feed Forward Neural Network
FFT:	Fast Fourier Transformation
GRNN:	Generalized Regression Neural Network
HBN:	Brinell Hardness Number
HSC	High Speed Cutting
HSM	High Speed Milling
HV:	Vicker Hardness
i:	Tooth number (Theoretical model surface roughness profile recreation)
κ	Kappa angle (^{o})
L:	Cutting length (mm)
Mg:	Magnesium (%)
Mn:	Manganese (%)
MRA:	Multiple Regression Analysis

MRR: Material removal rate (cm^3/min)

MRR_1: Material removal rate after the first pass (cm^3/min)

MRR_2: Material removal rate when reaching tool life criterion (cm^3/min)

Mo: Molybdenum (%)

n: Amount of samples in the EM equation

n: The number of peak (Theoretical model surface roughness profile recreation)

n*: Revolution per minutes (rpm)

r: Tool nose radius (mm)

R^2: Multiple correlation coefficient

R^2_{adjust}: Adjust multiple correlation coefficient

Ra: Experimental Surface Roughness Average Arithmetic mean value (μm)

Rap: Predicted Surface Roughness (μm)

Ra_T: Trained Surface Roughness (μm)

Ra_V: Validated Surface Roughness (μm)

RBNN: Radial Base Neural Network

RE: Relative Error (%)

RE*: Relative Error average (%)

RE_P: Relative Error between predicted and experimental values (%)

RE_T: Relative Error between trained y experimental values (%)

RE_V: Relative Error between validated and experimental values (%)

rms: Root mean square average roughness (μm)

RMS: Root Mean Square acceleration (g)

S: Standard deviation

S/N: Signal-to-Noise ratio

Si: Siliceous (%)

t: Cutting time (min)

T: Tool life (mm)

T_1: Tool life after the first pass(mm)

T_2: Tool life once reaching tool life criterion (mm)

T_e: Represents the experimental value of any variable.

TG: Total sum of "p" square differences (cutting parameters)

$T_{i\,(p)}$: Total per level.

TT: Total sum of each TG

V: Cutting speed (m/min)

VB: Experimental tool flank wear (mm)

VB_1: Experimental tool flank wear after the first pass (mm)

VB_2: Experimental tool flank wear when reaching tool life criterion (mm)

VB_P: Predicted tool flank wear (mm)

W: Workpiece width (mm)

Y_e: Represents the values of the calculated output of any variable in the EM equation.

Z: Number of teeth

Zn: Zinc (%)

List of Figures

List of Tables

1 Introduction

In recent years, our world has gone through many changes. These changes can be related to the environment, society, technology, etc. In the case of technology changes, although some of them have affected our environment, others have changed or improved our life quality.

Technological change is a term that is used to describe the overall process of invention, innovation and diffusion of technology or processes. In essence, it is the invention of a technology or a process, the continuous process of improving a technology and its diffusion throughout industry or society.

One of the most important commercial sectors in the world is manufacturing since it is the chief wealth-producing sector of an economy. Manufacturing industries use various technologies and methods, widely known as manufacturing processes and they are broadly categorized into engineering, construction, electronics, chemical, energy, textile, food and beverage, metalworking, plastic and transport and telecommunication industries. Each of these industries are important for an economy as they employ a large share of the labour force and produce materials required by sectors of strategic importance.

Product quality has always been one of the most important elements in manufacturing operations. In view of the present global economy and competition, continuos improvement in quality has become a major priority, particularly for major corporations in industrialized countries, such as USA, UK, Germany, Japan, etc (Kalpakjian, 2003).

Quality assurance is the total effort made by a manufacturer to ensure that its product conform to a detailed set of specifications and standards. These standards cover several parameters, such as dimensions, surface finish, tolerances, composition, color and mechanical, physical and chemical properties. Quality assurance is the responsibility of everyone involved with design and manufacturing. Prevention of defects in products and on-line inspections are now major goals in all manufacturing activities, since the quality must be built into a product and not merely checked after the product has been made (Kalpakjian, 2003).

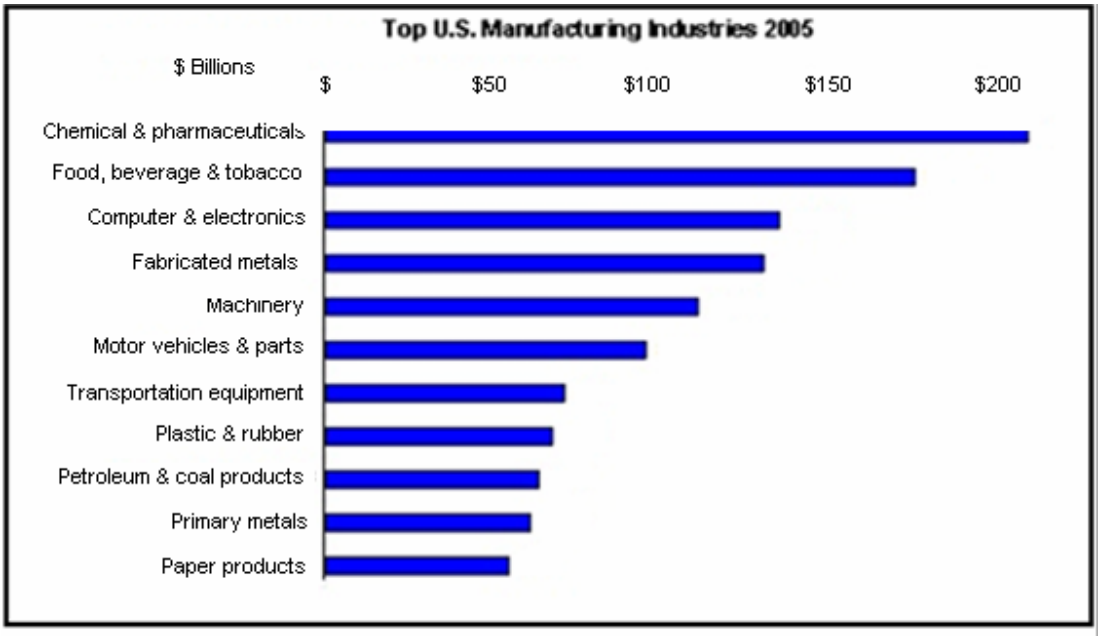

www. case-europe (2005)

a)

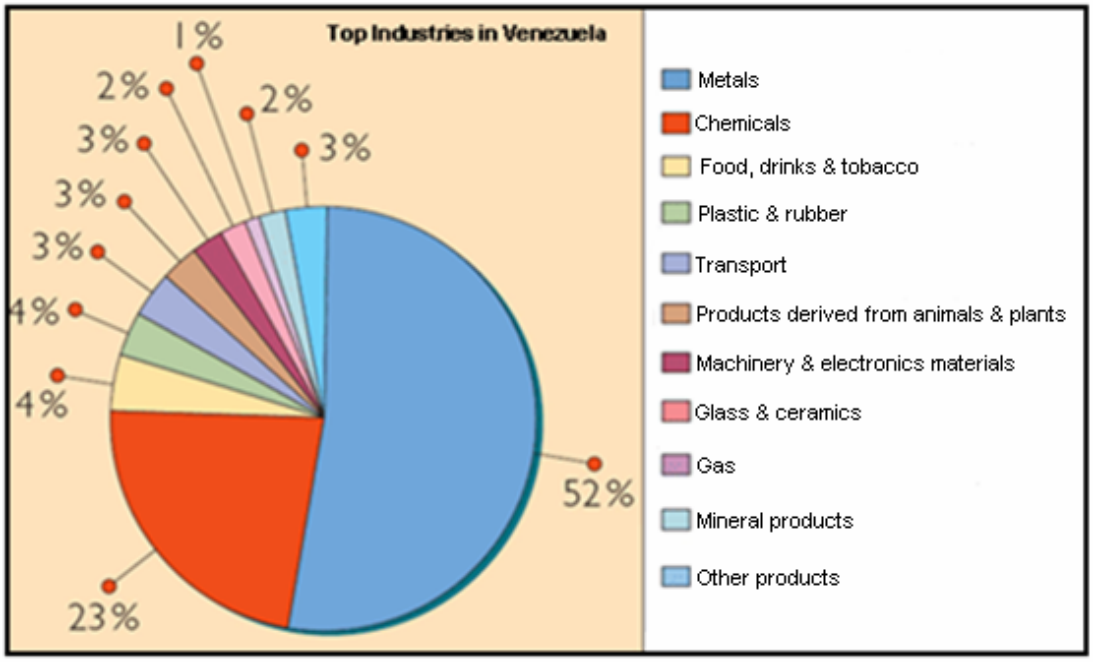

http://ve.kalipedia.com.

b)

Figure 1.1- Top Manufacturing industries a) USA and b) Venezuela

The range of technologies involved in the manufacturing sector is growing each day with the introduction of improved equipment and tools in order to produce high quality final products, with specific characteristics, such as: dimensional accuracy,

etc. Figure 1.1 shows an example of the top manufacturing industries in the developed and developing countries such as the USA and Venezuela respectively, where it is observed in both cases the importance of the metal working industry within the manufacturing sector. In Figure 1.2, an example of the world automobile production share by country is presented.

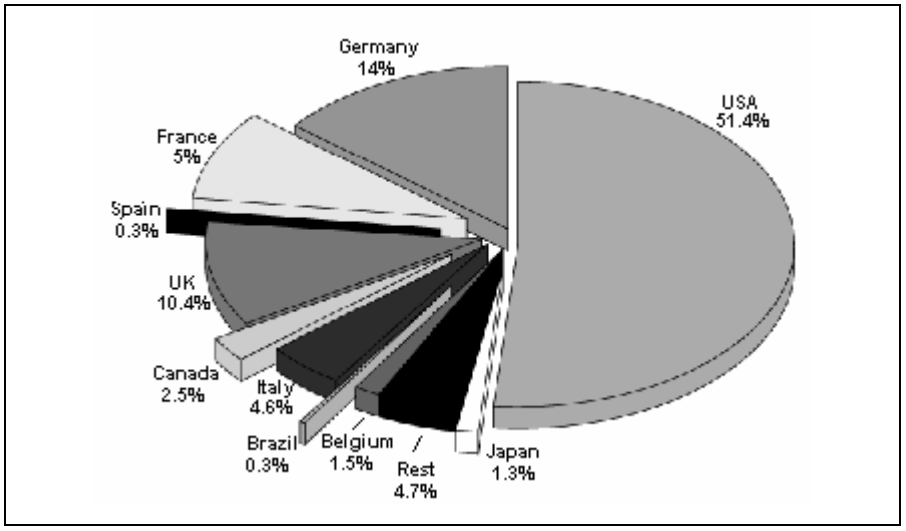

a)

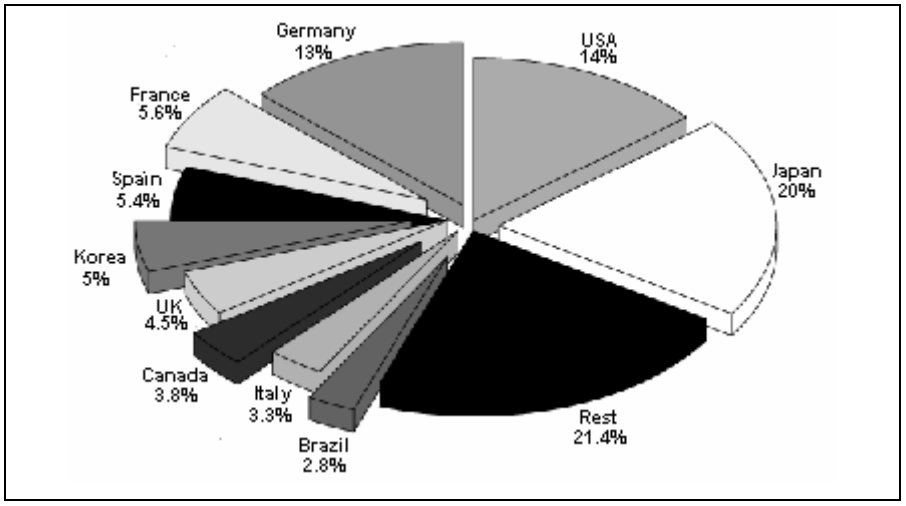

b)

Figure 1.2- World automobile production share by country. a) 1960 and b) 1990 www.ilo.org (2000)

As observed in Figure 1.2 some countries have reduced their production, however in other cases such as Japan their production increased more than 15 times from 1960 to 1990, where it must be highlighted that this country deals every minute with quality improvement been recognized as a manufacturing powerhouse.

Parts manufactured by casting, forming, and various shaping processes often require characteristics, which are obtained by a subsequent manufacturing operation called machining. The machining processes use power-driven machine tools such as: lathes, milling machines and drilling and machining centres. A sharp cutting tool removes the excess material in the workpiece that needs to achieve a desired dimensional accuracy or a specific geometric feature, in order to obtain the product that meets the specifications set out by engineering drawings.

The machining processes require specific attention to guarantee the quality of a final product against certain manufacturing specifications. Besides the obvious problems related to correct dimensions, one of the biggest problems is achieving the correct finish or surface smoothness on the workpiece. Surfaces are commercially and technologically important for a number of reasons. Few reasons are: 1) esthetic; a smooth and free of scratches surface are more likely to give a favorable impression to costumer, 2) surfaces affect safety, 3) surfaces interact with its environment, due to its influence on mechanical properties such as: wear, corrosion and lubrication (Kim, 1997; Medicus, 2001; Saï, 2005 and Groover, 2002).

General defects caused by and produced during component manufacturing can be responsible for inadequate surface integrity. These defects are usually caused by a combination of factors, such as defects in the original material, the method by which the surface is produced, and lack or proper control of process parameters that can result in excessive stresses and temperature. For example, roughness is a measure of the texture of a surface and is a consequence of the cutting parameters, tool geometry, etc used during the machining process. Depending on how rough the surface is (deepness of the grooves left by the tool on the machined surface) a piece can wear more quickly and have higher friction coefficients than a smoother surface (Groover, 2002).

High speed cutting has become one of the most promising advanced manufacturing technologies in the last decade, due to its potential for high production rates, since the technique combines high cutting speeds with increased feed rates (Kalpakjian 2003). This results in a high chip-forming rate and lower milling forces, producing an improved surface quality and tighter tolerances. However, appropriate tools and cutting parameters should be used in order to complete the machining

process with out damaging the tool. In this case, engineers must assist themselves with statistical methods in order to optimize the process by saving costs and time production. An example of these methods is the Signal-To-Noise ratio developed by Taguchi. This method allow the selection of optimal combination of parameters in order to achieve a desire goal, such as smooth surface, small tool wear, higher amount of material removal, etc. (Lin T, 2002; Ghani, 2004; Lin S, 2007).

Finally, it can be concluded that the achievement of quality pieces can be reached by using advance technologies, supported by the use of statistical methods to optimize product design and manufacturing processes.

2. Overall description of the work

2.1 Introduction

The evaluation of surface quality is primarily based on the surface roughness, which in turn plays an important role in wear resistance, ductility, tensile, and fatigue strength for machined parts, which is why it cannot be neglected at the design stage. Even though in the recent years much research has been conducted on the influence of cutting parameters on the surface roughness, tool wear, etc, there are still gaps that are need to be understood and analyzed, especially when using new material-tool combinations, higher cutting speeds, etc. Due to these facts, it is important to ascertain the influence of the different factors involved on the cutting process, in order to select the appropriate combination of parameters that provide the desired surface quality. This will depend on the properties of the workpiece material and cutting tool, the cutting conditions and the process phenomena. Another issue that must be taken into account in manufacturing is the tool life, since tool wear influences the quality of the workpieces, as well as the cost and time of production, by reducing tool changing times.

HSM is considered, after the turning process, the second most widely used machining process, especially in the die/mould, "aerospace" and automotive industries, where workpiece quality is an important factor to be achieved (Groover, 2002). This is the main factor of why the prediction and control of the surface roughness and the tool wear are challenges to researchers.

In recent years there have been several proposals regarding different models for surface roughness predictions during a milling process, however, these models are based on computational analysis and complex mathematical calculus and basically addressed for the use of end milling processes and for round inserts when using a face milling process under specific number of teeth and tool diameter.

2.2 Aim and objectives

The aim is to improve prediction methods to estimate surface roughness on face milling parts when using square inserts, since published models for surface roughness prediction are focused on round inserts. In addition, square inserts also allow shoulder cuts.

.

The general objectives of this research are:

1. To develop different models based on mathematical, computational and geometrical analysis, for the prediction of the surface roughness during a face milling process when using square inserts, considering the tool runout deviations, the tool diameter, the number of cutting teeth and the cutting parameters involved in the process.
2. To support and evaluate the developed models by a research methodology that includes conducting machining experiments.
3. To identify the best model for the prediction of surface roughness when face milling with square inserts on the basis of the evidence available from the comparison of models performance with experimental results.

The specific objectives of this research are:

1. To analyze the influence of the cutting parameters, such as: the cutting speed, feed per tooth, axial depth of cut, tool nose radius and static tool runouts (axial and radial deviations) on surface roughness during the HSM of aluminium alloy 7075-T7351.
2. To analyze the influence of the cutting parameters, such as: the cutting speed, feed per tooth and axial depth of cut on the tool wear and surface roughness of 416 martensitic stainless steel after a face milling process.
3. To study the relationship between tool wear and surface roughness when face milling 416 martensitic stainless steel.
4. To conduct surface characterization analysis of Al 7075-T7351 and 416 martensitic stainless steel.

The models that will be developed will be validated with experimental research conducted in aluminium alloy 7075-T7351, due to its importance in the die/mould and aerospace industries and because Venezuela has a huge reservoir of bauxite the

main component of the aluminium. Finally, experiments in 416 SS will be used to understand the HSM process and due to its importance in the Venezuelan oil companies, since it is used in the fabrication of valve parts, pump shafts, etc. Also, all the experiments will be conducted under different cutting conditions in order to investigate and validate the boundaries of applications of both selected materials

The justification for undertaking the research reported in this thesis is, to make a new contribution to the manufacturing field by developing different models for surface roughness prediction and reconstruction of the 2D surface roughness profile, when face milling with square inserts, without the presence of tool wear. The other possible benefit in predicting the surface roughness, prior to the machining process, is the selection of the optimal combination of cutting parameters to achieve a desired value of roughness; this will represent decreases in the time and the cost of production by eliminating trial and errors practices.

Additionally, in order to accomplish these objectives and understand the influence of the cutting parameters and the relationship between the surface roughness and the tool wear, experimental studies were conducted on 416 martensitic stainless steel bars previous to aluminium alloy 7075-T7351 experiments. Finally, surface characterization studies in both, 416 martenstic stainless steel and Al 7075-T7351 were conducted. This includes: surface roughness, microstructure and microhardness analysis, and chip measurements.

2.3 Desired outcomes of the research

Once investigating the objectives the desired outcomes are:

- A mathematical, computational and theoretical model that allows to predict the surface roughness when face milling with square inserts.
- To identify and quantify the importance of static tool runouts (axial and radial deviations) on the surface roughness.
- To identify and quantify how to characterize a machined surface after a milling process and the importance of conducting this technique for the evaluation of a surface.

- To identify and quantify the influence of the cutting parameters on the surface roughness, tool wear, tool life, material removal and machine-tool vibrations when conducting a machining process.
- Methods that will allow the selection of optimal parameters for best tool performance, small tool wear and smooth surfaces for face milling processes.

2.4 Research methodology

As previously stated the aim of this research is to develop models for surface roughness prediction when high speed milling is to improve prediction methods to estimate surface roughness on face milling parts.

In order to reach the objectives and make a new contribution to knowledge, square inserts were selected as there is an absence of models for surface roughness prediction with these inserts and due to the fact that this geometry allows shoulder cuts. The models to be developed should be validated with experimental data obtained by HSM Al 7075-T7351. This material was selected due to its importance in the die/mould, automotive and aerospace industries. Previous to the Al7075-T7351 experiments, a 416 SS will be used to gain an understanding of the HSM process. This material is very important in the Venezuelan oil companies, since it is used in fabrications of valve parts, pump shafts, etc.

All the experiments were conducted in a HSM Deckel Maho 50 evolution milling centre and for the Design of Experiments, the Taguchi method was followed. This method allows the use of only a fraction of the full factorial combination of experiments reducing the time and cost. The cutting parameters selected for the study are the cutting speed, feed per tooth, axial depth of cut and the tool nose radius, since from previous research it was observed the importance of these parameters on the surface roughness, tool life, etc.

Once the 416 SS has been milled under dry cutting conditions the influence of the cutting parameters on the surface roughness, tool life and material removal will be analysed, as well as the influence of the tool wear on the surface roughness. For the tool wear, measurements the tool life criteria suggested by the ISO-Standard 8688-1 will be followed and for the surface roughness measurement, the Taylor-Hobson contact equipment used.

The Al 7075-T7351 will be HSM under a Minimum Quantity of Lubrication (MQL). Once the experiments are completed, the surface roughness will be measured

with a Pro-Scan 2000 non-contact equipment. Three areas of the machined surface will be measured and the Ra value, 2D profile, and 3D topography obtained. In addition surface characterization (microstructure, microhardness and chip geometry) analysis will also be conducted in order to analyze the influence of the cutting parameters on the surface roughness. As an extra contribution, the spindle's and workpiece vibrations will be measured in order to know how much these variables affect the surface roughness. The Ra value and the 2D profiles will be used as the target outputs of the models to be developed.

The Al 7075-T7351 results will be used to validate the models for surface roughness prediction and before developing them the Tchebysheff theorem will be applied in order to secure a good performance of the models.

Three models will be explored, with the cutting parameters as the inputs of the models. The first model is a mathematical model based on the Fourier series. The second model is a computational model based on Artificial Neural Networks. For this model a number of networks will be selected for study, the Radial Base (RBNN), the FeedForward (FFNN) and the General Regression (GRNN).

The third model is a theoretical model based on a geometrical analysis where the tool trail left on the machined surface will be reproduced.

Finally all the models will be compared by calculating the %Rep (predictive relative error) which is the difference between the predicted and experimental values of surface roughness.

2.5 Scope of the Thesis

The thesis has been organized into three main sections; namely, a literature review and state of the art, martenstic stainless and aluminium alloy studies and the analysis and modelling stage. The work done during each of these stages is illustrated in Figure 2.1 and as can be observed is presented in this thesis in Chapters 3 to 9, including general conclusions and recommendations for further work.

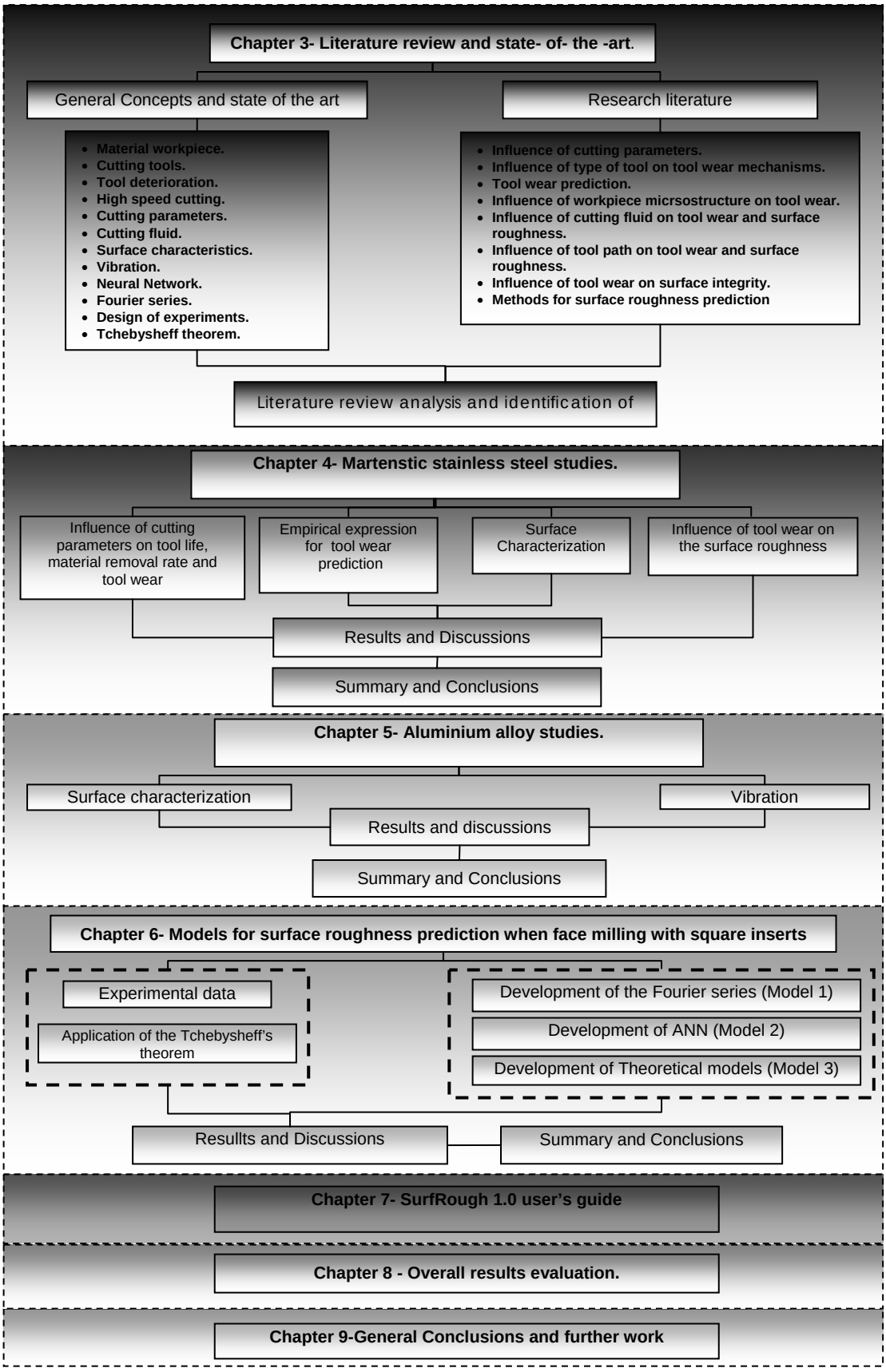

Figure 2.1- Diagram of overall thesis structure.

When analyzing Figure 2.1 it is observed that Chapter 3 includes a relevant literature review, where general concepts, state of the art and identification of knowledge gaps are presented.

Chapter 4 reports the experimental studies for martenstic stainless steel. This chapter is organized in six sections. A brief introduction leads to the second section where the influence of the cutting parameters on tool life, material removal rate and tool wear, as well as the best combination of cutting parameters for a best tool performance is presented. A third section presents an empirical expression for tool wear prediction. A fourth section includes the surface characterization analysis, where a complete study regarding surface roughness, microstructure and microhardness is presented. The fifth section includes an analysis of the influence of tool wear on surface roughness and the sixth section includes a summary and conclusions of these studies.

Chapter 5 reports the experimental studies of aluminium alloy. This chapter is organized in six sections. A brief introduction and description of the experimental set-up leads to the third section where a complete surface characterization analysis is presented. This section includes different studies, such as: 2D and 3D surface roughness analysis, microstructure, microhardness and chip's morphology analysis. The fourth section describes the influence of the cutting parameters on the surface roughness, as well as the optimal combination of cutting parameters in order to achieve a smooth surface. Section 5 shows the influence of the RMS acceleration of the spindle and the workpiece on the machined surface roughness when cutting under specific conditions. This has been performed in order to determine how much this factor, affects the surface roughness of the milled specimens, and if so, if it needs to be included on the development of the different models for surface roughness prediction. Finally, section six presents a summary and the general conclusions of these studies.

Chapter 6 presents the development of different models for surface roughness prediction when face milling with square inserts. The developed models were supported and evaluated by a research methodology (Taguchi method) by conducting experimental measurements obtained over a wide range of cutting conditions when

face milling an aluminium alloy (7075-T7351). This chapter is divided in five sections. A brief introduction leads to section 2, where Tchebysheff's theorem is applied, in order to guarantee the later adjustment of the different developed models, for surface roughness prediction. A third section presents the development of a mathematical model based on the Fourier series. Section four presents the development of Artificial Neural Networks computational models such as: Radial Base, Feed Forward and General Regression. This section also presents an analysis of the performance assessment for the selection of the ANN that achieved the best result when comparing it to the experimental surface roughness data. The fifth section presents the development of different theoretical models, based on geometric analysis. The models are: front cutting, back cutting and front-back cutting processes. The last section includes a summary and conclusions of this part of the research.

Chapter 7 presents the SurfRough 1.0 pilot software User's Guide. This chapter is divided in three main sections. A brief introduction leads to the second section, where a detailed content of all the fields that are involved in the SurfRough 1.0 is presented. The last section presents the summary and general conclusions of this chapter.

Chapter 8 presents an overall result evaluation of the different developed models. The chapter is divided into four sections. An introduction leads to the second section where a comparison between the predicted values of surface roughness obtained by applying the different developed models, with the experimental values, is reported. Section 3 presents a comparison between the 2D profiles (predicted and experimental), as well as a proposal of the best model that describes the prediction of surface roughness when face milling with square inserts. The final section includes a summary and significant conclusions of this study.

Finally, Chapter 9 presents the contribution of this thesis by reporting general conclusions drawn from this research as well as suggestions and recommendations made by the author that might be valuable for future studies of surface roughness predictions during face milling processes.

3 Literature review and state-of-the-art

3.1 Introduction

In order to reach specific characteristics such as dimensional accuracy, surface texture and production of geometrical features in parts manufactured by casting, forming, and various shaping processes, a finish process is required. This finishing process is achieved by machining operations.

Machining is one of the most important group of manufacturing processes is that use material removal methods in which power-driven machine tools, such as lathes, milling, and drilling machines, are used with a sharp cutting tool to mechanically shear the material and achieve a desired geometry, dimensional accuracy and specific surface roughness. In the particular case of surface roughness, this is influenced by factors such as: the cutting conditions, workpiece material, cutting geometry, tool wear, tool errors, machine-tool vibrations, etc and even though many studies have been conducted in the area there are still many gaps that need to be filled.

In this chapter, general concepts employed in the milling of workpiece materials as well as an analysis of different articles published in the area, with identification of various gaps are presented.

3.2 General concepts and state-of-the-art.

3.2.1 Material workpiece

Workpiece material plays an extremely important role in the engineering and food industries, the manufacturing of medical components, and in high corrosion applications. Depending on their mechanical, physical, chemical properties, etc; these behave different depending on the environment they are working in.

This thesis will be concentrate on stainless steel and aluminium and its alloys due to their importance in industries such as oil, automotive, aerospace, etc.

- **Stainless Steels**

As its name suggests stainless steels are characterized primarily by their corrosion resistance, high strength, and high chromium content. This ability to resist corrosion attack is attributed to the self healing and nonporous chromium oxide film that forms in the presence of oxygen. A minimum of 12% chromium is required to form this film. (Edwards and Endean, 1990)

In addition to chromium, other alloying elements in stainless steels are: nickel, molybdenum, copper, titanium, silicon, manganese, columbium, aluminium, nitrogen, and sulphur. The higher the carbon content, the lower the corrosion resistance of the stainless steels. This is due to the fact that the carbon combined with the chromium forms chromium carbide, which lowers the passivity of the steel. (Kalpakjian, 2003)

Unique to any other alloy system, the stainless steel family covers a temperature range from -454 ˚F (-234 ˚C) to above 1800 ˚F (982 ˚C), where within this range it exhibits strength, toughness, and corrosion resistance superior to most metals. Also, stainless steels are divided according to their microstructure and crystalline structure. (Lindberg, 1983).

Figure 3.1, shows the Schaeffer diagram where the effect of alloying elements on the basic structure of Cr-Ni stainless steel can be observed.

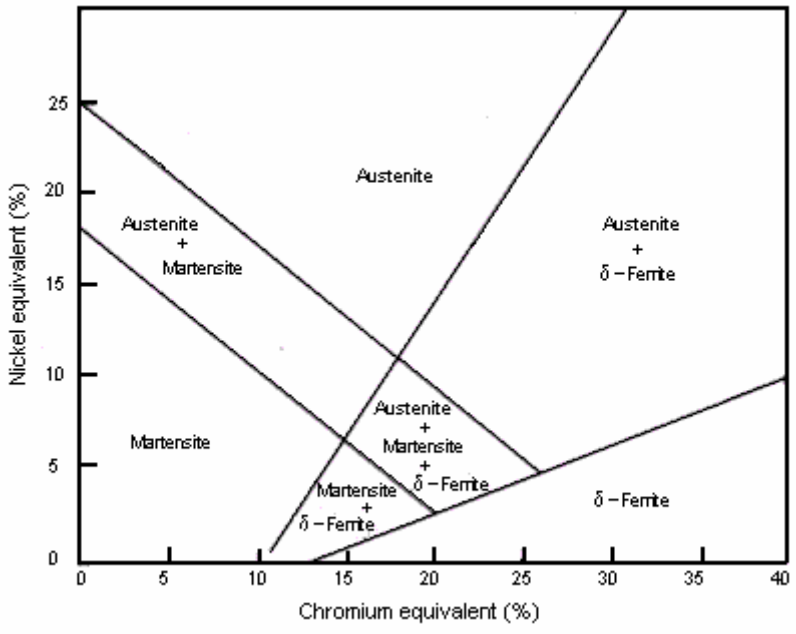

Figure 3.1- Schaeffer diagram for stainless steels.
(http://steel.keytometals.com)

As observed from this figure there are a few types of stainless steel and a detail follow:

- **Austenitic stainless steels (200 and 300 series)**

These steels are chromium-nickel steels and they contain 16% to 26% of chromium and from 6% to 22% of nickel. These steels are the most ductile, so they can easily be formed, although, with increasing cold work, their formability is reduced. These steels are nonmagnetic and have excellent corrosion resistance, although are susceptible to stress-corrosion cracking. As a group, they have considerably better corrosion resistance than martensitic stainless steels.

Finally, they are used in a wide variety of applications, such as kitchenware, fittings, welded constructions, furnace and heat-exchanger parts, as well as in components for several chemical environments, (Lindberg, 1983; Kalpakjian, 2003).

- **Ferritic stainless steels (400 series)**

This type of steel may contain 12% to 27% of chromium. They are magnetic and have a lower ductility when compared to austenitic stainless steels.

These steels can be hardened by cold working, but not with heat treatment and they are generally used for non-structural applications such as, kitchen equipment and automotive trim. The type 430 is the more typical. (Lindberg, 1983; Kalpakjian, 2003)

- **Martensitic stainless steels (400 and 500 series)**

This type does not contain nickel. They are magnetic and have high strength, hardness, and fatigue resistance, and good ductility, but moderate corrosion resistance and are not suitable for marine or other chloride exposure. The maximum corrosion resistance is achieved in the hardened condition with a smooth surface finish.

These steels have chromium content from 11.5% to 18%, with enough carbon to render them hardenable by heat treatment. As the carbon content goes up, so does the range of mechanical properties that can be obtained by heat treatment. Grade 416 has the highest machinability of any stainless steel, at about 85% of that of a free-machining carbon steel. As for most other free-machining stainless steels the

improvement in machinability is achieved by addition of sulphur, which forms manganese sulphide inclusions. The addition of sulphur also lowers the corrosion resistance, weldability and formability to below that of its non-free machining equivalent Grade 410. (Lindberg, 1983).

Also the grade 416 is sometimes used in the unhardened or hardened and highly tempered condition because of its low cost and machinability, and is typically used for cutlery, surgical tools, instruments, valves, pump shafts, automatic screw machined parts, motor shafts, studs, gear, springs, etc, (Kalpakjian, 2003).

Table 3.1 show the mechanical properties and chemical composition of different stainless steels and Table 3.2 the percentage of machinability of few stainless steels.

Table 3.1- Mechanical properties and chemical composition of different stainless steels

	Alloy	Tensile (ksi)	Yield (ksi)	Rockwell Hardness	%C	%Cr	%Ni	%Cu
Austenitic	**18-8**	80-150	40 min	B85-95	0.08	17-20	8-13	0-4.5
	302	70-125	40 min	B85-95	0.15	17-19	8-10	-
	303	90-125	40 min	B85-95	0.15	17-19	8-10	-
	304	85-150	40 min	B85-95	0.08	18-20	8-10.5	1
	304L	Slightly lower than 304	Slightly lower than 304	Slightly lower than 304	0.03	18-20	8-12	1
	305	80-140	40 min	B85-95	0.12	18-20	10.5-13	1
	309	100-120	40 min	B85-95	0.20	17-19	12-15	-
	310	100-120	60-80	B85-95	0.25	22-24	19-22	-
	316	85-140	40 min	B85-95	0.08	24-26	10-14	2-3.5
	316L	Slightly lower than 316	Slightly lower than 316	Slightly lower than 316	0.03	16-18	10-14	2-3.5
	317	100-120	60-80	B85-95	0.08	16-18	11-15	3-4.5
	321	100-120	60-80	B85-95	0.08	18-20	9-12	-
	347	100-120	60-80	B85-95	0.08	17-19	9-13	-
Martensitic	**410**	180 Heat treated	150 Heat treated	C34	0.15	11.5-13.5	-	-
	416	180 Heat treated	150 Heat treated	C34-45	0.15	12-14	-	-
	420	250 Heat treated	200 Heat treated	C45	0.15 min	12-14	-	-
Ferritic	**405**	70-75	40-45	B65-75	0.08	11.5-14.5	-	-
	430	70-75	40-45	B65-75	0.12	16-18	-	-

www.marfas.com

Table 3.2- Percentage of machinability of few stainless steels.

Alloy	% Machinability
302	50
310	30
316	35
317	35
410	55
416	90
420	45

www.quakerchem.com

- **Aluminium and aluminium alloys**

The most important factors of these materials are their high strength-to-weight ratio, their corrosion resistance by many chemicals, their high thermal and electrical conductivity, their non-toxicity, reflectivity, and their ease of formability and machinability; also they are nonmagnetic. Aluminium and its alloys are being used for applications ranging from containers and packaging to aircraft and aerospace components as well as in electrical appliances.

There are two types of wrought-aluminium alloys:

- Alloys that can be hardened by cold-working and are not heat treatable.
- Alloys that can be hardened by heat treatment.

Aluminium alloys are identified by four digits and by a temper designation that shows the condition of the material. Table 3.3 shows how aluminium alloys are identified by the first digit as follows:

Table 3.3- Aluminium alloy identification and their typical application

	Alloying Element	Typical application
1XXX	Commercially pure aluminium 99.6 % - 99.9 %	• Excellent corrosion resistance • High electrical and thermal conductivity • Good workability and low strength • Not heat treatable
2XXX	Copper 3.8 % - 6.8 %	• High strength-to-weight ratio • Low resistance to corrosion • Heat treatable
3XXX	Manganese 0.4 % - 1.5 %	• Good workability • Moderate strength • Not generally heat treatable
4XXX	Silicon 4.5 % - 6.0 %	• Lower melting point • Forms an oxide film of a dark-gray to charcoal color • Not generally heat treatable
5XXX	Magnesium 2.2 % - 5.5 %	• Good corrosion resistance and weldability • Moderate to high strength • Not heat treatable
6XXX	Magnesium and silicon Mg. 0.35 % - 0.7 % Si. 0.3 % - 0.9 %	• Medium strength • Good formability machinability and weldability • Corrosion resistance • Heat treatable
7XXX	Zinc 0.8 % - 7.3 %	• Moderate to very high strength • Heat treatable
8XXX	Other element	

Table 3.4 shows the heat treatment designations for wrought and cast aluminium.

Table 3.4- Heat treatment designation for wrought and cast aluminium

Designation	Temper characteristics
F	As fabricated (by cold or hot work or by casting)
O	Annealed (from the cold-worked or the cast state
H	Strain-hardened by cold working (for wrought products only)
T	Heat treated
W	Solution-treated only (unstable temper)

Table 3.5 shows the mechanical poperties of Al 7075 and Table 3.6 the percentage of machinability of different alumimium alloys.

Table 3.5- Mechanical properties of Al 7075.
All values are minimum long transverse mechanical properties except where noted.

Temper	Thickness in.(mm)	Tensile strength Ksi (MPa)	Yield Strength Ksi (MPa)	Elongation (%)
0	0.015-2.000	40 (max)	21 (max)	9-10
Sheet & Plate	(0.38-50.80)	(276)	(145)	
T6	0.008-0.249	74-78	63-69	5-8
Sheet	(0.203-6.320)	(510-538)	(434-476)	
T651	0.250-4.000	78-67	67-54	9-3
Plate	(6.35-101.60)	(538-462)	(462-372)	
T76	0.125-0.249	73	62	8
Sheet	(3.18-6.32)	(503)	(427)	
T7651	0.250-1.00	72-71	61-60	8-6
Plate	(6.35-25.40)	(496-490)	(421-414)	
T73	0.040-0.249	67	56	8
Sheet	(1.02-6.32)	(462)	(386)	
T7351	0.250-4.000	69-61	57-48	7-6
Plate	(6.35-101.60)	(476-421)	(393-331)	

Table 3.6- Percentage of machinability for aluminium alloys wrought and cast.

Material-Cast	Machinability (%)	Material-wrought	Machinability (%)
A-132-T	110	2011	200
A-214	200	2014-T	140
A-356-T	140	2017-T	140
B-113	180	2024-T	150
D-132-T	130	3003	180
108	140	3004	180
112	180	5052	190
122-T	140	5056	190
135-T	190	4032-T	110
212	160	6051-T	140
218-T	240	6061-T	190
220-T	230	6063-T	190
319-T	160	7075-T	120
333-T	130	Aluminium-bronze (5%Al)	60
355-T	160		
750-T	180		

www.quakerchem.com

3.2.2 Cutting tools

Success in metal cutting depends upon the selection of the proper cutting tool (material and geometry) for a given work material. Cutting tools can be subjected to hostile environments involving high temperatures and stresses; consequently they must possess the following properties:

- Hardness particularly at elevated temperature.
- Toughness, so that sudden loading of the tool (in interrupted cutting) does not chip or fracture the tool.
- Chemical inertness with respect to the workpiece.
- Wear resistance, to maximize the life of the tool.

The first three properties are satisfied by selecting the correct material for a given cutting operation, although the high temperatures and stresses produced when cutting at high speeds means that wear is inevitable, (Edwards and Endean, 1990).

However, the most satisfactory tool will usually be the one corresponding to the minimum total cost of performing a required operation to the specified accuracy. Thus, the best tool material will not necessarily be the one that gives the longest life; factors such as machinability, tool material cost, and the practical levels of cutting speeds and feeds for a given tool material play important roles in the selection of the best tool material for a particular operation.

With the increased use of numerically controlled machine tools, reliability and predictability of performance are of greater significance than before and these items must be given greater weight in selecting tool material for such applications, (Shaw, 1991).

- **Face milling cutter**

In face milling, the cutter is mounted on a spindle having an axis of rotation perpendicular to the workpiece surface. The cutter rotates at a rotational speed and the workpiece moves along a straight path at a linear speed.

With the relative motion between the cutter teeth and the workpiece, a face milling cutter leaves feed marks on the machined surface similar to those left by turning operations. The terminology for a face milling cutter, as well as the various angles, is shown in Figure 3.2. The side view is shown in Figure 3.3, where it is observed that the lead angle has a direct influence on the underformed chip thickness. As the lead angle increases, the undeformed chip thickness decreases, and the length of contact increases. (Kalpakjian, 2003)

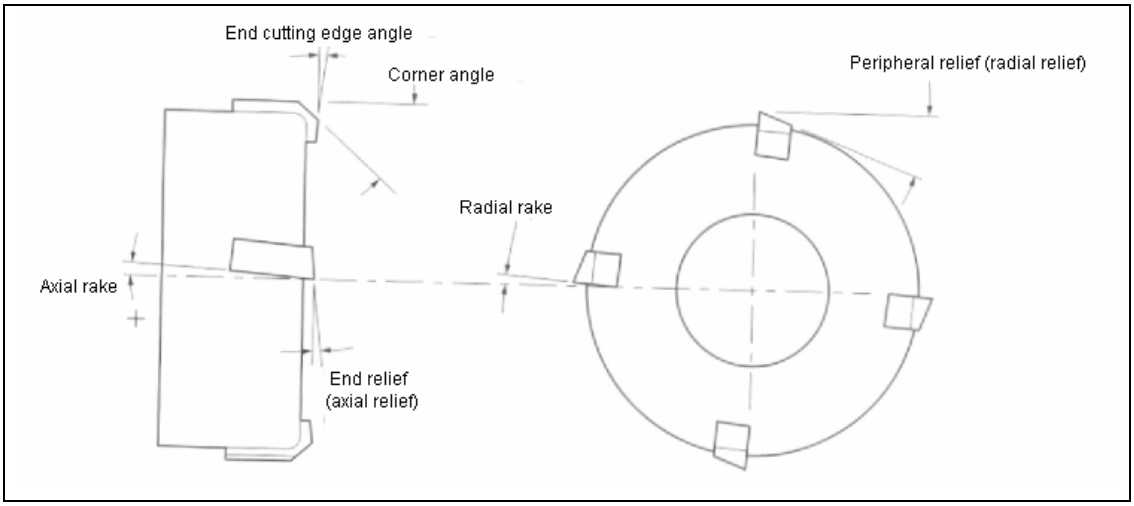

Figure 3.2- Terminology for a face-milling cutter (Kalpakjian, 2003)

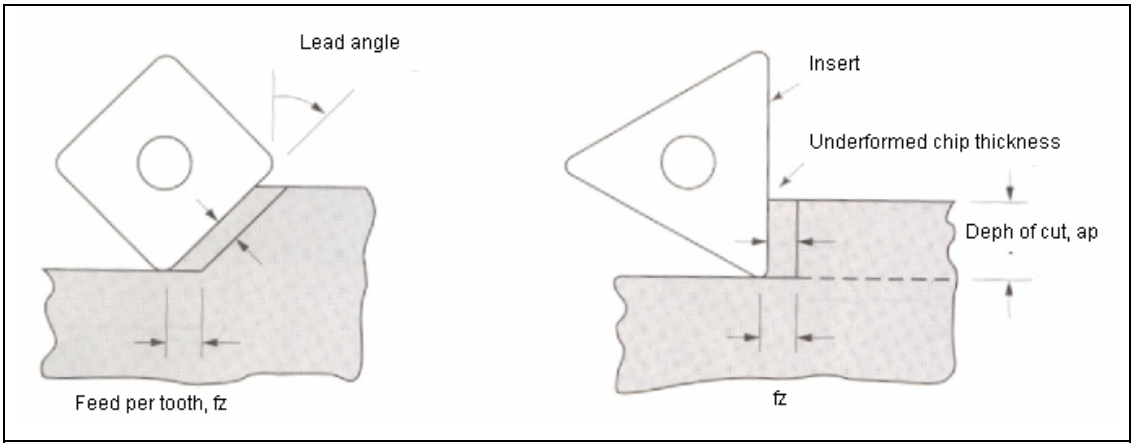

Figure 3.3- The effect of lead angle on the undeformed chip thickness in face milling (Kalpakjian, 2003)

Many types of tool have been developed in recent years in order to improve the cutting processes. These include high carbon steels and low/medium alloy steels, high speed steels (HSS), cast cobalt alloys, cemented carbides, cast carbides, coated carbides, coated high speed steels, ceramics, sintered polycrystalline cubic boron nitride (cBN), sintered polycrystalline diamond and single-crystal natural diamond, (DeGarmo, 1988).

- **Carbide tools**

These are made from nonferrous alloys and are called sintered (or cemented) carbides because they are manufactured by powder metallurgy techniques.

Carbide tools are made by mixing pure tungsten powder under high heat with pure carbon in the ratio of 94% and 6%, respectively, by weight. The resulting compound WC (tungsten carbide) is then mixed with cobalt until the mass is homogenous. The powder mixture is compacted at high pressure and sintered in a furnace at 1371 ˚C. After cooling, the carbide tool is ground and in some cases, subjected to further finishing operations, (Lindberg, 1983).

Carbide tools are much harder and chemically more stable, they have better hot hardness, high stiffness and lower friction; and they operate at higher cutting speeds than those made with HSS and cobalt alloys, (DeGarmo, 1988).

Because of their high hardness over a wide range of temperatures, high elastic modulus and thermal conductivity, and low thermal expansion, carbides are among the most important versatile and cost-effective tool and die materials for a wide range of applications (Kalpakjian, 2003).

The two basic groups of carbides used for machining operations are tungsten carbide and titanium carbide. In order to differentiate them from coated tools, plain carbides are usually referred to as uncoated carbides, (Lindberg, 1983).

Cemented carbide tools are available in insert form in many different shapes; squares, triangles, diamonds, and rounds. They can be either brazed or mechanically clamped onto the tool shank. The latter is more popular because when one edge becomes dull, the insert is rotated or turned over for a new edge, (DeGarmo, 1988)

In order to improve the hardness and surface condition of the tool to withstand the high cutting forces and temperatures presented during high cutting, these tools are coated with hard materials.

- **Coated tools**

Because of their unique properties, coated tools can be used at high cutting speeds, thus reducing the time required for machining operations and hence, costs. Coated tools can improve tool life by as much as 10 times that of an uncoated tool.

Coated tools must have the following characteristics:

- High hardness at elevated temperatures.
- Chemical stability and inertness to the workpiece material.
- Low thermal conductivity.
- Good bonding to the substrate to prevent flaking.
- Little or no porosity.

Commonly used coating materials include titanium-nitride (TiN), titanium-carbide (TiC), titanium-carbonitride (TiCN), and aluminium oxide (Al_2O_3). Generally, these coatings are applied on tools and inserts by Chemical Vapour Deposition (CVD) and Physical Vapour Deposition (PVD) techniques. The CVD process is the most commonly used coating application method for carbide tools with multiphase and ceramic coatings, (Kalpakjian, 2003). The PVD coated carbides with TiN coatings, on the other hand, have a higher cutting edge strength, lower friction, lower tendency to form a built-up edge, and are smoother and more uniform in thickness.

3.2.3 Tool deterioration (ISO 8688-1)

All changes in a cutting part of a tool caused by the cutting process are tool deterioration.

There are three major classes of tool deterioration: tool wear, brittle fracture and plastic deformation.

a) Tool wear: is a change in the shape of the cutting part of a tool from its original shape, resulting form the progressive loss of tool material during cutting.

Cutting tools are subjected to forces, temperature, and sliding; all these inputs induce wear. Because of its effects on the quality of the machined surface and the economics of machining, tool wear is one of the most important and complex aspects of machining operation.

Wear depends on the tool and workpiece material (i.e. physical, mechanical, and chemical properties), tool geometry, properties of cutting fluids (if used), and various other operating parameters. The types of wear on a tool depend on the relative roles of the foregoing variables, (Kalpakjian, 2003).

The flank wear, as the name indicates, takes place on the flanks of the cutting edge, mainly from the abrasive wear mechanisms. This is usually the most normal type of wear. In the end, excessive flank wear will lead to poor surface texture, inaccuracy and increasing friction at the edge changes shape. (Sandvik, 1994)

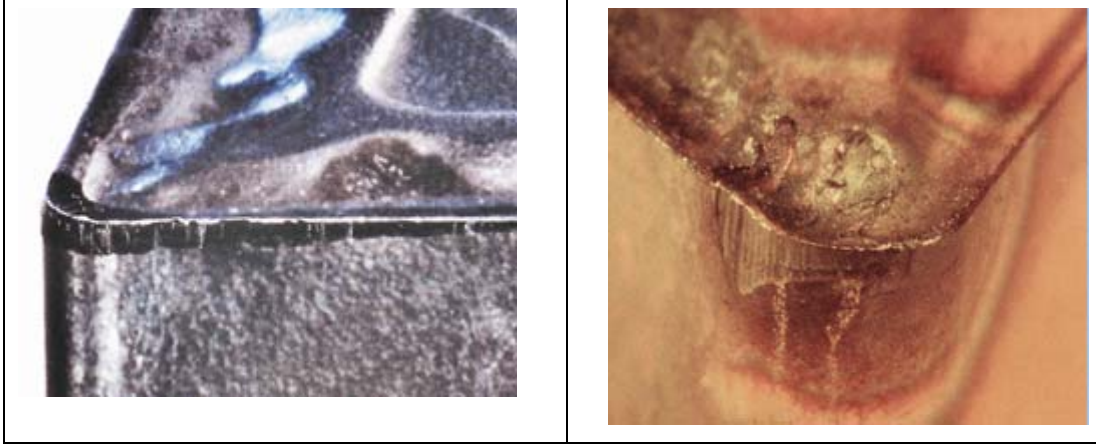

a) **b)**

Figure 3.4- Tool wear.a) Flank wear and b) Crater wear

b) Brittle fracture: is when a cutting tool loses a fragment of material resulting from a crack during the cutting process. This type of wear can be divided in 1) chipping of the cutting edge, where it ussualy occurs due to the cycles of loading and unloading; this leads to particles of material leaving the material surface. Intermmittent cutting is a frequent cause of this wear type and 2) fracture, this type of wear can be catastrophic. Edge fracture is often also the end of the line for other wear types.

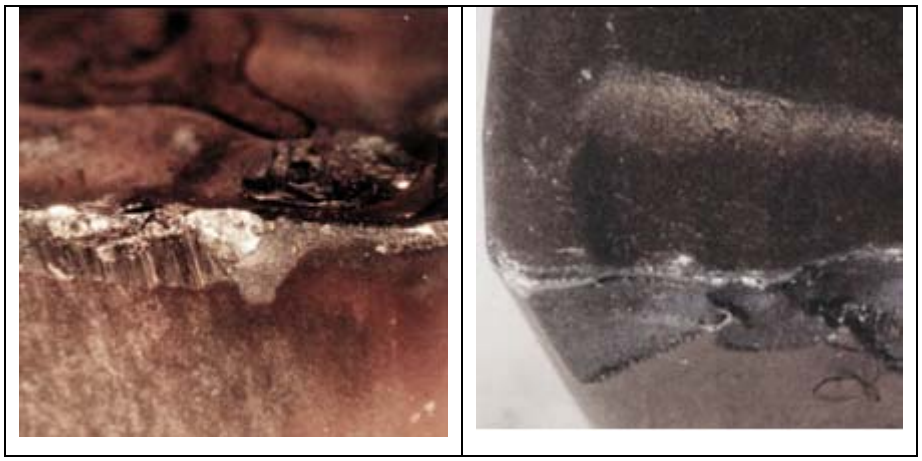

a) **b)**

Figure 3.5- Brittle fracture types. a) Chipping of the cutting edge and b) Fracture.

c) Plastic deformation: is any distortion of the cutting part of the tool from its original shape without initial loss of the tool material during the cutting process. This type of wear takes place as a result of combined high temperatures and high pressure on the cutting edge. The typical bulging of the edge will lead to even higher temperatures, geometry deformation, chip flow changes until a critical stage is reached. (Sandvik, 1994)

Figure 3.6- Plastic deformation on a cutting tool

- **Types of wear**

The progressive wear of a tool takes place in two distinct ways: flank wear and crater wear.

a) Flank wear

This type of wear is generally attributed to:

1. Sliding of the tool along the machined surface, causing adhesive and/or abrasive wear, depending on the materials involved.
2. Temperature rise, because of its influence on the properties of tool material.

b) Crater wear:

The factors affecting flank wear also influence crater wear, but the most significant factors in crater wear are temperature and the degree of chemical affinity between the tool and the workpiece. The rake face of the tool is subjected to high levels of stress and temperature, in addition to sliding at relative high speeds, (Boothroyd, 1989).

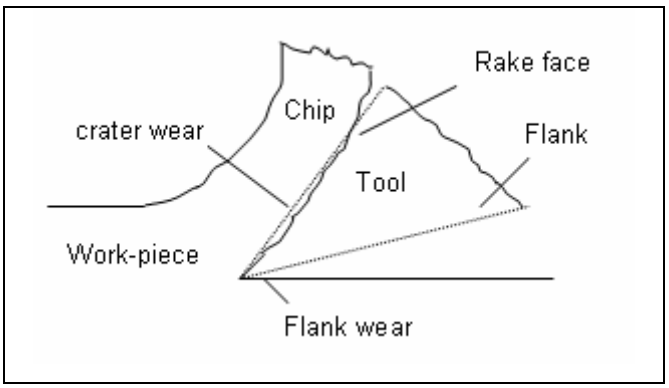

Figure 3.7- Regions of tool wear in metal cutting

3.2.3.1 Tools wear mechanisms

The study of wear between two metallic surfaces is complicated because it involves several unique mechanisms.

At low cutting speeds mechanical mechanisms governs tools wear such as, abrasion and adhesion and at higher cutting speeds, thermal mechanisms govern tool wear such as, diffusion and oxidation. Each of these wear mechanisms will be described. (Lindberg 1983, Boothroyd, 1989 and Kalpakjian, 2003).

- **Abrasive wear**

Abrasion takes place when hard constituents in the workpiece microstructure or underside of the chip pass over the tool face or flank and remove tool material by mechanical action. Highly strain-hardened fragments of a built-up edge or inclusion produce grooves or scratches on the softer surface. It is generally more pronounced on the flank surface of the tool.

A convenient way of studying abrasive wear is in terms of specific energy, which is the work required to remove a unit volume of material, (Shaw, 1991).

- **Adhesive wear**

Metal cutting junctions between the chip and tool materials are formed as part of the friction mechanism; when these junctions are fractured, small fragments of tool material can be torn out and carried away on the underside of the chip on the new work-piece surface.

- **Diffusion wear**

This type of wear involves the transfer of atomic particles from the tool to the workpiece and from the workpiece to the tool.

Diffusion is accelerated by high temperatures caused by rapid movement of the work material near the tool surface. This process takes place within a very narrow reaction zone at the interface between the two materials producing weakening of the surface structure of the tool.

Diffusion wear is often accompanied by decomposition of a component of one of the sliding surfaces. For example, in cutting ferrous alloy with a tungsten carbide tool at high speed (temperature), α-iron is transformed to γ-iron on the surface of the chip. The γ-iron has a strong affinity for carbon, the tungsten carbide (WC) crystals in the surface decompose and the carbon released diffuses into the surface of the chip, (Shaw, 1991).

- **Fatigue wear**

In a milling process, the cutting teeth enter and exit the workpiece producing temperature fluctuations and cutting forces that can produce cracks and later fracture

of the cutting edge. This thermomechanical combination is known as fatigue wear. (Boothroyd, 1978)

- **Oxidation wear**

This is also known as corrosive wear and is caused by chemical or electrochemical reactions between the surfaces and the environment. At the elevated temperature range at which a cutting tool operates, oxidation can cause rapid wear. As oxidation takes place, it weakens the tool matrix and thus the cutting edge strength. The oxides that form are easily carried away, leading to increased wear.

Figure 3.8 illustrates the tool wear mechanisms described above.

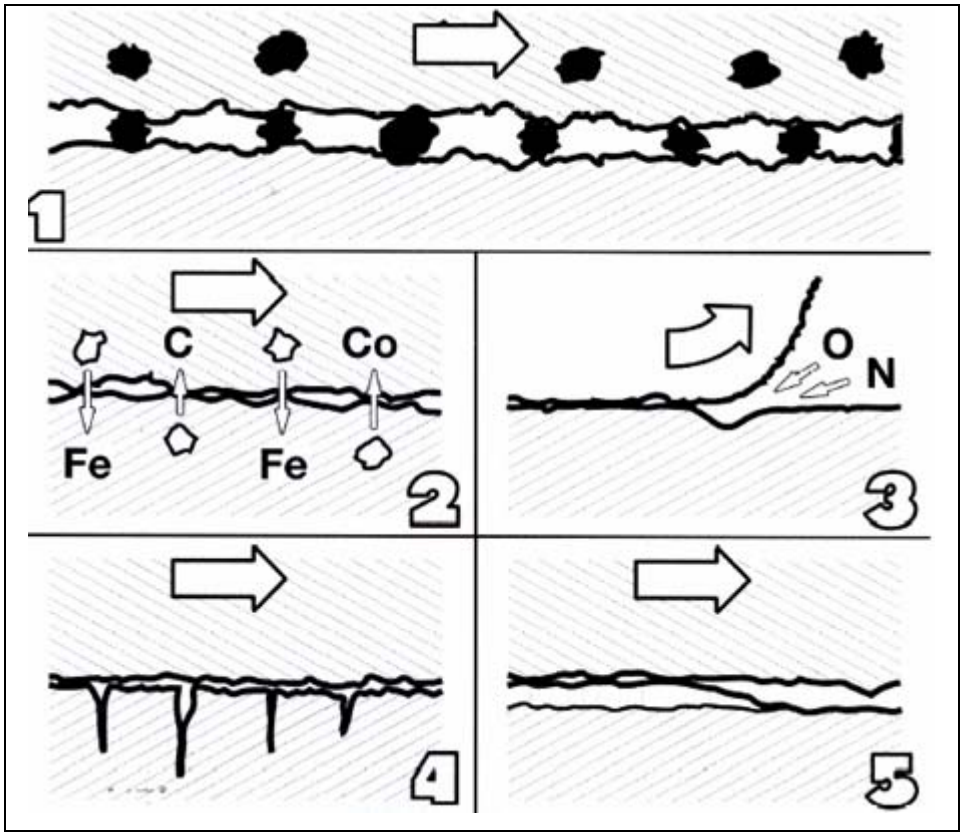

Figure 3.8- Tool wear mechanisms: 1) Abrasion, 2) Difusion, 3) Oxidation, 4) Fatigue, 5) Adhesion (Sandvik, 1994)

3.2.4 High Speed Cutting, HSC (Kalpakjian, 2003)

High speed cutting has become one of the most promising advanced manufacturing technologies in the last decade.

What was considered High Speed Cutting just a few years ago is today regarded as conventional. Many factors are driving machine shops to faster metal cutting rates. These factors include better and more capable machine tools and CNC processors that allow the machine to accurately cut at increasingly higher speeds and feeds.

HSC is one of the modern technologies, which in comparison with conventional cutting enables to increase efficiency, accuracy and quality workpieces and at the same time to decrease costs and machining time.

One of the most important of all High Speed Cutting methods is the HSM process, which generally uses high cutting speeds and shallow depths of cut.

HSC is being mainly used in three industrial sectors due to their specific requirements. The first category is industry, which deals with machining aluminium to produce automotive components, small computer parts or medical devices. This industry needs fast metal removal and typically due to their high volume of manufacturing involves many machining operations.

The second category, which is the aircraft industry, involves machining of long aluminium parts, often with thin walls. The third industry sector is the die/mould industry which requires dealing with finishing of hard materials. In this category it is important to machine with high speed and to keep high accuracy. This industry machines parts such as:

- Die casting dies: this is an area where HSC can be utilized in a productive way as most casting dies are made of hard tool steels and have a moderate or small size.

- Forging dies: most forging dies are suitable for HSC due to their complex shape. The surface is very hard and often prone to cracks.

- Milling of electrodes in graphite and copper: is an excellent area for HSC. Graphite can be machined in a productive way with Ti (C,N), or diamond coated solid carbide endmills.

- Modelling and prototyping of dies and moulds: is one of the earliest application areas of HSC. Easy to machine materials such as non-ferrous, for example aluminium are used. The cutting speeds are high and the feeds are also very high.

- **High Speed Milling (HSM)**

High speed milling is a technique that combines high spindle speeds with increased feed rates. This results in a high chip-forming rate and lower milling forces, producing an improved surface quality and closer tolerances (Groover 2002 and Kalpakjian 2003).

In HSM applications, cuts are shallow and the engagement time for the cutting edge is extremely short. The feed is said to be faster than the time for heat propagation.

HSM allows for a productive cutting process in small-sized components. Roughing, semi-finishing and finishing is economical to perform when the total material removal is relatively low. In addition, the HSM process achieves productivity in general finishing and it is possible to achieve extremely good surface finishes, often as low as Ra~0.2 μm.

For most workpiece materials, increasing cutting speed leads to lower cutting forces. The higher temperature in the flow-zone and reduced ontact area contribute towards this effect. The decrease in forces varies with the type and condiction of material and the range of cutting speed in question.

There are few disadvantages of the HSM such as, higher acceleration and deceleration rates, and spindle start and stop result in faster wear of guide ways, ball screws and spindle bearings, leading to higher maintenance costs. Also HSM

requires specific process knowledge, programming equipment and interfaces for fast data transfer needed. In addition, it can involve a considerable "trial and eror" period. Good work and process planning is necessary, along with significant safety precautions and safety enclosing (bullet proof covers).

Finally, tools adapters and screws need to be checked regularly for fatigue cracks

3.2.5 Cutting conditions (Datsko 1966)

The cutting conditions in machining usually refer to those variables that are easily changed at the machine tool by the operator and that affect the rate of metal removal and the machined surface roughness. They are: the cutting speed and the size of cut, besides the tool geometry.

- Cutting speed (V): is defined as the largest of the relative velocities between the cutting tool and the workpiece material. In the case of a milling process is the cutter that moves to provide the cutting speed. This variable is expressed with the units of meter or feet per minute.

  Each metal under a specific metallurgic and mechanical condition needs a different cutting speed, since this parameter depends on the heat treatment that has been applied.

  In order to know the proper cutting speed to machine an specific material it is important to consider: workpiece material, tool material, tool's diameter, required surface roughness, depth of cut, rigidity of the cutter, etc. Equation 3.1. shows how to calculate the cutting speed:

$$V = \frac{\pi \cdot D \cdot n^*}{1000} \tag{3.1}$$

Where:

V = Cutting speed (m/min)

D = Tool diameter (mm)

n^* = Spindle speed (rpm)

Figure 3.9 illustrates the cutting speed and the parameters related to this variable.

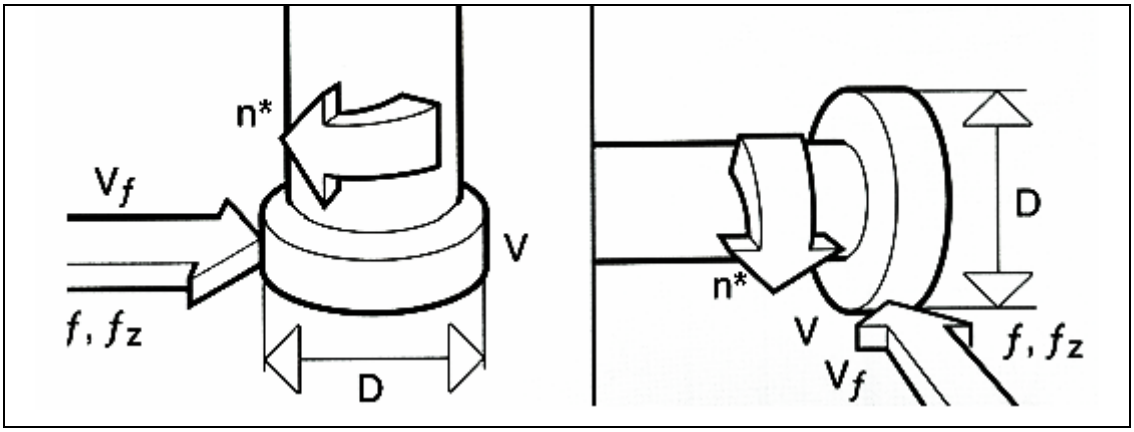

Figure 3.9- Cutting speed and parameters related to the cutting process. (n*=spindle speed, V=cutting speed, fz=feed per tooth, D=tool diameter). (Sandvik, 1994).

- Depth of cut (d): is defined as the distance the cutting tool projects below the original surface of the work and is expressed in mm. The depth of cut determines one of the linear dimensions of the cross-sectional area size of cut. In general, an increase in the depth of cut will result in a nonlinear increase in temperature and a decrease in tool life. With regard to the milling process there are two types of depth of cut, the axial depth of cut (ap) and the radial depth of cut (ar). Figure 3.10 illustrates the axial and radial depth of cut during a machining process
  a. *Axial depth of cut* (ap): is measured along the tool axis. Is the depth the tool penetrates into the workpiece
  b. *Radial depth of cut* (ae): is measured along the cutting tool diameter. Is the distance by which the tool covers the workpiece surface.

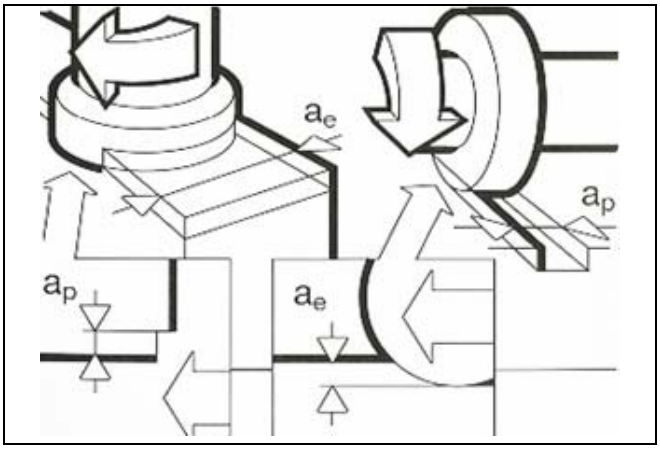

Figure 3.10- Cutting depth in face and peripheral milling (Sandvik, 1994).

- Feed (f): is defined as the relative movement between the tool and the workpiece during a machining operation. On the milling machine is expressed in millimeters or inches per tooth, although the machine controls are designed with the units millimeters or inches per min, which is the product of the basic feed times the number of teeth in the cutter times the revolution per minute of the cutter. The feed is the second linear dimension that determines the cross-sectional area of the size of the cut. In a milling process, this variable is denoted "fz".The capability of each tooth sets the limits for the tool. This variable is expressed in equation 3.2.

$$fz = \frac{V_f}{n* \cdot z} \tag{3.2}$$

Where:

fz = feed per tooth (mm/rev*teeth)

V_f = Feed speed (mm/min)

$n*$ = spindle speed (rpm)

z = number of cutting teeth

Figure 3.11 illustrates the feed and the parameters related to this variable.

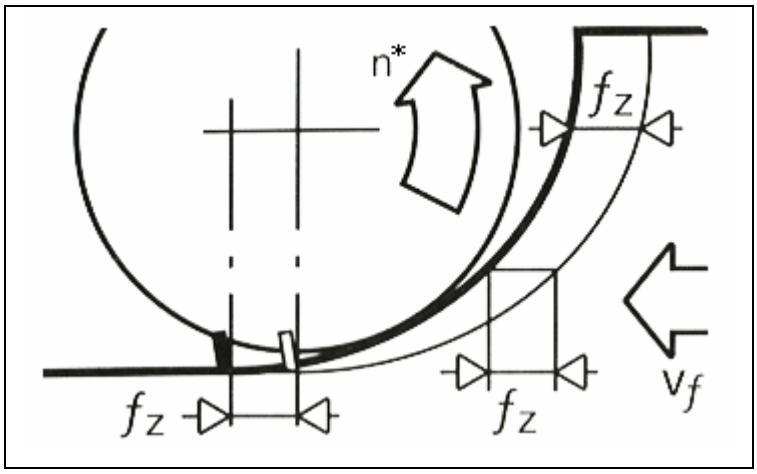

Figure 3.11-Feed variable and the parameters involved. (Sandvik, 1994)

3.2.6 Machinability

Chips may be cut from some materials with relative ease and from others only with the greatest difficulty. This difference may be attributed to the "machinability" of the respective materials. (Black, 1996)

Machinability is made up of a combination of five criteria:

1. Wear resistance
2. Specific cutting pressure
3. Chip breaking
4. Built-uo-edge formation
5. Tool coating character

The most significant variables indicating machinability are tool life and the quality of surface finish produced. Conditions of the materials which determine machinability are composition, heat treatment and microstructure. The measurable mechanical properties of hardness, tensile strength and ductility give some indication of the machining properties to be expected.

The machinability index is a numerical value that designates the degree of difficulty or ease with which a particular material can be machined. Originally based on turning B1112 with a tool life of 60 minutes at a cutting speed of 180 sfpm.

3.2.7 Surface characteristics

Once a workpiece has been machined a surface is created. This new surface can show straight, circular or radial lays. The lay is the direction the predominant surface pattern and the determination of the surface texture is made at 90^{o} to the lay.

In some cases where it is not possible to form an opinion as to the direction of the lay, then it is usual to make measurements in several directions, and to accept the maximum value as a roughness height parameter.

Engineered components must satisfy surface texture requirements such as: roughness and waviness, being the arithmetic average, "Ra" the principal method to assess quality.

Surface integrity (SI) is used to describe the quality and condition of the surface region of a component. The combination of stress and elevated temperatures generated during machining can lead to defects, or alterations of the microstructure, microhardness, cause surface cracking, craters, folds, inclusions, plastic deformation and residual stresses in the finished part. (Kalpakjian, 2003)

Thus the SI describes not only the topological (geometric) features of surfaces and their physical and chemical properties, but their mechanical and metallurgical properties and characteristics as well. Surface integrity is an important consideration in manufacturing operations because it influences properties, such as fatigue, strength, resistance to corrosion, and service life. The defects produced from different machining procedures can significantly affect the performance of the final component. Therefore, it is critical for industries, like aerospace, to know and understand the effects of changing operating parameters before new machining strategies are accepted.

The SI studies covers:

- Surface texture (roughness and lay)
- Macrostructure (macrocracks and surface defects)
- Microstructure (microcracks, plastic deformation, phase transformation, recast layers and selective etching)
- Microhardness

- **Surface texture**

Surface texture is related to quality and precision of machined parts, and that is why it has become an important factor to be considered during a machining process, since is the final factor that controls the machinability of a material.

Every machining operation leaves characteristic evidence on the machined surface. This evidence is in the form of finely spaced micro irregularities left by the cutting tool. Each type of cutting tool leaves its own individual pattern which therefore can be identified. This pattern is known as surface finish or surface roughness.

The texture of the surface of a component arises from the way the material of the component was processed. The description of surface texture as a geometric property is complex, but normally uses the measurable quantities of flaws, waviness, roughness and lay, (Edwards and Endean, 1990).

a) Flaws or defects: are random irregularities, such as scratches, cracks, holes, depressions, seams, tears, and inclusions, (Kalpakjian, 2003).

b) Waviness: is a form of regular deviation from a flat surface. It may be caused by deflections of tools, dies or work-piece during manufacture and is quantified by the width and height of the wave, (Edwards and Endean, 1990).

c) Roughness: consists of closely spaced, irregular deviation on a smaller scale than waviness. It is often superimposed on waviness. Roughness is expressed in terms of its height, its width, and the distance on the surface along which it is measured, (Edwards and Endean, 1990; Kalpakjian, 2003).

d) Lay or directionality: is a description of the predominant surface pattern, which is usually discernible by eye. The lay of a surface is highly dependent on the manufacturing process, (Kalpakjian, 2003).

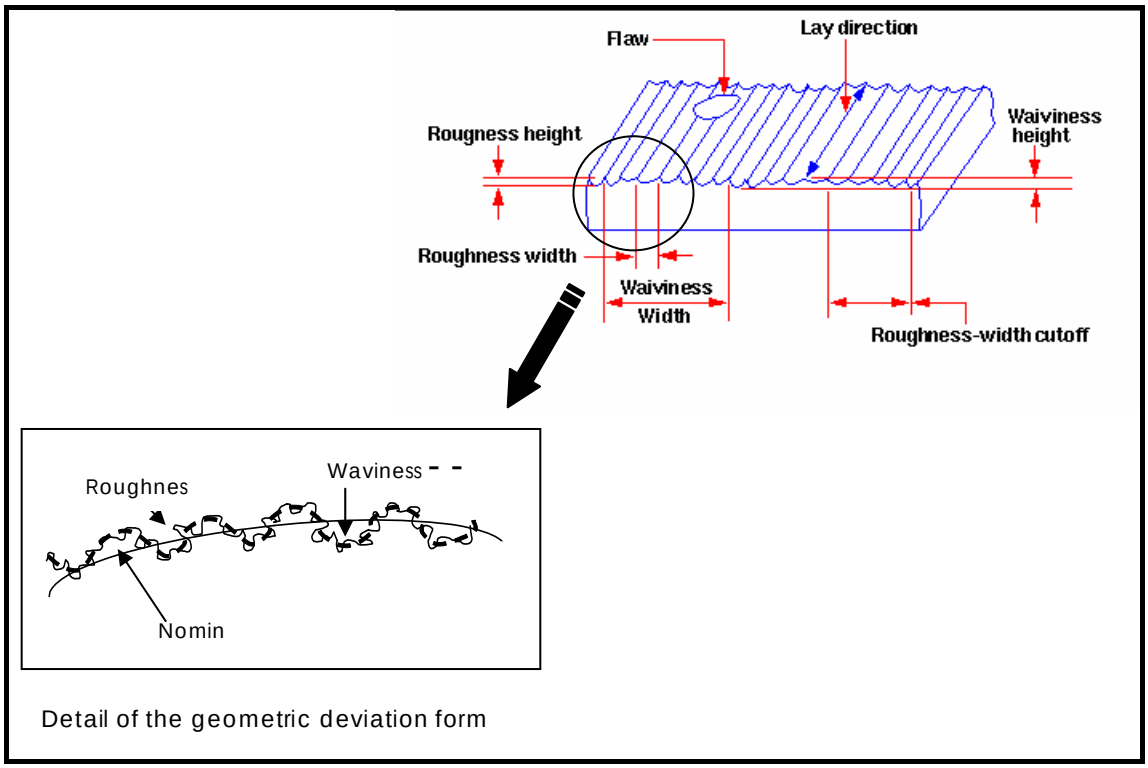

Figure 3.12- Details of a workpiece surface texture. Kalpakjian, 2003

- **Surface roughness** (Boothroyd, 1989)

The final surface roughness obtained during a practical machining operation may be considered as the sum of two independent effects:

1. The "ideal" surface roughness: results from the geometry of the tool and the feed rate.
2. The "natural" surface roughness: results from the irregularities in the cutting operations,(i.e. vibrations, machine movement, cutting parameters, etc)

Surface roughness is generally described by two parameters: arithmetic mean value and root-mean-square average.

a) Arithmetic mean value, R_a

It is also called AA (arithmetic average), or CLA (centre-line average).

This value is obtained by measuring the mean deviation of the peaks from the centre-line of a trace, the centre line being established as the line above and below which there is an equal area between the centre line and the surface trace.

Modern tracer instruments have the capability of giving the arithmetic mean value as a meter reading and the shape of the surface as a magnified tracing, (Shaw, 1991):

$$Ra = \frac{Y_1 + Y_2 + Y_3 + ... + Y_n}{n} \tag{3.3}$$

b) Root mean square average (rms)

The geometric average, root mean square, is more sensitive to occasional highs and lows, making it a valuable complement to Ra, (Lindberg, R, 1990):

$$rms = \sqrt{\frac{Y_1^{\,2} + Y_2^{\,2} ... + Y_n^{\,2}}{n}} \tag{3.4}$$

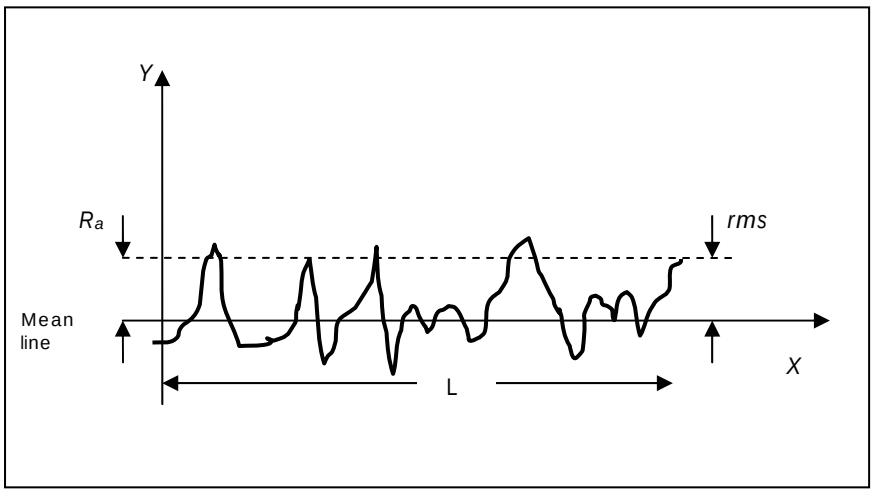

Figure 3.13- Arithmetic surface roughness average, Ra and geometric, root mean square, rms

- **Factors that affects surface roughness**

The height, shape, arrangement and direction of all surface irregularities on the workpiece depend upon a number of factors such as:

a) The machining variables: cutting speed, feed and depth of cut.

b) The tool geometry: the design and geometry of the cutting tool also plays a vital role in determining the quality of the surface. Some geometric factors, which affect the achieved surface finish include: nose radius, rake angle, side cutting edge angle, and cutting edge (Doyle, 1985).

c) Workpiece and tool material combination and their mechanical properties: depending on the combination some advantages such as a decrease in tool wear can be obtained.

d) Quality and type of the machine tool. Vibrations between the workpiece, machine tool and cutting tool: metal cutting processes are inherently cyclic. Cutting forces build up as the tool penetrates the material and deflect the tool, even if slightly. Vibration increases when cutting forces become out of phase with the tool forces. Also cyclic vibrations in other factors, such as depth of cut, material properties, friction forces, and rubbing of the tool nose, affect vibrations. Strong vibration in metal cutting is called chatter. It may become quite noisy and unpleasant, can damage tools and machines, and defaces work surface with patterns called chatter marks. Remedies to decrease chatter are to reduce speed, raise feed, and increase dampening capacity and rigidity of tooling and machine, (Doyle, 1985).

- **Measuring surface roughness,** (Kalpakjian, 2003)

Instruments can be used to obtain an enlarged tracing of the surface irregularities; this tracing is known as the surface profile.

The most commonly used instruments feature a diamond stylus travelling along a straight line over the surface. The distance that the stylus travels, which can be varied, is called the cut-off.

Surface roughness can be observed directly through interferometer, optical or scanning-electron microscopy, or atomic-force microscopy. These latter are especially useful for imaging very smooth surfaces for which features cannot be captured by the less sensitive instruments.

- **Microstructure analysis**

This involves removing a small sample from the workpiece surface that are prepared for examination by mounting in bakelite followed by grinding/polishing using a selection of abrasive media. The exact abrasive and polishing route is dependant on the material being investigated. The selection of a grinding and polishing route is critical to ensure that no additional damage is introduced into the specimen. Polished samples are chemically etched to reveal grain boundaries and other microstructural features with a microscope fitted with a digital camera

- **Microhardness analysis**

The Microhardness measurement is conducted with a diamond indenter utilising loads from as little as 5g. This produces very small indentations (between 0.01 and 0.1 mm across), which allow individual grains/phases in an alloy and near surface regions in cross-sections to be measured.

- **Vicker hardness test.**

The Vickers hardness test method consists of indenting the test material with a diamond indenter, in the form of a right pyramid with a square base and an angle of 136 degrees between opposite faces subjected to a load of 1 to 100 kgf. The full load is normally applied for 10 to 15 seconds. The two diagonals of the indentation left in the surface of the material after removal of the load are measured using a microscope and their average calculated. The area of the sloping surface of the indentation is calculated. The Vickers hardness is the quotient obtained by dividing the kgf load by the square mm area of indentation. (www.gordonengland.co.uk)

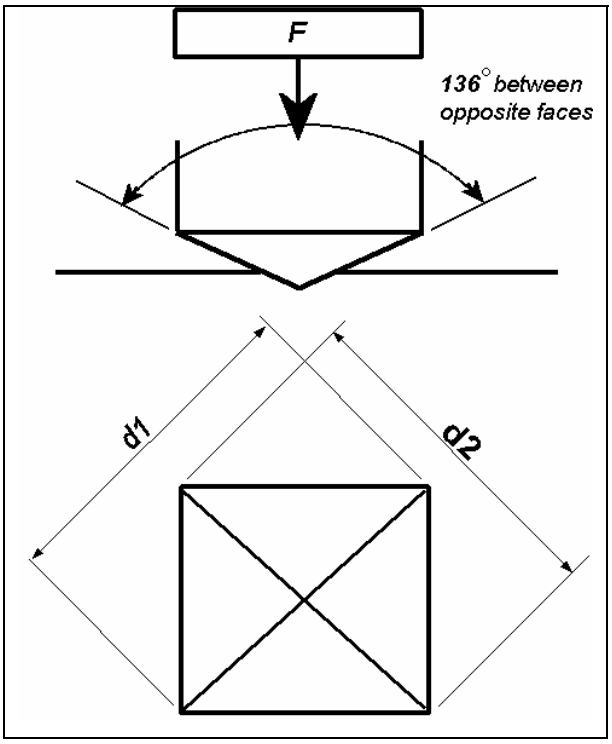

Figure 3.14-Vickers Indentation Test

The Vickers Hardness (HV) is the quotient obtained by dividing the load expressed in kilograms-force (F) by the sloping area of the indentation expressed in mm^2 (d = Arithmetic mean of the two diagonals, d1 and d2 in mm)

$$HV = \frac{2F(136°/2)}{d^2} = \frac{1.854F}{d^2} \tag{3.5}$$

When the mean diagonal of the indentation has been determined the Vickers hardness may be calculated from the formula, but is more convenient to use conversion tables. The Vickers hardness should be reported like 400 HV/10, which means a Vickers hardness of 400, was obtained using a 10 kgf force.

Different loading settings give practically identical hardness numbers on uniform material, which is much better than the arbitrary changing of scale with the other hardness testing methods.

The advantages of the Vickers hardness test are: 1) extremely accurate readings can be taken and 2) just one type of indenter is used for all types of metals and surface treatments.

3.2.8 Workhardening theory

Dislocations are defects in the orderly arrangement of a metal's atomic structure between the actual and theoretical strength of metals. A slip plane containing a dislocation requires less shear stress to allow slip than does a plane in a perfect lattice.

Dislocations are defined quantitatively by means of a Burgers vector, which is the distance, in multiple of the lattice parameter, which is needed to close a straight-sided loop around a dislocation when going the same number of lattice distances in all four directions. There are two types of dislocations: edge and screw. A characteristic of an edge dislocation is that lies perpendicular to its Burgers vector and a screw dislocation lies parallel to its Burgers vector. (Datsko, 1966)

Although the presence of a dislocation lowers the shear stress required to cause slip, dislocations can:

- Become entangled and interfere with each other.
- Be impeded by barriers, such as grain boundaries and impurities and inclusions in the materials.

Entanglements and impediments increase the shear stree required for slip. Entanglement is like moving two humps at different angles across a carpet: where they cross, the two humps interfere with each other's movement, and their combined effect is to make more difficult to move the carpet.

The effect of an increase in shear stress that causes an increase in the overall strength of the metal is known as work hardening or strain hardening. The greater the deformation, the greater the number of entanglements, hence an increase in the metal's strength. Work hardening is used extensively for strengthening metals in metalworking processes at room temperature. Typical examples are producing sheet

metal for automobile bodies and aircraft fuselages by rolling, making the head of a bolt by forging and strengthening wire by reducing its cross-section by drawing it through a die. (Kalpakjian, 2003)

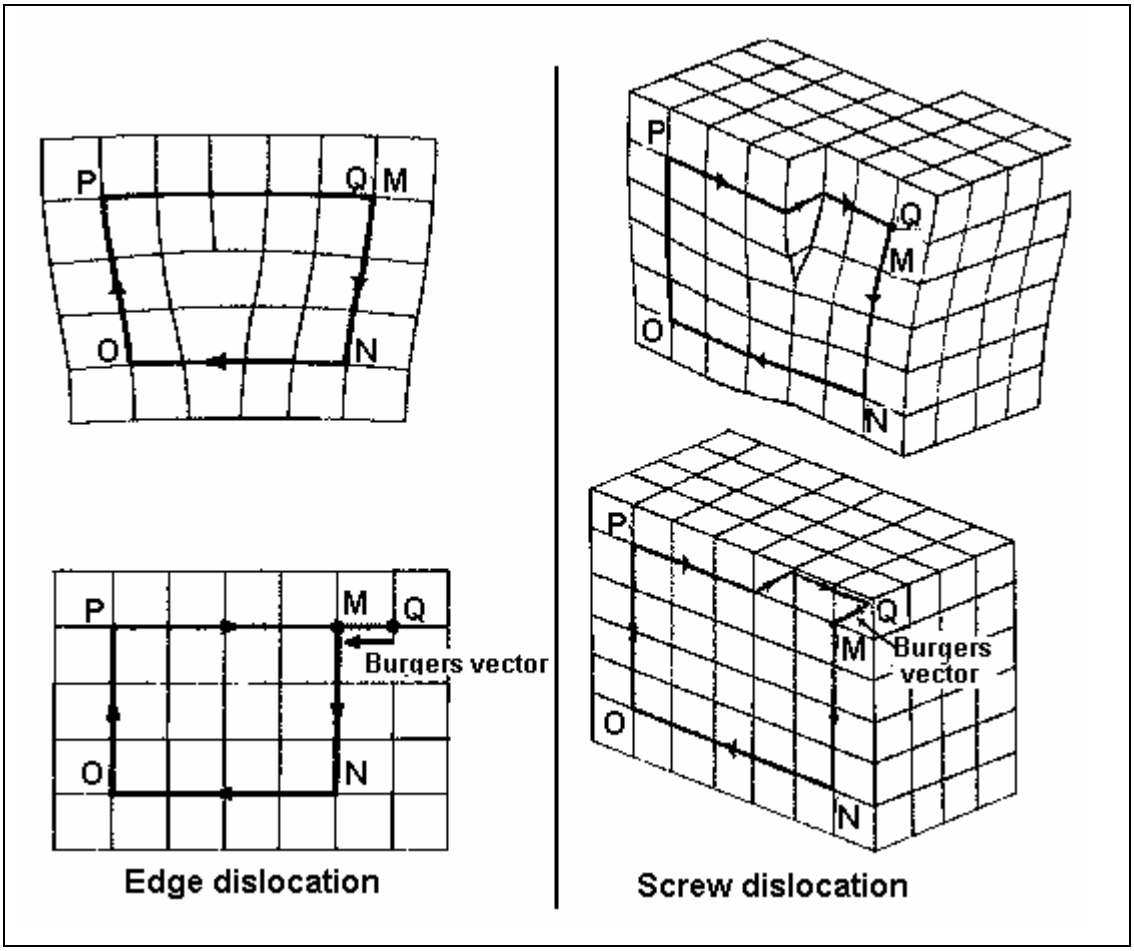

Figure 3.15- Types of dislocations.

3.2.9 Vibration

A vibration in its general sense is a periodic motion, i.e., a motion which repeats itself in all its particulars after a certain interval of time, called the period of the vibration and usually designated by the symbol *T*. The simplest kind of periodic motion is a harmonic motion. In a machine, vibration is a result of internal dynamic forces created by the elements that compose the equipment.

The harmonic motion is the simplest form of vibration and when plotted as a function of time, it is represented by a sinusoidal curve as observed in Figure 3.16.

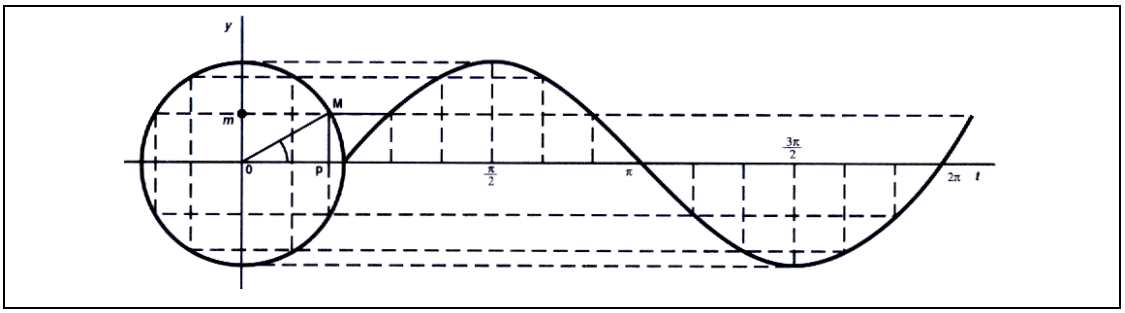

Figure 3.16- Simple harmonic motion

The vibration is probably the best parameter to judge dynamic conditions such as balance and bearing stability, to detect flaws in rolling element bearings, and to recognize excessive dynamic stress applied to components, such as blading and gear teeth. Machinery vibration is normally a combination of various harmonic motions, with different amplitudes and frequencies, together with random motions (Mitchell, 1981).

The RMS amplitude (Root Mean Square) value gives an estimate of the energy content of the vibration signal, and it is a widely used descriptor for the estimation of vibration severity from casing or external measurements.

Real life systems, such as a machine and foundation, are not single degree of freedom systems. They are made up of a combination of masses, springs, and dampers where each can move and rotate in six degrees of freedom.

Table 3.7 shows the illustrated vibration diagnostic chart (Mitchell, 1981). This chart can be used to analyze the bahaviour of rotating elements that composed a HSM machine.

Table 3.7- Illustrated vibration diagnostic chart, (Mitchell, 1981).

Problem Source	Typical spectrum	Remarks
Normal spectrum	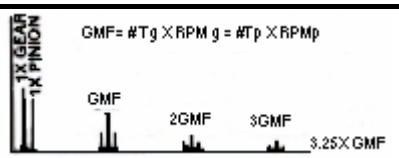	Normal spectrum shows 1X and 2X RPM, along with Gear Mesh Frequency (GMF). GMF commonly will have running speed sidebands around it. All peaks are low amplitude, an no natural frequencies of gears are excited
Tooth wear	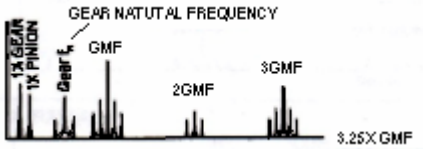	Key indicator of tooth wear is excitation of Gear natural Frequency, along with sidebands around it spaced at the running speed of the bad gear. GMF may or may not change in amplitude, although high amplitude side bands surrounding GMF usually occur when wear is noticeable. Sidebands may be a better wear indicator than GMF frequencies themselves
Tooth load	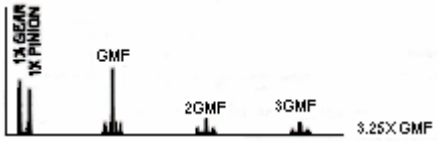	GMF are often very sensitive to load. High GMF amplitudes do not necessarily indicate a problem, particularly if sidebands frequencies remain low level and no gear natural frequencies are excited. Each analysis should be performed with system at maximum operating load.
Gear eccentricity and backlash	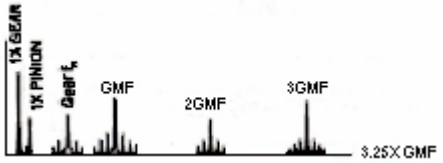	Fairly high amplitude sidebands around GMF often suggest gear eccentricity, backlash, or non-parallel shafts which allow the rotation of one gear to "modulate2 the running speed of the other. The gear with the problem is indicated by the spacing of the sideband frequencies. Improper backlash normally excites GMF and gear natural Frequency, both of which will be sidebanded at 1X RPM. GMF amplitudes will often decrease with increasing load if backlash is the problem.
Gear misalignment	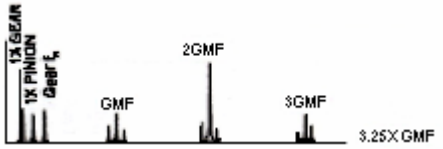	Gear Misalignment almost always excites second order or higher GMF harmonics which are sidebanded at running speed. Often will show only small amplitude 1X GMF, but much higher levels at 2X or 3X GMF. Important to set F_{MAX} high enough to capture at least2 GMF harmonics if traducer systems has the capability.
Cracked/ Broken tooth	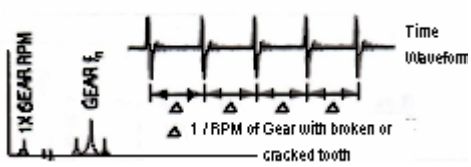	A cracked or broken tooth will generate high amplitude at 1X RPM of this gear, plus will excite gear natural frequency (fn) sidebanded at its running speed. It is the best detected in time waveform which will show a pronounced spike every time the problem tooth tries to mesh with teeth on the mating gear. Time between impacts (Δ) will correspond to 1/speed of gear with the problem. Amplitude of impact Spikes in Time Waveform often will be much higher than that of 1X gear RPM in FFT
Hunting Tooth problems	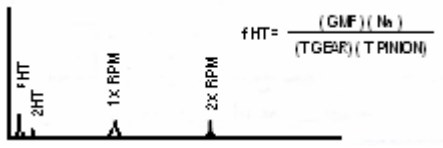	Hunting tooth frequencies (f_{HT}) is particularly effective for detecting faults on both the gear and pinion that might have occurred during the manufacturing process or due to mishandling. It can cause quite high vibration, but since it occurs at low frequencies predominately less than 600 CPM, it is often missed. A gear set with this tooth repeat problem normally emits a "growling" sound form the drive. The maximum effect occurs when the faulty pinion and gear teeth both enter the mesh at the same time.

- **Fourier transform**

A Fourier transform is a method whereby the variation of a quantity as a spectral function (e.g. plotted against frequency) from the variation quantity as a function of period (e.g. plotted against time) is obtained.

In many instances where there is a concern with the frequency or spectral response of a system to a pulse or complex distribution of amplitude with time, the Fourier transform relates the distribution of the signal expressed in terms of time with its distribution in terms of frequency. In other cases, where there is a coherent spatial distribution across an aperture, the relationship exists between the reception or transmission pattern of the system in terms of the sine of the angle of projection and the distribution of the field along the aperture of the system. (Bracewell, 1999)

3.2.10 Neural Networks

Neural network analysis is a subject lying at the intersection of psychology, mathematics, neuron science and system theory. Currently this field is experiencing rapid development because of its applications, which include: robotics, pattern recognition and understanding human brain-mind processes. The point of view is modelling biological nervous systems since it is a dynamical system with one-way interconnections. (Harvey, 1994)

- **Neural network architecture**

A neural network consists of a number of elementary units called neurons, which are simple processors that takes one or more inputs and produces an output.

Each input has an associated weight that determines the intensity of the input. A network can be trained to perform certain tasks where the data is fed into the network through an input layer, it is processed through one or more intermediate hidden layers and finally it is fed out to the network through an output layer.

It must be highlighted that the best network architecture is generally reached by trial and error, after considering different combinations of number of neurons in the

hidden layer, the number of hidden layers, spread parameter, learning rate, etc, depending on the type of neural network that has been used. Figure 3.17 shows a general scheme of an artificial neural network.

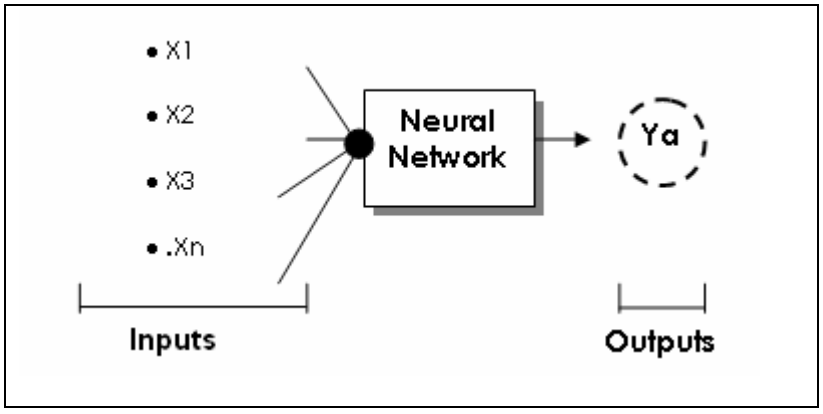

Figure 3.17- Inputs and outputs of the network

- **Radial Base Neural Network (RBNN)**

This network architecture can be designed in a very short period of time since it consists of three layers: 1) input layer, 2) hidden layer and 3) output linear layer.

There are only two types of Radial Base Network, the newrbe (exact design) and the newrb (more efficient design). The newrb, architecture iteratively creates one neuron at a time and there are added to the network until the sum-squared error falls beneath an error goal or a maximum numbers of neurons have been reached (MATLAB user's Guide).

- **Feed Forward Neural Network (FFNN)**

This network is one of the most popular multi-layer architecture, proving to be an excellent universal approximation of non-linear functions. Its ability to map complex input-to-output relationships with acceptable error, best demonstrates its suitability. There are many variations of a feed forward network and the most common one is the Lavenberg-Marquardt algorithm. This algorithm is designed to approach second-order training speed without having to compute the Hessian Matrix, being the fastest method for training moderate-sized feed forward neural networks, (MATLAB user's Guide).

- **Generalized Regression Neural Network (GRNN)**

This type of network is often used for function approximation. It has a radial basis layer and a special linear layer. The first layer is just like the newrbe network and it has as many neurons as there are input/ target vectors, (MATLAB user's Guide).

3.2.11 Fourier series

Mathematics is the science of patterns since it seeks for patterns in numbers, in space, in science, in computers and in imagination.
Mathematical theories explain the relations among patterns functions and map, in order to explain and predict natural phenomena that fit the patterns, (Steen, 1988).

The Fourier series provides a set of mathematical tools which enables waveforms of any form to be broken down into a number of sinusoidal with different frequencies, amplitudes and phases.

- **Periodic waveforms**

A periodic waveform is defined as being one for which the entire set of values repeats itself at regular intervals; the time between successive repetitions is being called the periodic time or period. In mathematical terms, a function of time $f(t)$ can be defined as periodic if it has the same value when considered at the time t+T, for example; $f(t) = f(t+T)$. In Figure 3.18 different examples of periodic forms are presented, (Bolton, 1995).

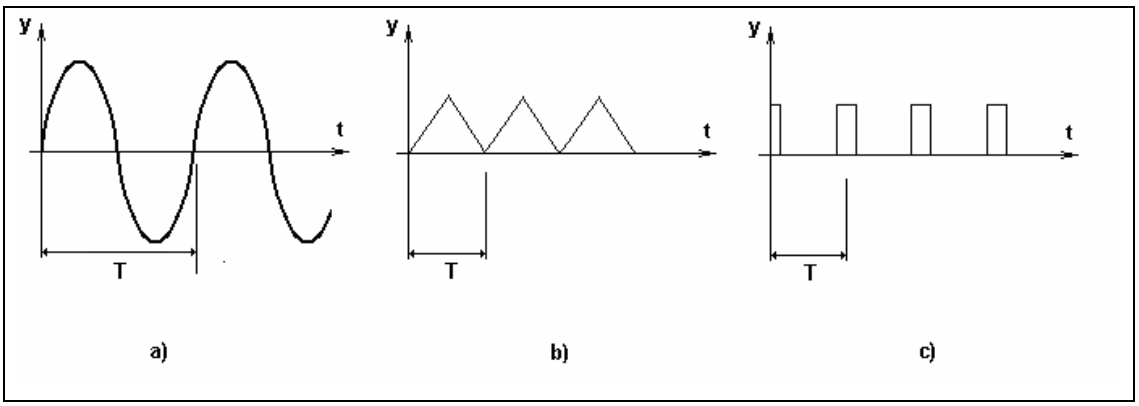

Figure 3.18- Examples of periodic waveforms.

In Figure 3.18, a) shows a signal with a sinusoidal waveform, where the signal varies with the time, keep on repeating themselves every T seconds, b) a signal with a triangular waveform and c) a signal with a pulsed waveform.

T is the periodic time. Thus if a waveform has a periodic time of 3 seconds then we have $f(t) = f(t+3)$.

3.2.12 Design of experiments. Taguchi Method (Montgomery, 1997)

The most efficient method of experimental planning is Design of Experiments (DoE), which incorporates the orthogonal arrays (OAs), developed by Taguchi, to successfully design and conduct fractional factorial experiments that can collect all the statistically significant data with the minimum possible number of repetitions.

The selection of the appropriate OA is based on the following criteria: the numbers of factors and interactions of interest, the number of levels for the factors of interest and the desired experimental resolution or cost limitation.

A Taguchi design, or an orthogonal array, is a method of designing experiments that usually requires only a fraction of the full factorial combinations. An orthogonal array means the design is balanced so that factor levels are weighted equally. Because of this, each factor can be evaluated independently from all the other factors, so the effect of one factor does not influence the estimation of another factor. The disadvantages of this method are: 1) the results are only relative and do not exactly indicate what parameter has the highest effect on the performance characteristic value, 2) does not take into account the interactions between parameters, 3) is inappropriate for a dynamically changing process such as a simulation study and 4) it is applied most effectively at early stages of process development.

In robust parameter design, such as Taguchi, first choose the control factors and their levels and choose an orthogonal array appropriate for these control factors. The control factors comprise the inner array. At the same time, determine a set of noise factors, along with an experimental design for this set of factors. The noise factors comprise the outer array.

The experiment is carried out by running the complete set of noise factor settings at each combination of control factor settings (at each run). The response data from each run of the noise factors in the outer array are usually aligned in a row, next to the factors settings for that run of the control factors in the inner array.

3.2.13 Pareto ANOVA diagram

The application of the Pareto ANOVA (Analysis of Variance) diagram gives the opportunity of knowing the contribution of each studied independent variable on the dependent variable.This method represents a simplified ANOVA method that employs the Pareto principle and the technique requires less knowledge that the ANOVA method, but it adjusts very well to engineer and industries practices.

For the application of this method, it is required a specific amount of independent variables and one or few dependent variables.

Once the target variable is obtained, comparisons as observed in Table 3.8 are applied, (Canavos, 1988).

Table 3.8- An example of how to fill the comparison table with the level of contributions of each cutting parameter on the target variable.

	Addition of the target variable for each factor's level				
Level	**A**	**B**	**C**	**D**	**Total**
1	$T_{1\,(A)}$	$T_{1\,(B)}$	$T_{1\,(C)}$	$T_{1\,(D)}$	---
2	$T_{2\,(A)}$	$T_{2\,(B)}$	$T_{2\,(C)}$	$T_{2\,(D)}$	---
3	$T_{3\,(A)}$	0	$T_{3\,(C)}$	$T_{3\,(D)}$	---
Square differences addition (TG)	$TG\,(A) = [T_{1\,(A)} - T_{2\,(A)}]^2 + [T_{2\,(A)} - T_{3\,(A)}]^2 + [T_{3\,(A)} - T_{1\,(A)}]^2$	$TG\,(B) = [T_{1\,(B)} - T_{2\,(B)}]^2$	$TG\,(C) = [T_{1\,(C)} - T_{2\,(C)}]^2 + [T_{2\,(C)} - T_{3\,(C)}]^2 + [T_{3(C)} - T_{1\,(C)}]^2$	$TG\,(D) = [T_{1\,(D)} - T_{2\,(D)}]^2 + [T_{2\,(D)} - T_{3\,(D)}]^2 + [T_{3\,(D)} - T_{1\,(D)}]^2$	$TT = \Sigma$ row
Contribution on the target variable (%)	$\frac{TG\,(A)}{TT}$ **(%A)**	$\frac{TG\,(B)}{TT}$ **(%B)**	$\frac{TG\,(C)}{TT}$ **(%C)**	$\frac{TG\,(D)}{TT}$ **(%D)**	Σ row = 100

$Ti_{(P)}$: Total per level. i= level, p= cutting parameter
TG : Total sum of the "p" square differences (cutting parameter)
TT: Total sum of each TG

The respective Pareto diagram is built in order to illustrate what is exposed in Table 3.7. For this illustration a table is made, where the first row of the diagram (see Figure 3.19) corresponds to the percentage of contribution of each studied variable on the target variable from the highest values to the lowest value.

The second row of the diagram corresponds to the addition of each percentage of contribution of each studied variable (column by column), in order to obtain the accumulative effect of each contribution. Finally, the respective bar chart is superimposed on to the table.

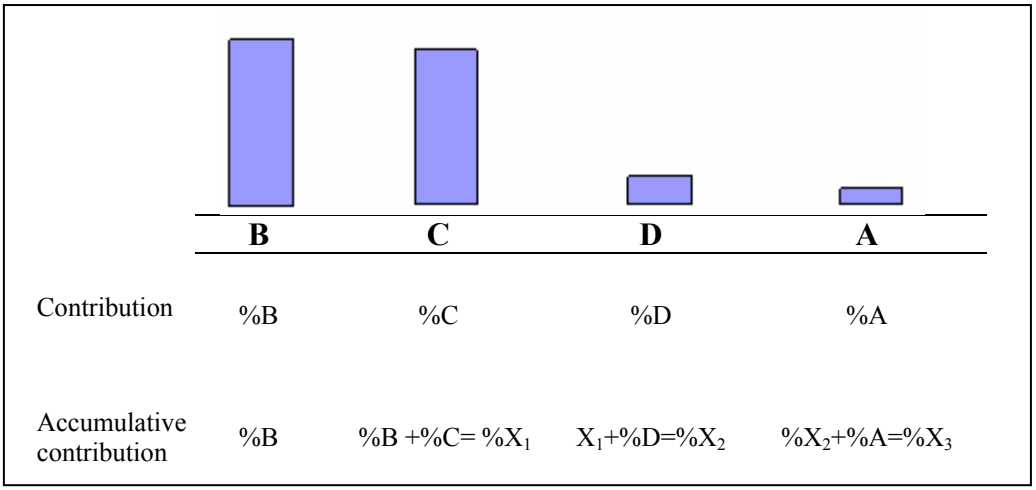

Figure 3.19- Pareto ANOVA diagram.

3.2.14 Tchebysheff theorem

When using any method in statistic design, a random variable presents a low variance (S2) and/or low standard deviation (S), it will be expected that the major part of the values will be grouped much closer to the media (μ). The standard deviation is a statistic that tells you how tightly all the various examples are clustered around the mean in a set of data. When the examples are pretty tightly bunched together and the bell-shaped curve is steep, the standard deviation is small. When the examples are spread apart and the bell curve is relatively flat, that tells you you have a relatively large standard deviation. For this reason, the probability that a random variable takes a value in between certain intervals around the media is higher than a random variable with a higher standard deviation. If the probability is described in terms of a surface, it will be expected for any type of distribution with a small standard deviation that most part of its area is located closed to the media (μ), such as illustrated in Figure 3.20. (Canavos, 1988)

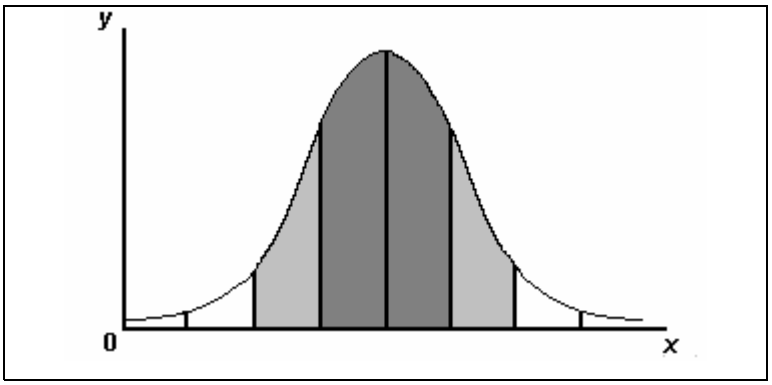

Figure 3.20- Normal distribution curve showing different areas for different values of standard deviations.

One standard deviation away from the mean in either direction on the horizontal axis (the dark gray area on the above graph) accounts for somewhere around 68%. Two standard deviations away from the mean (the dark and light gray areas) account for 95 %. And three standard deviations (the dark gray, light gray and white areas) account for about 99%.

Tchebysheff, was a Russian mathematician who discovered that the fraction of the area between any two symmetric values around the mean, are related to the standard deviation. Based in his observations he postulated the theorem that is named after him and expresses the following:

"In any data sample or probability distribution, nearly all the values are close to the mean value, and provide a quantitative description of "nearly all" and "close to".

More precisely, no more than $1/K^2$ of the values are more than K standard deviations away from the mean.

$$P(X) \geq 1 - \left(\frac{1}{K^2}\right) \qquad \mu - K \cdot S < X < \mu + K \cdot S \qquad (3.6)$$

3.3 Research literature

In order to compete in the worldwide market, the most important objective for manufacturing industries is to obtain better workpiece quality with reduced production cost and shorter production time.

To accomplish this objective, many researches have focused on studying the influence of tool materials, tool geometry, path strategies, etc, on workpiece surface roughness. In addition to the influence of the tool and the machining process on the causes, mechanisms, and the types of wear, of the cutting tool during high speed machining processes.

A wide range of publications have been analyzed in order to know and understand the influence of the different factors that affect a machined surface, tool life and tool wear. Also research related to the prediction of surface roughness has been reviewed.

Despite all the studies in the area there are always gaps that need to be understood and fulfilled due to the constant introduction of improved machine-tools, and tools in order to reach higher quality standards on machined pieces by achieving smoother surfaces. Another factor that needs to be kept in mind is the fact that the machining process is a dynamic process, so any change during the process can change the results dramatically.

The different papers that were reviewed in order to support this research as well as the identification of possible gaps now follow.

- **Influence of cutting parameters and type of tool on tool life and wear**

In 1997, Elbestawi et al, studied the effect of the different tool path directions on the cutting tool performance when high speed milling H13 tool steel. Dry and wet cutting conditions were used and the effect of coolant on the tool life was also determined. The optimum cutting conditions have been specified based on the modes of tool failure, tool life and surface integrity produced.

In 1998, Kopac studied the influence of the cutting parameters and the influence of the type of tool on tool wear mechanisms. He studied the influence of the cutting material and coating on tool quality and tool life and concluded that machining on the basis of “dry” cutting requires modern cutting tools (cermets) coated with TiN, TiC or Al_2O_3 due to higher temperatures on the cutting edge. In addition, the

diffusion wear process was considered since it was shown that this process has a greater effect at higher temperatures.

In 1999, D'Errico, et al, studied the possibility of high-speed milling and dry cutting operations with different tools when machining AISI 1045. They concluded that the following coatings, TiAlCN, TiN, TiCn and TiALNbN, do not provide an efficient thermal barrier against diffusive wear, which is the most important wearing mechanisms during dry metal cutting at relative high cutting speed (V= 600 m/min). The results also showed that using cermet as tool substrate, the uncoated tool is the most appropriate, from economic and cutting efficiency point of view. When machining an Al-based alloy, the best performing coating is TiAlNbN, since it allows a decrease of the cutting forces, and the tool wear. In some cases PVD coatings of hard metal substrates increases the wear resistance in the wet cutting of Al-based alloys.

In 2001, Dolinsek et al. concluded that the oxidation process of the protective coating of the tool and oxidation of workpiece, is one of the mechanisms causing the extensive wear of end mill tools. When the protective coating is removed from the tool tip, a further wearing process accompanied by increased cutting resistance and elevated temperatures is demonstrated as the sudden chipping of the cutting edges and catastrophic failure of the tool.

Lin, T. in 2002, studied the performance of a TiN-coated carbide tool in the face milling of stainless steel. An orthogonal array, the signal-to-noise (S/N) ratio, and the analysis of variance (ANOVA) were employed to study the performance characteristics in face milling operations. The results show that these methods are usefull to optimize the cutting parameters for a certain objective.

Mativenga and Hon in 2003, demonstrated that multi-layer TiAlN coated carbides generate the best surface finish, while the uncoated tool and TiAlN + WC/C lubricant coating led to a severe degradation of surface finish when increasing spindle speed.

Also in 2003, Corduan et al. studied the wear mechanisms of PCD, CBN and TiB_2 coating tools, when turning Ti-6Al-4V titanium alloy. They concluded that

CBN tools must be used with finishing cutting conditions in order to achieve a suitable tool life. Regarding the coated carbide tool, the coating protects the tool from diffusion and adhesion before its delaminating.

In 2003, Dabade et al. analyzed the cutting process performed using a specifically designed and fabricated self-propelled rotary inserts face milling cutter. Statistically designed experiments were performed using Taguchi method with surface roughness and chip cross-sectional area as response variables. The results show that inclination angle is the most significant factor influencing both surface roughness and chip cross-sectional area and can give better results in the range of 30-45 degrees.

The performance of multilayered (TiN/TiCN/TiN) carbide inserts when high speed milling AISI 304 stainless steels was studied by Abou-El-Hossein et al. in 2005. They concluded that tool wear increased with cutting speed, while at the same time, a decrease in tool wear was observed with increase of the cutting feed. It was also found that the built up edge phenomenon occurred at high values of feeds and medium cutting speeds (190 and 225 m/min).

In 2004, Ghani et al. applied the Taguchi optimization methodology, to optimize cutting parameters in end milling when machining hardened steel AISI H13 with TiN coated P10 carbide insert tool under semi-finishing and finishing conditions of high speed cutting. An orthogonal array, signal-to-noise (S/N) ratio and Pareto analysis of variance (ANOVA) were employed to analyzed the effect of the cutting speed feed rate and the depth of cut. The result show that the optimal combination for low resultant cutting force and good surface finish are high cutting speed, low feed rate and low depth of cut. The study shows that the Taguchi method is suitable to solve the stated problem with minimum number of trials as compared with a full factorial design.

Regarding the influence of coating thickness, Bousakis et al. in 2004, studied the performance of PVD coated cemented carbides inserts with variable film thickness on the rake and flank face during a milling process. The results indicated that coating thickness diminishing on the tool rake significantly affects the milling performance, in comparison with a corresponding decrease on the tool flank. In general, a

symmetric distribution of the coating thickness on tool rake flank leads to an enhanced cutting performance. Later in 2005, Bousakis et al. investigated the feasibility of increasing the wear resistance of cemented carbide tool through micro-blasting of their PVD coatings during a milling process. They concluded that tool life increases through micro-blasting of films, deposited on micro-blasted polished substrates and also a comparable lower enhancement of the wear resistance can be attained through micro-blasting of films, on ground micro-blasted substrates.

In 2008, Childs et al. studied the influence of cemented carbides and single crystal diamond round nosed tool on the surface finish of 1000 series aluminium after a turning and facing process. They concluded that when machine tool limits are avoided, surface roughness values decreased 0.02 times at the insert edge radius.

Ravindra et al. 2008, studied the surface quality of a chemically vapor deposited (CVD) polycrystalline SiC material to be used in an optics device such as a mirror. Besides improving the surface roughness of the material, the research also emphasized increasing the material removal rate (MRR) and minimizing the diamond tool wear. The surface quality was improved using a Single Point Diamond Turning (SPDT) machining operation.

In 2009, Dilipak et al. studied the effect of the number of milling cutter inserts on the metal removal and the machining time when milling AISI D3. The machinability tests were carried out in dry cutting conditions at various cutting speeds, feed rates and with different number of inserts. The results show that the machining time decreased and the tool flank wear increased when increasing the cutting speed, number of inserts and feed rate. The flank wear increased gradually until the first 0.2 mm, but the wear rate increased significantly when above this point under different cutting conditions.

In 2009 Sahin compared the tool life between ceramics and cubic boron nitride (CBN) cutting tools when machining hardened bearing steels. An Orthogonal design, signal-to-noise ratio (S/N) and analysis of variance (ANOVA) were employed to determine the effective cutting parameters on the tool life. First order linear and exponential models were carried out to find out the correlation between cutting time

and independent variables. Second order regression model was also extended from the first order model when considering the effect of cutting speed, feed rate, hardness of cutting tool and two-way of interactions amongst these variables. The results indicated that the cutting speed has the most influence on the tool life, followed by the tool hardness. The CBN cutting tool showed the best performance than that of ceramic based cutting tool.

- **Influence of the type of tool on tool wear mechanisms**

Wear mechanisms have been studied by few researchers and among them it can mention the works made by Elbestawi et al. in 1997. They performed some experiments using several grades of PCBN ball-nose end mills with various type of edge for the high speed milling of H13 tool steel. They concluded that higher contents of CBN (90%) on PCBN tools are recommended for milling hardened tool steel and that the main mode of tool failure was classical flank wear. Low CBN fraction volume (65%) tools fail generally by chipping. Also the higher the cutting speed the thinner the chips produced.

In 2002, Molinari and Nouari, showed that the dominant damage mechanism at high cutting speed is diffusion wear, due to higher temperatures produced by friction at the tool-chip interface. They also presented a modelling of diffusion wear, which allows optimizing high speed cutting process in terms of tool life and volume of material removal.

Koshy, et al. in 2002, machined AISI D2 (HRC=58), using indexible insert ball nose end mills employing carbide and cermets tools, and solid carbide ball nose end mills. They concluded that chipping, adhesion and attrition were, in general, the governing mechanisms responsible for tool wear and that PCBN tools failed by fracture of the cutting edge. However, better surface roughnesses were obtained with PCBN end mills.

In 2002, Liu et al. studied the wear patterns and mechanisms of cutting tools during high-speed face milling of different working material such as: cast iron, 45# tempered carbon steel, 45# hardened carbon steel. They demonstrated that lower

CBN content in the PCBN tool is not suitable for the high speed machining of steels with hardness less than 45-50 HRC and that it is necessary to select a higher CBN content PCBN tool (more than 90% CBN) in intermittent high-speed operations such as milling.

The tool wear of different coated tools when machining alloyed tool steel (X38CrMoV5, 47-48 HRC) with a high speed milling process was studied by Sokovic et.al. in 2004. In this work they concluded that, single-layer of TiAlN (0.96 % Ti, 0.04% Al) tool, showed uniform, not so strong flank wear with the beginning of central wear and that end mill cutters, coated with dry lubricating coating TiAlN + WC/C, are not preferred to be used in high speed milling of alloyed steels, due to the presence of strong central wear.

Shimada et al. in 2004, proposed an erosion test in order to simulate the wear process of a diamond tool during turning of stainless steel. Their results would be useful to extend the application of a diamond tool for machining a variety of ferrous metals that have been known to wear diamond tools rapidly.

In 2005, Wang et al. analyzed the wear mechanism of the BCBN (binderless cubic boron nitride) tool, in high speed milling of Ti-6Al-4V. This tool showed a longer tool life at high cutting speeds when milling titanium alloys. Also they concluded that non-uniform flank wear was found to be the dominant wear pattern of BCBN tool, even though there were some micro-grooves on the flank face. Due to this result they considered that BCBN appears to become a new cutting tool material for high-speed machining of titanium alloys.

Different coated tools were evaluated by Aslan, in 2005. Tool performance evaluation was based on the surface finish of the workpiece and tool flank wear. The experiments were conducted in the high speed milling of hardened X210Cr12 cold-work tool steel. The results showed that TiCN and TiCN+TiAlN coated carbide and TiAlN coated cermets tools exhibited much shorter tool lives compared to mixed ceramic with Al_2O_3+TiCN and CBN tools. Also, CBN tools had a much slower flank wear rate than ceramic tool and has much superior chip removal capacity compared with coated cemented carbides and cermets tools.

Also, Kishawy et al. in 2005**,** determined the effect of different process parameters on tool wear, cutting forces and surface quality when face milling aluminium alloys. They found that by increasing the tools clearance angle and radius of the cutting edge and the volume of lubricant, the existence of material adhered to the machined surface and tools cutting edge could be minimized. Further study is required to completely quantify this phenomenon and to identify its causes and prevention method.

In 2005, Myung et al. suggested that fractal analysis could be used as an effective tool for in-process monitoring of tool wear. Experiments were carried out on high-hardened die steel using uncoated and coated tools (TiN, TiAlN), in high-speed cutting conditions. They concluded that a TiAlN coating tool is the proper tool to analyze fractal dimension of machined surface. In addition, they showed that fractal dimension and tool wear shows a similar tendency associated with the increase in surface roughness.

Finally, in 2009 Siller et al. studied the impact of a special carbide tool design on the process viability of the face milling of hardened AISI D3 steel, in terms of surface quality and tool life. Experimental results show that surface roughness values from 0.1 to 0.3 μm can be obtained in the workpiece with an acceptable level of tool life. The tool performance is based on tool wear characterization. For the parameters optimal selection, frequency histograms of surface roughness distribution were obtained establishing the relationship between the milling process parameters (cutting speed and feed per tooth), surface roughness and tool wear morphology.

- **Tool wear prediction**

Regarding statistical models of tool wear, Gatto and Iuliano, in 1997, proposed a statistical model of tool wear when milling Inconel 718 with different tools (coated an uncoated). They demonstrated that (TiAl) coated ceramic is less influenced by the increase in cutting speed and feed rate than the uncoated and CrN coated ceramic tool. Finally, different wear mechanisms along the tool-chip contact length may be

attributed to the variation of the plastic deformation energy and also a tool safety area is obtained.

In 2002, Tay et al. studied the topography of the flank wear surface of a coated carbide insert when turning AISI 4340 steel was studied. They concluded that there is a good relationship between the maximum flank wear and roughness parameters of the flank wear surface. The greater the roughness value of the flank wear surface, the higher the friction of the tool on the workpiece. Therefore greater heat generation will occur, which could cause tool failure.

In 2004, Choundhury and Srinivas, presented a mathematical model to predict tool wear during a turning process. The proposed model can be used to estimate the flank wear by means of the index of the diffusion coefficient, and other cutting parameters. The same year (2004), Korkut et al. studied the influence of cutting speed on tool wear and surface roughness when turning AISI 304 austenitic stainless steel. The results show a decrease in tool wear when increasing the Cutting speed up to 180 m/min. Surface roughness (Ra) was also decreased with increasing the cutting speed. A correlation was made between the tool wear/surface roughness and the chips obtained when cutting speeds at 120, 150 and 180 m/min.

Later in 2005, Kishawy et al. determined an analytical model of tool wear, specifically for abrasion mechanisms during a turning process of metal matrix composites. The model was also used to study the effect of tool nose radius on the progress of tool wear. The proposed model agrees with the measured tool wear data.

In 2005, Sai W, studied the tool wear when turning AISI 4340 steel at speeds between 325 and 1000 m/min. The flank wear was measured in connection to cutting time and the results show that an increase in cutting speed causes a higher decrease of the time of the second gradual stage of the wear process. This is due to the thin coat layer which is rapidly peeled off when high-speed turning. The investigation included the realization of a wear model in relation to time and to cutting speed and an empirical model, that relates the tool life with the cutting speed.

Other works related to tool wear were conducted by Gopalsamy et al. in 2009. They presented equations for the prediction of tool wear and surface roughness. The equations were based on a multiple regression analysis. The experiments were conducted on hardened steel when using an end milling process. As Design of Experiments the Taguchi method was applied. The signal-to-noise ratio and an analysis of variance (ANOVA) were applied to study the performance of the cutting speed, feed and depth of cut, on the machined surface finish and the tool life. The results showed that cutting speed is the most influencing parameter and that chipping and adhesion were the main causes of tool wear. Also, it was observed that the Taguchi method match closely with the ANOVA results.

In 2009 Calamaz et al. studied the tungsten carbide (WC-Co) tool wear under dry machining of the hard-to-cut titanium alloy Ti6Al4V. Machining tests were conducted in the orthogonal cutting framework and showed a strong evolution of the cutting forces and the chip profiles with tool wear. The wear mechanisms were identified using cutting force measurements, scanning electron microscope observations and optical profilometer analysis. The results showed that the chip formation mechanisms during dry cutting process are quite dependent of the worn tool geometry.

Also in 2009 Rashed et al, predicted the tool wear based on artificial neural network (ANN) approach. The studies were conducted on A356/SiC metal matrix composites (MMCs) prepared using rheocasting route. The ANN model was obtained to aid in prediction and optimization of the wear rates of the composites. The results have shown that ANN is an effective tool in the prediction of the properties of MMCs.

- **Influence of workpiece microstructure on tool wear**

In 2003 Poulachon et al. demonstrated that the microstructure of hardened tool steels also has an influence on tool wear. Studies were carried out in PCBN tools during a turning process (V = 180 and 230 m/min, f = 0.08 and 0.12 mm/rev, and d = 0.2 mm). They concluded that the major influencing factor on the tool wear is the presence of various carbides in the steel microstructure. The hardness of these carbides varies significantly, causing different wear rates. The microstructure of the

chips reveals the presence of different amounts of white layers when machining these steels.

In 2006, Campbell et al. studied microstructural characterization of Al-7075-T651 chips and workpieces after a high-speed orthogonal machining. The results showed a decreased of the surface hardness after the machining process.

Rashad et al. in 2006 studied the effect of heat treatment conditions on the surface roughness of 7116 structural aluminium alloy during a turning process. The specimens were prepared by casting to attain the required chemical composition, and then hot extruded to form bars. The results show that the material hardness has a pronounced effect on the formation of built-up edge (BUE) for the material under investigation.

In 2009, Derakhshan conducted and experimental investigation in order to analyze the effect of the workpiece hardness and the cutting speed on the surface roughness when hard turning AISI 4140 with CBN tools. His results showed that when the turning operation a thermal softening was reached in cutting area (between tool edge and surface of workpiece) that made easier the plastic deformation for chips. Also he found that the hard particles in workpieces effect on tool wear producing an increase on the surface roughness.

- **Influence of cutting fluid on tool wear and surface roughness**

Due to the fact that coolants or cutting fluids are dangerous for the environment and human health, the movement towards green manufacturing cutting operations will be one of the most important challenges in the near future.

Some investigations have been made regarding the influence of lubricants on tool wear and surface roughness, since the implementation of dry machining cannot be accomplished by simply turning off the cooling lubricant supply. The minimization of cutting fluid leads to economical benefits by way of saving lubricant costs and workpiece/tool/machine cleaning cycle time. The concept of minimum quantity lubrication (MQL) has been suggested since a decade ago as a means of addressing

the issues of environmental intrusiveness and occupational hazards associated with the airborne cutting fluid particles.

In 2004, Weinert et al. concluded that the reduction of cooling lubricants in modern cutting technologies of dry machining and MQL (Minimum Quantity Lubricant) has led to significant advancements in machining technology. In 2005, Mativenga, evaluated coated tools on H13 tool steel during high speed milling using minimum-quantity lubricant (MQL) in order to reduce the thermal shock of flood coolant. Despite that the TiAlN + WC/C tools showed the best performance, in terms of wear it is not recommended for finishing operations since it affects the surface integrity of tool steel. It was also concluded that effective coatings led to a lower wear rate. Compared with the uncoated tool, effective coatings distinguish and broaden secondary wear, where nearly uniform wear rate can be assumed.

Research made by Kishawy et al. in 2005, described the results of application of different coolant strategies to high- speed milling of aluminium alloy A356 for the automotive industry; where the effect of flood coolant, dry cutting, and minimum quantity of lubricant (MQL) technologies on tool wear, surface roughness and cutting forces were analyzed.

In 2006, Dhar et al. studied the effect of MQL on tool wear and surface roughness when turning AISI 4304 steel. Their studies showed a significant reduction in tool wear rate and surface roughness when comparing it to a dry process, mainly due to a reduction in the cutting zone temperature which improved the chip–tool interaction and maintained the sharpness of the cutting edges.

In 2009, Braghini et al. studied the influence of cooling and lubrication on the tool wear mechanisms. The experiments were conducted on precipitation-hardened martensitic stainless after an end milling operation. The results showed that the tool wear mechanisms are directly influenced by the cooling and lubrication condition to which the tool is exposed, especially in interrupted cutting processes.

Also in 2009, Xavior et al. studied the influence of cutting fluids on tool wear and surface roughness during turning of AISI 304 with carbide tool. They selected

coconut oil as one of the cutting fluids due to its thermal and oxidative stability which are comparable to other vegetable-based cutting fluids used in the metal cutting industry. The results show that the coconut oil reduced the tool wear and improved the surface roughness.

- **Influence of tool path on tool wear and surface roughness**

Regarding the influence of tool path on tool wear and surface roughness, the research made by Diniz and Filho, in 1999**,** demonstrated that the relative positions of tool and workpiece have a strong influence on flank wear and, consequently, on tool life and surface finish of the workpiece. Also they showed that as the distance between the end of the cutter diameter and the beginning of the workpiece is increased, the flank wear value increases throughout the tool life. Their studies were conducted on AISI 1045 carbon steel during a conventional milling process.

In 2000, Ng et al. studied the influence of the direction of cut when milling Inconel 718. The coating performance of the tool during the process was also studied. They concluded that horizontal downwards cutter orientation generated the longest length of cut. In addition workpiece surface improved, primarily due to a low specific force and absence of vibration. Regarding coating of the tool, they concluded that TiAlN performed better than CrN coating.

Toh, in 2003, dedicated his effort studying the influence of path strategies on tool life and wear. He studied the influence of three different cutter paths (raster, single direction raster and offset) on tool life and tool wear during rough high-speed milling of hardened AISI H13 tool steel. He concluded that the tool life in terms of length of cut was higher when using a raster strategy. Also depth of cut notch wear was observed at all axial depth of cut employed, regardless of the cutter path strategy used. The same year (2003) he presented other results when studying the influence of the cutter path strategies on the surface topography of H13 hardened hot work tool steel, when high-speed rough milling was employed. He concluded that raster strategy in general gave lower workpiece surface roughness values compared with single-direction raster down milling at all axial depths of cut employed.

Vivancos et al. in 2004, presented a mathematical model of surface roughness prediction in HSM of hardened steels for injection moulds using factorial designs of experiments combined with techniques of regression. They concluded that climbing machining leads to better surface finish compared to conventional machining and in both cases, the radial depth of cut is the most affecting parameter. Also they showed that it is possible to obtain surface values corresponding to the ones obtained with grinding processes when using high-speed machining process.

Later, in 2005, Toh studied the design, evaluation and optimization of cutter path strategies when HSM mould and die materials. He concluded that the number of cutting levels and the cutter path strategies adopted on each level has a significant effect on machining time. Also he demonstrated that although flat end mills are superior to ball nose end mills in terms of metal removal rate and production of a low work-piece surface roughness on a plane surface, the nature of the die/mould cavities restricts the use of a flat end mill for finishing.

In 2009, de Oliveira et al. studied the wear mechanisms of tools used in semi-finishing operations of hardened steels for dies and molds. Several milling experiments were carried out to cut AISI H13 using a high-speed milling process. The results show that the inclination of the machined surface strongly influences tool life and tool wear. At the beginning of tool life, the wear was caused mainly by abrasion on the flank face and diffusion and attrition on the rake face. At the end of tool life, the mechanisms were adhesions and microchipping at the cutting edge.

- **Influence of tool wear on workpiece surface integrity**

Surface quality and integrity of machined surfaces are affected among others by metallurgical changes, microhardness alterations and residual stresses and the factors that affect the surface texture in a face milling process are as follows:

- Selection of cutter geometry.
- The accuracy of grinding of the selected angle of the cutter teeth.
- The setting of the teeth relative to the cutter body.
- The alignment of the machine spindle to the worktable.

Relatively little research has been conducted in an attempt to predict the surface finish from the process parameters. This is the main reason why relatively spare data on surface integrity (SI) following HSM can be reviewed, compared to the large number of papers available on SI for turning processes.

Experiments made by Che-Haron in 2001 showed that surface finish tends to become rougher toward the end of tool life concluding that this result was probably due to the deformation of the flank face or adherence of the workpiece material at the tool nose. Regarding changes in microhardness some differences were found when comparing the initial cut to the final cut and when cutting under dry conditions a thin layer of disturbed or plastically deformed layer was formed immediately underneath the machined surface. These results were obtained when turning titanium alloy.

In 2002, Axinte, presented an empirical model for surface integrity of hardened AISI H13 hot work tool steel, when HSM using solid carbide ball nose end mill coated with TiAlN. The experiments showed that no white layers or other microstructural alteration were observed during the process and this is possible due to the low values of cutting speed used during the experiments (200-300 m/min).

Other research such as Medicus et al. in 2001, conducted some work oriented to tool wear and surface finish in HSM of aluminium bronze. In their work they demonstrate the possibility of using high speed machining with tungsten carbide tooling in order to significantly reduce machining times and minimize or eliminate hand polishing and grinding.

Experiments conducted by Saï, in 2005, intended to optimize the cutting parameters to minimize surface roughness in up-face milling. A mathematical model was developed for roughness and cutting parameter calculation. The experiments revealed that at low cutting speed a poor surface quality was obtained, but on the other hand, a high cutting speed resulted in more roughness due to vibration. Also he concluded that if the cutting speed is limited by the maximum speed of machine spindle, the tool life, the production time or production cost, an optimal value of the feed can be used to minimize the surface roughness.

Very little work has been reported on phase transformation and microstructure of the ASB (Adiabatic Shear bands) and white layers and between these works, investigations done by Chunzheng in 2005, included the studied of the ASB and white layers induced during high speed cutting of high strength low alloy steel, after a turning process.

Previous studies have found that ASBs and white layers are similar in appearance, and moreover the white layers seem to be branches of the ASBs, but they are formed due to different mechanisms. The white shear bands result from the adiabatic shear development, whereas the white layers mainly occur due to the intense friction between the bottom of the chip and the rake surface of the tool. The white layers can be found in many material removal processes such as turning, grinding, etc.

Also, in 2005, Poulachon et al. studied the appearance of white layers and the associated effects of cutting parameters at varying tool-wear rates. The result showed that the thickness of these layers depends on the nature of the microstructure of the workpiece material.

The machining technology of aluminium alloy surfaces with a good surface finish and edge finishing is very important and required in many industries. In 2001, Balkrishna, studied the high-speed face milling process of 7075-T6 aluminium in terms of cutting forces, chip morphology, and quality of the finished surface with two commonly used cutting tool materials, i.e., carbide and diamond. They concluded that surface roughness improved with cutting speed up to 1524 m/min, beyond which it showed degradation and that an increase of depth of cut shows a slightly deterioration of the workpiece surface roughness.

Experiments made by Kim, in 1997, revealed the possibility of machining a mirror-like aluminium alloy without built-up edges and burrs using the designed diamond end mill at HSM. Experiments were done on aluminium alloy, A1-2024 where kerosene was used as a cutting fluid, since it is one of the most popular coolants for mirror-like aluminium machining. They concluded that overall, surface roughness increased as the axial depth of cut was increased above 0.5 mm, that the

radial depth of cut does not influence surface roughness and regarding the influence of the feed per tooth on the surface roughness shows that an increase on the feed per tooth causes an increase on the surface roughness, but in this case the rate of increase is smaller than in the case of the axial depth of cut.

Aluminium used in the field of aviation and die/mould production is required to have a very precise machined surface. However, the machining of aluminium using conventional tools at conventional cutting speeds shortens the tool life and has an adverse effect on the surface quality and edge quality, because of the formation of built-up edges and burrs. Therefore, aluminium parts require deburring and finishing processes such as polishing after cutting. Thus the machining of a ductile material such as aluminium occurs at a low cutting temperature at high speed, which can improve surface accuracy and surface roughness by restraining the formation of built-up edges, (Kim, 1997).

In 2006 Babur et al. developed a statistical model for surface roughness estimation on AISI 1040 during a high-speed flat end milling process under wet cutting conditions, using machining variables such as spindle speed, feed rate, depth of cut, and step over. First- and second order models were developed using experimental results of a rotatable central composite design, and assessed by means of various statistical tests.

In 2009 Ginting et al. studied the machined surface integrity of titanium alloy under the dry milling process. The surface roughness, the lay, defects; microhardness and microstructure alterations were analyzed. The result show that the CVD-coated carbide tool fails to produce a better Ra value compared to the uncoated tool. The lay is found to be dependent on cutting speed and feed speed directions. Microhardness is altered down beneath the machined surface where a soft subsurface caused by thermal softening in the ageing process was obtained.

- **Methods for surface roughness prediction**

With regard to surface roughness prediction, several studies have been made especially using computational methods such as: Artificial Neural Networks (ANN), Genetic Algorithms (GA) and Respond Surface Methodology (RSM).

In 1999, Tsai et al. developed an artificial neural network (ANN) model based on backpropagation to predict the output neuron-surface roughness Ra values. The studies were made in an end milling process showing that the proposed ANN surface recognition model has a high accuracy rate (96% – 99%) for predicting surface roughness under a variety of combinations of cutting conditions.

In 2001, Baek et al. analyzed the effects of the insert runout errors and the variation of the feedrate on the surface roughness and the dimensional accuracy on a face-milling operation using a surface roughness model. The validity of the developed model was proved through cutting experiments on AISI 1041.

Mansour et al. in 2002 developed a mathematical model for surface roughness prediction for the end milling EN32M (a semi-free cutting carbon casehardening steel with improved merchantability). The model has been developed, in terms of cutting speed, feedrate, and axial depth of cut. The effect of these cutting parameters on the surface roughness has been carried out using design of experiments and the response surface methodology (RSM). A first-order equation covering the speed range 30-35 m/min and a second-order generation equation covering the speed range 24-38 m/min were investigated in dry condition.

In 2003, Fang proposed an analytical model that takes into account the chip curling effect in milling operations. The results show that chip morphology and machining parameters, such as the chip up-curl radius, the chip thickness, and the tool-chip contact length, simultaneously change with varying undeformed chip thickness during each tooth cycle.

Continuing with numerical models, in 2004 Franco, et al. developed a model to predict milling surface profile and surface roughness when using round insert cutting tools. They incorporated a random value generation algorithm for tool axial and

radial errors. The same year, Wang, (2004), analyzed the influence of cutting conditions such as: cutting speed, feed, depth of cut, concavity and axial relief angles as well as tool geometry on the surface roughness when slot end milling AL2014-T6. The developed surface roughness models for both dry cutting and coolant conditions were built using the response surface methodology (RSM) and the experimental results showed that the dry-cut roughness was reduced by applying cutting fluid.

In 2005, Oktema et al. developed an effective methodology to determine the optimum cutting conditions leading to minimum surface roughness when end milling aluminium 7075-T6 mold surfaces. For this research, they coupled response surface methodology (RSM) with a genetic algorithm (GA).

In 2005 Sai et al. developed mathematical models for roughness and optimal cutting parameter calculation. The results show that lower cutting speeds give poor surface quality, due to the formation of a built-up edge. On the other hand, higher cutting speeds result in more roughness due to vibrations.

In 2006, Ryu et al. studied plane surface generation mechanism when flat end milling MC901 plastic material. The Surface topography parameters such as RMS deviation, skewness and kurtosis were used to evaluate the generated surface texture characteristics.

In 2007, Lin et al. established a relationship between the cutting variables and surface roughness in the process of high-speed machining. For this purpose, the finite element method and neural network were coupled to construct the surface roughness prediction model. The surface roughness obtained from the calculations is compared with the experimental results conducted in the laboratory and with other research studies. The simulation results show that feed rate is the most important cutting variable dominating the surface roughness.

Jesuthanam et al. in 2007, proposed the development of a novel hybrid Neural Network (NN) trained with Genetic Algorithm (GA) and Particle Swarm Optimization (PSO) for the prediction of surface roughness. The results showed that

the proposed hybrid neural network was found to be competent in terms of computational speed and efficiency over the neural network model.

In 2008, Franco et al. studied the influence of back cutting on the surface finish after face milling operations. Their model included static tool runouts and the height deviations that affect the surface marks provoked by back cutting. The theoretical predictions obtained by the developed model were compared with experimental values of surface roughness obtained after milling carbon steel when using round insert cutting tools.

In 2008 Surmann et al, studied the influence of tool vibrations on the surface roughness. A geometric model for predicting the surface roughness when tool vibrations are present is developed. The model enables one to predict and minimize the roughness and location error of the flank surface.

Finally, in 2009, Arizmendi et al. presented a model for surface topography when considering tool vibration. The experiments were conducted when end milling Al 7075. The results showed a good agreement between the model and the cutting results.

3.4 Research gaps:

Based on the literature reviewed above a number of research gaps have been identified and are outline below.

- To the authors knowledge there has been no studies reported on materials such as 416 martensitic stainless steel and Al 7075-T7351 related to tool wear, surface roughness, etc.
- In addition, there has been no reported studies on surface roughness prediction for HSM processes when using square inserts for 416 martensitic stainless steel and Al 7075-T7351.
- There are a number of limited studies on the development of a mathematical model for surface roughness prediction and 2D surface roughness profile

reproduction based on the Fourier series. The author believes that these studies show potential for further investigations.

3.5 Literature review analysis

Once the literature was reviewed and analyzed the importance of knowing specifics aspects related to the machining process as an important area in the manufacturing industries was understood.

As was observed, many researchers have focused their efforts on analyzing the influences of cutting parameters, tool wear, tool geometry, etc, on surface roughness and a smaller amount of researchers were focused on surface roughness prediction when using a face milling process especially using computational software. Between all the possible gaps that still need to be studied, the prediction of surface roughness when face milling with square inserts was selected. The literature survey indicates the absence of studies when using square geometry tools and this geometry allows producing shoulder cuts.

Also, the models will be validated with experiemtnal data obtained by HSM Al 7075-T7351 due to its importance in the aerospace industry where low weight and strength materials (such this alloy) are require for the fabrication of frames, fuselage, etc.

Taking advantage of this gap in knowledge, different models for the surface roughness prediction based on mathematical, computational and geometrical analysis will be developed when using a face milling process with square inserts, making a new contribution to the machining field especially in HSM.

The theoretical model based in geometric analysis is considered as a general expression since it can be extended for the application of any tool diameter with any number of teeth.

All the developed models must be validated with experimental data in order to assure their reliability. The experimental data that will be used for the models validation is obtained by face milling AL 7075-T7351 under MQL cutting conditions and cutting speeds up to 1600 m/min.

The basic knowledge of milling and the understood of the influence of the cutting parameters on tool wear, tool life, etc were obtained by milling 416 martensitic stainless steel bars.

These materials, 416 martensitic stainless steel and Al 7075-T7351 were selected for the different studies due to the absence of research in the area, despite their used in important industries such as the oil industries and the automotive and aerospace industries respectively.

The machining of stainless steel generally gives short tool lives, a limited metal removal rate, large cutting forces and high power consumption; this is due to their high temperature strength, rapid work hardening during machining and reactivity with most tool materials during high cutting speed. Regarding the use of aluminium alloy in fields such as aerospace and for injection moulds for polymer parts, very precise machined surfaces must be generated. However, the machining of aluminium using conventional tools and conventional cutting speeds shortens the tool life and has an adverse effect on the surface quality and edge quality, because of the formation of built-up edges and burrs. Therefore, aluminium parts require finishing processes that can be obtained with adequate tools and high speed machining.

Finally the Taguchi method was followed by Design of Experiment since, as observed from the literature review, the use of this method allows the opportunity to save time and cost in experiments due to the fact that it requires only a fraction of the full factorial combinations. Also by studying the Signal-to-Noise ratio, also developed by Taguchi, the optimal combination of cutting parameters to reach a specific surface roughness, as well as a decrease in tool wear can be obtained.

4 Martensitic stainless steel studies

4.1 Introduction

In machining processes, surface roughness is an important quality characteristic. The combination of cutting parameters, the tool wear, the machine-tool vibrations, etc, are a few of the variables that affect in a higher or less degree the roughness of a machined surface.

The lack of any specified surface finish in engineer drawings or in the achievement of a not adequate roughness can be the source of a final problem. Most decisions about which roughness should a material have depends on a combination of different factors such as: environment, temperature of operation, strength required, etc.

As previously stated in Chapter 3, tool wear is one of the variables that influence the surface roughness, so in order to achieve a required surface with a minimum production cost and maximum production rate, a decision regarding changing the tool before the machining of any new batch of parts must be made. If the tool is replaced before starting a new batch, it will be safe for the process, however the premature tool replacement incurs extra costs and increases machine downtime. If the tool is not changed, a continual use of a worn tool beyond its life limit can induce in-process tool failure and/or defective parts.

During the past years there has been extensive research and development regarding tool wear, tool life, surface roughness, etc and the results have provided lots of knowledge, Lin T, 2002, Ghani 2004, Abou-El-Hossein, 2005. However many gaps still need to be filled since depending on the material workpiece-tool combination a different result can be obtained.

The 416 Martensitic stainless steel is used in the fabrication of parts widely used in the oil and automotive industries. Some applications are; valve parts, pump shafts, automatic screw machined parts, motor shafts, washing machine components, bolts and nuts, studs and gears. However, despite its use, no research has been found related to this material, and the topic of this thesis. Also, the author recognises that 316SS is also widely used however this material has a machinability of approximately 40% less compared with the 416SS which has a machinability of 90% (www.quakerchem.com)

This chapter presents the research that has been performed to fill gaps identified in Chapter 3 and make a new contribution to knowledge, by studying the influence of cutting parameters on tool wear, tool life, material removal rate and surface roughness when face milling 416 stainless steel.

This chapter is divided into five (5) sections. The first four represent analysis of results and the last section summarizes and concludes the present work.

Section 4.2: Includes the influence of the cutting parameters on the tool life, the material removal rate and the tool wear, as well as the best combination of cutting parameters for a best tool performance.

Section 4.3: Includes an empirical expression for the tool wear prediction

Section 4.4: Includes a surface characterization analysis which includes surface roughness, microstructure and microhardness tests.

Section 4.5: Presents the analysis of the influence of the tool wear on the surface roughness.

Section 4.6: Includes the general conclusions obtained from all these studies.

Figure 4.1 shows a schematic overall description of the development of this study.

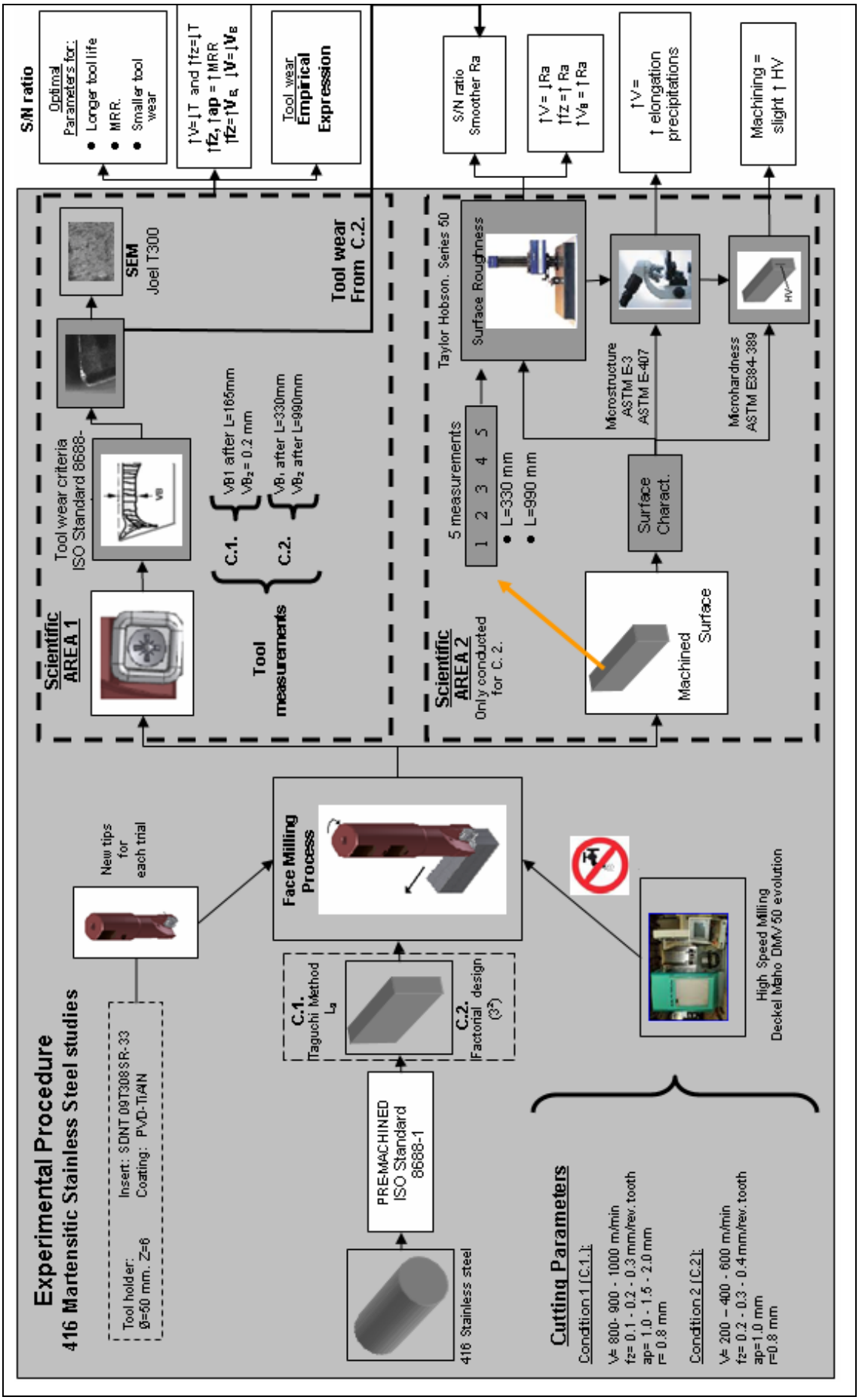

Figure 4.1- Schematic diagram of the different studies conducted on the 416 martensitic stainless steel.↑ increase, ↓ decrease

When analyzing Figure 4.1, it can be observed that the study is divided into two main areas, both sharing the milling process although under different cutting conditions and before going into a detail explanation of each of this area the starting point of them is explained first.

As observed in the diagram, the 416 martensitic stainless steel round bars were pre-machined into square bars following the suggestions made by the ISO Standard 8688-1, which is a specific standard for face milling operations.

The specimens were milled using a HSM, Deckel Maho 50 evolution CNC machine under a dry cutting condition. A tool shank with 6 teeth was used for the cutting process.

Two combinations of cutting parameters were selected. Condition 1 was conducted at high cutting speeds (800-900 and 1000 m/min), with different feed per tooth and axial depth of cut. Condition 2 was conducted at lower cutting speeds (200-400 and 600 m/min), different feed per tooth and a constant axial depth of cut. In both cases a constant value of tool nose radius r=0.8 mm was used.

The idea of selecting different combination of cutting parameters was to give knowledge regarding their influence on the tool wear. It must be highlighted that new inserts were used for each trial machined under different cutting condition.

Regarding the main areas of study, it can be observed that:

Scientific Area 1 corresponds to the study of the influence of the cutting parameters on the tool life, the material removal rate and the tool wear. The tool wear was measured on the insert that presented the highest wear when cutting under experiment 1 and 2, cutting conditions. The results of these studies concluded (after applying the Signal-to-Noise (S/N) ratio developed by Taguchi), which is the best combination of cutting parameters for a best tool performance, when using condition 1 cutting parameters.This study also allowed the development of an empirical expression for tool wear prediction. Tool wear results obtained from condition 2

cutting parameters were linked to the results of surface roughness obtained under the same conditions.

Scientific Area 2 corresponds to the surface characterization conducted on the 416 martensitic stainless steel machined surface. This study was only conducted for condition 2 cutting parameters. The surface characterization analysis included: surface roughness measurements, microhardness measurement and microstructure analysis. These studies gave information regarding the influence of the tool wear on the surface roughness as well as the influence of the cutting parameters on the machined surface microstructure and microhardness. Sections 4.2, 4.3, 4.4 and 4.5 present the detail explanation of each of the studies.

4.2 Scientific Area 1: Influence of the cutting parameters on the tool life, the material removal rate and the tool wear, and the selection of cutting parameters for a best tool performance.

As previously stated, martensitic 416 stainless steel bars, with the following geometry, ∅= 76.2 mm and L= 165 mm were used. These round bars were pre-machined into a square shape bar of 165 x 70 x 30 mm as suggested by the ISO Standard 8688-1. Table 4.1 shows the chemical composition and Table 4.2 shows the mechanical properties of this martensitic stainless steel. Figure 4.2 shows the final geometry of the bars used for the experiments and Figure 4.3 shows the original microstructure of the 416 stainless steel used for the study.

Table 4.1- Chemical Composition of 416 stainless steel

%C ± 0.01	%Cr ± 0.01	% Mn ± 0.01	% Si ± 0.01	%Mo ± 0.01
0.13	12.50	1.25	1.00	0.58

Table 4.2- Mechanical Properties of 416 stainless steel

Ultimate Strength (MPa)	510
Yield Strength (MPa)	274
Brinell Hardness*	270

* Load: 3000 Kg. Indentation $Ø_{ball}$: 10 mm

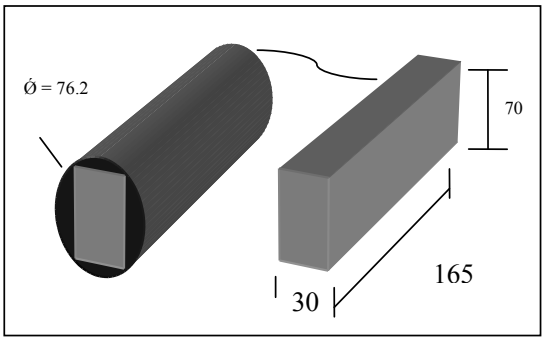

Figure 4.2- Shape and basic dimensions of the workpiece used for the experiments. (Units in mm)

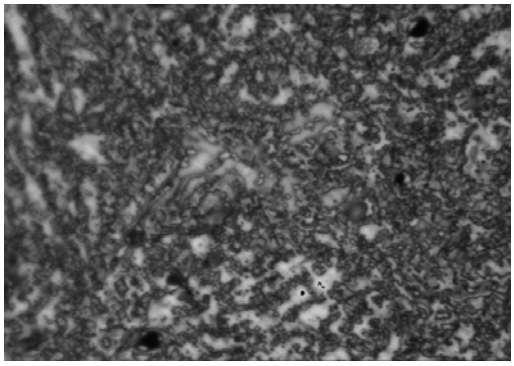

Figure 4.3- Original microstructure of the 416 stainless steel bar used in the experiments.

A cutting tool with a standard insert holder of diameter, $Ø_{Tool}$= 50 mm, and Z=6 (Z=number of teeth) was selected, with the following insert characteristic: SDNT 09T308SR-33, Grade HCN2235 (PVD-TiAlN coating). This type of insert is recommended for stainless steel cutting operations under dry cutting conditions. Figure 4.4 shows the geometry of the insert used for the study.

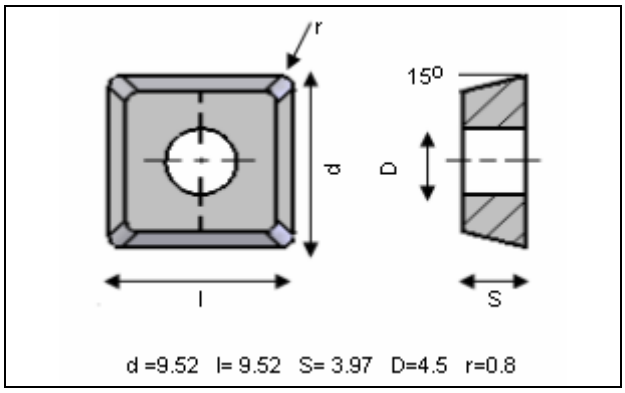

Figure 4.4- Geometry and dimensions of the insert used for the experiments. Units in mm.

A tool diameter of $Ø_{Tool}$= 50 mm was selected for the experiment in order to machine the whole width of the workpiece in just one single pass, since the tool diameter is bigger than the workpiece width ($Ø_{Tool}$= 50 mm > 30 mm).

This condition ($Ø_{Tool}$ > W), as well as a symmetric position, between the tool and the workpiece, will achieve a better performance of the tool (longer tool life), as suggested by Diniz and Filho (1999). Figure 4.5 shows a schematic of the cutting process.

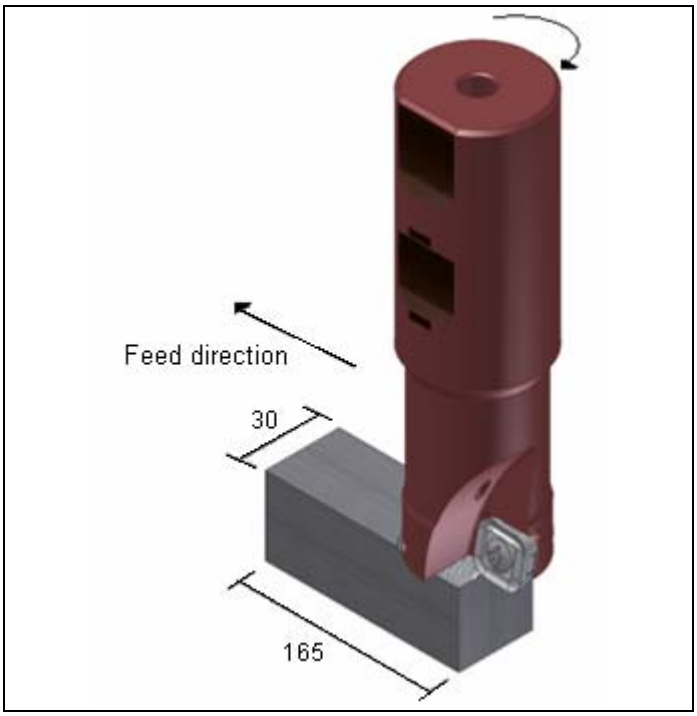

Figure 4.5- Scheme of the cutting process

The variables chosen for the study were the cutting speed, the feed per tooth and the axial depth of cut. Since from previous research, outlined in the literature review (Chapter 3), it was observed that these variables have the highest influence on tool life and on the surface roughness of the workpiece. Table 4.3 shows the values of the selected cutting parameters.

Table 4.3- Selected cutting parameters for Condition 1.

Level	V (m/min)	fz (mm/rev * tooth)	ap (mm)	r (mm)
Low (1)	800	0.1	1.0	0.8
Medium (2)	900	0.2	1.5	0.8
High (3)	1000	0.3	2.0	0.8

Although it is known that the cutting speed values selected for this experiment are much higher than the recommended from the tool supplier (V= 60-200 m/min), the intention of this selection is to investigate and validate the boundaries of application for this insert material and workpiece combination, representing a new contribution to knowledge.

For face milling operations a Deckel Maho, DMV 50 evolution, high speed vertical machine centre was used, with a maximum spindle speed of 18.000 rpm. All the tests were conducted under dry cutting conditions, using the cutting parameters showed in Table 4.3.

The Taguchi method was selected as Design of Experiment (DoE) since from previous research it was observed its advantage in reducing cost and time experiments (Lin, 1998 and 2002). Table 4.4 shows the L_9 orthogonal array for the four cutting parameters to be studied. The values 1 to 3 indicate the levels of the three cutting parameters as defined in Table 4.3.

Table 4.4- L_9 orthogonal array for the experiments with Condition 1.

Trial	V	fz	ap	r
1	1	1	1	1
2	1	2	2	1
3	1	3	3	1
4	2	1	2	1
5	2	2	3	1
6	2	3	1	1
7	3	1	3	1
8	3	2	1	1
9	3	3	2	1

The evaluation of tool performance was based on the tool life and the material removal rate, whereby a good performance was defined by achieving a longer tool life with a maximum amount of material removal rate.

The most commonly used criterion to identify tool life is tool flank wear and in order to define a correct tool deterioration criterion, the ISO Standard 8688-1 was followed. This standard is specific for face milling operations where different values of flank wear criteria are suggested. The maximum value of flank wear considered in this standard is VB=0.5 mm, but in order to reduce the time of experiments a limit value of tool flank wear of 0.2 mm was selected. This value represents the lowest numerical value of tool deterioration suggested by this standard. Once the insert reached this value, tool life has been reached; although if chipping or cracking was shown before a VB= 0.2 mm, then tool life will also be considered as over.

It must be highlighted that for all trials new inserts were used, in order secure tool wear and tool life results. Only the insert which presented the highest deterioration out of the six inserts was the one selected for the study.

The tool wear was measured twice during each trial and by using a NIKON 18724 optical microscope, following the tool wear criteria suggested by ISO Standard 8688-1.

The first measurement (VB_1) was performed after face milling 165 mm of length, which corresponds to the first pass and the second measurement (VB_2) when the tool flank wear land reached about 0.2 mm.

Figure 4.6 shows a schematic of the flank wear measurement.

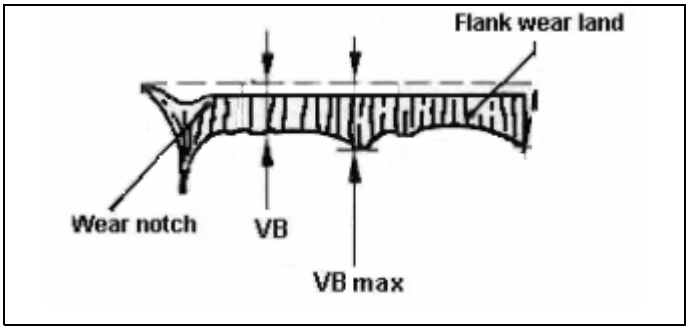

Figure 4.6- Schematic of tool flank wear measurement

In order to determine the effect of each cutting parameter on the tool life, material removal rate and surface roughness, the statistical measure of performance, called Signal-to-Noise ratio (S/N), developed by Taguchi, was applied. This measure also allowed the identification of the optimal combination of cutting parameters for a specific objective; which in the case study corresponds to a small tool wear for a longer tool life and a small value of surface roughness.

For this analysis, the S/N ratio, larger-the-best formula was applied, for the tool life and the material removal rate since they both need to be maximized and the S/N ratio smaller-the-best formula for the tool wear and the surface roughness studies.

4.2.1 Results and analysis of results

Once the experiments were concluded the following results were obtained. To present a better understanding, the results were divided into three (3) sub-sections:

- Influence of the cutting parameters on the tool life.
- Influence of the cutting parameters on the material removal rate.
- Influence of the cutting parameters on the tool wear.

- **Influence of the cutting parameters on the tool life**

In order to analyze how a combination of cutting speed, feed per tooth and axial depth of cut affects tool life, the S/N ratio for tool life for each trial after the first pass (T_1) and after the tool has reached the tool life criterion (T_2) was calculated. The results are shown in Table 4.5 and are illustrated in Figure 4.7.

Table 4.5- Tool life and Signal-to-Noise (S/N) ratio, for tool life for each trial, after the first pass and once reaching the tool life criterion.

Trial	T_1 (sec)	T_2 (sec)	S/N T_1 *	S/N T_2 **
1	4.20	**130.8**	12.46	42.33
2	2.16	60.0	6.69	35.56
3	1.38	31.2	2.80	29.88
4	3.78	67.8	1.55	36.62
5	1.86	24.6	5.39	27.82
6	1.26	21.0	2.01	26.44
7	3.36	30.6	10.53	29.71
8	1.68	18.6	4.51	25.39
9	**1.14**	4.20	1.14	12.46

* The larger-the-best S/N ratio = $-10\log(1/T_1^2)$ ** The larger-the-best S/N ratio = $-10\log(1/T_2^2)$

- See Appendix A for calculus example

As it can be observed from Table 4.5, the longest tool life achieved with these cutting parameters (condition 1) is 130.8 sec and the shortest tool life is 4.20 sec. Even though these values do not represent ideal tool life figures, and are not what industry may try to use, they allow us to understand the trend of the behaviour of tool wear for this material, under dry milling conditions, as well as to establish the limits of realistic cutting data for this tool-workpiece combination. Also it is observed an increased of around 900% in the tool life by using low combination of cutting parameters (trial 1) when compared to value of tool life obtained when using high combination of cutting parameters (trial 9).

Figure 4.7 shows the S/N ratio for the tool life for each of the trials, after the first pass (T_1) and when reaching the tool life criterion of VB=0.2 mm (T_2).

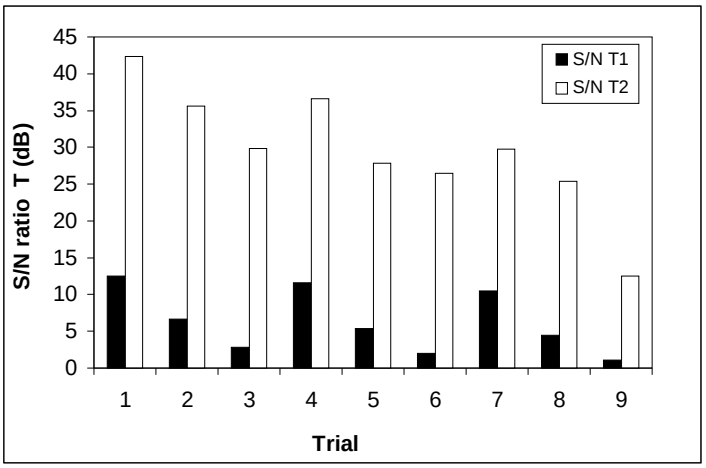

Figure 4.7- Signal-to-Noise (S/N) ratio for the tool life for each of the trials, after the first pass (T_1) and after reaching tool life criterion (T_2)

As observed in Figure 4.7, the higher the value of the S/N ratio, the bigger the tool life achieved. From this fact, trials 1, 4 and 7 gave the best results in terms of the S/N ratio, when cutting a length of 165 mm and when reaching the tool life criterion.

Each of these trials was conducted under different combinations of cutting speed, feed per tooth and axial depth of cut. Trial 1 gave the best result for a longer tool life, using a combination of the lowest levels of the selected cutting parameters studied (V=800 m/min, fz= 0.1 mm/rev * tooth and ap= 1.0 mm). These experiments reflect the expected impact of lower temperatures and lower levels of cutting forces in extending the tool life.

In order to analyze the individual influence of each cutting parameter on tool life, the S/N ratio for each of the cutting parameters under study was calculated, giving the results shown in Table 4.6 and illustrated in Figure 4.8.

Table 4.6- S/N ratio for the tool life, for each of the cutting parameters, after the first pass (T_1) and after reaching the tool life criterion (T_2).

		S/N ratio for T_1	S/N ratio for T_2
V (m/min)	800	7.32*	35.93
	900	6.32	30.30
	1000	5.39	22.52
fz (mm/rev*tooth)	0.1	11.51	36.22**
	0.2	5.53	29.59
	0.3	1.98	22.93
ap (mm)	1.0	6.33	31.39
	1.5	6.46	28.22
	2.0	6.24	29.14

* [S/N T_1 (1) + S/N T_1 (trial 2) + S/N T_1 (trial 3)]/3

** [S/N T_2 (trial 1) + S/N T_2 (trial 4) + S/N T_2 (trial 7)]/3

- See Appendix A for calculus example

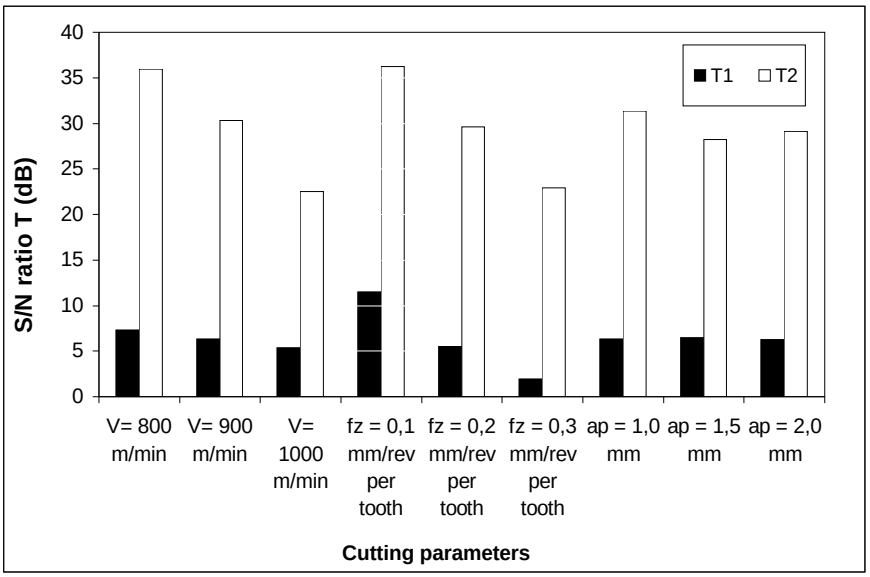

Figure 4.8- S/N ratio for tool life for each cutting parameter.

As observed in Figure 4.8, tool life decreases when increasing the cutting speed (smaller S/N ratio). Also, it can be observed that when cutting the first 165 mm length of cut, it seems that the cutting speed has a relatively small influence on tool life (T_1), but once the tool has been cutting for more than 1 pass (>165 mm), it is more noticeable that a longer tool life (T_2) will be obtained when using a low cutting speed.

This result is due to the fact that a high cutting speed increases the temperature in the cutting edge of the tool, causing heat related wear mechanisms, especially during dry machining conditions. This result is in agreement with previous research, (Ghani, 2004).

Regarding the influence of the feed per tooth on the tool life, it can be observed that, as the feed per tooth is increased, the tool life decreases for both cases, when cutting a length of 165 mm and when reaching the tool life criterion. This result is probably due to the fact that a higher level of cutting force is needed in order to remove a bigger amount of material.

With respect to the influence of the axial depth of cut on the tool life, it seems that this parameter does not have much influence on the tool life at the beginning of the cutting process (L= 165 mm) and a definite pattern could not be obtained when the tool life reached the tool life criterion; although it can be observed that the variation of the S/N ratio for tool life, when using an axial depth of cut higher than 1.0 mm is negligible. This is in agreement with the research made by Tsann-Rong, (2002).

When comparing the influence of each cutting parameter on the tool life, specially when reaching the tool life criterion (T_2), it can be observed that an increase in cutting speed of 25% (from 800 m/min to 1000 m/min) causes a more noticeable reduction of the tool life (around 26%), when compared with the feed per tooth variable, where an increase of 100% of this variable (from 0.1 mm/rev*tooth to 0.2 mm/rev*tooth) produced a decrease of around 50 % of the tool life. These results agree with the research made by Abou-El-Hossein, (2005).

From these results, it appears that the optimal combination of cutting parameters in order to obtain a longer tool life is: V=800 m/min, fz= 0.1 mm/rev*tooth and ap= 1.0 mm.

- **Influence of the cutting parameters on the material removal rate**

Since productivity or volume of material removed per unit time is a very important indicator for tool performance and the metal cutting operation, this factor was also calculated.

The material removal rate results and S/N ratio results, for the material removal rate, after the first pass and once reaching the tool life criterion are shown in Table 4.7 and illustrated in Figure 4.9.

Table 4.7- Material removal rate (MRR) and S/N ratio for MRR for each trial, after the first pass and once reaching the tool flank wear of 0.2mm

Trial	MRR_1 (cm^3/min)	MRR_2 (cm^3/min)	S/N MRR_1*	S/N MRR_2**
1	70.71	70.39	36.99	36.95
2	208.97	207.90	46.40	46.36
3	422.11	418.85	52.51	52.44
4	118.81	118.27	41.50	41.46
5	316.62	313.90	50.01	49.94
6	237.46	240.43	47.52	47.62
7	175.90	174.71	44.91	44.85
8	175.87	175.65	44.90	44.89
9	399.11	424.29	52.02	52.55

* The larger-the-best S/N ratio = -10log (1/ MRR_1^2)
** The larger-the-best S/N ratio = -10log (1/ MRR_2^2)
- See Appendix A for calculus example

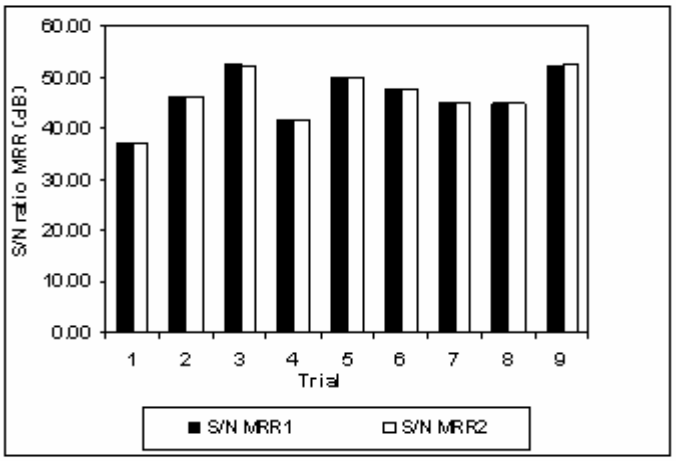

Figure 4.9- S/N ratio for material removal rate Signal-to-Noise (S/N) ratio for each trial**.**

When analyzing Figure 4.8, it can be observed that for both cases (after the first pass and after reaching the tool life criterion) trials 3 and 9 seem to give the better results. Also, it is observed that an increase of 350% on material removal was obtained by using the highest combination of cutting parameters (trial 9 with 399.11 cm^3/min) when compared with the lowest combination of cutting paramenters (trial 1 with (70.71 cm^3/min).In addition, the S/N ratio for each individual cutting parameter was calculated and the results are shown in Table 4.8 and illustrated in Figure 4.10.

Table 4.8- S/N ratio for material removal rate, for each cutting parameter after the first pass and after reaching the tool life criterion.

		S/N ratio for MRR_1	**S/N ratio for MRR_2**
V (m/min)	800	45.30	45.25
	900	46.34	46.34
	1000	47.28	47.43
fz (mm/rev*tooth)	0.1	41.13	41.08
	0.2	47.11	47.06
	0.3	50.68	50.87
ap (mm)	1.0	43.13	43.15
	1.5	46.64	46.79
	2.0	49.14	49.07

* [$S/NMRR_1$ (1) + $S/NMRR_1$ (trial 2) + S/N MRR_1 (trial 3)] /3

** [$S/NMRR_2$ (trial 1) + $S/NMRR_2$ (trial 4) + $S/NMRR_2$ (trial 7)]/3

- See Appendix A for calculus example

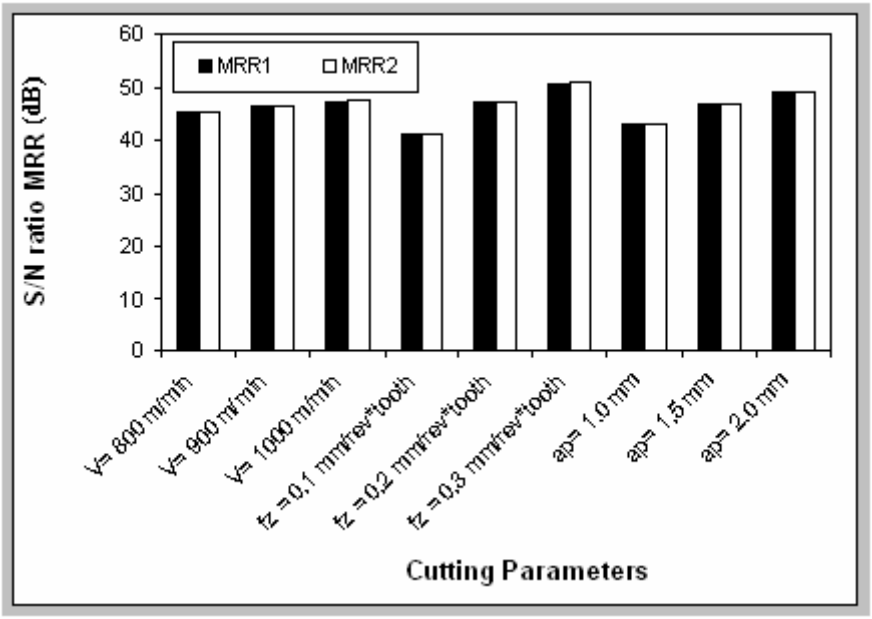

Figure 4.10- Material removal rate Signal-to-Noise (S/N) ratio for each cutting parameter.

In Figure 4.9 it can be observed that the cutting speed has a small influence on the material removal rate for the three levels of cutting speed being studied. Also the variation on S/N ratio for the material removal rate is only 4% when increasing the cutting speed by 25%. Finally, the feed per tooth and the axial depth of cut are the variables that have the most direct influence on the material removal rate.

These results were expected, since these parameters determine the size of the chip. Both of these parameters have practically the same influence on material removal rate since when increasing “fz” and “ap” by 100% each, in separate experiments, the corresponding increase in material removal was 14.5% and 13.7% respectively.

From these results, the optimal combination of cutting parameters for a maximum material removal rate was found to be: V= 1000 m/min, fz=0.3 mm/rev*tooth and ap=2.0 mm. The combination of these variables will be considered as the optimal combination for a good performance of metal cutting operation, yielding a volume of material removal rate of 494.56 cm^3/min.

Table 4.9 shows the best combination of variables for the longest tool life and for maximum volume of material removal rate.

Table 4.9- Optimal cutting condition for a maximum tool life and a maximum material removal rate when face milling 416 SS.

V (m/min)	fz (mm/rev x tooth)	ap (mm)	T (sec)	MRR (cm^3/min)
800	0.1	1	130.8	70.71
1000	0.3	2	4.2	494.56

When analyzing Table 4.9, it can be observed that the cutting conditions that produced the maximum tool life yielded a material removal rate (MRR) which is only 14.29% of the maximum value achieved, and the main corresponding benefit is in the rapid improvement of the tool life from 4.2 seconds to 130.8 seconds. Clearly the combination of machining variables must be selected on the basis of how tool performance is going to be judged in each case, either by achieving a longer tool life or by obtaining a maximum amount of material removal rate.

- **Influence of the cutting parameters on the tool wear**

The following results of tool wear were obtained once face milling the 416 martensitic stainless steel bars, under the conditions shown in Table 4.3 and 4.4.

Figure 4.11, shows an insert's new flank edge and Table 4.10 shows the tool flank wear values obtained after the first pass, which correspond to a cutting length of 165 mm.

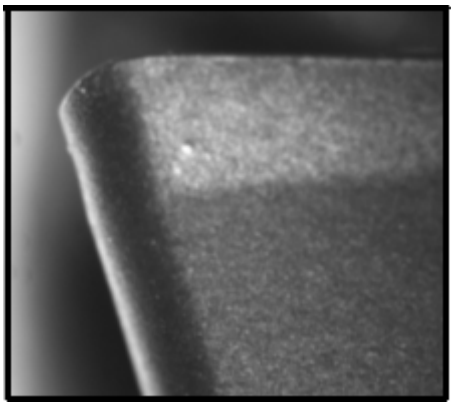

Figure 4.11- Detail of the insert's new edge

Table 4.10- Tool flank wear value after the first single pass for each trial.

Trial	V (m/min)	fz (mm/rev * tooth)	ap (mm)	r (mm)	VB_1 (mm)
1	800	0.1	1.0	0.8	0.04
2	800	0.2	1.5	0.8	0.04
3	800	0.3	2.0	0.8	0.06
4	900	0.1	1.5	0.8	0.05
5	900	0.2	2.0	0.8	0.06
6	900	0.3	1.0	0.8	0.08
7	1000	0.1	2.0	0.8	0.08
8	1000	0.2	1.0	0.8	0.09
9	1000	0.3	1.5	0.8	0.09

The tool's flank wear pictures for the first pass (L= 165 mm) for each trial are not included since the tool flank wear value obtained for each studied condition was too small.

The Figure 4.12 shows a picture of flank wear insert value of about VB= 0.2 mm when face milling under different cutting conditions.

Trial	**1**	**2**	**3**
	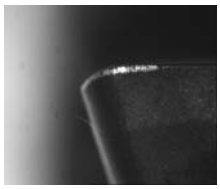	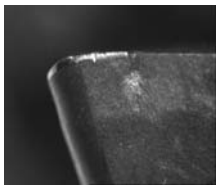	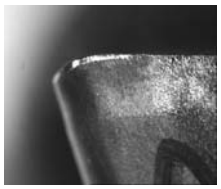
VB_2	0.21	0.19	0.20
Trial	**4**	**5**	**6**
	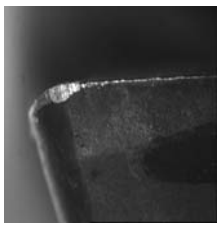	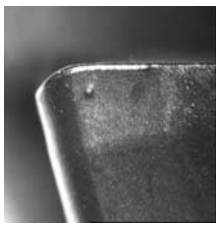	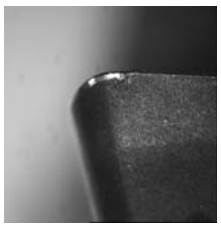
VB_2	0.24	0.19	0.20
Trial	**7**	**8**	**9**
	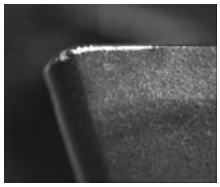	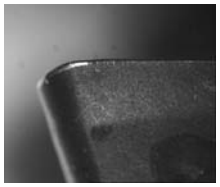	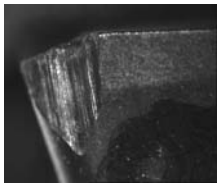
VB_2	0.19	0.19	chipping

Figure 4.12- Picture and value of tool flank wear for each trial after reaching about VB_2=0.2mm

When analyzing Figure 4.12, it can be observed that in general, all the tools failed due to flank wear except for the tool corresponding to trial 9. In trial 9, tool flank chipping was observed before tool flank wear. This occurred at the highest values of cutting conditions (V=1000 m/min, fz=0.3 mm/rev*tooth and ap=1.5 m). A 10% increase in cutting speed (800-900 or 900-1000 m/min) represents a significant reduction in tool life and indeed in tool wear from 31.2 sec for trial 3, to 21.0 sec in trial 6 to 4.2 sec in trial 9. This shows that cutting speed is the primary parameter affecting the tool wear. In addition, the trials show that the main mechanism of tool wear was “abrasion”. These results are in line with the research made by Lin (1998).

In order to complement these results, scanning electron graphs were obtained using a Joel, T300 Scanning Electron Microscope (SEM). Figure 4.12 shows the pictures of different stages of an insert used to cut under specific cutting conditions,

where Figure 4.13 c, shows the abrasion mechanism with a more detail. In this case the development of grooves and ridges in the direction of the chip sliding against the tool is observed.

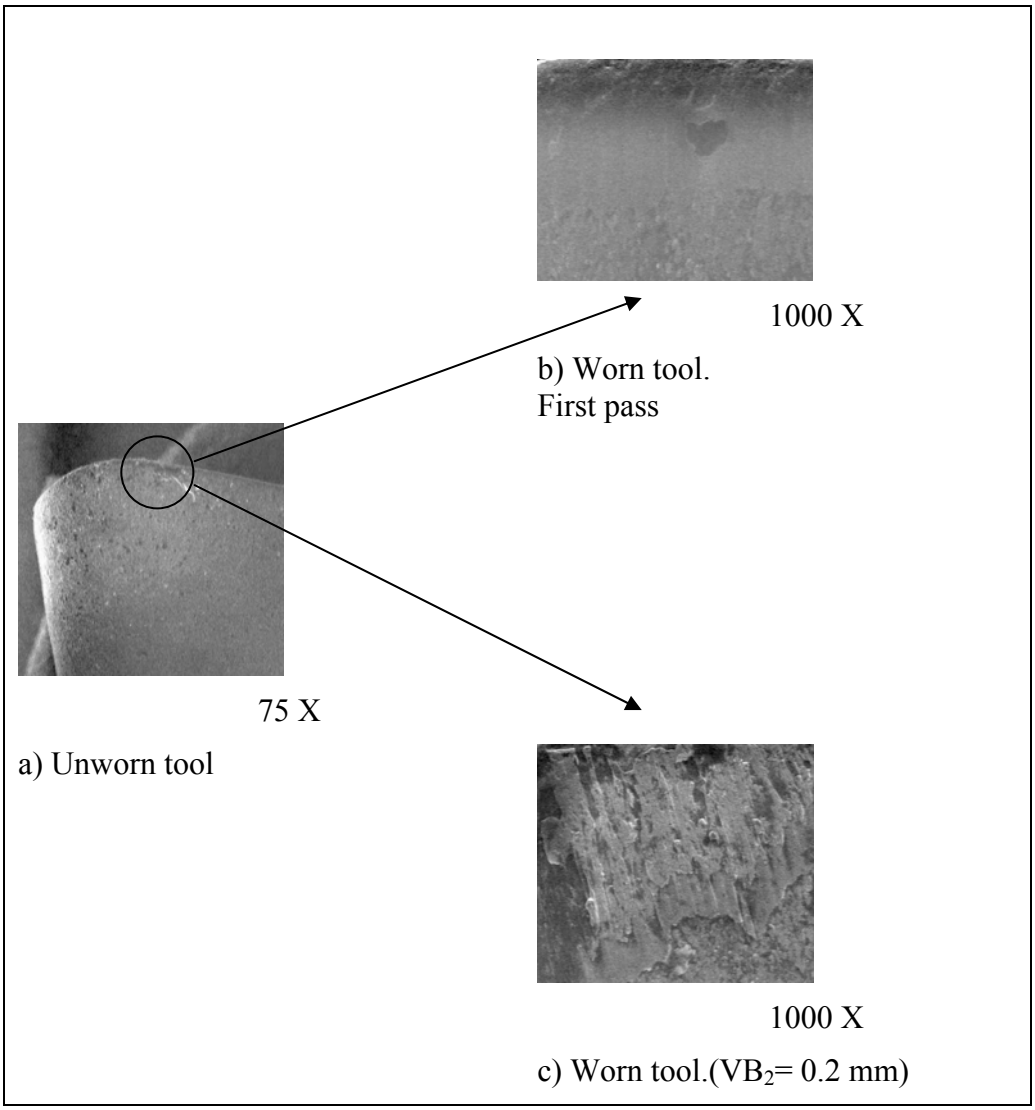

Figure 4.13- Electro Scan Microscope pictures of the insert used in trial 4, V=900 m/min, fz=0.1 mm/rev * tooth, ap=1.5 mm. a) Unworn tool, b) Worn tool after the first pass and c) worn tool when reaching VB_2=0.2 mm.

From the tool behaviour for trial 9 conditions, it can be observed that, the tool failed because it chipped before reaching VB=0.2 mm. This is probably due to the fact that as a higher speed was used for this trial, a higher temperature was generated. Also, the fluctuations of temperature due to the characteristic behaviour of the milling process, (periodic tool movement, *in and out,* of the workpiece) caused a thermal cycling which in combination with thermal shocks were responsible for the

thermal-fatigue and eventual tool failure. This result agrees with research made by Ghani, (2004).

In order to analyze the influence of each cutting parameter on tool wear the S/N ratio for the tool flank wear, after the first pass (L=165 mm) was calculated. This study also allows the selection of the optimal combination of parameters for a better tool performance. The influence of each cutting parameter on flank wear is shown in Table 4.11 and illustrated in Figure 4.14.

Table 4.11- Signal-to-Noise (S/N) ratio for tool wear for each cutting parameter after the first pass

		S/N ratio for VB_1
V (m/min)	800	26.78*
	900	24.13
	1000	21.26
fz (mm/rev*tooth)	0.1	25.31**
	0.2	24.44
	0.3	22.43
ap (mm)	1.0	23.60
	1.5	24.96
	2.0	23.60

* [S/N ratio VB1 (trial 1) + S/N ratio VB1 (trial 2) + S/N ratio VB1 (trial 3)]/3
** [S/N ratio VB1 (trial 1) + S/N ratio VB1 (trial 4) + S/N ratio VB1 (trial 7)]/3

- See Appendix A for calculus example

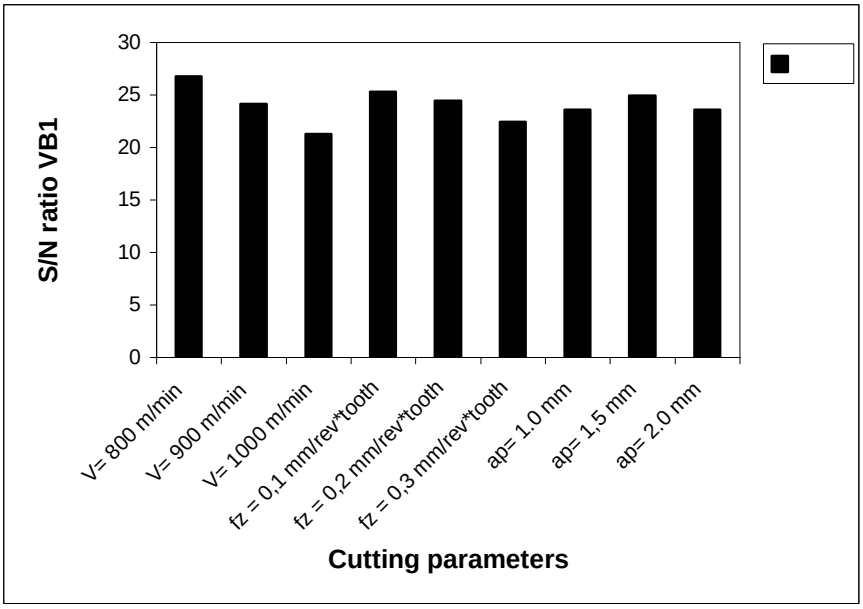

Figure 4.14- Signal-to-Noise (S/N) ratio for VB_1 for each cutting parameter after the first pass

When analyzing Figure 4.14, it can be observed that the tool flank wear increases when increasing the cutting speed (smaller S/N ratio). This result is in agreement with previous results such as the ones made by Elbestawi (1997), Choundhury (2004) and Abou-El Hossein (2005), where it was concluded that as cutting speed increases the increase in temperature is higher in the cutting edge, increasing the tool wear especially when machining under a dry cutting condition, such as in these experiments.

Figure 4.14 also shows the influence of the feed per tooth on the tool flank wear. In this figure it can be observed that tool flank wear increases when increasing the feed per tooth. This result is probably due to the fact that, as the feed increases, the contact area between the chip and the tool also increases, generating a higher friction on the tool, which is equivalent to a higher temperature in this area. This result is in agreement with previous research, (Ghani, 2004).

Other researchers, such as Abou-El-Hossein, (2005); found a different result regarding the influence of feed per tooth on tool flank wear. Their results showed that the tool flank wear increases when using low values of feed per tooth. This is probably due to the fact that their experiments were conducted at a low cutting speed (150-260 m/min), instead of higher cutting speeds such as the ones used in this research (800-1000 m/min) and by Ghani, (2004).

Regarding the influence of the axial depth of cut on the tool flank wear, a definite pattern was not obtained, although it can be observed that the tool flank is smaller when using ap= 1.5 mm. This result is probably due to the fact that as the axial depth of cut increases; the size of the chip also increases, causing a larger contact area between the chip and the tool.

To conclude it can be observed that lower values of tool flank wear are obtained when using low values of cutting speed and low values of feed per tooth. With these results it seems that the cutting speed is the variable that has most influence on the tool flank wear followed by the feed per tooth and then the axial depth of cut.

Once analyzing the influence of each cutting parameter on the tool flank wear, in order to obtain a better tool performance which will be for this case of study, a small tool flank wear for a longer tool life, the optimal combination of cutting parameters is: V=800 m/min, fz=0.1 mm/rev * tooth, ap= 1.5 mm.

4.3 Empirical expression for tool wears prediction.

By using the tool wear data obtained from the milling process results, an empirical analytical expression of tool flank wear for face milling 416 SS is developed. In this case, multiple regression analysis (MRA) is applied and different adjustments such as: lineal, exponential, polynomial and exponential were evaluated. The selection of the model is based on the one that fulfilled all the statistical variables, such as: 1) high values of the multiple correlation coefficients R^2 and R^2_{adjust}, 2) adequate residual distribution and 3) a linear tendency of the residuals against a normal distribution. (Lipson, 1973 and Freund, 1994). From these facts, the model that fulfilled all the statistical variables is the potential model which is presented in equation 4.1.

$$VB_P = 10^{-8.62} \cdot V^{2.79} \cdot fz^{0.28} \cdot ap^{0.04} \cdot t^{0.42} \qquad (4.1)$$

R^2: 96 % R^2_{adjust}: 95 %

where:

VB_P: Predicted tool flank wear (mm)
V: Cutting speed (m/min)
fz: Feed per tooth (mm/rev * tooth)
ap: Axial depth of cut (mm)
t: Cutting time (min)

From the relationship shown in equation 4.1, it can be observed that, once again the cutting speed has the highest influence on the tool flank wear, followed by the cutting time and then the feed per tooth. Also it can be observed that the axial depth of cut has very small influence on tool flank wear.

In order to evaluate the efficiency and the ability of the developed empirical expression to predict the tool flank wear (VB_P), the $\%RE_P$ (Relative Error percentage) criterion is used, as it is defined in equation (4.2).

$$\%RE_P = \left| \frac{VB - VB_P}{VB} \right| \cdot 100 \tag{4.2}$$

where:

$\%RE_P$: Relative Error in % between predicted and experimental values

VB: Experimental tool flank wear (mm)

VB_P: Predicted tool flank wear obtained by using eq 4.1 (mm)

Table 4.12 shows the experimental value of tool wear obtained after the first pass and the predicted value obtained from equation 4.1, also the $\%RE_P$ is reported.

Table 4.12- Experimental, predicted and $\%RE_P$ for tool flank wear after cutting the first pass for each trial.

Trial	V (m/min)	fz (mm/rev * tooth)	ap (mm)	VB_1 (mm)	VB_P (mm)	RE_P (%)
1	800	0.1	1.0	0.04	0.047	16.2
2	800	0.2	1.5	0.04	0.043	7.2
3	800	0.3	2.0	0.05	0.041	18.1
4	900	0.1	1.5	0.05	0.062	24.9
5	900	0.2	2.0	0.06	0.057	4.6
6	900	0.3	1.0	0.08	0.053	24.7
7	1000	0.1	2.0	0.07	0.081	1.4
8	1000	0.2	1.0	0.09	0.072	20.1
9	1000	0.3	1.5	0.09	0.069	23.6
					RE_P* (%)	15.66%

As observed, the % RE_P* (Relative Error average) between the experimental and the predicted value is 15.66%. This value can be considered as a good approximation considering that the resolution of the tool microscope used to measure the tool flank wear is 0.01 mm.

4.4 Scientific Area 2: Surface characterization analysis

In this part of the study the same experimental set-up used in section 4.2 was applied regarding the workpiece, the tool insert and the equipment characteristics.

Regarding the selection of cutting parameters, in this part of the study only the cutting speed and the feed per tooth were taken into account as process variables as shown in Table 4.13.

Table 4.13 shows the selected cutting parameters for this study.

Table 4.13- Selected cutting parameters for Condition 2.

Level	V (m/min)	fz (mm/rev * tooth)	ap (mm)
Low (1)	200	0.2	1.0
Medium (2)	400	0.3	1.0
High (3)	600	0.4	1.0

All the tests were conducted under dry cutting conditions and in this case since the axial depth of cut is constant, a factorial design (3^2) was used. Table 4.14 shows the array used for this study.

Table 4.14- Array for the experiments with condition 2.

Trial	V	fz	ap
1	1	1	1
2	1	2	1
3	1	3	1
4	2	1	1
5	2	2	1
6	2	3	1
7	3	1	1
8	3	2	1
9	3	3	1

Also, for this case study, the signal-to-Noise (S/N) ratio was also applied in order to obtain the effect of each cutting parameter on surface roughness as well as to identify the optimal combination of cutting parameters to achieve low values of surface roughness.

For this analysis, the smaller-the-best formula for the S/N ratio was applied since a lower tool wear will prolong tool life and a smooth surface roughness will allow a better performance of a workpiece in a highly corrosive environment.

Once the specimens had been machined, the surface roughness was measured. A Taylor Hobson Series 50, roughness tester, with a resolution of 0.001 μm was used for this purpose. A cut-off of 0.8 mm and an evaluation length of 6.4 mm were used, which is recommended by the manufacturers for face milling operations.

The machined surface was measured across the direction of the feed and these measurements were performed every 330 mm length cut until the tool flank wear reached around VB=0.5 mm.

Five measurements were taken each time as shown in Figure 4.15 where extreme values were ignored.

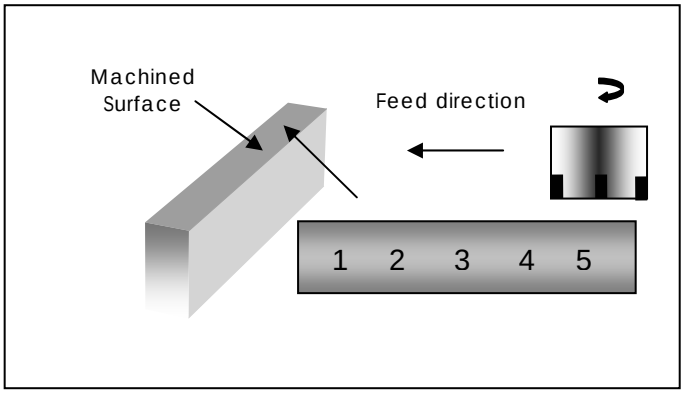

Figure 4.15- Scheme indicating the areas where surface roughness measurements were taken**.**

Once the surface roughness test was completed, the microstructural analysis was carried out in order to analyze possible metallurgical changes below the machined surface. This test was conducted on samples 1, 3, 4, 7 and 9 following the ASTM E-3 standards. In order to reveal the microstructure, the samples were etched with NaOH

(20%) reactive as suggested by the ASTM E-407 standards. After this procedure, samples were observed in an optical microscope equipped with a digital camera for microstructural analysis.

Finally, in order to complete the surface integrity analysis, microhardness analysis was carried out to study the microhardness changes below the machined surface. This test followed the ASTM E 384-399 Standard Test Method for Microindentation Hardness of Materials, and was conducted using a Buehler hardness equipment, applying a load of 200 grf for 15 sec. The first measurement was spaced 50 μm apart from the machined surface. A total of 7 measurements from 50 μm to 1000 μm to the centre of the specimen were taken. In each of this distance 5 measuements were taken and the average of them is reported as observed in Figure 4.16.

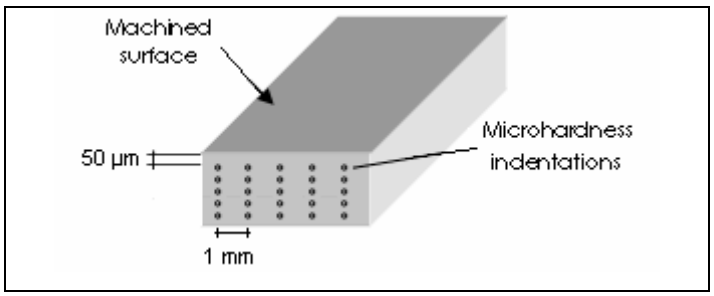

Figure 4.16- Scheme of microhardness indentation measurements

4.4.1 Results and analysis of results

Once all the experiments were concluded, the following results were obtained and for a better understanding, the results were divided into four (4) subsections:

- Influence of the cutting parameters on the surface roughness.
- Influence of the cutting parameters on the machined surface microstructure.
- Influence of the cutting parameters on the microhardness.
- Influence of the tool wear on the surface roughness.

- **Influence of cutting parameters on the surface roughness**

The relationship between surface roughness and the cutting parameters is observed in Figures 4.17 and 4.18.

Figure 4.17 shows the influence of cutting speed on surface roughness for a different values of feed per tooth (Condition 2) when cutting a workpiece length of L=330 mm (Fig 4.17a.) and a length of L=990 mm (Fig 4.17b.)

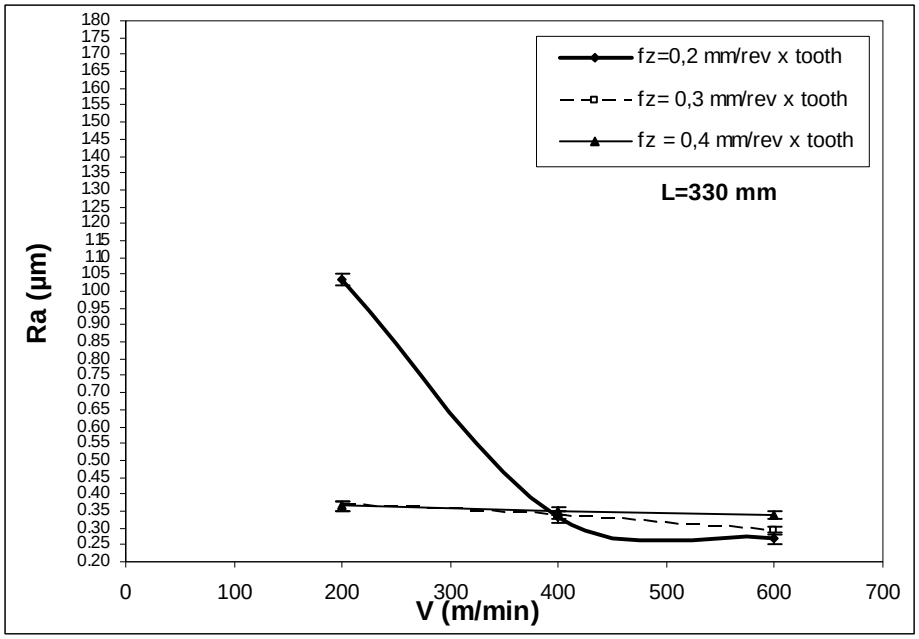

a)

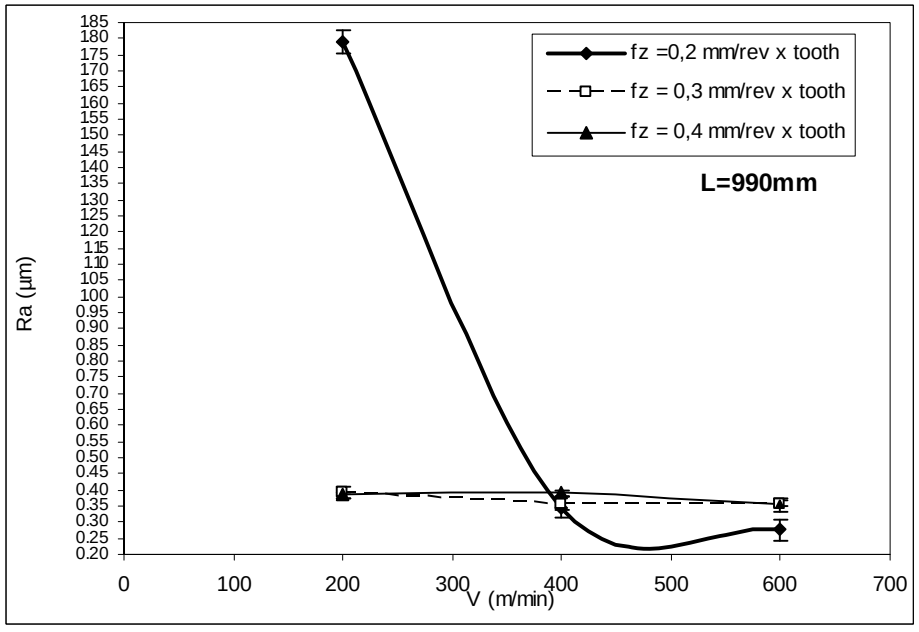

b)

Figure 4.17- Surface roughness vs. cutting speed for different feed per tooth and constant ap=1.0 mm. a) L=330mm b) L=990 mm.

When analyzing the influence of cutting speed on surface roughness (Fig. 4.17) it can be observed that there is a huge improvement in roughness when the cutting speed is increased from 200 m/min to 400 m/min when using a low value of feed per tooth (fz=0.2 mm/rev* tooth). This result is probably due to a suppression of built-up-edge formation in this range of cutting speed. Also, when using a low feed per tooth, the material removal involves mechanical "rubbing" rather than efficient cutting, as a result of insufficient chip thickness, due to a small contact length between the tool and the chip. An improvement of surface roughness is observed when using a fz =0.3 mm/rev * tooth and fz =0.4 mm/rev x tooth, when cutting at low values of cutting speed.

When comparing the two figures 4.17a and 4.17b, it can be observed that the surface roughness increases when machining a higher length of cut, especially when using a V=200 m/min and fz =0.2 mm/rev * tooth. This result is due to the fact that the tool starts to wear out shortly after starting to cut, increasing the roughness of the workpiece surface since it is less sharp and also because there is more time contact between the tool and the chip when using low values of cutting speed and feed per tooth. This result agrees with previous researchers such as the studies made by Sai, (2001 and 2005), and Korkut, (2004).

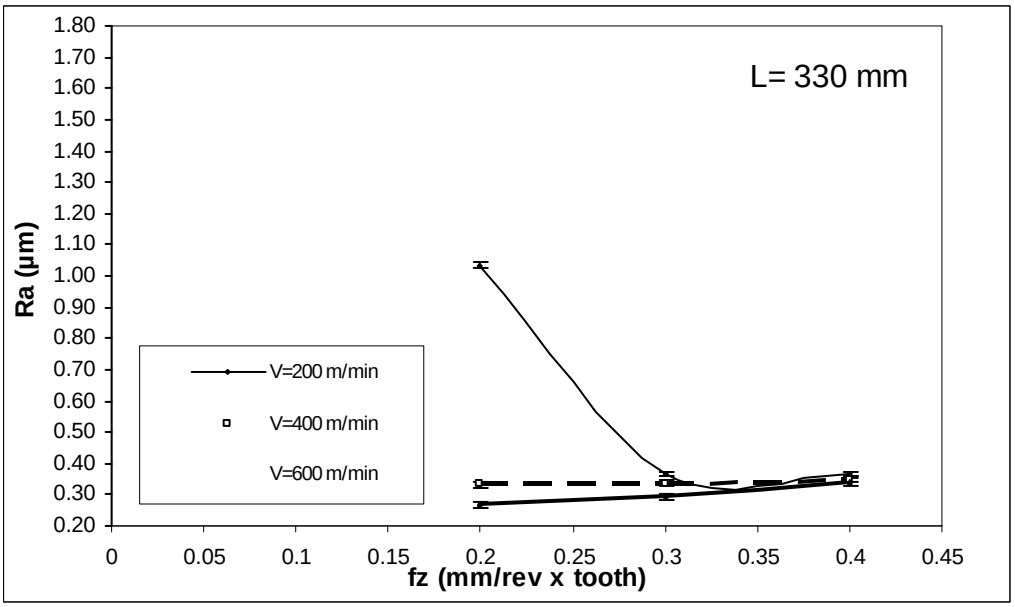

a)

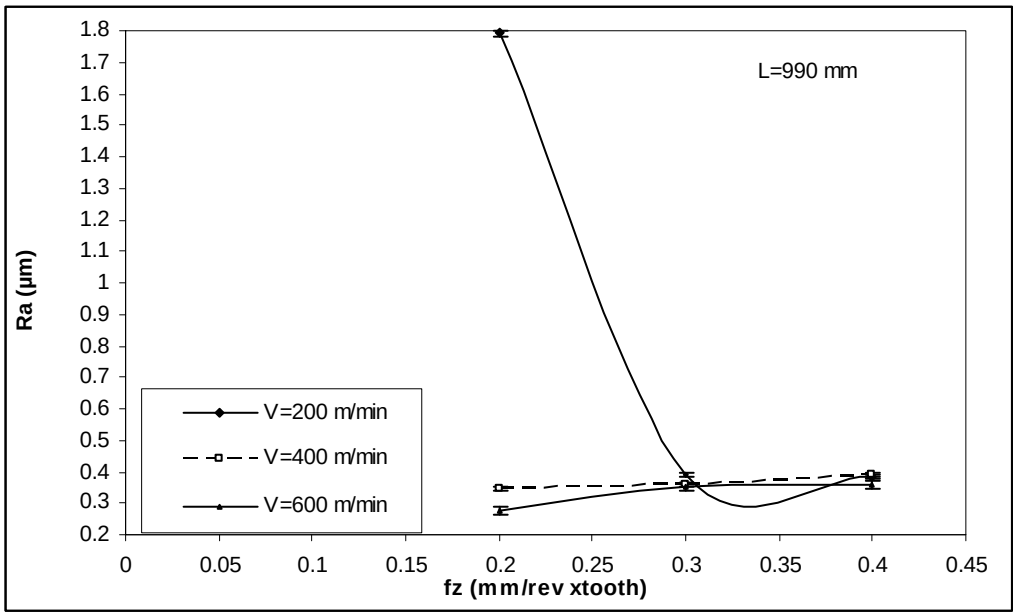

b)

Figure 4.18- Surface roughness vs. feed per tooth for different cutting speeds. a) L=330mm b) L=990 mm

Figure 4.18 shows the relationship between surface roughness and feed per tooth for different cutting speeds and different lengths of cut. When analyzing this figure, it can be observed in general, that surface roughness increases slightly when increasing the feed per tooth in the cutting speed range between 400 m/min to 600 m/min. This result is due to the fact that as the feed per tooth increases, the section of

the sheared chip also increases because the metal resists the rupture and requires larger effort for chip removal thus increasing the cutting forces.

Regarding the high value of roughness obtained when using a fz =0.2 mm/rev*tooth and V=200 m/min, this result is probably due to the fact that at low cutting speed the temperature profile is not sufficient to eliminate built-up-edge that in turn deteriorates the quality of surface. The small feed also involves a higher amount of mechanical "rubbing" that induces vibration. However, as previously stated, an increase of the cutting speed probably produces a suppression of built-up-edge formation in this range of cutting speed. In addition, an increase of cutting speed produces an increase of temperature in the cutting zone, this fact makes the metal machined more plastic and consequently the efforts necessary for machining the workpiece decrease. Finally it was observed that, an increase of 300% of the cutting speed represented an improvement of roughness of 60%, when using f=0.2 mm/rev*tooth, while an increase of 100% of the feed per tooth represented an increase of around 40% of the surface roughness.

In order to obtain the best combination of parameters for a low value of surface roughness which is recommended for a corrosive environment, the statistical S/N ratio was applied using the smaller-the-best formula. Figure 4.19 shows the S/N ratio for surface roughness (Ra) for different cutting parameters.

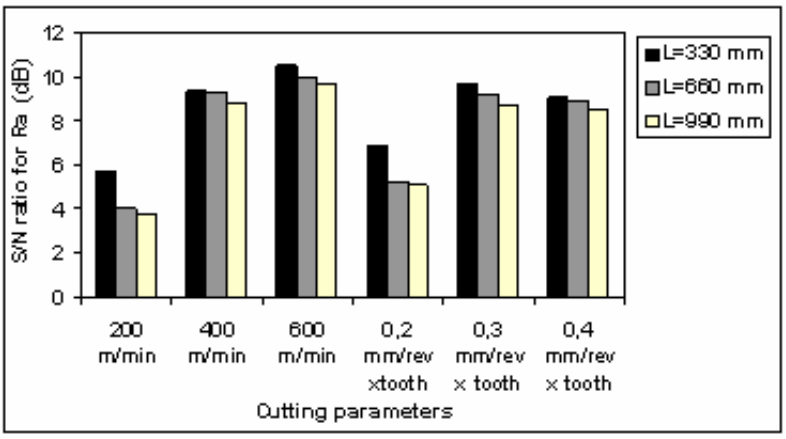

Figure 4.19- S/N ratio for Ra for different cutting parameters when machining different length of cut.

When analyzing Figure 4.19 it can be observed that the surface roughness improves when increasing the cutting speed (high values of S/N ratio). Regarding the feed per tooth, under the established cutting conditions, a definite pattern cannot be observed, although it seems that in general an improvement of the surface roughness is obtained when using fz = 0.3 mm/rev * tooth. The best combination of cutting parameters, for low values of roughness is V=600 m/min and fz=0.3 mm/rev * tooth, since it allows the achievement of a low value of roughness.

- **Influence of the cutting parameters on the machined surface microstructure**

As observed in Figure 4.20, this martensitic stainless steel show black elongated shapes, however there is not a noticeable difference between the microstructures when changing the cutting conditions.

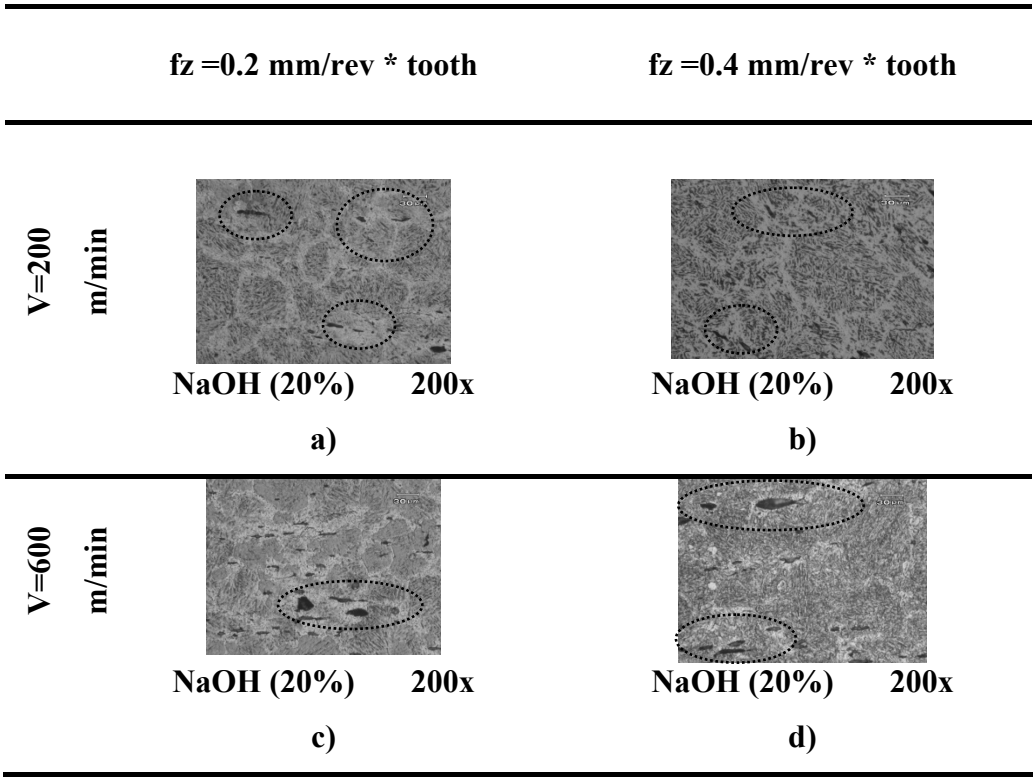

Figure 4.20- Surface microstructure after face milling machining at different cutting conditions

An Electro Dispersive X-Ray (EDX) analysis was conducted to this material in order to analyse these black elongated shapes and the results are shown in Figure 4.21. As expected, a considerable percentage of manganese and sulphur is presented, corroborating the presence of this precipitate (manganese sulphide) which are a characteristic of this material when heat treated. (Metals Handbook, 1972).

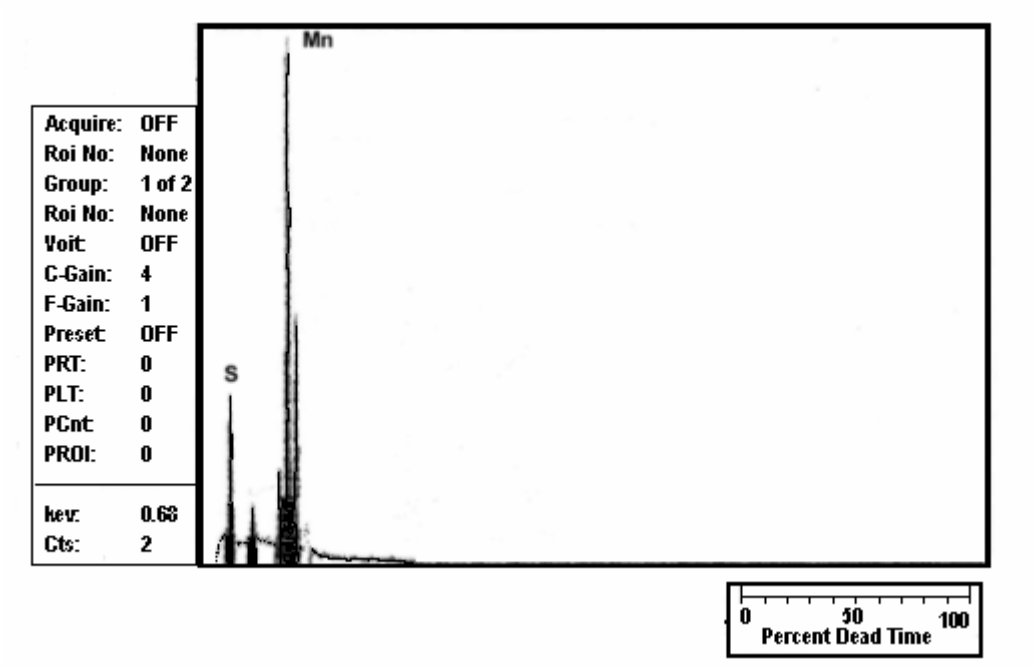

Figure 4.21- Electro Dispersive X-Ray (EDX) analysis obtained in 416 martensitic stainless steel machined at V=600 m/min and fz = 0.4 mm/rev*tooth

- **Influence of the cutting parameters on the microhardness**

Figures 4.22 and 4.23 show the influence of cutting speed and feed per tooth respectively on the surface hardness of the specimen from the machined surface towards the centre of the workpiece, when face milling under different cutting conditions.

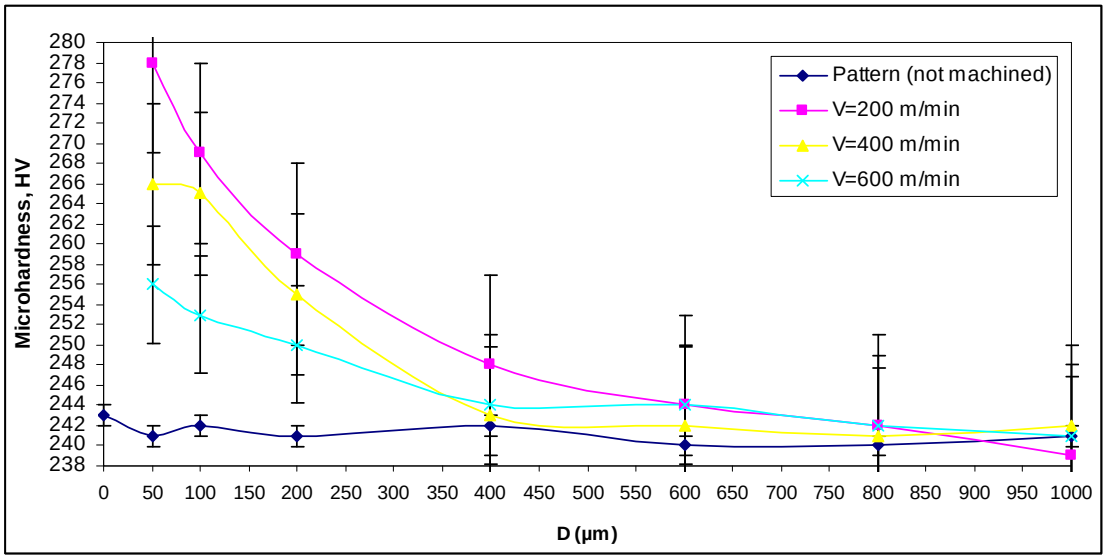

Figure 4.22- Hardness vs. Distance from the machined surface towards the centre of the specimen in mm (D) when face milling at different cutting speed and at a constant feed per tooth of fz=0.2 mm/rev* tooth

In Figure 4.22, it can be observed that, in general that the specimens machined increased their surface hardness when compared to the original specimen (not machined). In general, the overall variation of microhardness did not vary more than 15% when compared to the pattern surface. This increase in microhardness is related to the fact that as the cutting process is conducted the material is deformed in the sublayer of the workpiece, causing an entanglement of the dislocations and hence an increase in the metal's strength, which could be increased by the presence of any inclusion, precipitation, etc. Also as observed, as the cutting speed is increased the surface microhardness is decreased, probably due to the fact that as the cutting speed is increased there is less contact time between the tool and the chip, easing the plastic deformation of the chip. In addition, when machining at low cutting speeds, the built-up-edge formation is generated which produces a less clean cut and as a consequence more distortion in the surface layer. Finally, an increase of 100% in the cutting speed produced a decrease of 4% in microhardness.

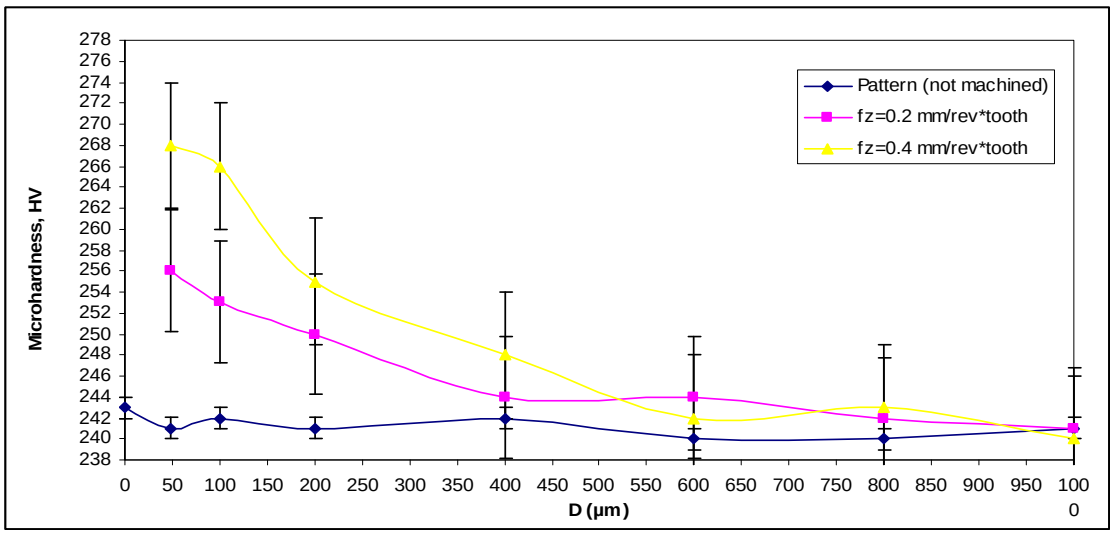

Figure 4.23- Hardness vs. Distance from the machined surface to the centre of the specimen in mm (D) when face milling at different feed per tooth and at a constant cutting speed of V=200 m/min

When analyzing Figure 4.23 it can be observed that once again the microhardness values of the machined specimens are higher than the original specimen (not machined) and that an increase of 100% in the feed per tooth produces an increase of 4% of the surface microhardness. This result is due to the fact that as the feed per tooth is increased the volume of material that has been removed is also increased. This fact produces an increase in the strain on the material that has been machined, producing an increase in the hardness of the material near the machined surface.

- **Influence of the tool wear on the surface roughness**

For this case study, the tool flank wear measurements were performed every 2 single passes (330 mm of length of cut = workpiece length x 2) up to a length of cut that will give a maximum tool flank wear of 0.5 mm as suggested in ISO Standards 8688-1. All the tool wear measurements were conducted using a Nikon 18724 optic microscope.

Figure 4.24 and 4.25 show the relationship between surface roughness and the tool wear respectively for different cutting conditions. Figure 4.24 shows the influence of the tool flank wear on surface roughness for different feed per tooth when machining at V=600 m/min.

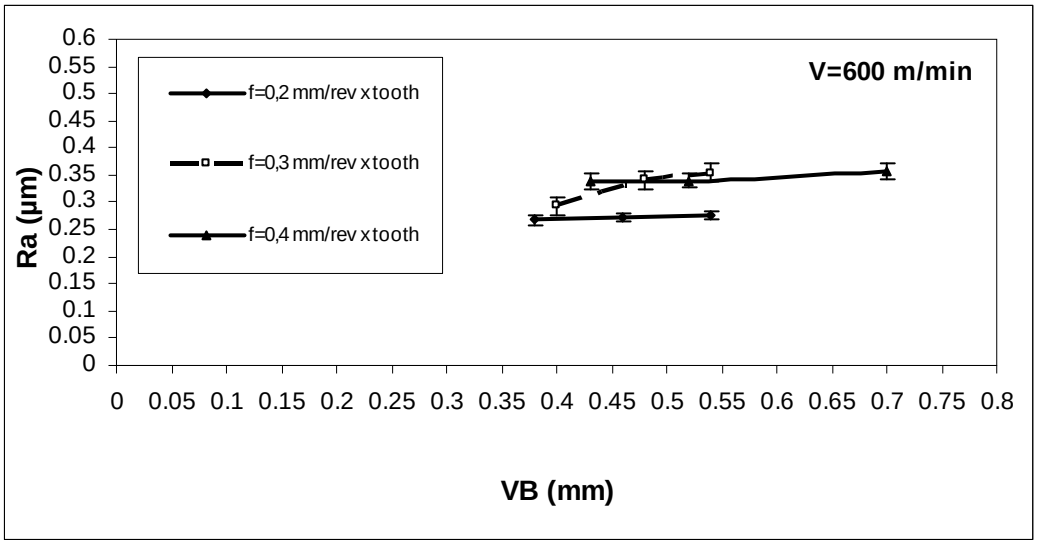

Figure 4.24- Surface roughness vs. tool wear for different feed per tooth when cutting at V=600 m/min

Figure 4.25 shows the influence of the tool flank wear on the surface roughness for different cutting speeds when using a fz = 0.4 mm/rev * tooth.

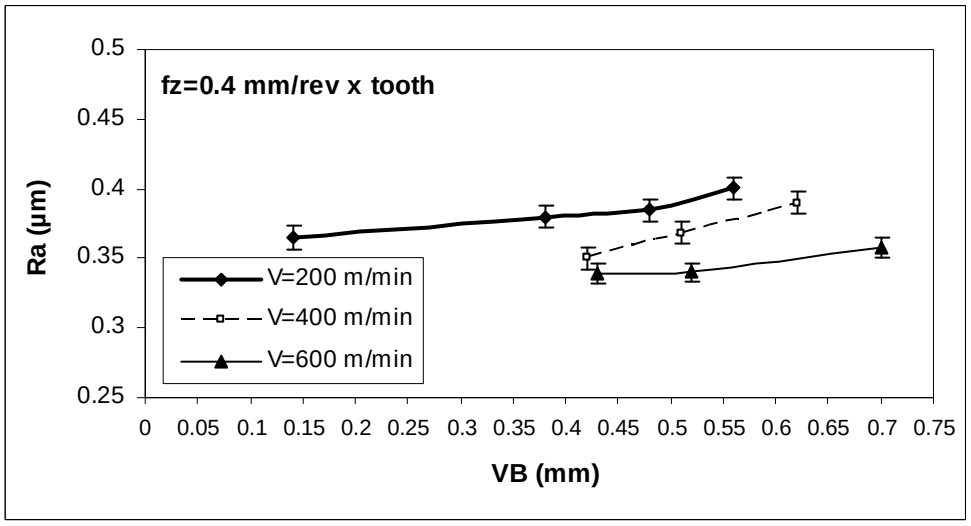

Figure 4.25- Surface roughness vs. tool wear for different cutting speeds when machining at fz=0.4 mm/rev * tooth

In both Figures 4.24 and 4.25, it can be observed that, in general, an increase in the tool wear produces a corresponding increase of the value of surface roughness, for a particular set of cutting data. This is due to the fact that the rubbing process which occurs especially when using low values of cutting speed, produces more wear on the tool, giving rise to a less pronounced cutting edge and an increase of the surface contact between the workpiece and the tool. An increase of 25% of the tool wear produced an increase of 30% in surface roughness this more prevelant when using f=0.3 mm/rev*tooth. This situation leads to a reduction in cutting efficiency in removing the material, where it is more difficult to achieve a clean cut. This result remained constant for all the established conditions and it also agrees with previous studies made by Aslan, (2005).

4.5 Summary and general conclusions

In this study a new contribution to knowledge is provided by through the optimal combination of cutting parameters in order to achieve longer tool life, maximum material removal and low tool wear when face milling 416 martensitic stainless steel with PVD-TiAlN coated carbides square inserts. The conclusions drawn from this research are:

- A longer tool life was achieved when using low values of cutting speed, feed per tooth and axial depth of cut, where an increase of around 900 % in tool life was observed when using a low combination of cutting parameters.
- A maximum material removal rate of 399 cm^3/min was obtained when using the highest values of these cutting variables. This value represents an improvement of 350% when compared to 71 cm^3/min obtained when using a combination of low values of cutting parameters.
- An increase of 25% on the cutting speed produced an increase of 4% in the material removal rate.
- The machined surface microhardness did not vary more than 15% due to workhardening when compared with the original specimen.
- An increase of 100% of the cutting speed produced a decreased of 4.0 % of the surface microhardness while an increase of 100% of the feed per tooth produced an increased of 4.0 %.
- It was observed that, an increase of 300% of the cutting speed represented an improvement of roughness of 60%, when using f=0.2 mm/rev*tooth, while an increase of 100% of the feed per tooth represented an increase of around 40% of the surface roughness.
- It was corroborated that tool performance can be judged from the tool life or volume of material removal and that abrasion was the main tool wear mechanism presented in the inserts when cutting under the selected conditions.
- The combination of cutting speed and feed per tooth is of significant importance for controlling tool flank wear, since an increase of 25% in tool wear produced an increase of 30% in surface roughness when using f=0.3 mm/rev*tooth.

5 Aluminium alloy studies

5.1 Introduction

In machining, a surface can be defined as a border between a machined component and its environment. The defects produced from different machining procedures can significantly affect the performance of the final component. Therefore, it is critical for industries, like aerospace, to know and understand the effects of changing operating parameters before new machining strategies are accepted.

The term “surface integrity” is used to describe the attributes of a machined surface and its relationship to functional performance. In general, surface integrity can be divided into two aspects: the external topography of surfaces (surface finish); and the microstructure, mechanical properties and residual stresses of internal subsurface layers.

Performance characteristics that are usually sensitive to surface integrity include; fatigue strength, fracture strength, corrosion rate, and tribological behaviour (such as friction, wear and lubrication, and dimensional accuracy). Notches, scratches or pits on the surface would be expected to act as fatigue crack initiation sites since depending on it the parts can be introduced to specific environments.

Extensive research has been developed regarding surface integrity and even though the results have provided lots of knowledge (Balkrishna 2001, Che-Haron 2001, Axinte 2002 and Poulachon 2005); there are still many gaps that need to be filled specially when analyzing an important material such as aluminium alloy 7075.

This chapter presents the research that has been performed to fill gaps identified in Chapter 3 and make a new contribution to knowledge, by studying the surface characterization and the vibrations occurred during the face milling process of aluminium alloy 7075-T7351 under a wet cutting condition.

This chapter is divided into five sections. The first of the four sections presents a detail explanation of the experimental set up. The next three sections represent analysis of results and the last section summarizes and concludes the present work.

Section 5.2: Describes the experimental set-up conducted for the aluminium alloy studies.

Section 5.3: Describes the surface characterization analysis of the machined surface which includes different studies, such as: 2D and 3D surface analysis, microstructure, microhardness, and the chip's morphology analysis

Section 5.4: Describes the influence of the cutting parameters on the surface roughness as well as the optimal combination of cutting parameters in order to achieve a smooth surface

Section 5.5: Describes the influence of the RMS acceleration of the spindle and the workpiece on the machined surface roughness

Section 5.6: Describes the general conclusions of these studies

Figure 5.1 shows a schematic overall description of the development of this study.

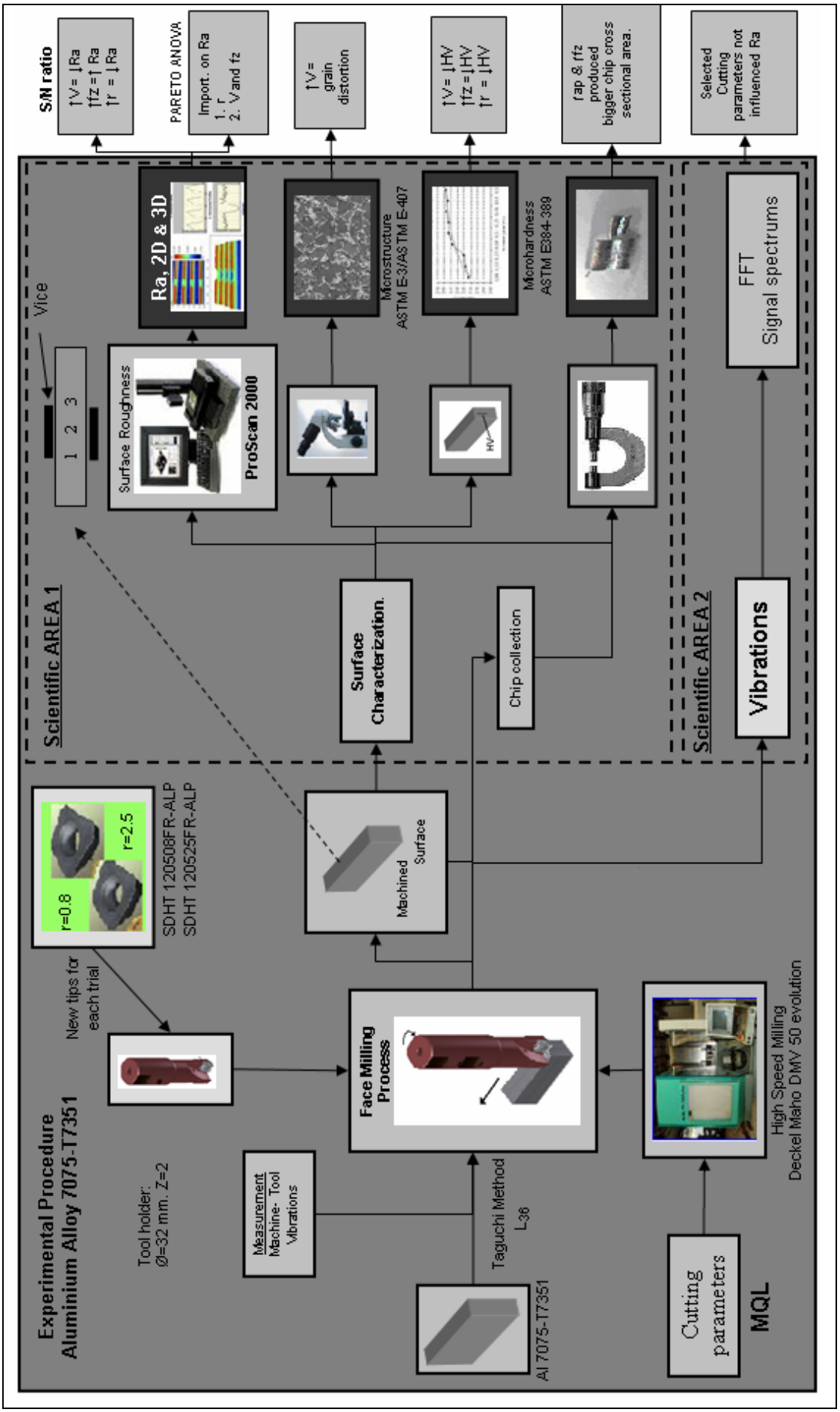

Figure 5.1- Schematic diagram of the different studies conducted on the AL 7075-T7351.↑ increase ↓decrease

When analyzing Figure 5.1, it can be observed that the study is divided into two main areas, both sharing the first stage of experiment which corresponds to the face milling process.

As observed, AL 7075-T7351 square bars where milled in a HSM Deckel Maho 50 evolution CNC machine under a wet cutting condition (MQL), where a tool holder of 2 teeth was used for the cutting process. New inserts were used for each trial and two different inserts were studied, where basically the tool nose radius was changed. The Taguchi method was used and a total of 36 trials were conducted.

During the milling process vibrations data were collected in the tool holder and in the machined workpiece.

Also after milling each trial, the chips were collected and registered for further analysis.

With regard to the main areas of study it can be observed that:

Scientific Area 1 corresponds to the surface characterization of the milled surface. This study includes surface roughness measurement, microstructure analysis, microhardness and chip measurements. From the surface roughness measurements, the surface roughness value, the 2D profile and the 3D maps of each milled surface was obtained.

Scientific Area 2 corresponds to the analysis of the vibration data collected during the milling process. This study was conducted in order to give knowledge on how much this variable affects the resultant surface under the studied cutting conditions and, indeed if it needs to be included in the development of the models.

Sections 5.2 presents the experimental set-up used for the studies and sections 5.3, 5.4 and 5.5 presents a detail explanation of each of the conducted studies.

5.2. Experimental set-up for the aluminium alloy studies

As previously stated, aluminium alloy 7075-T7351 square bars with dimensions 333.3 x 76.2 x 31.75 mm were used, as suggested by ISO Standard 8688-1.

Table 5.1 and Table 5.2 show the chemical composition and the mechanical properties of this aluminium alloy.

Table 5.1- Chemical Composition of Al 7075-T7351

% Al ± 0.1	% Cr ± 0.007	% Cu ± 0.013	% Mg ± 0.381	% Zn ± 0.019
87.1	0.174	1.586	2.693	5.240

* Varian Spectrophotometer. Model AA-275. (Weight percentage)

Table 5.2- Mechanical Properties of Al 7075-T7351

Ultimate Strength (MPa)	593
Yield Strength (MPa)	448
Vickers Hardness*	155

* Load=100 grf for a time of 30 sec.

A cutting tool with a standard insert holder of $Ø_{Tool}$= 32 mm, with two cutting teeth (Z=2), was used for the experiment. Two types of indexable inserts SDHT 120508FR-ALP CWK26 and SDHT 120525FR-ALP CWK26 were used for the experiment; where the first one corresponds to a 0.8 mm of tool nose radius and the second to a 2.5 mm of tool nose radius. This type of insert is recommended for the machining of aluminium alloy under a wet cutting operation. Figure 5.2 shows a scheme of the insert geometry used for this study.

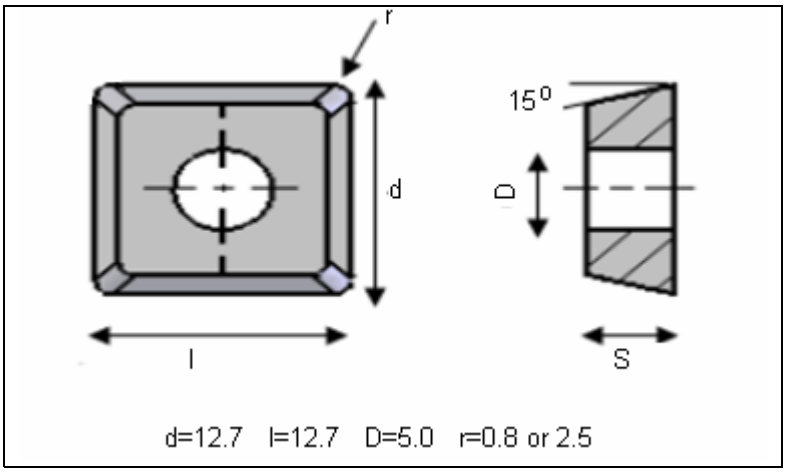

Figure 5.2- Schematic of the geometry of the insert used for the experiments. Units in mm.

Once again following the suggestions made by researchers Diniz and Filho in 1999, a tool diameter bigger than the workpiece width was selected in order to machine the whole width of the workpiece in just one single pass, ($Ø_{Tool}$= 32.0 mm > 31.75 mm). Also a symmetric position between the tool and the workpiece was used in order to achieve a better tool performance (longer tool life). Figure 5.3 shows a schematic of the cutting process.

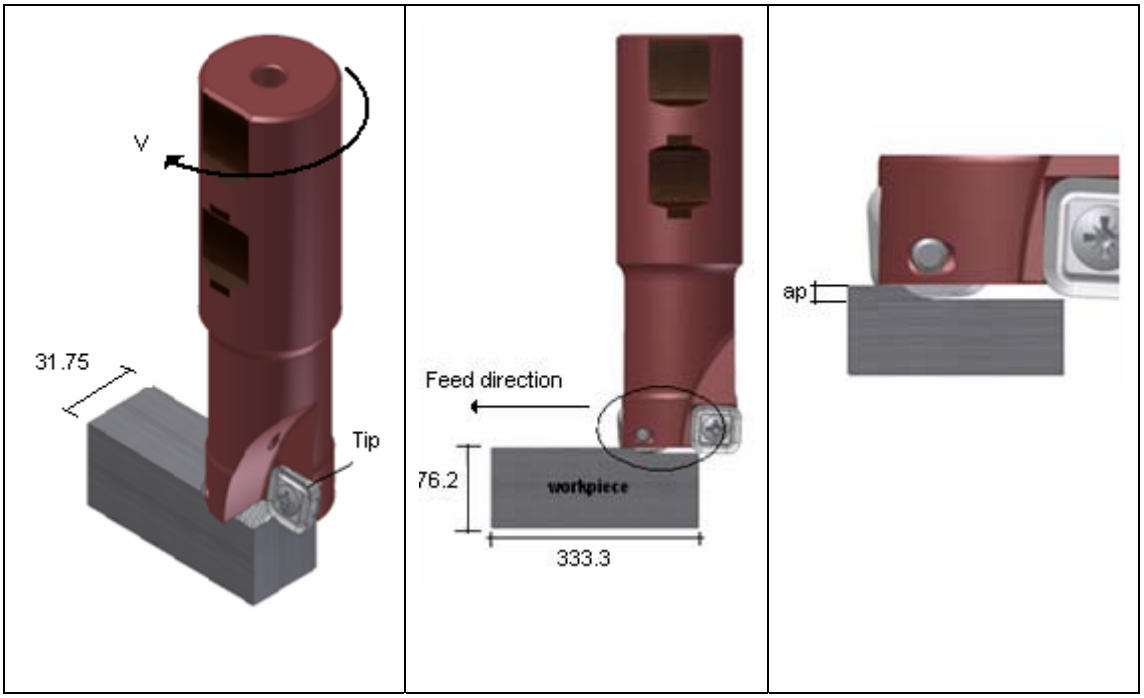

Figure 5.3- Schematic of the cutting process for Al 7075-T7351

The cutting parameters selected for this study were, the cutting speed, the feed per tooth, the axial depth of cut and the tool nose radius and the values were recommended by the tool supplier for the selected workpiece-tool combination. Selected cutting parameters are shown in Table 5.3.

Table 5.3 - Selected cutting parameters for Al 7075-T7351 studies.

Level	V (m/min)	fz (mm/rev*tooth)	ap (mm)	r (mm)
1	600	0.1	3.0	0.8
2	800	0.2	3.5	2.5
3	1000	0.3	4.0	
4	1200			
5	1400			
6	1600			

Six (6) levels were selected for the cutting speed, three (3) levels for the feed per tooth and the axial depth of cut; and two (2) levels for the tool nose radius parameter.

A Deckel Maho, DMV 50 evolution, high speed vertical machine centre, with a maximum spindle speed of 18.000 rpm was used for the face milling operation. All the experiments were conducted under MQL (Minimum Quantity of Lubricant), since: 1) tool wear was not considered as a criterion that will affect the result of the cutting process due to the small amount of material that was removed from the workpiece, (one single pass of 333.3 mm) 2) new inserts were used for each trial and 3) this material needed to be cut under a MQL cutting condition.

For the Design of Experiment (DoE) the Taguchi method was applied, selecting a L_{36} ($2^1 * 6^1 * 3^2$) mixed-level design array. Table 5.4 shows the orthogonal array for the four (4) selected cutting parameters. The values 1 to 6 indicate the levels of the four cutting parameters as defined in Table 5.3.

Table 5.4- L_{36} orthogonal array selected for Al 7075-T7351 studies**.**

	Trial	V	fz	ap	r
Group 1	**1**	1	1	1	1
	2	1	2	2	1
	3	1	3	3	1
	4	2	1	2	1
	5	2	2	3	1
	6	2	3	1	1
	7	3	1	3	1
	8	3	2	1	1
	9	3	3	2	1
Group 2	**10**	1	1	1	2
	11	1	2	2	2
	12	1	3	3	2
	13	2	1	2	2
	14	2	2	3	2
	15	2	3	1	2
	16	3	1	3	2
	17	3	2	1	2
	18	3	3	2	2
Group 3	**19**	4	1	1	1
	20	4	2	2	1
	21	4	3	3	1
	22	5	1	2	1
	23	5	2	3	1
	24	5	3	1	1
	25	6	1	3	1
	26	6	2	1	1
	27	6	3	2	1
Group 4	**28**	4	1	1	2
	29	4	2	2	2
	30	4	3	3	2
	31	5	1	2	2
	32	5	2	3	2
	33	5	3	1	2
	34	6	1	3	2
	35	6	2	1	2
	36	6	3	2	2

5.3 Scientific Area 1: Surface characterization analysis

The surface characterization analysis is used to describe the quality and condition of a surface region and therefore encompasses studies such as 2D and 3D surface roughness analysis, the microstructure analysis, the microhardness analysis and the chip's morphology studies.

Once the samples were machined, they were put on a bench for surface roughness measurement. The roughness was measured across the direction of the machined surface lay (feed direction) using a white lamp profilometer ProScan 2000.

The roughness average value of each specimen was determined by measuring three points, located in the centre of the specimen, specifically, 8 cm away from the edge of the workpiece and just where the vice was retaining the workpiece. The idea of measuring the roughness at the workpiece centre, was in order to make sure that the obtained values of surface roughness were not affected by possible vibrations due to the impact of the tool entering the workpiece. Then an average of these three (3) values was used to represent the surface roughness value of the specimen (Ra). The surface roughness values measured within the measuring area are sufficient to represent the roughness of each workpiece, (Tsai 1999).

In this case study, the sample size for the surface roughness measurements was 4 mm in the ***X*** direction and 4 mm in the ***Y*** direction. In order to cover this 4x4 mm^2 area, 1335 steps with a size of 0.003 mm each was used by the profilometer ProScan 2000. These values are recommended by the ProScan manufacturers guide, for face milling operations. Once the measuring procedure was concluded the filter for the waviness was applied in order to report the exact value of roughness.

Once the surface roughness was measured, the surface characterization analysis was conducted. Here 2D and 3D surface analysis were carried out by analyzing the surface profile and the surface topography obtained from each trial after the milling process.

When completing the surface roughness measurement and later analysis, the microstructure analysis was conducted, and in this case the specimens were ground and polished following the ASTM E-3 standards. This test was carried out in order to analyze possible metallurgical changes below the machined surface. The samples were etched with a solution of 950 ml absolute methanol + 15 ml nitric acid + 50 ml of perchloric acid. This reactive is suggested by the ASTM E-407 Standard Practice for Microetching Metals and Alloys. After this procedure, the samples were observed in an optical microscope equipped with a digital camera for microstructure analysis.

In order to analyze possible microhardness changes below the machined surface a microhardness analysis was conducted. This study was performed following the ASTM E-384-399 Standard Test Method for Microindentation Hardness of

Materials. In this case, the test was conducted using a Shimadzu hardness equipment using a load of 100 grf for a period of 30 sec. A total of 5 measurements spaced 1 mm apart were taken; from the machined surface towards the centre of the sample as was shown in Figure 4.16. It must be highlighted that it is common to obtain a difference of around 100 HV between measurements on the same sample, since the material pattern used to calibrate the hardness equipment has a range from 738 to 874 HV.

In order to complete the surface characterization study, the chips from each specimen were collected after the face milling process, for morphology studies. Pictures of the chips were obtained by using an Olympus SZ61 optical magnifier at 9X and the chip's width (Cw) and thickness (Ct) was measured by using a TESSA micrometer with a range of 0-25 mm and 0.01 mm of resolution.

Since 36 experimental trials were conducted, the results of each study involved in the surface characterization, were divided into four (4) groups as shown in Table 5.4.

Group 1, corresponds to the specimens machined with V= 600 m/min, 800 m/min, 1000 m/min and r = 0.8 mm.

Group 2, corresponds to the specimens machined with V= 600 m/min, 800 m/min, 1000 m/min and r = 2.5 mm.

Group 3, corresponds to the specimens machined with V= 1200 m/min, 1400 m/min, 1600 m/min and r = 0.8 mm.

Group 4, corresponds to the specimens machined with V= 1200 m/min, 1400 m/min, 1600 m/min and r = 2.5 mm.

5.3.1. Results and analysis of results

Once the experiments were concluded the following results were obtained. To present a better understanding, the results were divided into three sub sections:

- 2D and 3D surface roughness analysis.
- Microstructure analysis.
- Microhardness analysis.
- Chip morphology analysis.

- **2D and 3D surface roughness analysis**

The analysis of the surface roughness will give knowledge of how the machined surface is affected by the cutting conditions used during the process. It must be highlighted that the measurement of each machined surface roughness corresponding to each trial gives knowledge of the surface roughness value (reported in Appendix B. Table 1) and the 2D and 3D map when using a non-contact lamp profilometer.

Tables 5.5 and 5.6 show a few of the surface roughness profiles obtained from specimen of each group, when machined under different cutting conditions with r = 0.8 mm and r = 2.5 mm respectively. The rest of the profiles can be observed in Appendix B Tables 2 and 3.

Table 5.5- 2D surface roughness profile of a few Al 7075-T7351 specimens cut under different cutting conditions with r = 0.8 mm

TRIAL	Cutting parameters	Axis	Surface roughness Ra, profile
2	V= 600 m/min fz= 0.2 mm/ rev x tooth ap= 3.5 mm	x=132.947 mm z = 15.950 µm	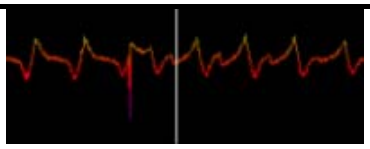
6	V= 800 m/min fz= 0.3 mm/ rev x tooth ap= 3.0 mm	x=140.993 mm z = 6.354 µm	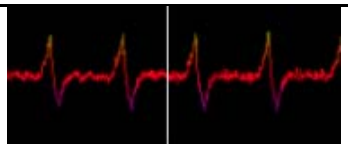
	V= 1000 m/min fz= 0.1 mm/ rev x tooth ap= 4.0 mm	x =118.939 mm z =4.260 µm	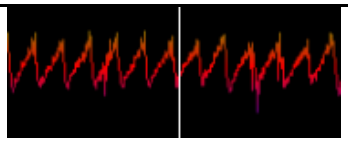
9	V= 1000 m/min fz= 0.3 mm/ rev x tooth ap= 3.5 mm	x =100.032 mm z = 7.400 µm	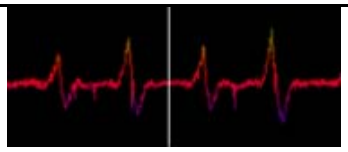
21	V= 1200 m/min fz= 0.3 mm/ rev x tooth ap= 4.0 mm	x=100.032 mm z =7.400 µm	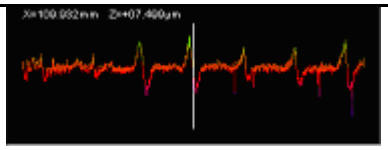
23	V= 1400 m/min fz= 0.2 mm/ rev x tooth ap= 4.0 mm	x=138.060 mm z =7.008 µm	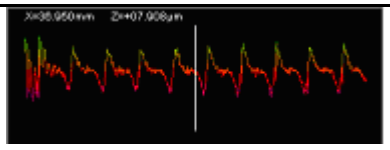
24	V= 1400 m/min fz= 0.3 mm/ rev x tooth ap= 3.0 mm	x =101.080 mm z =10.012 µm	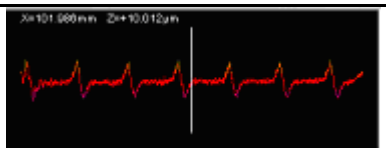
27	V= 1600 m/min fz= 0.3 mm/ rev x tooth ap= 3.5 mm	x =122.001 mm z =3.047 µm	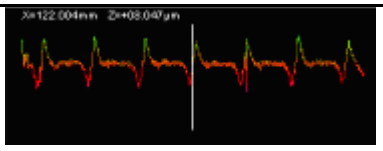

Table 5.6- 2D surface roughness profile of a few Al 7075-T7351 specimens cut under different cutting conditions with r = 2.5 mm

TRIAL	Cutting parameters	Axis	Surface roughness Ra, profile
10	V= 600 m/min fz= 0.1 mm/ rev x tooth ap= 3.0 mm	x=112.080 mm z=4.316 µm	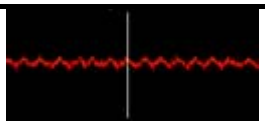
13	V= 800 m/min fz= 0.1 mm/ rev x tooth ap= 3.5 mm	x=127.180 mm z=9.960 µm	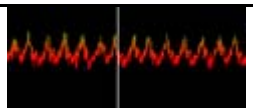
15	V= 800 m/min fz= 0.3 mm/ rev x tooth ap= 3.0 mm	x=109.012 mm z=9.210 µm	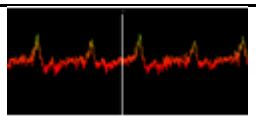
16	V= 1000 m/min fz= 0.1 mm/ rev x tooth ap= 4.0 mm	x=115.230 mm z=5.841 µm	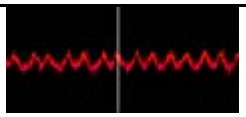
28	V= 1200 m/min fz= 0.1 mm/ rev x tooth ap= 3.0 mm	x=123.080 mm z=7.860 µm	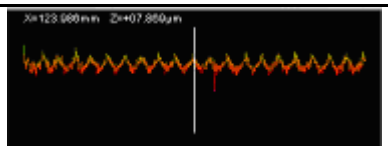
31	V= 1400 m/min fz= 0.1 mm/ rev x tooth ap= 3.5 mm	x=100.830 mm z= 5.333 µm	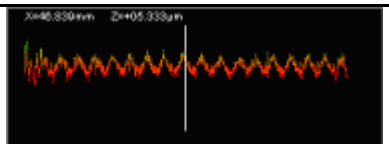
34	V= 1600 m/min fz= 0.1 mm/ rev x tooth ap= 4.0 mm	X=15.068 mm z=4.220 µm	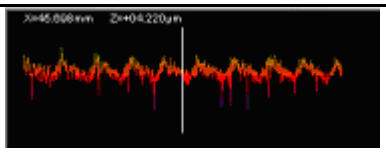
35	V= 1600 m/min fz= 0.2 mm/ rev x tooth ap= 3.0 mm	x=111.032 mm z=5.038 µm	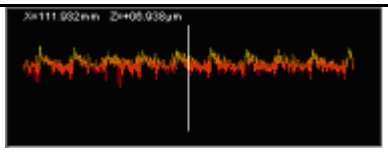

As observed from Tables 5.5 and 5.6 the surface roughness profile of each of the specimens show a periodic and harmonic function, with no kind of irregularity that could lead to an imperfection on the machined surface. This result indicates that apparently no defect on the tool (such as wear) or high enough vibrations were presented during the milling process. Since as stated from previous research a rougher surface will be obtained when the tool is reaching the end of its life, (Che-Haron, 2001).

Table 5.7 shows a comparison between the surface roughness profiles obtained when machining at a constant cutting speed (V = 800 m/min) and a constant tool nose radius (r = 2.5 mm), but using different feed per tooth and axial depth of cut. The selected trials are 13, 14, and 15. When analyzing the surface roughness profiles of these specimens, it can be observed that the amplitude between the peaks of the profile increases as the feed per tooth increases. This result is due to the fact that, as the feed is increased, the tool displacement is bigger along the machined surface, removing a higher amount of material, making the furrows deeper and broader. This result can be appreciated when analyzing the machined surface where the tool trail can be easily observed. This behaviour was kept constant for all the conditions where the cutting speed remained constant and the feed per tooth was increased. This result is in agreement with research made by Koshy, (2002), Korkut, (2004) and Rashad, (2006).

Table 5.7- 2D surface roughness profile comparison, between specimens corresponding to trials 13, 14 and 15 (V = 800m/min, r = 2.5 mm and different fz and ap).

TRIAL	Cutting parameters	Surface roughness profile
13	V= 800 m/min fz= 0.1 mm/ rev *tooth ap= 3.5 mm	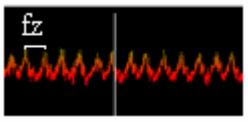
14	V= 800 m/min fz= 0.2 mm/ rev *tooth ap= 4.0 mm	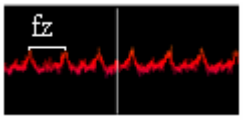
15	V= 800 m/min fz= 0.3 mm/ rev *tooth ap= 3.0 mm	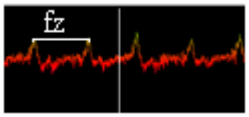

In Table 5.8, a comparison between trial 7 and 16 is observed. In these cases the specimens were cut at a constant cutting speed, feed per tooth and axial depth of cut, but with different tool nose radius.

Table 5.8- 2D surface roughness profile comparison, between specimens corresponding to trials 7 and 16.

TRIAL	Cutting parameters	Surface roughness Ra, profile
7	V= 1000 m/min fz= 0.1 mm/ rev x tooth ap= 4.0 mm r=0.8 mm	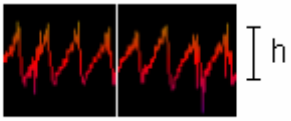
16	V= 1000 m/min fz= 0.1 mm/ rev x tooth ap= 4.0 mm r=2.5 mm	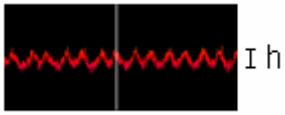

When analyzing the profiles presented in Table 5.8, the surface roughness profile height (h) decreases as the tool nose radius is increased, resulting in a smoother surface. This is due to the fact that there is more surface contact between the tool nose radius and the workpiece surface, generating smaller peaks on the trail. Also when cutting edges are fresh the surface roughness can be considered as a geometrical result of the stepover of the cutter and the tool radius. This result can be related to the results obtained by Ghani in 2004, (even though, his research was conducted in an end milling process), where the height of the tooth mark is inversely related to the radius of the cutter.

Once the 2D surface roughness of all the specimens was analyzed, the surface topography of each specimen was studied. Tables 5.9 and 5.10 show the surface topography obtained for a few different trials, machined under different cutting conditions, the rest of the surface topographies are presented in Appendix B, Table 4 and 5. The analysis of these plots was based on a visual presentation of the processed topographic data. In this case study, the visual presentations are isometric projections which are referred to a 3D object on a 2D medium. An important property of this type of projection is that the distance along the projection axes, retained their original proportion, giving a realistic view of the 3D surface as observed in the results shown in Table 5.9 and 5.10 which remained constant for all the studied established conditions (Stout, 2000).

Table 5.9- Surface topography of a few Al 7075-T7351 specimens machined under different cutting conditions with r = 0.8 mm

Trial	Surface topography	Trial	Surface topography
2 **V=600 m/min,** **fz=0.2 mm/rev*tooth,** **ap=3.5 mm**	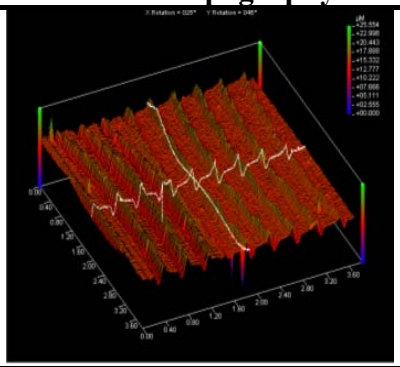	**6** **V=800 m/min,** **fz=0.3 mm/rev*tooth,** **ap=3.0 mm**	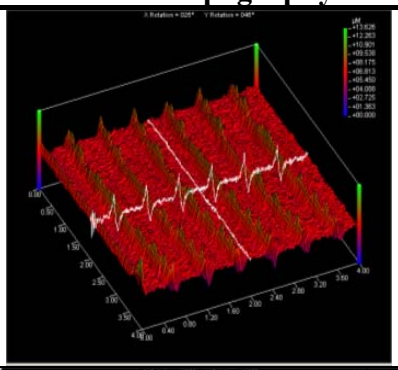
7 **V=1000 m/min,** **fz=0.1 mm/rev*tooth,** **ap=4.0 mm**	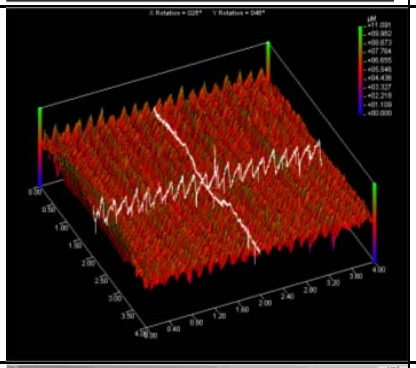	**9** **V=1000 m/min,** **fz=0.3 mm/rev*tooth,** **ap=3.5 mm**	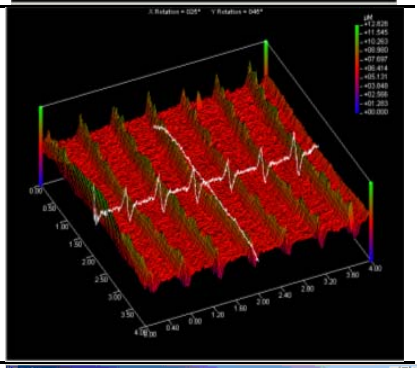
21 **V=1200 m/min,** **fz=0.3 mm/rev*tooth,** **ap=4.0 mm**	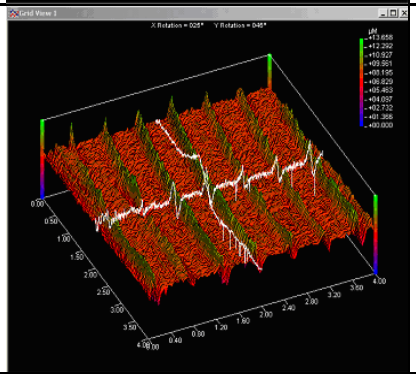	**23** **V=1400 m/min,** **fz=0.2 mm/rev*tooth,** **ap=4.0 mm**	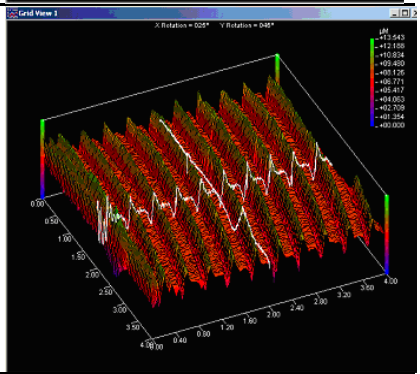
24 **V=1400 m/min,** **fz=0.3 mm/rev*tooth,** **ap=3.0 mm**	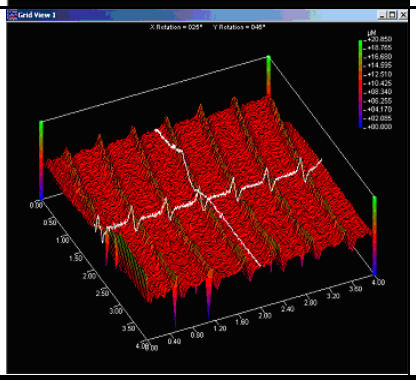	**27** **V=1600 m/min,** **fz=0.3 mm/rev*tooth,** **ap=3.5 mm**	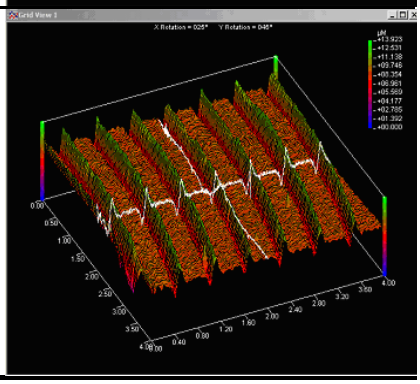

Table 5.10- Surface topography of a few Al 7075-T7351 specimens machined under different cutting conditions with r = 2.5 mm

Trial	Surface topography	Trial	Surface topography
10 **V=600 m/min,** **fz=0.1 mm/rev*tooth,** **ap=3.0 mm**	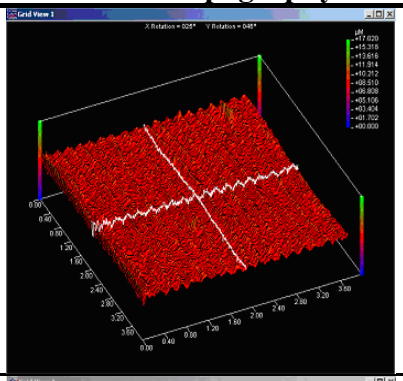	**13** **V=800 m/min,** **fz=0.1 mm/rev*tooth,** **ap=3.5 mm**	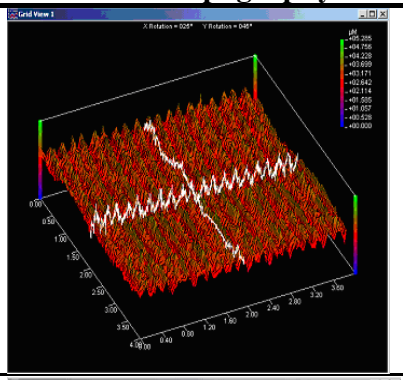
15 **V=800 m/min,** **fz=0.3 mm/rev*tooth,** **ap=3.0 mm**	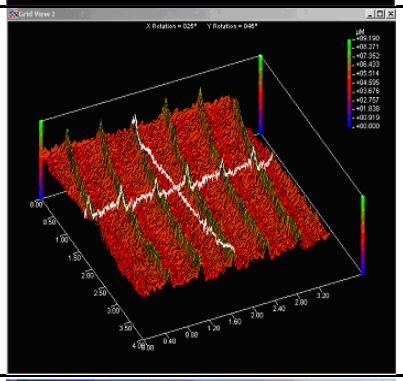	**16** **V=1000 m/min,** **fz=0.1 mm/rev*tooth,** **ap=4.0 mm**	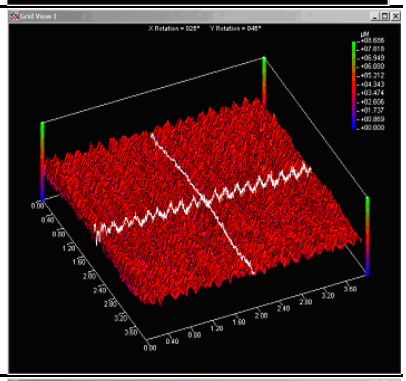
28 **V=1200 m/min,** **fz=0.1 mm/rev*tooth,** **ap=3.0 mm**	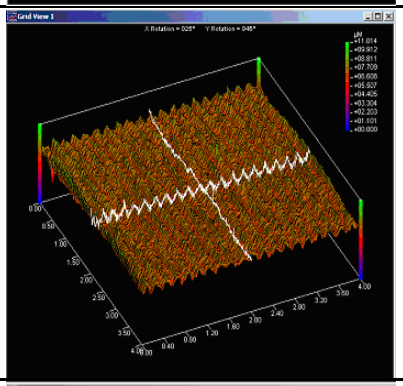	**31** **V=1400 m/min,** **fz=0.1 mm/rev*tooth,** **ap=3.5 mm**	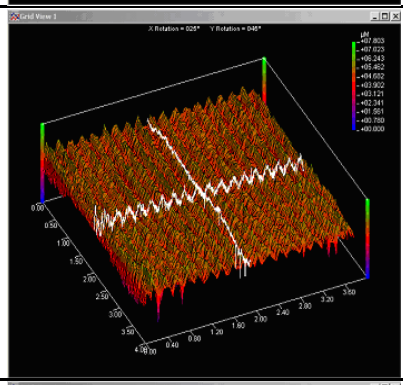
34 **V=1600 m/min,** **fz=0.1 mm/rev*tooth,** **ap=4.0 mm**	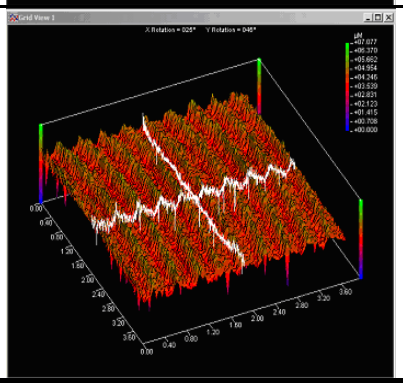	**35** **V=1600 m/min,** **fz=0.2 mm/rev*tooth,** **ap=3.0 mm**	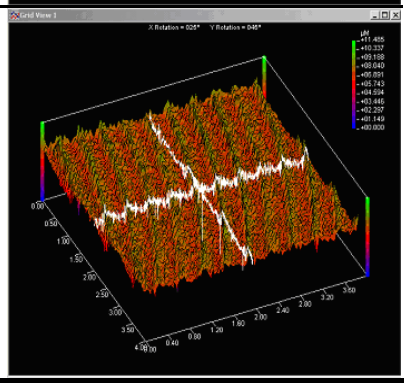

When analyzing Tables 5.9 and 5.10, where the surface topography obtained for few Al 7075-T7351 specimens, machined under different cutting conditions are presented, it is observed that, in general milling operations generate a surface texture that is essentially composed of periodic elements. All the studied topographies showed a periodic reflectance pattern indicating no tool deterioration during the machining process. This result is probably due to the fact that the cutting length was not big enough to wear the tool and also because a MQL was used during the process where a reduction of thermal shock were probably obtained, as the results conducted by Weinert et al. (2004) and Dhar et al. (2006). This last researcher obtained a significant reduction in tool wear rate and surface roughness when using MQL, mainly due to a reduction in the cutting zone temperature which improved the chip–tool interaction and maintained the sharpness of the cutting edge.

Also, it must be highlighted that Kang in 2005 concluded that when tool wear was present, a poor surface shape with a conspicuous lay structure was produced, and as observed from our results inconspicuous lay structure was obtained in our experiments when machining under the established studied conditions.

- **Microstructure analysis**

Figure 5.4 shows the original aluminium alloy 7075-T7351 microstructure (not machined). This microstructure will be used to compare the microstructure obtained in each specimen cut under different cutting conditions.

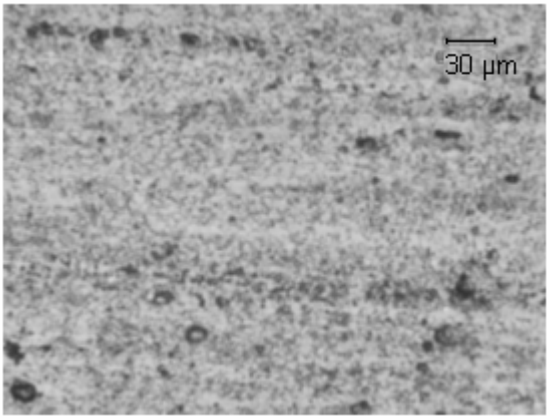

Figure 5.4- Original microstructure of the Al 7075 - T7351, 30µm. (not machined)

Tables 5.11 and 5.12 show the microstructure of few Al 7075-T7351 specimens machined under different cutting conditions with r = 0.8 mm and r = 2.5 mm respectively. Appendix B, Tables 6 and 7 show the rest of these results.

Table 5.11- Microstructure of a few Al 7075-T7351 specimens machined under different cutting conditions with r = 0.8 mm**.**

TRIAL	Cutting parameters	(30µm)	(20 µm)
2	V= 600 m/min fz = 0.2 mm/ rev x tooth ap = 3.5 mm	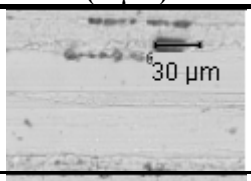	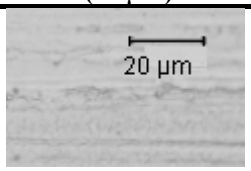
6	V= 800 m/min fz = 0.3 mm/ rev x tooth ap = 3.0 mm	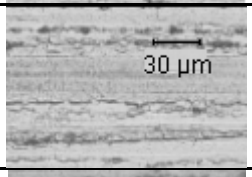	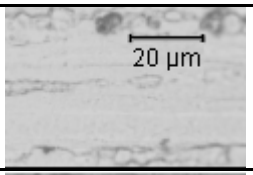
7	V= 1000 m/min fz = 0.1 mm/ rev x tooth ap = 4.0 mm	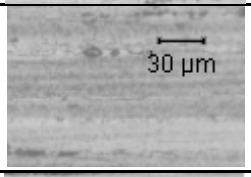	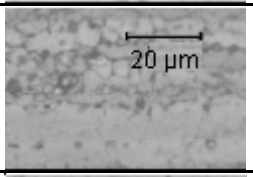
9	V= 1000 m/min fz = 0.3 mm/ rev x tooth ap = 3.5 mm	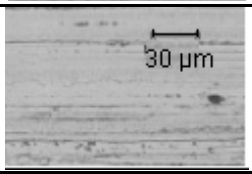	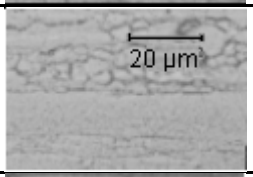
21	V= 1200 m/min fz = 0.3 mm/ rev x tooth ap = 4.0 mm	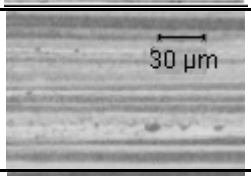	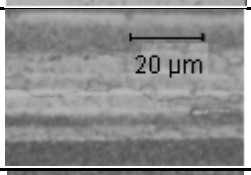
23	V= 1400 m/min fz = 0.2 mm/ rev x tooth ap = 4.0 mm	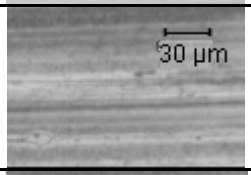	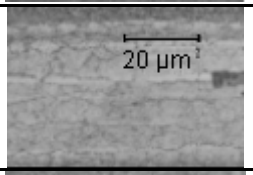
24	V= 1400 m/min fz= 0.3 mm/ rev x tooth ap = 3.0 mm	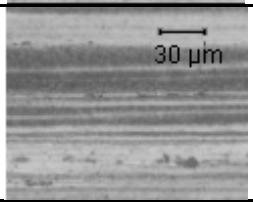	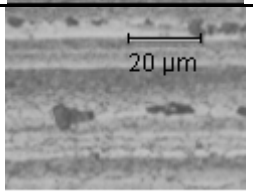
27	V= 1600 m/min fz = 0.3 mm/ rev x tooth ap = 3.5 mm	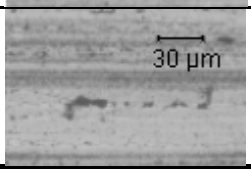	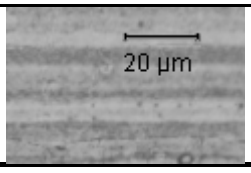

Table 5.12- Microstructure of a few Al 7075-T7351 specimens machined under different cutting conditions and r = 2.5 mm

TRIAL	Cutting parameters	(30µm)	(20 µm)
10	V= 600 m/min fz = 0.1 mm/ rev x tooth ap = 3.0 mm	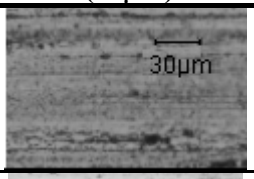	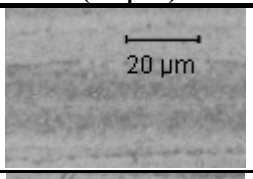
13	V= 800 m/min fz = 0.1 mm/ rev x tooth ap = 3.5 mm	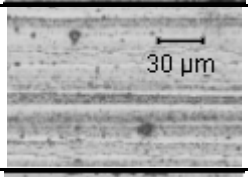	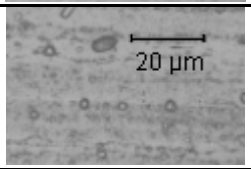
15	V= 800 m/min fz = 0.3 mm/ rev x tooth ap = 3.0 mm	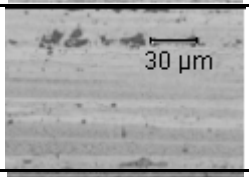	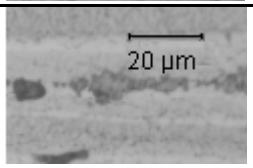
16	V= 1000 m/min fz = 0.1 mm/ rev x tooth ap = 4.0 mm	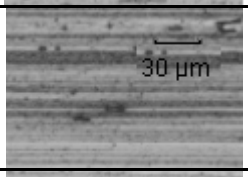	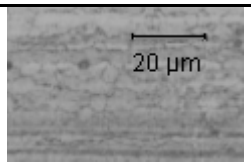
28	V= 1200 m/min fz = 0.1 mm/ rev x tooth ap = 3.0 mm	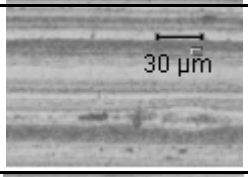	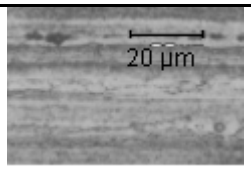
31	V= 1400 m/min fz = 0.1 mm/ rev x tooth ap = 3.5 mm	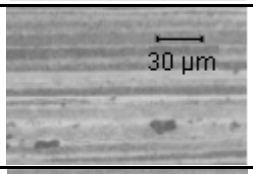	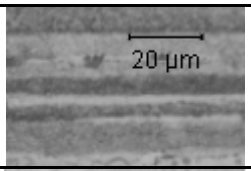
34	V= 1600 m/min fz = 0.1 mm/ rev x tooth ap = 4.0 mm	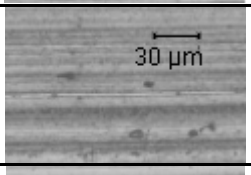	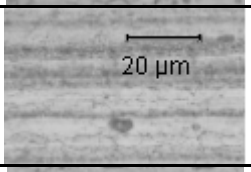
35	V= 1600 m/min fz = 0.2 mm/ rev x tooth ap = 3.0 mm	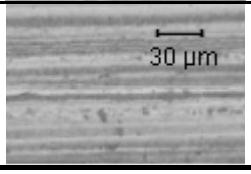	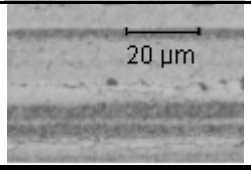

After analyzing each microstructure, it was observed that the grain structure near the machined surface is lined up consistent to the face milling direction. This is due to the plastic deformation the material has gone through due to the cutting process. The dislocations start to slip and if they find an obstacle (grain boundary, impurities, etc) they start to pile up producing an entanglement and an increase in shear stress. The increase of the shear stress causes an increase in the overall strength of the metal. No other considerable microstructure changes were noticed, probably due to the fact that the thermal conductivity of this material is 155 W/m ^{o}K. This factor helped to release the heat generated during the cutting process through the chip avoiding major changes in the surface microstructure of the workpiece. Finally, as previously stated this material offers good machinability, giving curled or easily broken chips with good to excellent surface finish.

- **Microhardness analysis**

Once the microstructure analysis was concluded, the microhardness tests were conducted and selected results are shown in Figure 5.5. When face milling aluminium alloy at V= 600 m/min, 800 m/min and 1000 m/min using a 0.8 mm tool nose radius, different feed per tooth and different axial depth of cut.

In this figure, the values of Vickers hardness obtained from the machined surface at the centre of the specimen are plotted. The first measurement was conducted 50μm from the machined surface up to 1000 μm and this distance is named D.

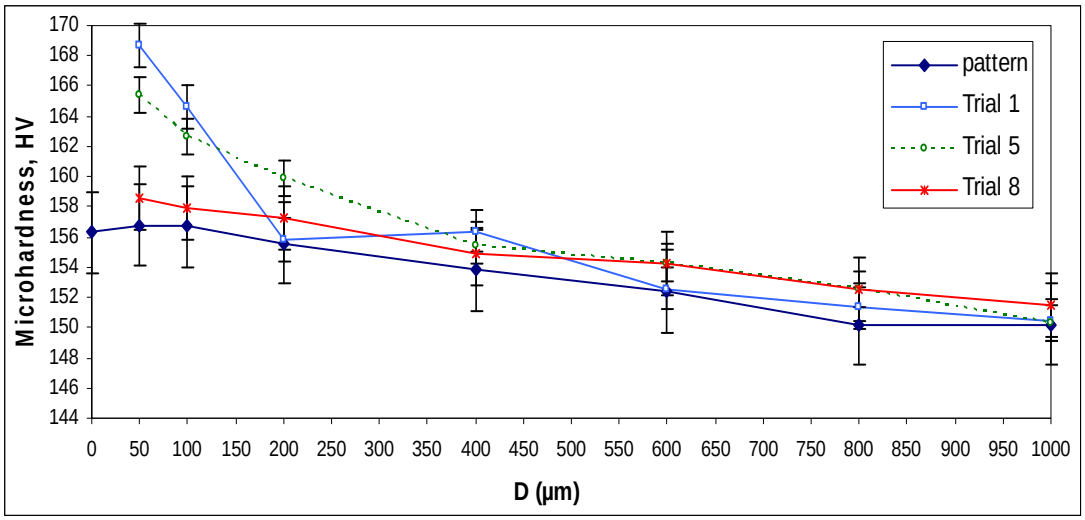

Figure 5.5- Vickers hardness (HV) vs. Distance from the machined surface towards the centre of the specimen (D) when face milling aluminium alloy at V= 600 m/min , 800 m/min and 1000 m/min using a 0.8 mm tool nose radius different feed per tooth and different axial depth of cut.

When analyzing the Figures 5.5, it can be observed that in general a higher value of microhardness was obtained near the machined surface, and is evaluated in more detail below. The result maintained constant for all the established conditions, and is probably due to an increase in surface deformation that ultimately leads to an increase in the workhardening of the machined surface dominated by plastic deformation, since no evidence of microstructure changes were observed.

In order to analyze the influence of the cutting speed, feed per tooth and the tool nose radius, different graphs were developed and presented in Figures 5.6, 5.7 and 5.8, respectively

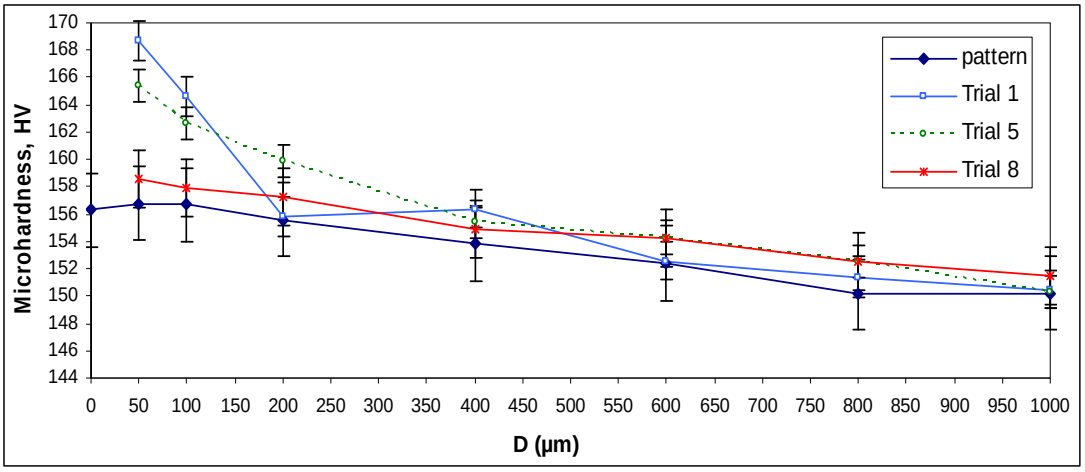

Figure 5.6- Vickers hardness (HV) vs. Distance from the machined surface towards the centre of the specimen (D) when face milling at a constant fz=0.1 mm/rev*tooth and r=0.8mm. Trial 4, V=800 m/min, ap=3.5 mm; Trial 19, V=1200 m/min, ap=3.0mm, Trial 25, V=1600 m/min, ap=4.0 mm

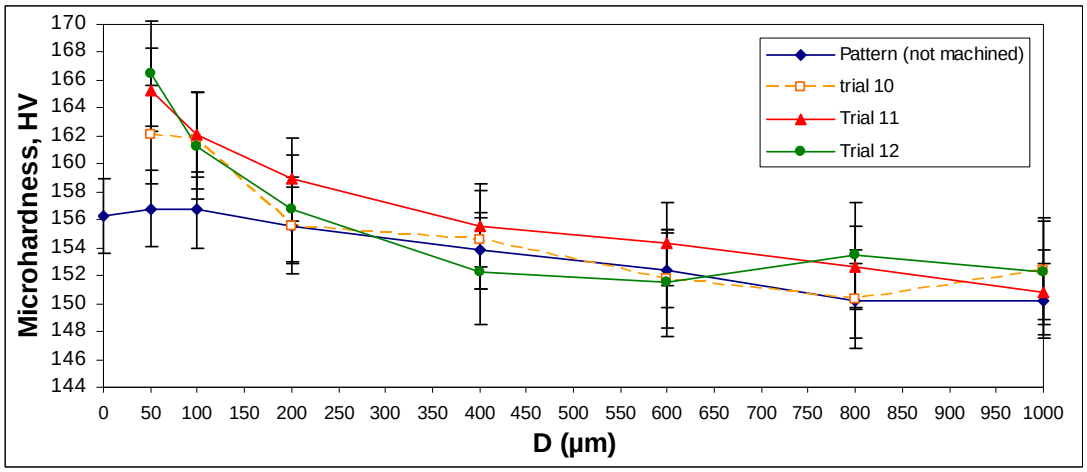

Figure 5.7- Vickers hardness (HV) vs. Distance from the machined surface towards the centre of the specimen (D) when face milling at a constant V=600 m/min and r= 2.5 mm. Trial 10, fz=0.1 mm/rev*tooth, ap= 3.0 mm, Trial 11, fz=0.2 mm/rev*tooth, ap= 3.5 mm, Trial 12 fz=0.3 mm/rev*tooth, ap= 4.0 mm.

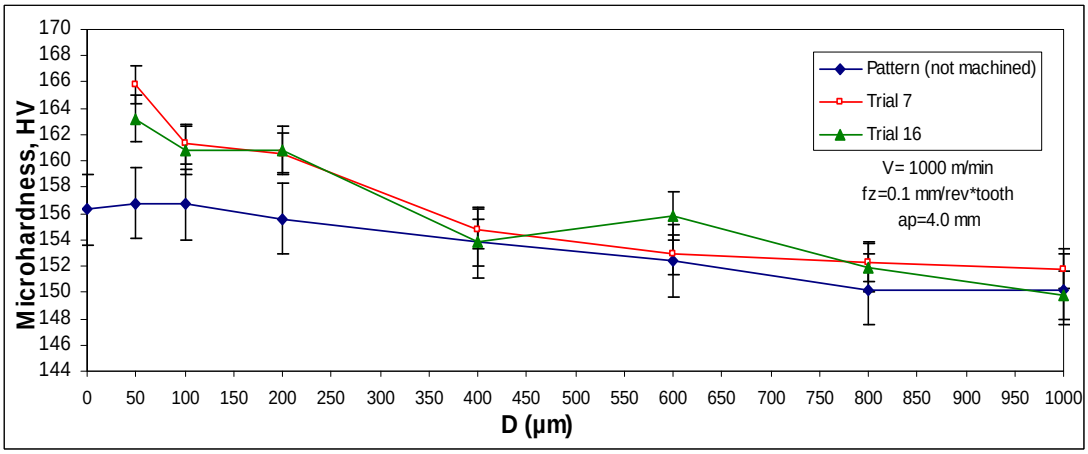

Figure 5.8- Vickers hardness (HV) vs. Distance from the machined surface towards the centre of the specimen (D) when face milling at a constant V=100 m/min and fz=0.1 mm/rev*tooth. Trial 7, r = 0.8mm and Trial 16, r = 2.5 mm.

When analyzing Figure 5.6, the influence of the cutting speed on the surface microhardness can be observed. In general, an increase of 30% of the cutting speed represents a decrease (3.0% – 4.0%) of the surface hardness. This is due to the fact that as the cutting speed is increased the chip has less contact time with the tool, producing probably a thermal softening in the cutting area (between the tool edge and the workpiece surface) potentially easing the plastic deformation of the chip.

When analyzing Figures 5.7 and 5.8, where the influence of the feed per tooth and the tool nose radius on the surface microhardness can be observed, it seems that when increasing the feed per tooth 100% an increase of 2.0% - 3.0% of the microhardness is observed, probably due to an increase in plastic deformation since more energy is required to remove the chip. With regard to the influence of the tool nose radius on the microhardness it is observed that as the tool nose radius is increased there is more contact length between the chip and the tool and the material is removed more softly producing a decrease in the microhardness of around 3%. With regards, the influence of the axial depth of cut on the surface microhardness a defined pattern was not observed. It must be highlighted that, even though the results show a small variation of surface microhardness when analyzing the influence of each cutting parameters, it is observed that in general the overall variation of microhardness when comparing it with the pattern sample (not machined) did not vary more than 12% due to work hardening effect. This result is in consistent and in agreement with Toh, 2004.

- **Chip morphology analysis**

The chips of each sample were collected after the face milling process in order to conduct the chip morphological study. In Tables 5.13 and 5.14 few chip samples of Al 7075-T7351 specimens machined under different cutting conditions with r = 0.8 mm and r = 2.5 mm respectively are presented. Appendix B, Tables 8 and 9 show the rest of these results.

As observed, the obtained chips are typical of milling processes and are defined as a stable and continuous chip because their shape and geometry agree well with the in-cut segment of the cutter in the stable process. Also it is observed that in general, the feed per tooth and the axial depth of cut has a strong influence on the chip size and that it is the cutting speed alone that is sufficient to give rise to the different mechanism of chip formation. These results are in agreement with previous research (Shouckry (1981), Ning (2001), Poulachon (2003), Fang (2003), Dabade (2003) and S_eref Aykut (2007)).

Also it was observed that the measurements showed that the chip width kept nearly constant along the chip length direction and that some chips showed a saw-tooth type shape, where even though the mechanisms of saw-tooth formation have not been well understood,. Some researchers have addressed this formation to surface crack propagation, (Guo 2004). Regarding this result, the trials that showed the chips with a little saw-tooth type shape were the ones where a feed per tooth of 0.3 mm/rev*tooth was used. This result is in agreement with results made by S_eref Aykut, (2007).

Table 5.13- Chip morphology obtained in few AL 7075- T3751 specimens machined under different cutting conditions with r=0.8 mm

Trial	Cutting parameter	Cw (mm)	Ct (mm)	Cross-sectional area (mm^2)	9X magnifier
2	V= 600 m/min fz= 0.2 mm/rev*tooth ap= 3.5 mm	3.4	0.22	0.748	
6	V= 800 m/min fz= 0.3 mm/rev*tooth ap= 3.0 mm	3.1	0.3	0.930	
7	V= 1000 m/min fz= 0.1 mm/rev*tooth ap= 4.0 mm	4.0	0.12	0.480	
9	V= 1000 m/min fz= 0.3 mm/rev*tooth ap= 3.5 mm	3.4	0.28	0.952	
21	V= 1200 m/min fz= 0.3 mm/rev*tooth ap= 4.0 mm	4.0	0.31	1.240	
23	V= 1400 m/min fz= 0.2 mm/rev*tooth ap= 4.0 mm	3.9	0.18	0.702	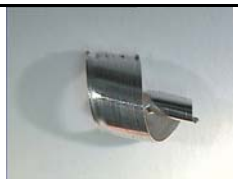
24	V= 1400 m/min fz= 0.3 mm/rev*tooth ap= 3.0 mm	3.1	0.22	0.682	
27	V= 1600 m/min fz= 0.3 mm/rev*tooth ap= 3.5 mm	3.5	0.31	1.085	

Table 5.14- Chip morphology obtained in AL 7075- T3751 specimens cut under different cutting conditions with r=2.5 mm

Trial	Cutting parameter	Cw (mm)	Ct (mm)	Cross-sectional area (mm^2)	9X magnifier
10	V= 600 m/min fz= 0.1 mm/rev*tooth ap= 3.0 mm	3.0	0.2	0.600	
13	V= 800 m/min fz= 0.1 mm/rev*tooth ap= 3.5 mm	3.5	0.22	0.770	
15	V= 800 m/min fz= 0.3 m/rev*tooth ap= 3.0 mm	3.0	0.22	0.660	
16	V= 1000 m/min fz=0.1mm/rev*tooth ap= 4.0 mm	3.8	0.18	0.684	
28	V= 1200 m/min fz= 0.1 mm/rev*tooth ap= 3.0 mm	3.0	0.11	0.330	
31	V= 1400 m/min fz= 0.1 mm/ rev*tooth ap= 3.5 mm	3.5	0.12	0.420	
34	V= 1600 m/min fz= 0.1 mm/rev*tooth ap= 4.0 mm	4.0	0.14	0.560	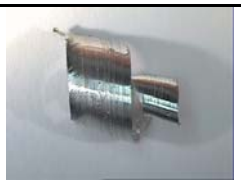
35	V= 1600 m/min fz= 0.2 mm/rev*tooth ap= 3.0 mm	3.0	0.21	0.630	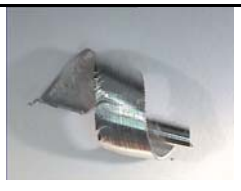

This type of chip (continuous chip) is attributed to the shearing process, which is dependent on the geometry of the cutter.

The shearing process begins when the cutting edge starts to penetrate the workpiece and the primary deformation zone moves accordingly to the cutter rotation. The chip starts to slide over the rake face angle as it is formed and curled. This shearing process finishes when the created chip is shaved away and the curling of the chip stops at the same time when the tooth leaves the workpiece.

During the milling process, a large amount of the cutting heat is transfered to the chips, where it is observed that the chip becomes curlier as observed in the case of chips cut at higher cutting speed. This result is observed when comparing chips obtained from trial 11 and trial 35 as shown in Table 5.15. In addition, it must be highlighted that no other significant variation regarding chip morphology was found when varying the cutting speed, since this material offers good machinability (110%).

Table 5.15- Comparison between chip geometry corresponding to specimens 11 and 35 cut with different cutting speed

Trial	Cutting parameter	9X magnifier
		
11	V= 600 m/min fz= 0.2 mm/rev*tooth ap= 3.5 mm	
35	V= 1600 m/min fz= 0.2 mm/rev*tooth ap= 3.0 mm	

Regarding the changes on the chip size, it is observed that when increasing the axial depth of cut and the feed per tooth a higher cross sectional area was obtained. Table 5.16 shows a comparison between the chips obtained from trials 28 and 30 were the axial depth of cut and the feed per tooth are increased. These results are in

agreement with the research made by Shouckry (1981), Ning (2001), Poulachon (2003), Fang (2003), Dabade (2003) and S_eref Aykut (2007).

Table 5.16- Comparison between chip geometry corresponding to specimens 28 and 30 cut with r=0.8 mm, different axial depth of cut and feed per tooth

Trial	Cutting parameter	9X magnifier
		
28	V= 1200 m/min fz= 0.1 mm/rev*tooth ap= 3.0 mm	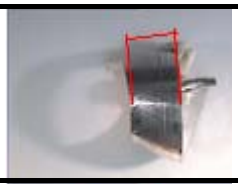
30	V= 1200 m/min fz= 0.3 mm/rev*tooth ap= 4.0 mm	

With regard to the influence of the tool nose radius, it was observed that a curlier chip was obtained when cutting with a smaller tool nose radius, since when a larger tool nose radius was used there is a greater contact length between the chip and the tool and the material is removed more softly. This result is presented in Table 5.17, where a comparison between the chip of trial 6 and 15 and trial 25 and 36 is presented.

Table 5.17- Comparison between chip geometry corresponding to specimens cut with a different tool nose radius

Cutting parameters / r (mm)	V= 800 m/min fz= 0.3 mm/rev*tooth ap= 3.0 mm (9X magnifier)	V= 1600 m/min fz= 0.1 mm/rev*tooth ap= 4.0 mm (9X magnifier)
0.8		
2.5		

5.4 Influence of the cutting parameters on the surface roughness and the optimal combination of cutting parameters in order to achieve a smooth surface.

In order to know the influence of each cutting parameter on the surface roughness, the S/N ratio smaller-the-best formula was applied. From these results the best combination of cutting parameters can be obtained in order to achieve a smooth surface.

5.4.1 Results and analysis of results

Once all the experiments were conducted Figure 5.9 shows the influence of each cutting parameter on the surface roughness once applying the S/N ratio smaller-the-best formula. As previously stated Appendix B, Table 1 presents the surface

roughness value, Ra (experimental average of surface roughness) obtained when cutting each specimens under different cutting conditions.

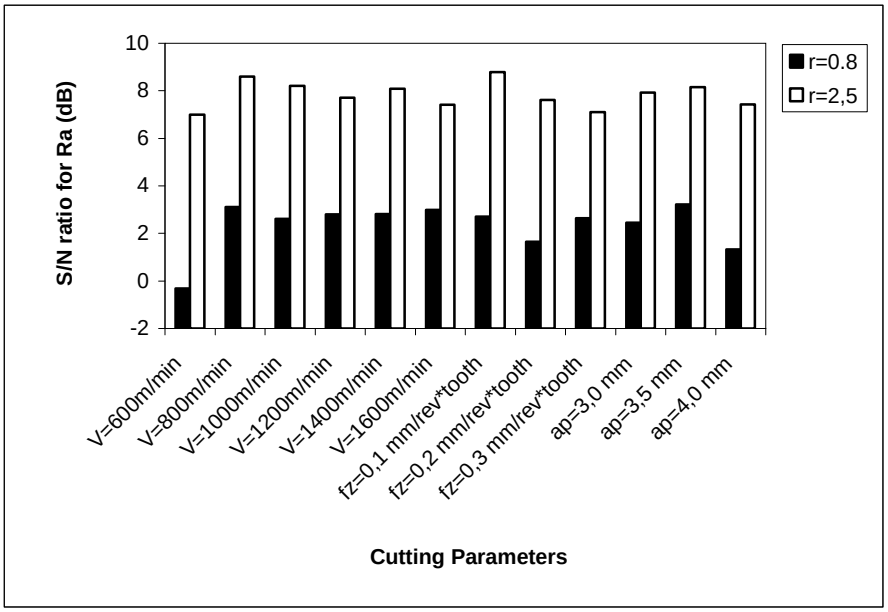

Figure 5.9- S/N ratio for Ra for the different cutting parameters when face milling Al 7075-T7351

As observed in Figure 5.9 in general, a better surface roughness was obtained when face milling with a big tool nose radius (r = 2.5 mm). This is due to the fact that smaller peacks are formed reducing the height of the surface roughness profile. This result is in agreement with the research made by Petropoulos (1973).

When analyzing the influence of the cutting speed on the surface roughness it is observed that a rougher surface was obtained when cutting at V=600 m/min, being more noticeable when using a tool nose radius of 0.8 mm. The optimal cutting speed in order to achieve a smooth surface is obtained when using V= 800 m/min for both tool nose radius. Cutting speeds higher than 800 m/min seem to have a stable behavior and this is probably due to the fact that at low cutting speeds the built up edge phenomenon was presented and then suppressed when increasing the cutting speed. This result is consistant with previous research such as Koshy (2002), Mansour (2002), Korkut (2004) and Rashad (2006).

This trend was also expected, because as the cutting speed increases the heat generated in the shear zone cannot be conducted away during the very short interval of time in which the material passes through this zone. Therefore, the temperature rise softens the material aiding grain boundary dislocation and thus reducing the surface roughness. Also the result of getting a better surface roughness when increasing the cutting speed can be explained in terms of the velocity of the chips, which is faster at higher cutting speeds, leading the chip being in contact with the newly formed surface of the workpiece for a shorter time (Ghani, 2004).

Regarding the influence of the feed per tooth on the surface roughness, it is observed that by using high values of feed per tooth a rougher surface is obtained, especially when using a r= 0.8 mm. This is due to the fact that the maximum chip thickness is increased, producing an increase of the cutting forces and thereby an increase of the surface roughness. This result is in agreement with research made by Koshy (2002), Mansour (2002), Korkut (2004) and Rashad (2006).

When using a tool nose radius of 0.8 mm it is noticed that the best roughness is obtained not only when using the smaller feed per tooth (fz= 0.1 mm/rev* tooth) but also when using the highest value of feed per tooth (fz=0.3 mm/rev*tooth). This result could be attributed to the so called “size effect”, which manifests as a rise in the specific cutting pressure or in energy per unit volume with a decrease in the underformed chip thickness. This result is in agreement with the research made by Petropoulos (1973).

With respect to the influence of the axial depth of cut on the surface roughness, a established behaviour was not observed, although it is observed that when using a tool nose radius of 2.5 mm the influence of axial depth of cut is negligible when comparing the influence of the other cutting parameters on the surface roughness and that a better result is obtained when using an axial depth of cut of 3.5 mm. This result can be also explained with the help of a model for surface irregularities shown in Figure 5.10. As evident from the model, when the selected depth of cut is larger than the tool nose radius, this does not contribute directly to the change in height of surface irregularities.

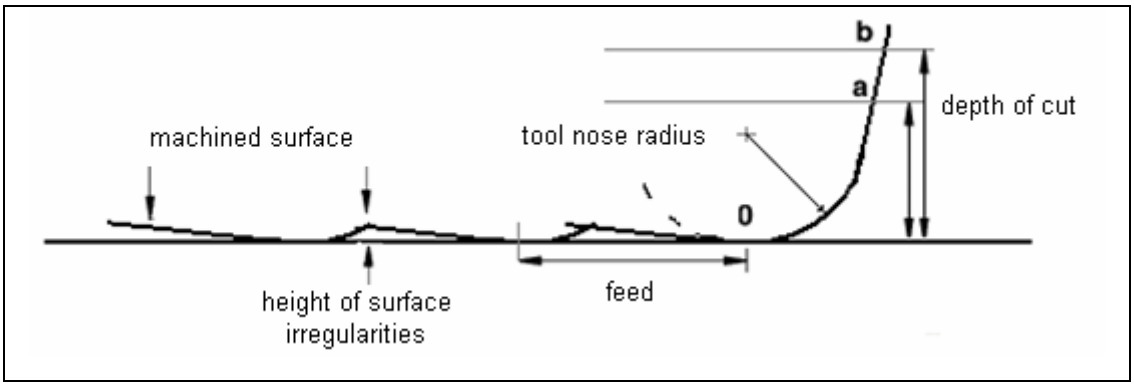

Figure 5.10- Model to represent the effect of the depth of cut on the surface irregularities.

From these results it seems that the optimal combination of cutting parameters in order to achieve a smooth surface is: V= 800 m/min, fz= 0.1 mm/rev*tooth, ap= 3.5 mm and r= 2.5 mm.

In order to know the percentage of contribution of each studied variable on the surface roughness, the Pareto ANOVA, which is a simplified ANOVA method which uses Pareto principles, was applied. This Pareto ANOVA technique requires the least knowledge about the ANOVA method and is suitable for engineers and industrial practitioners.

Table 5.18, shows the Pareto ANOVA analysis for surface roughness under the studied conditions and Figure 5.11 shows the Pareto ANOVA diagram.

Table 5.18- Pareto ANOVA analysis for surface roughness.

Surface roughness addition of each factor level	Factor			
	r	**V**	**fz**	**ap**
1	13.65	4.56	5.67	6.704
2	7.37	3.28	7.49	7.096
3	0	3.11	7.86	7.22
4	0	3.33	0	0
5	0	3.24	0	0
6	0	3.5	0	0
Square difference Addition (TG)	39.44	14.72	14.70	0.84
Contribution ratio (%)	69.80	14.72	14.70	0.78

Pareto Diagram

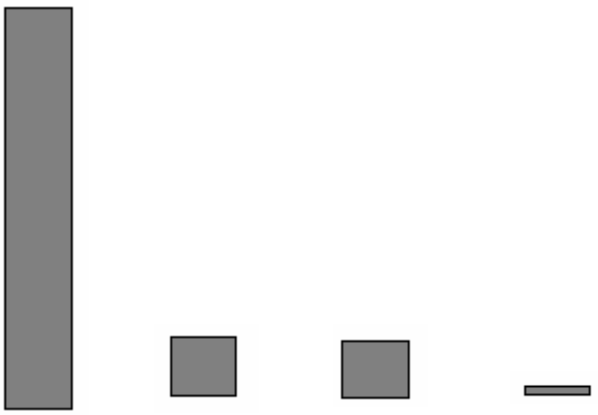

Cutting parameter	**r**	**V**	**fz**	**ap**
Contribution ratio (%)	69.80	14.72	14.70	0.78
Cumulative contribution (%)	69.80	84.52	99.22	100

Figure 5.11- Pareto ANOVA diagram for AL 7075-T7351 machined under different cutting conditions.

As observed the variable with most influence on the surface roughness is the tool nose radius, followed by the cutting speed, the feed per tooth with a similar contribution and finally with a negligible influence the axial depth of cut.

5.5 Scientific Area 2: Influence of the cutting parameters on the workpiece and tool vibration

As observed from Figure 5.1 the measurement of the machine-tool vibrations were conducted during the milling process. As previously stated, this study was conducted in order to develop knowledge related to how much this variable affects the resultant surface under the studied cutting conditions and indeed, if it needs to be included in the development of the models for surface roughness prediction, since from previous research, it was observed that vibrations degrade the surface finish, (Lin and Chang, 2007, Surman 2008).

5.5.1. Experimental set-up for vibrations data collection

During the milling process, the vibration data was collected employing two accelerometers, Model EGA-F±5/LOIMIR, sensitive 3.97mV/g with a response frequency of 3500 Hz. The accelerometer is a device to detect magnitude and direction of the acceleration as a vector quantity, and can be used to sense orientation, vibration and shock.

One accelerometer was located in the spindle in order to sense the spindle vibrations and the other accelerometer was located on the vice that was holding the workpiece, in order to register the workpiece vibration (in/out direction), both accelerometers were attached to the spindle and th vice with glue (Araldite Hardener). Also, a key phasor or proximity switch was used to identify the beginning of each revolution (spindle's RPM) as well as a phase signal reference. In Figure 5.12 a scheme of the experimental set-up for the rotation and vibration data collection can be observed.

In order to avoid the impact of the tool entering the workpiece, the vibration data was collected around the centre of the workpiece, (80 mm away from the workpiece edge towards the centre of the workpiece). The data was connected to an analog-to-digital (A/D) amplified board (this is to convert the analog signals to a digital

domain) and then transmitted to a personal computer for further processing and analyzing using, HP VEE version 5.0 software. The collection time for each run was about 3 sec at 2000 Hz (sampling frequency), since the enter frequency band was from 99.5 Hz-265 Hz.

The vibration data collected by each accelerometer in this experiment were discrete values which resulted from the machine-tool–workpiece system vibration during the cutting process. From these values, the RMS acceleration was calculated. In order to analyze the influence of each cutting parameter on the spindle and workpiece vibration the S/N ratio smaller-the-best formula was applied.

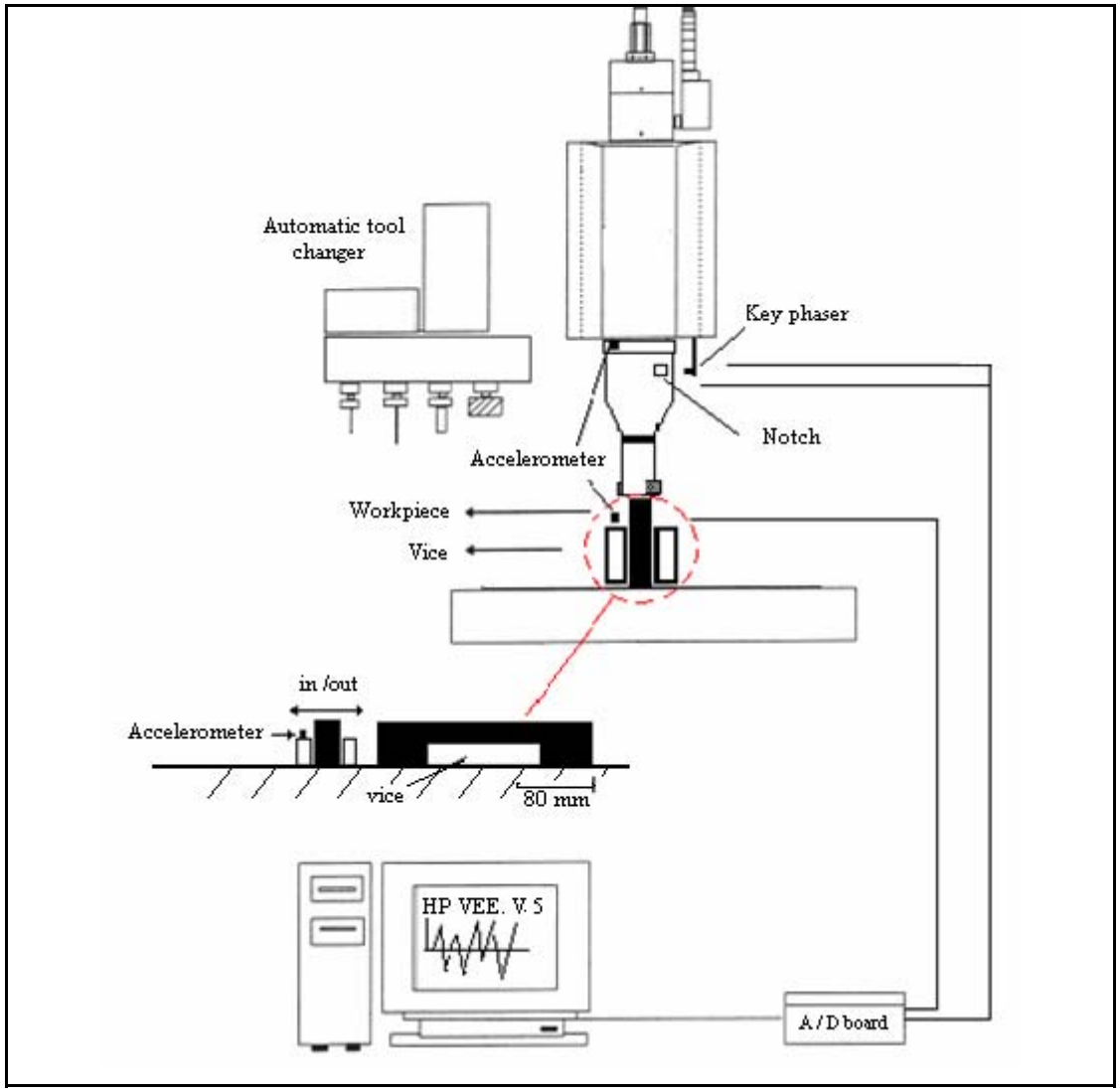

Figure 5.12- Scheme of the experimental set up for vibration data collection.

5.5.2. Results and analysis.

Once the machining process was completed, the following results were obtained. Only a few examples will be presented since a similar behaviour was obtained for each of the cases. In Figure 5.13 and Figure 5.14, an example of the vibration data collected for Trials 23 and 29 respectively can be observed. In these Figures, the voltage value against the time is presented for the spindle, the workpiece (in/out direction) and the key phasor.

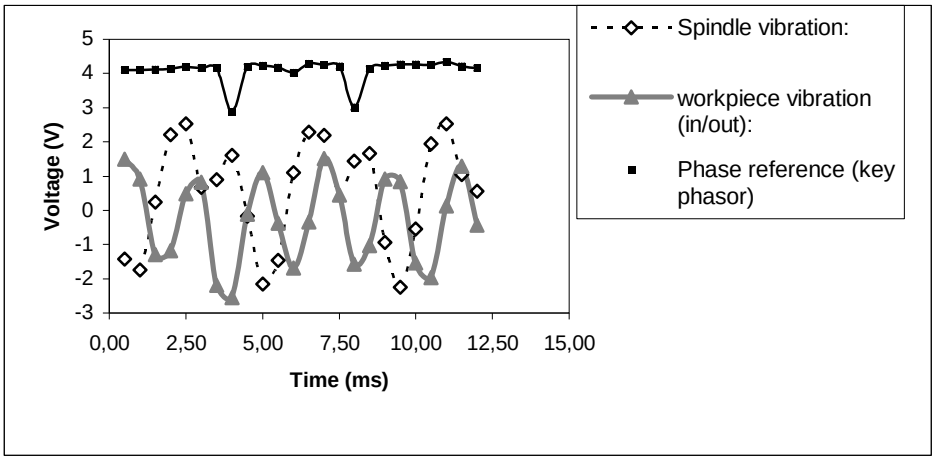

Figure 5.13- Voltage vs. time for trial 23 (V= 1400 m/min fz= 0.2 mm/rev*tooth ap= 4.0 mm, r= 0.8 mm) **a)** spindle and workpiece vibration, **b)** spindle rotation.

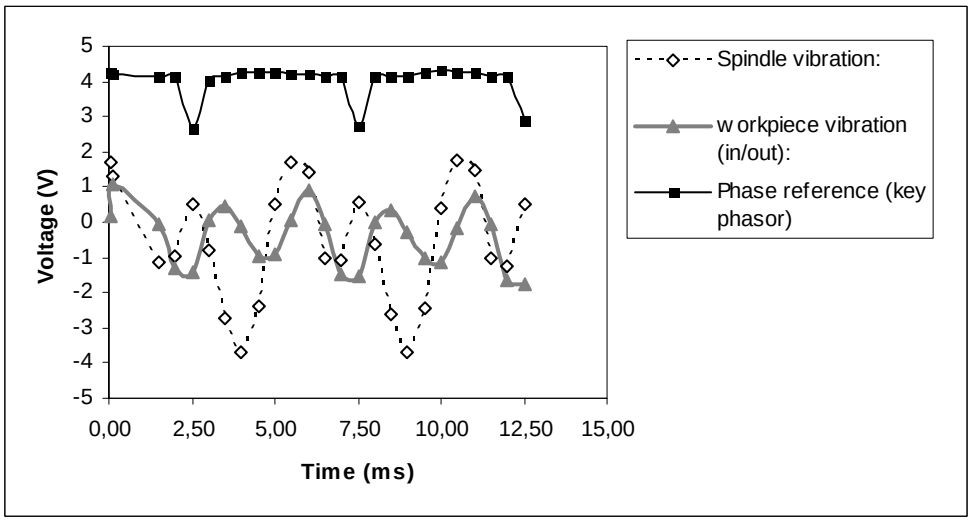

Figure 5.14- Voltage vs. time trial 29 (V= 1200 m/min fz= 0.2 mm/rev*tooth ap= 3.5 mm, r=2.5 mm) **a)** spindle and workpiece vibration, **b)** spindle rotation.

Figures 5.13 and 5.14 show similar behaviour regarding the signals shape. The key phasor signal shows the spindle rotation, where the pulse is observed when the magnetic tip passes over the notch on the spindle. This signal allows the measurement of the spindle rotational velocity and can also be used as a phase reference to the acceleration signals.

With regard to the vibration data obtained from the spindle and the workpiece, once again a constant behaviour is obtained when analyzing each of these curves. When observing the spindle vibrations, the peaks appear twice each revolution as well as in the workpiece (since two teeth are involve in the cutting process), but in this last one there is a phase lag. It must be highlighted that in most cases there is an out of phase between an excitation and an answer. This is like a "reaction time" that it needs to be transcured between a stimulus and its answer and it can be noticed that if the spindle vibration curve is moved towards the workpiece vibration curve both behaviours are similar. This result remained constant for all the established conditions.

- **Influence of the cutting parameters on the spindle and the workpiece vibration.**

Once the time vibration data from the spindle and the workpiece was collected the values were processed through a FFT (Fast Fourier Transform) using the MathCad software version 14 in order to obtain the signal spectrum of each trial.

The FFT uses the amplitude vs. time and transforme it to amplitude vs. frequency, since a vibration signal in the time domain is composed of many "simple signals" at different frequencies. When changing the signal under the time domain to the frequency domain, then the "simple signals" that composed the vibration signals are very welll identified. In addition, the contribution or the weight of each simple signal can be obtained.

Tables 5.19 and 5.20 show a few example of FFT spectra obtained in different trials as well as the RMS acceleration vibration amplitude when machining with r=0.8 mm and r=2.5 mm respectively.

Table 5.19- Few examples of FFT signal spectrum and RMS acceleration vibration amplitude of the spindle obtained during the face milling of a few Al 7075-T7351 specimens machined under different cutting conditions and r=0.8 mm.

Trial	RMS (g)	FFT signal spectrum
6 V= 800 m/min, fz= 0.3,rev*tooth ap= 3.0 mm , n*= 7958 rpm (132.6 Hz)	0.094	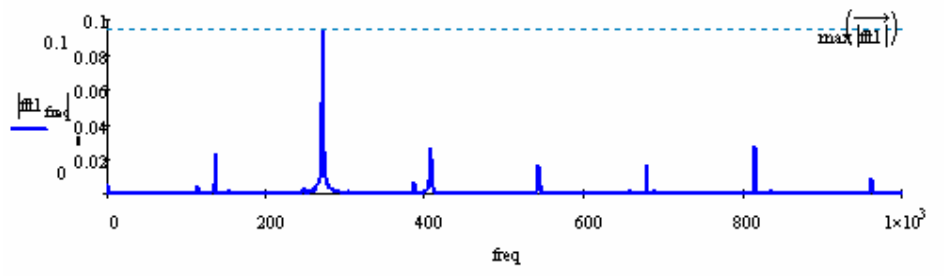
23 V= 1400 m/min, fz= 0.2 mm/rev*tooth ap= 4.0 mm, n= 13926 rpm (232 Hz)	0.384	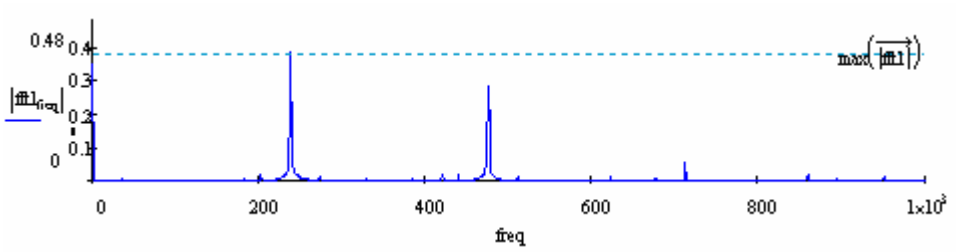

Table 5.20- Few examples of FFT signal spectrum and RMS acceleration vibration amplitude of the spindle obtained during the face milling of a few Al 7075-T7351specimens machined under different cutting conditions and r=2.5 mm

Trial	RMS (g)	FFT signal spectrum
13 V= 800 m/min, fz= 0.1 mm/ rev*tooth ap= 3.5 mm,n*= 7958 rpm, (132.6 Hz)	0.037	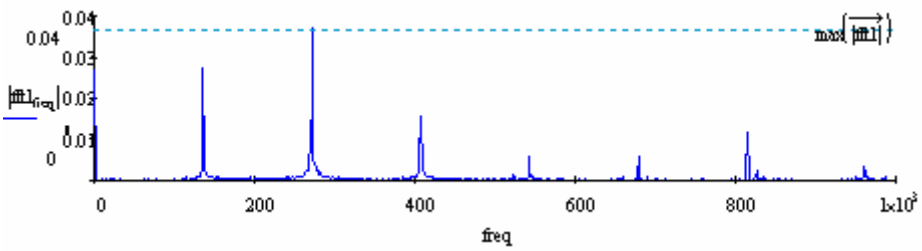
16 V= 1000 m/min, fz= 0.1 mm/rev*tooth ap= 4.0 mm, n*= 9947 rpm, (165.8 Hz)	0.017	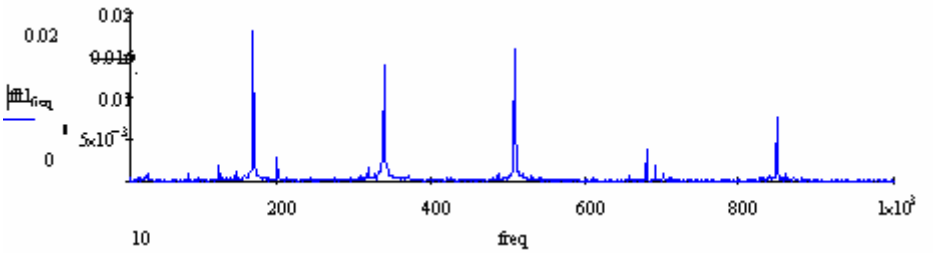

From each of the FFT signal spectra shown in Tables 5.19 and 5.20, the vibration coming from the rotating parts of the machine-tool equipment can be observed. Each of these sets is at different frequencies, and this is explained with the peaks observed in each spectrum, where they appear in an exact fraction of the spindle speed. It is also observed that in general all the FFT signal spectrums presented a harmonic behaviour, where no irregularities pointed to possible gear wear or loosing of machine parts that in turn could influence the surface roughness. As stated in the

literature review, Chapter 3, section 3.2.7, any distortion presented in the signal spectrum is indicative of irregularities in the tool-machine equipment.

In order to analyze how much influence each trial (specific combination of cutting parameters) has on the spindle RMS acceleration, the S/N ratio for the RMS acceleration of the spindle was calculated based on the smaller-the-best formula. The lower the vibration on the spindle, the smaller the influence of this variable on the machined surface. Figure 5.15 shows the influence of each trial on the S/N ratio for RMS acceleration of the spindle when milling under different cutting conditions.

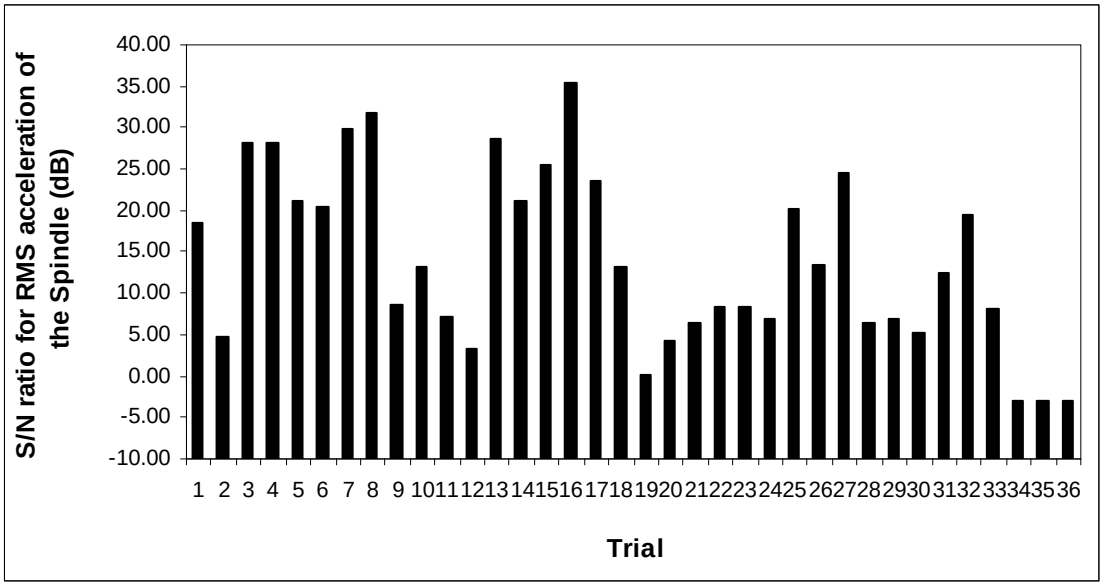

Figure 5.15- S/N ratio for RMS acceleration of the spindle for each trial cut under different cutting conditions when face milling Al 7075-T7351.

Figure 5.15, shows that trial 16 (V= 1000 m/min, fz=0.1mm/rev*tooth, ap= 4.0 mm and r=2.5 mm) gave the lowest RMS acceleration of the spindle and the highest RMS acceleration was obtained when using trial 35 cutting conditions combination (V=1600 m/min, fz=0.2mm/rev*tooth, ap= 3.0 mm and r=2.5mm). It must be highlighted that an increase in the spindle rotation does not necessarily produce an increase on the spindle's vibrations, since the response of a mechanical system is not linear. There are modal frequencies where the equipment will vibrate excessively but far away from these frequencies the vibrations will decrease almost immediately.

In order to analyze the influence of the workpiece vibrations (in/out direction) on the machined surface, the same study was conducted and a few of the results are observed in Tables 5.21 and 5.22. Here the FFT signal spectra obtained for each trial

cut with r=0.8 mm and r=2.5 mm respectively is presented. Also the influence of each trial on the RMS acceleration of the workpiece is observed in Figure 5.15.

Table 5.21- Few examples of FFT signal spectrum and RMS acceleration vibration amplitude of the workpiece obtained during the face milling of few Al 7075-T7351specimens machined under different cutting conditions and r=0.8 mm

Trial	RMS (g)	FFT signal spectrum
6 V= 800 m/min, fz= 0.3 mm/rev*tooth ap= 3.0 mm, n*= 7958 (132.6 Hz)	0.679	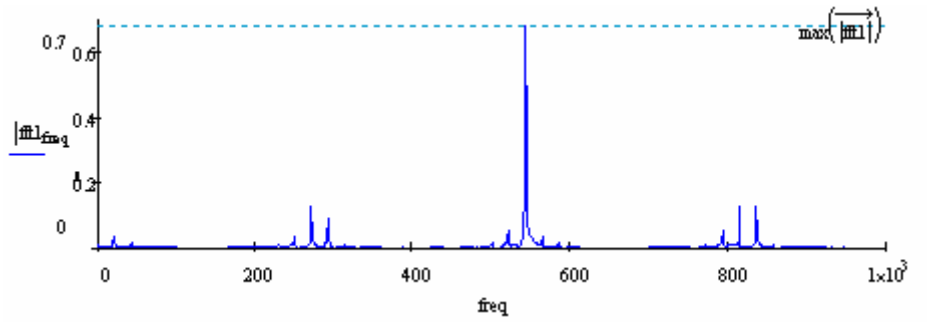
23 V= 1400 m/min, fz= 0.2 m/rev*tooth ap=4.0mm, n*= 13926 rpm, (232 Hz)	0.671	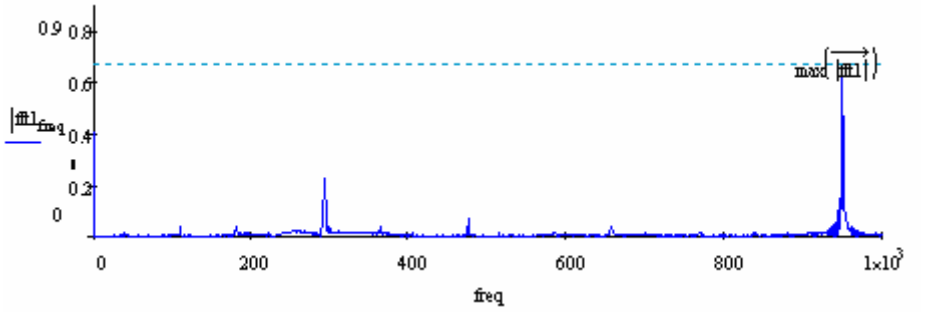

Table 5.22- Few examples of FFT signal spectrum and RMS acceleration vibration amplitude of the workpiece obtained during the face milling of few Al 7075-T7351 specimens machined under different cutting conditions and r=2.5 mm

Trial	RMS (g)	FFT signal spectrum
13 V= 800 m/min fz= 0.1 mm/ rev*tooth ap= 3.5 mm, n*= 7958 rpm, (132.6 Hz)	0.310	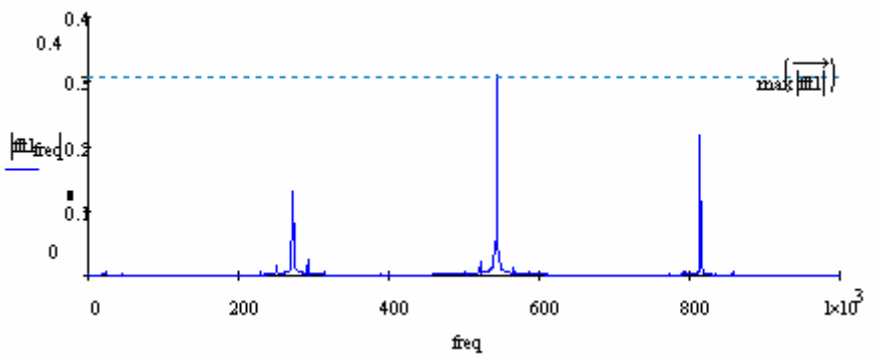
16 V= 1000 m/min, fz= 0.1 mm/rev*tooth ap= 4.0 mm, n*= 9947 rpm, (165.8 Hz)	0.018	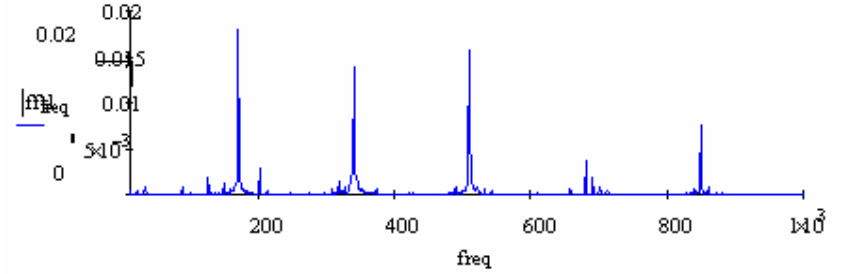

Once again, in general, all FFT signal spectra show the same harmonic behavior. This statement is supported by the fact that, during the study, the tool-machine equipment run in perfect shape-as it was expected. It is important to remark that the HSM machine used for this study was practically new, with few working/runnig

hours. There is no evidence of wear on internal gears or on other functional pieces in the signal under the frequency domain (FFT spectra).

In order to know how much influence each trial has on the RMS acceleration, the S/N ratio for the RMS of the workpiece was calculated based on the smaller- the-best formula, since the less the vibration the smaller the influence on the machined surface. The results are shown in Figure 5.16.

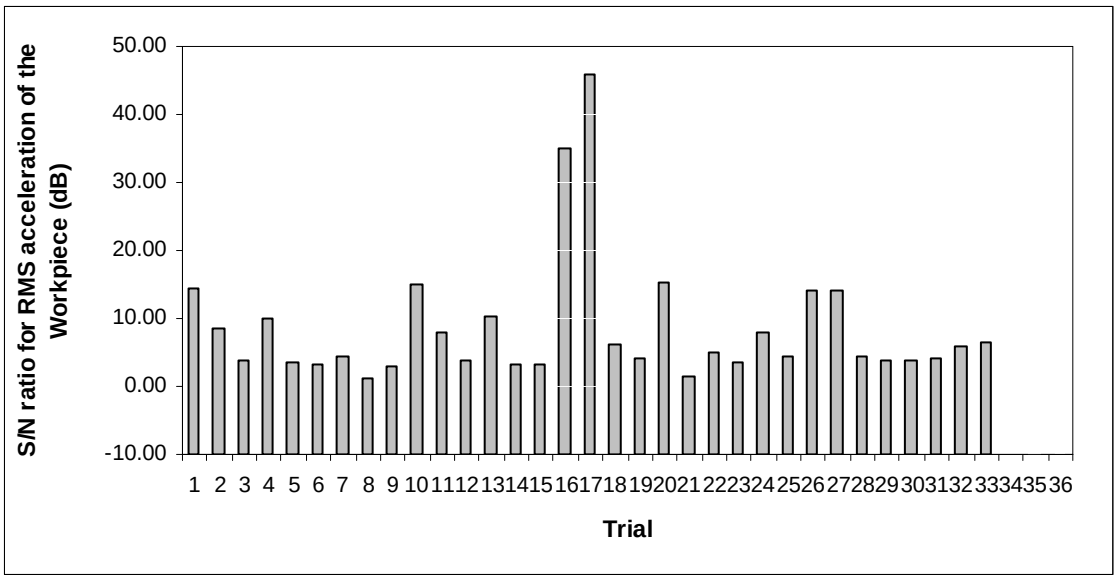

Figure 5.16- S/N ratio for RMS acceleration of the workpiece for each trial cut under different cutting conditions when face milling Al 7075-T7351

When analyzing the behaviour of each trial on the RMS acceleration of the workpiece it can be observed that trial 17 (V= 1000 m/min, fz=0.2 mm/rev*tooth, ap= 3.0 mm and r=2.5 mm) gave the smaller vibrations on the workpiece (higher S/N).

In order to analyze the influence of each cutting parameter on the spindle and on the workpiece vibrations, the S/N ratio smaller-the-best formula was also applied and the results can be observed in Figure 5.17.

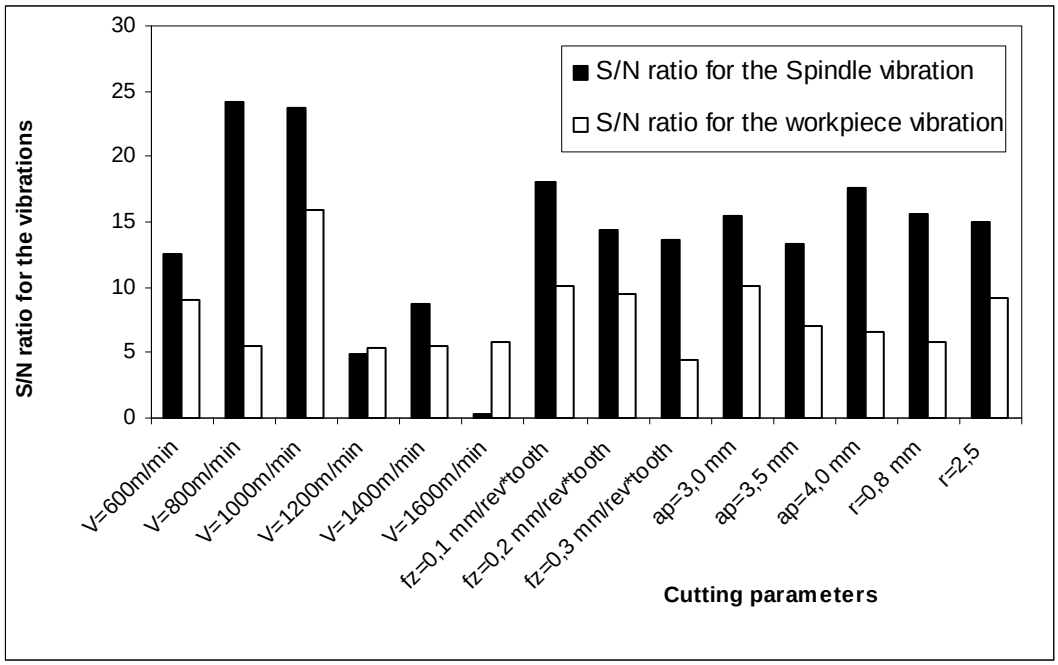

Figure 5.17- S/N ratio for RMS (spindle and workpiece) for different cutting parameters when face milling Al 7075-T7351

In Figure 5.17, the influence of the cutting speed on the spindle RMS acceleration can be observed. There is a reduction on the RMS acceleration when increasing the cutting speed from 600 m/min to 800 m/min where this last value seems to be the optimal value for a smaller RMS acceleration. Above V= 800 m/min it shows that the tendency varies and a defined pattern is not obtained. This result was expected since this type of behaviour (high and low values of vibrations) is typical in systems with multiple degrees of freedom (such as the HSM centre), where the modal frequencies are often presented. (See Chapter 3, section 3.2.9)

With regard to the influence of the feed per tooth on the RMS acceleration, it is observed that as this value increases higher values of RMS are obtained. This result is due to the fact that a higher amount of material is being removed from the workpiece increasing the cutting forces during the milling process.

With respect to the influence of the axial depth of cut on the RMS acceleration of the spindle, an established behaviour was not observed, although it seems that a smaller RMS acceleration is obtained when using ap= 4.0 mm. With regard to the influence of this variable on the RMS acceleration of the workpiece, it can be observed that as the axial depth of cut is increased, higher values of the RMS

acceleration are obtained. This result was expected due to the fact that the axial depth of cut is related to the chip cross sectional area where as this variable is increased a higher amount of material is being removed from the workpiece, increasing the cutting forces during the milling operation. However, as there is not a consistant relationship between RMS and the cutting parameters it is believed that the RMS is a weak tool for such analysis. Although the FFT is a very useful tool to identify any equipment problem.

When analyzing the influence of the tool nose radius on the RMS acceleration of the spindle, the results demonstrate that this variable has a negligible influence. However, when analyzing its influence on the RMS acceleration of the workpiece, it seems that a smaller vibration is obtained when using r=2.5 mm. This result can be associated with the fact that a better surface roughness is obtained when using a bigger tool nose radius since the surface contact between the tool nose radius and the workpiece is increased.

Finally, these results show that the variable that has most influence on the RMS acceleration of the spindle and the workpiece is the cutting speed, followed by the feed per tooth, the axial depth of cut and finally the tool nose radius. This result is in agreement with previous research (Tsai, 1999).

In Table 5.23 the optimal combination of cutting parameters for a lower RMS acceleration (lower vibrations) of the spindle and the workpiece are presented.

Table 5.23- Optimal cutting parameters in order to achieve low vibrations during the milling process of Al 7075-T7351

	V (m/min)	fz (mm/rev*tooth)	ap (mm)	r (mm)
Spindle	1000	0.1	4.0	2.5
Workpiece	1000	0.2	3.0	2.5

In conclusion, the range of cutting parameters selected for this study has a negligible influence on the workpiece machined surface, since the RMS acceleration values of the spindle and the workpiece were not high enough. This is supported by the FFT signal spectrum of each trial where none of them showed changes on signals that could indicate, wear, looseness or excessive imbalance of the tool-machine equipment used in this study.

5.6 Summary and general conclusion

In this study, the basic research aims were to evaluate the influence of the cutting parameters on the surface characterization together with the best combination of cutting parameters that resulted in a smoother surface. From these studies the following conclusions were obtained:

- The surface characterization analysis gives a wide knowledge of how a material surface can change once it is introduced to a machining process.
- It was observed that the tool nose radius is the parameter that has the most influence on the surface roughness with a contribution of 69.80 %, followed by the cutting speed and feed per tooth with a contribution of 14.72 % and 14.70 % respectively.
- A neglected influence of the axial depth of cut on the surface roughness was observed since a value larger than the tool nose radius value was used.
- Based on the experiments, the optimal combination of cutting parameters in order to achieve a smooth surface when face milling 7075-T7351 is V=800 m/min, fz=0.1 mm/rev*tooth, ap= 3.5 mm and r=2.5 mm.
- The 2D and 3D images of surface roughness provide the information regarding possible tool wear when distortions on the profile or topography are presented.
- The machined surface microhardness surface microhardness varies by up to 12% due to workhardening when compared with the original pattern, which will have a significant effect when continuosly machining the same product..
- An increase of 30% of the cutting speed produced a decrease of between 3% - 4 % of the surface microhardness while an increase of 100% of the feed per tooth produced an increased of between 2% - 3 %. This shows that a change in either cutting speed or feed change is of little significance to the microhardness, though both of these parameters may start to have an impact in cutting when combined together.
- A curlier chip was obtained when increasing the cutting speed and when using low values of tool nose radius.
- The RMS graphs are a weak tool to obtain a relationship between vibrations and individual cutting parameters.
- The FFT graphs are a very useful tool to identify any equipment problem, such as gear teeth wear.

6 Models for surface roughness prediction when face milling with square inserts

6.1 Introduction

In Chapter 3 previous relevant literature relating to surface roughness, machining using the milling process and the influence of cutting parameters on the surface roughness has been reviewed and critiqued. During this process specific gaps in knowledge had been identified. This chapter presents the research that has been performed to fill these gaps, especially regarding the development of different models for the prediction of the surface roughness, when face milling with square inserts.

This new contribution will represent a valuable tool for researchers in the area since it will allow the prediction of roughness before conducting experiments, representing saving in cost and time.

It must be highlighted, that despite the influence of the tool wear on surface roughness, this variable is not included on the models since: 1) new inserts are employed during each trial, 2) the length of cut used for the milling process is small (330 mm) 3) studies were conducted under a MQL (Minimum Quantity of Lubrication) and 4) the inclusion of this variable would requiere a long time for experiments and a higher budget, considering it a complete separate study, outside the scope of this research.

The validation of the developed models is obtained by comparing the predicted values obtained by each of the models with experimental values obtained by face milling Al 7075-T7351. These experiments and their results are presented in Chapter 5.

This chapter, shows the development of the different models for surface roughness prediction when face milling under wet cutting conditions. The models are based on mathematical, computational and geometric analysis and each model considers factors such as cutting conditions, cutting geometry and tool runouts, since all of them affect the workpiece surface roughness.

This chapter is divided into five further sections. The first four represent analysis of results and the last section summaries and conclude the present work.

Section 6.2: Presents the application of the Tchebysheff's theorem.

Section 6.3: Presents the development of a mathematical expression based on the Fourier series for surface roughness prediction.

Section 6.4: Presents the development of different Artificial Neural Networks (ANN) for surface roughness prediction.

Section 6.5: Presents the development of a theoretical model based on a geometrical analysis for surface roughness prediction.

Section 6.6: Includes a summary and the general conclusions obtained from these studies

Figure 6.1 shows a schematic overall description of the development of this study. Also the connection between the experimental and theoretical values of surface roughness for the models validation is presented. Finally, as observed in the diagram, the selection of the best model for surface roughness prediction is obtained, however this selection is presented and analyzed in Chapter 8.

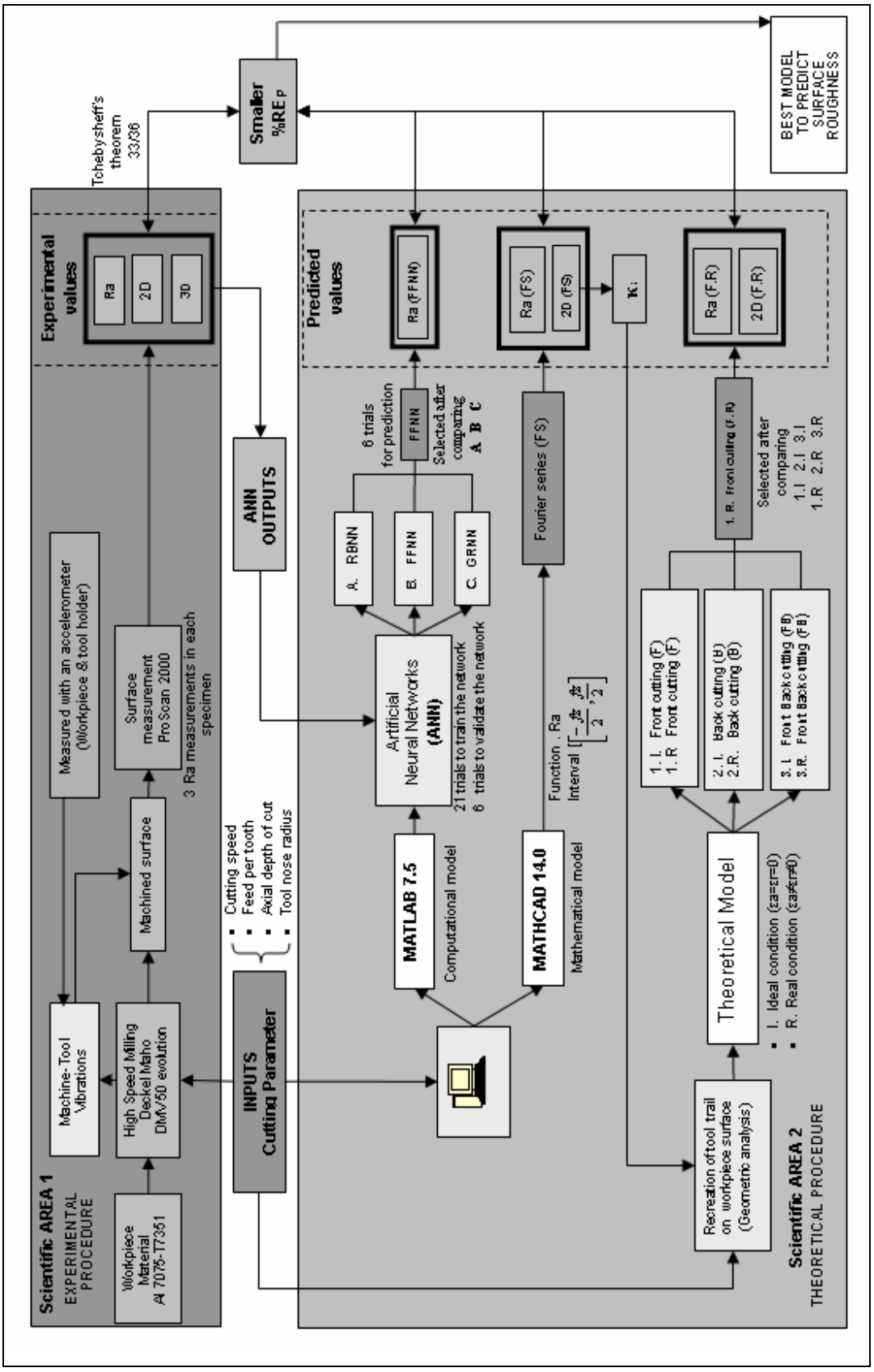

Figure 6.1- Schematic diagram of the development and comparison of different models for surface roughness prediction when face milling with square inserts

When analyzing Figure 6.1 it is observed that this study is divided into two main scientific areas. Scientific Area 1, corresponds to the experimental procedure conducted in Al 7075-T7351 during a face milling operation and Scientific Area 2, corresponds to the theoretical procedure followed for the development of the different models for surface roughness prediction.

As observed both areas are linked by the cutting parameters (input variables) and the experimental values of surface roughness and 2D profiles (output variables).

- **Scientific AREA 1:**

Experiments followed the Taguchi method of DoE, where 36 trials under different cutting conditions were conducted using Al 7075-T7351 on a Deckel Maho 50 evolution HSM machine. (This procedure is presented in detail in Chapter 5).

The parameters selected for the study (the cutting speed, the feed per tooth, the axial depth of cut and the tool nose radius) were based on their influence on the surface roughness as reported from previous research (Kopac, 1998, Poulachon 2003, Liu 2005). Also, as obtained from previous research, another factor that affects the surface roughness is the machine-tool vibrations generated during the cutting process (Saï, 2005, Arizmendi 2009). As explained in Chapter 5, section 5.5, this variable was measured on the workpiece and the tool holder, with accelerometers placed in specific places for this purpose. The measurement of this factor gives knowledge on how much it affects the resultant surface under the studied cutting conditions and, indeed if it needs to be included in the development of the models. As observed from Chapter 5, section 5.5, the results showed that this variable was not affecting the surface roughness values under the studied conditions and by using the specified equipment, so for this reason this variable is not introduced as an input to the developed models.

With regard to the surface roughness measurements, this variable was measured using a ProScan 2000 non-contact white lamp profilometer as extensively mentioned and illustrated in Chapter 5.

As we move along the flow chart it is observed that the experimental value of surface roughness (Ra) is used as the target output for the training of the Artificial

Neural Network, when considering the same cutting conditions and as a target output for all the developed models.

It must be highlighted that since the ANN does not reproduce the 2D profiles, only the 2D experimental profiles were considered as a target output for the Fourier series and the theoretical developed models.

- **Scientific AREA 2:**

This area involves the development of three surface roughness prediction models, each based on mathematical, computational and geometric analysis. Before developing the different models, Tchebysheff's theorem was applied, in order to secure a good performance of each of them. The results showed that 3 trials out of 36 were discharged, with the remaining 33 trials for the development and validation of the different models.

The assessment of each model is obtained by calculating the %RE, which is the relative error between the target output (experimental value of surface roughness) and the calculated output (trained, validated or predicted value of surface roughness depending on the case). The %RE is expressed by equation 6.1:

$$\%RE_X = \left| \frac{Ra - Ra_X}{Ra} \right| \cdot 100 \tag{6.1}$$

where:

$\%RE_x$: $\%\ RE_T$: Relative error between experimental and trained values

$\%\ RE_V$: Relative error between experimental and validated values

$\%\ RE_P$: Relative error between experimental and predicted values

Ra: Experimental value of surface roughness (μm).

Ra_X: Ra_T: Trained surface roughness (μm)

Ra_V: Validated surface roughness (μm)

Rap: Predicted surface roughness, (μm)

Once the $\%RE_P$ of each model is obtained, the performance assessment of each model is obtained by comparing them. The smaller $\%RE_P$ will represent the best model to predict the surface roughness.

A description of each of the models flow diagram observed in Figure 6.1 now follows:

- **Model 1:** is a mathematical model based on the Fourier series (FS). This model was selected since the experimental 2D profiles showed a harmonic and periodic behaviuor that could be represented by using the FS. For this case the MathCad 14 software was used to solve all the equations involved, as the function of the surface roughness is definined between the interval $\left[-\frac{f_z}{2},\frac{f_z}{2}\right]$.

Once the Fourier series of each milled surface was developed a detailed study of the series was conducted, where the kappa angle (κ_i, secondary entrance angle) was obtained for each cutting condition. The developed model allows the prediction of the surface roughness value and the reproduction of the 2D profile. The performance of this model is checked by calculating the $\%RE_P$ (the relative error between the experimental value of surface roughness and the predicted value of surface roughness). In this case this $\%RE_P$ is named $\%RE_P$ (FS).

- **Model 2:** is developed based on computational models, such as Artificial Neural Network This model was selected since they can be used to model complex relationships between inputs and outputs. Different networks were used such as: the Radial Base Neural Network (RBNN), the Feed Forward Neural Network (FFNN) and the Generalized Regression Neural Network (GRNN) and a comparison between them is conducted. As previously stated the inputs of each network are the cutting parameters selected in the experimental study (6 levels of cutting speed, 3 levels of feed per tooth, 3 levels of axial depth of cut and 2 levels for the tool nose radius). The output of each network is the experimental value of surface roughness obtained under specific cutting conditions. From the 33 trials used to develop the models, 21 trials were selected at random to train each network and six (6) trials were selected to validate the network.

Once the networks were validated, six trials were used to predict the surface roughness. The performance of each network is checked by using $\%RE_P$ between the target output (experimental surface roughness) and the calculated output (predicted value of surface roughness). When comparing the $\%RE_P$ between the different developed networks it was observed that the Feed Forward Neural Network (FFNN) $\%RE_P$, obtained the best results, especially when developing a FFNN for each studied tool nose radius. In this case the $\%RE_P$ is named $\%RE_P$ (FFNN)

- **Model 3:** is a theoretical model based on a geometric analysis developed by the reconstruction of the trail left by the tool on the milled surface. This model was selected since it is very illustrative and depends only on geometrical analysis. `In this case the model is a function of the feed per tooth, the cutting tool nose radius, κ_i angle (obtained from the Fourier series analysis) and the tool runout errors. These tool runout errors are the axial and radial deviations (εa and εr respectively) of the inserts when they are screwed to the tool holder and will be explained later with more detail. Three main models were developed based on a geometrical analysis and named: 1). Front cutting model, designated with the letter "F", 2). Back cutting model, designated with the letter "B" and 3). Front-Back cutting model, designated with the letters "FB". Also each of these models considered to cases: a letter "I" was designated for an ideal case which corresponds when tool runouts are not considered ($\varepsilon a = \varepsilon r = 0$) and a letter "R" was designated for the real case which corresponds when the static tool runouts are considered ($\varepsilon a \neq \varepsilon r \neq 0$). This study will enable the influence of these variables on the surface roughness to be determined. Once again, the assessment of each of the models is obtained by comparing the $\%RE_P$ of each of them. As previously mentioned this is the relative error between the experimental value of surface roughness obtained when milling the Al 7075-T7351 and the predicted value of surface roughness obtained by using the model. When comparing the $\%RE_P$ between the different developed models, it was observed that the Front cutting model that considered the real case (1.R.), obtained the best results. In this case the $\%RE_P$ is named $\%RE_P$ (F.R).

Finally, the selection of the best model that describes the prediction of the surface roughness when face milling with square inserts is obtained by comparing each $\%RE_P$ obtained in each of the developed models ($\%RE_P$ (FS), $\%RE_P$ (FFNN) and $\%RE_P$ (F.R)), where the smaller $\%RE_P$ will indicate which model to select.

6.2 Application of the Tchebysheff's theorem.

In order to secure a good performance of the different models developed in this research. Tchebysheff's theorem was applied for specimens cut with r = 0.8 mm and r = 2.5 mm respectively. The results are shown in Figures 6.2 and 6.3.

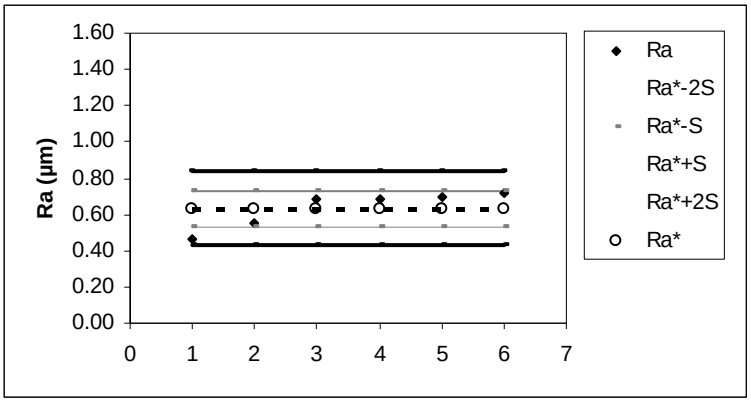

a)

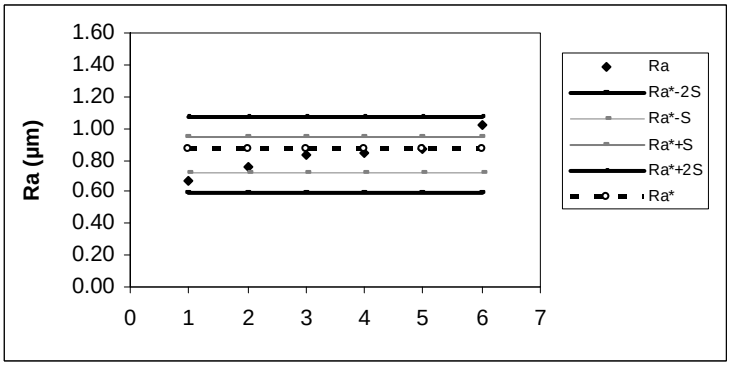

b)

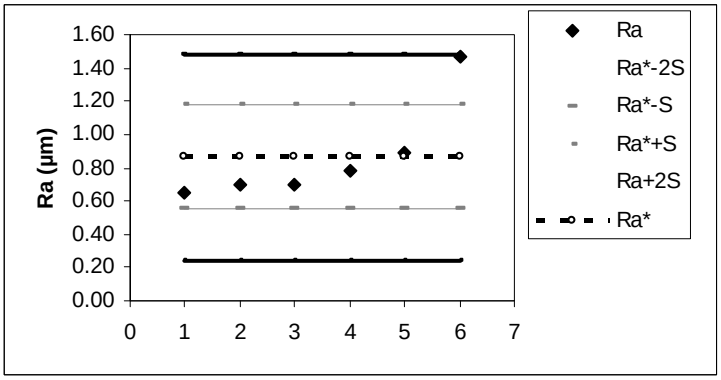

c)

Figure 6.2- Experimental surface roughness (Ra) distribution for Tchebysheff's theorem application for specimens milled with r=0.8 mm.
a) fz=0.1 mm/rev*tooth, b) fz=0.2 mm/rev*tooth and c) fz=0.3 mm/rev*tooth

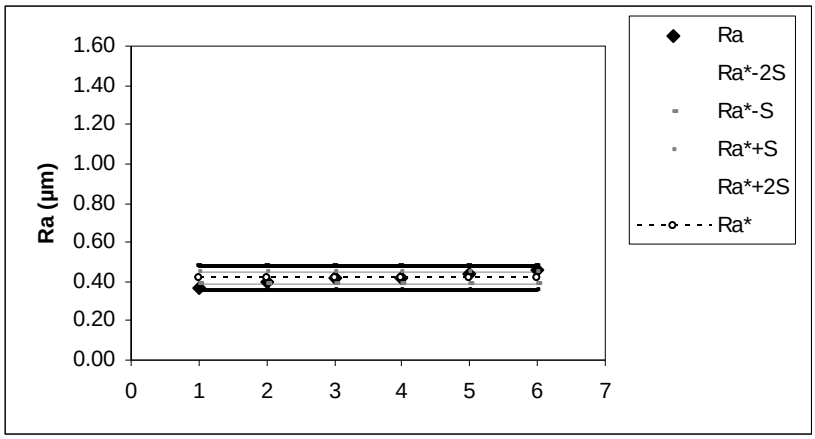

a)

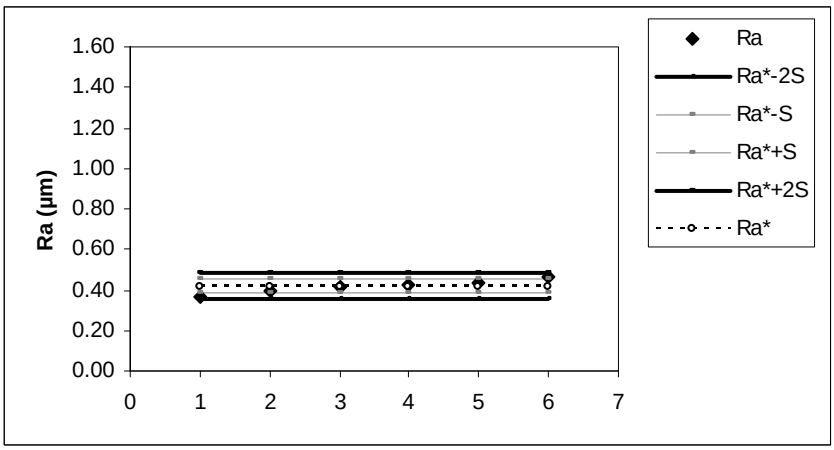

b)

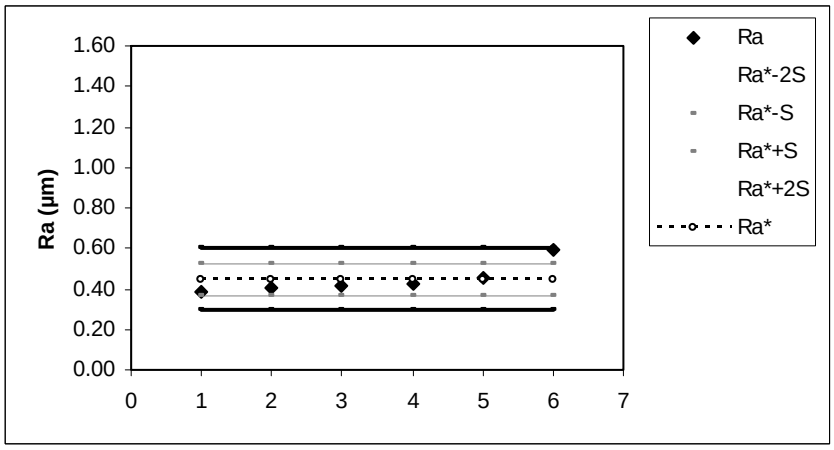

c)

Figure 6.3- Experimental surface roughness (Ra) distribution for Tchebysheff's theorem application for specimens milled with r=2.5 mm.
a) fz=0.1 mm/rev*tooth, b) fz=0.2 mm/rev*tooth and c) fz=0.3 mm/rev*tooth

When analyzing Figures 6.2 and 6.3, it is observed that in general the experimental surface roughness values are inside 95% of the normal distribution (between Ra*-2S and Ra*+2S, where Ra* represents the surface roughness average of the 36 trials and S the standard deviation) except for a few points that are just touching the boundaries of 95% of normal distribution (most of the examples in a set of data are close to the "average", while relatively few examples tend to one extreme or the other). From this, point #1 from Figure 6.2a, point #6 from Figure 6.2c and point #6 from Figure 6.3c are eliminated; this means that trials 25, 3 and 12, which belong to the points, previously mentioned, are not taken into account in the different models that are developed for surface roughness prediction.

It must also be highlighted that even though points #1 and #6 from Figures 6.3a and 6.3b are touching the boundaries of 95% of normal distribution these are not eliminated since the standard deviation obtained for the experimental surface roughness values of specimens milled with r = 2.5 mm is smaller when compared to the standard deviation obtained for the experimental surface roughness values of specimens milled with r = 0.8 mm (0.027 and 0.102 respectively).

Once Tchebysheff's theorem was applied and a total of 3 values out of 36 were discharged the different models were considered to develop.

6.3 Surface roughness prediction based on the Fourier series (Model 1)

As observed from Chapter 5, section 5.2, all the 2D experimental surface roughness profiles present a periodic and harmonic function for each set of cutting conditions; this behaviour led to the development of the Fourier series. The Fourier series leads to the development of an expression for surface roughness prediction and will also contribute as a support of the geometrical analytical model that is developed in section 6.5.

The Fourier series of a function, (in this case the surface roughness) defined in the interval $[-p, p]$, as shown in equation 6.2, where $p = \frac{fz}{2}$:

$$Ra(x) = \frac{a_0}{2} + \sum_{n=1}^{\infty}\left(a_n \cdot \cos\frac{n\cdot\pi}{p}\cdot x + b_n \cdot \sin\frac{n\cdot\pi}{p}\cdot x\right) \tag{6.2}$$

where:

$$a_0 = \frac{1}{p}\int_{-p}^{p} f(x)\cdot dx \tag{6.3}$$

$$a_n = \frac{1}{p}\int_{-p}^{p} f(x)\cdot \cos\frac{n\cdot\pi}{p}\cdot x\cdot dx \tag{6.4}$$

$$b_n = \frac{1}{p}\int_{-p}^{p} f(x)\cdot \sin\frac{n\cdot\pi}{p}\cdot x\cdot dx \tag{6.5}$$

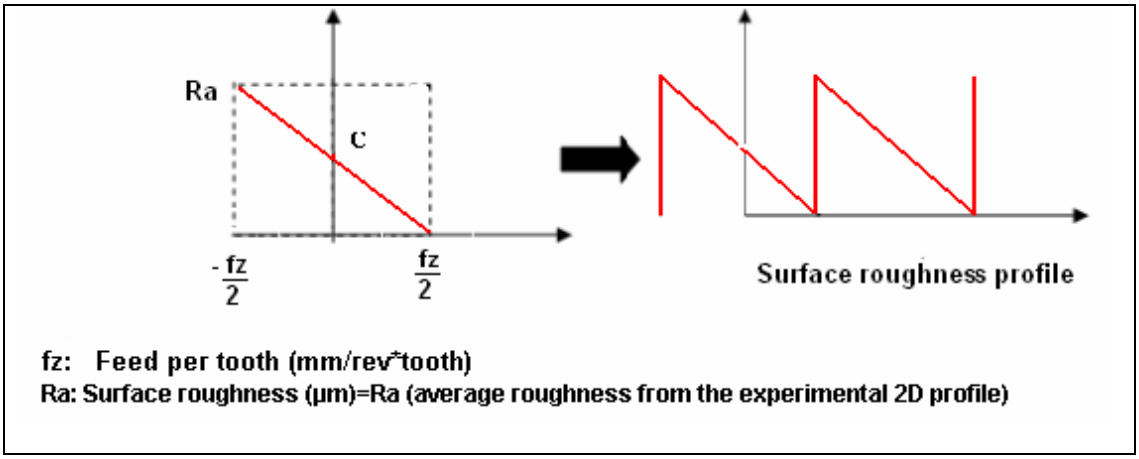

Figure 6.4- Diagram showing the geometry of the Fourier series

The maximum value of Ra reported in the Fourier series is Ra (the average roughness obtained from the 2D experimental profile), which is the value requiered.

The Fourier series is a first mathematical approach to the periodic behaviour obtained from the 2D experimental surface roughness profile. As observed the profiles presented a periodical behaviour, which is modelled by a line since the tool geometry used for the experiments is square.

The line $Ra(x) = mx + b$, defined between $\left[-\frac{fz}{2}, \frac{fz}{2}\right]$, where the minimum value is $Ra(x) = 0$ for $x = \frac{fz}{2}$ and the maximum value is $Ra(x) = Ra$ (average roughness) for $x = -\frac{fz}{2}$.

This is why the maximum value of the line will always be Ra (average roughness) since the valleys will always be Ra=0. It must be highlighted that some experimental measurements did not report Ra min or Ramax and this is why Ra (average roughness) was reported as the maximum Ra

Based on equation 6.2 and applying the diagram shown in Figure 6.4, the software MathCad 14 was used to solve equations 6.3, 6.4, and 6.5, respectively, and in order to obtain the Fourier series of each trial, equation 6.2 was developed considering the equations 6.6 to 6.15. Equation 6.16 represents the Fourier series used to develop all the 2D surface roughness profiles shown in Table 6.1, 6.2, 6.3 and 6.4:

$$f(x) = m \cdot x + c \tag{6.6}$$

$$a_0 = \frac{1}{p}\int_{-p}^{p} (m \cdot x + c) \cdot dx \tag{6.7}$$

$$a_0 = 2c \tag{6.8}$$

$$a_n = \frac{1}{p}\int_{-p}^{p} (m \cdot x + c) \cdot \cos\left(\frac{n \cdot \pi}{p} \cdot x\right) \cdot dx \tag{6.9}$$

$$a_n = \frac{2c \sin(n \cdot \pi)}{n \cdot \pi} = 0 \tag{6.10}$$

$$b_n = \frac{1}{p}\int_{-p}^{p} (m \cdot x + c) \cdot \sin\left(\frac{n \cdot \pi}{p} \cdot x\right) \cdot dx \tag{6.11}$$

$$b_n = \frac{2m \cdot \left(p^2 \cdot \sin(n \cdot \pi) - n \cdot \pi \cdot p^2 \cdot \cos(n\pi)\right)}{n^2 \cdot \pi^2 \cdot p} = \frac{-2m \cdot p(-1)^n}{n \cdot \pi} \tag{6.12}$$

$$m = \frac{Ra}{fz} \tag{6.13}$$

$$c = \frac{Ra}{2} \tag{6.14}$$

$$p = \frac{fz}{2} \tag{6.15}$$

$$Ra(x) = \frac{Ra}{2} + \sum_{n=1}^{\infty}\left(-\frac{Ra \cdot (-1)^n}{n \cdot \pi} \cdot \sin\left(\frac{2n \cdot \pi}{fz} \cdot x\right)\right) \tag{6.16}$$

The 33 Fourier series corresponding to the 33 trials obtained after applying the Tchebysheff's theorem are presented in four groups as follows:

Group 1: Includes the Fourier series profiles of trials conducted using a cutting speed of 600 m/min, 800 m/min and 1000 m/min and r = 0.8 mm. The results are shown in Table 6.1.

Group 2: Includes the Fourier series profiles of trials conducted using a cutting speed of 600 m/min, 800 m/min and 1000 m/min and r = 2.5 mm. The results are shown in Table 6.2.

Group 3: Includes the Fourier series profiles of trials conducted using a cutting speed of 1200 m/min, 1400 m/min and 1600 m/min and r = 0.8 mm. The results are shown in Table 6.3.

Group 4: Includes the Fourier series profiles of trials conducted using a cutting speed of 1200 m/min, 1400 m/min and 1600 m/min and a tool nose radius of 2.5 mm. The results are shown in Table 6.4.

Table 6.1- Fourier series for V = 600 m/min, 800 m/min, 1000 m/min and r=0.8 mm.

TRIAL	Cutting parameters	Fourier series
1	V= 600 m/min fz= 0.1 mm/ rev * tooth ap= 3.0 mm r = 0.8 mm	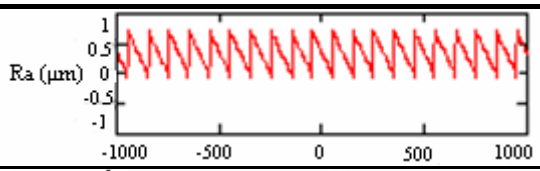
2	V= 600 m/min fz= 0.2 mm/ rev * tooth ap= 3.5 mm r = 0.8 mm	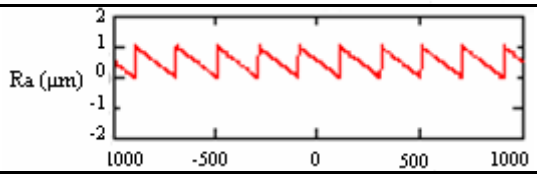
4	V= 800 m/min fz= 0.1 mm/ rev * tooth ap= 3.5 mm r = 0.8 mm	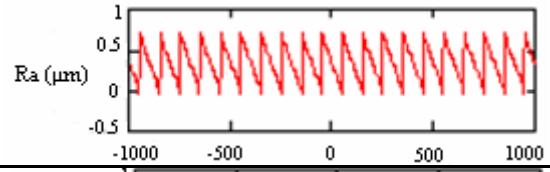
5	V= 800 m/min fz= 0.2 mm/ rev * tooth ap= 4.0 mm r = 0.8 mm	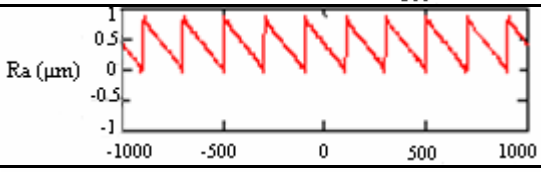
6	V= 800 m/min fz= 0.3 mm/ rev * tooth ap= 3.0 mm r = 0.8 mm	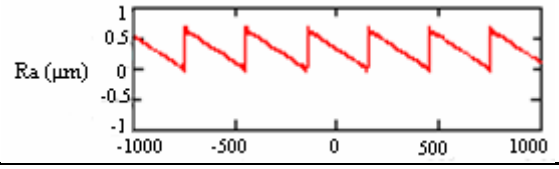
7	V= 1000 m/min fz= 0.1 mm/ rev * tooth ap= 4.0 mm r = 0.8 mm	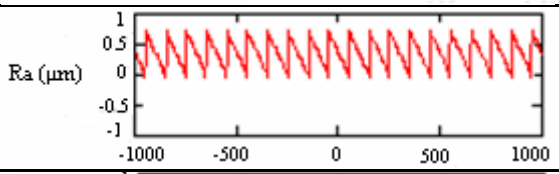
8	V= 1000 m/min fz= 0.2 mm/ rev * tooth ap= 3.0 mm r= 0.8 mm	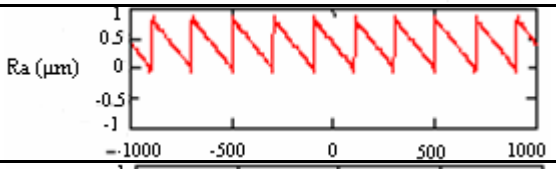
9	V= 1000 m/min fz= 0.3 mm/ rev * tooth ap= 3.5 mm r = 0.8 mm	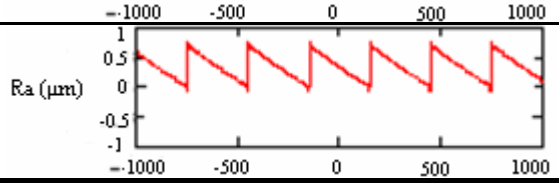

Table 6.2- Fourier series for V = 600 m/min, 800 m/min, 1000 m/min and r = 2.5 mm.

TRIAL	Cutting parameters	Fourier series
10	V= 600 m/min fz= 0.1 mm/ rev * tooth ap= 3.0 mm r =2.5 mm	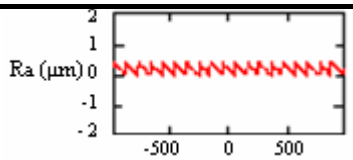
11	V= 600 m/min fz= 0.2 mm/ rev * tooth ap= 3.5 mm r = 2.5 mm	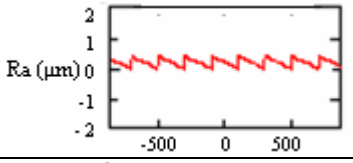
13	V= 800 m/min fz= 0.1 mm/ rev * tooth ap= 3.5 mm r= 2.5 mm	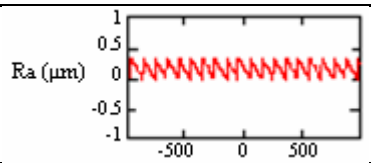
14	V= 800 m/min fz= 0.2 mm/ rev * tooth ap= 4.0 mm r = 2.5 mm	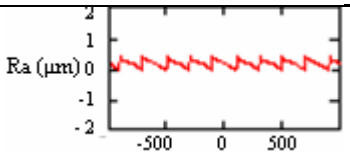
15	V= 800 m/min fz= 0.3 mm/ rev * tooth ap= 3.0 mm r = 2.5 mm	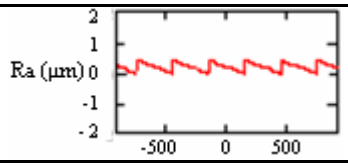
16	V= 1000 m/min fz= 0.1 mm/ rev * tooth ap= 4.0 mm r= 2.5 mm	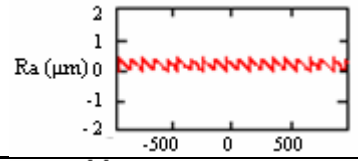
17	V= 1000 m/min fz= 0.2 mm/ rev * tooth ap= 3.0 mm r = 2.5 mm	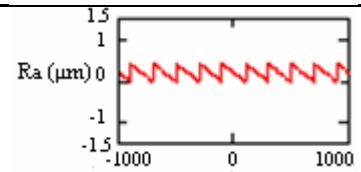
18	V= 1000 m/min fz= 0.3 mm/ rev * tooth ap= 3.5 mm r = 2.5 mm	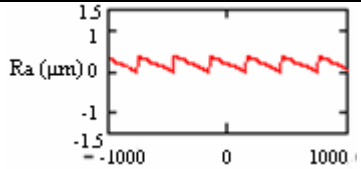

Table 6.3- Fourier series for V= 1200 m/min, 1400 m/min, 1600 m/min and r = 0.8 mm

TRIAL	Cutting parameters	Fourier series
19	V= 1200 m/min fz= 0.1 mm/ rev * tooth ap= 3.0 mm r = 0.8 mm	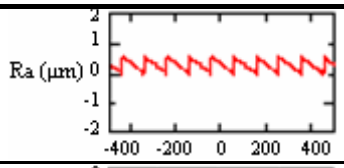
20	V= 1200 m/min fz= 0.2 mm/ rev * tooth ap= 3.5 mm r = 0.8 mm	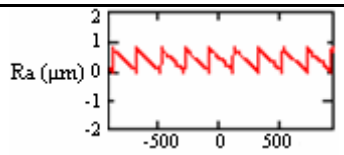
21	V= 1200 m/min fz= 0.3 mm/ rev * tooth ap= 4.0 mm r = 0.8 mm	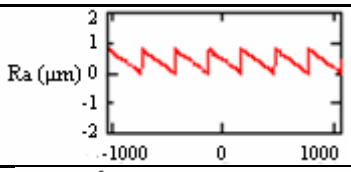
22	V= 1400 m/min fz= 0.1 mm/ rev * tooth ap= 3.5 mm r = 0.8 mm	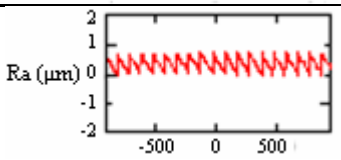
23	V= 1400 m/min fz= 0.2 mm/ rev * tooth ap= 4.0 mm r = 0.8 mm	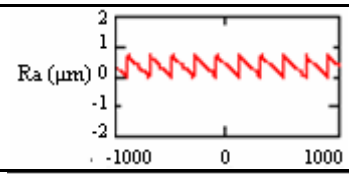
24	V= 1400 m/min fz= 0.3 mm/ rev * tooth ap= 3.0 mm r = 0.8 mm	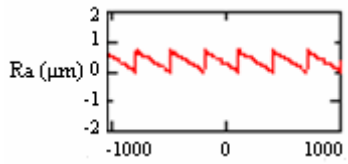
26	V= 1600 m/min fz= 0.2 mm/ rev * tooth ap= 3.0 mm r = 0.8 mm	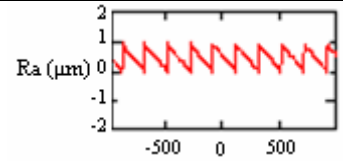
27	V= 1600 m/min fz= 0.3 mm/ rev * tooth ap= 3.5 mm r = 0.8 mm	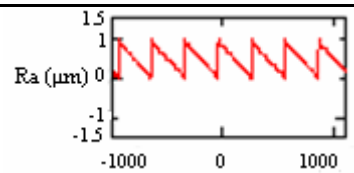

Table 6.4- Fourier series for V= 1200 m/min, 1400 m/min, 1600 m/min and r = 2.5 mm

TRIAL	Cutting parameters	Fourier series
28	V= 1200 m/min fz= 0.1 mm/ rev * tooth ap= 3.0 mm r = 2.5 mm	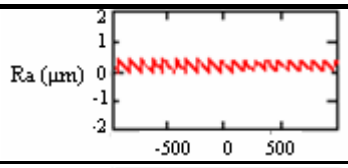
29	V= 1200 m/min fz= 0.2 mm/ rev * tooth ap= 3.5 mm r = 2.5 mm	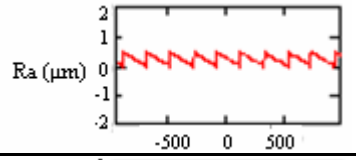
30	V= 1200 m/min fz= 0.3 mm/ rev * tooth ap= 4.0 mm r = 2.5 mm	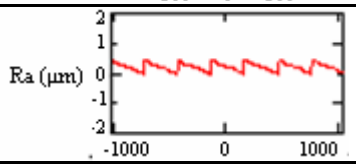
31	V= 1400m/min fz= 0.1 mm/ rev * tooth ap= 3.5 mm r = 2.5 mm	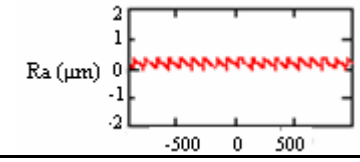
32	V= 1400m/min fz= 0.2 mm/ rev * tooth ap= 4.0 mm r = 2.5 mm	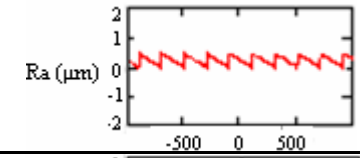
33	V= 1400m/min fz= 0.3 mm/ rev * tooth ap= 3.0 mm r = 2.5 mm	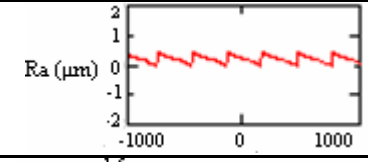
34	V= 1400 m/min fz= 0.1 mm/ rev * tooth ap= 4.0 mm r = 2.5 mm	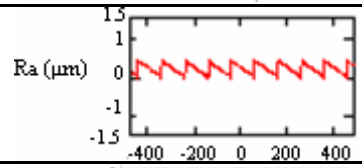
35	V= 1600 m/min fz= 0.2 mm/ rev * tooth ap= 3.0 mm r = 2.5 mm	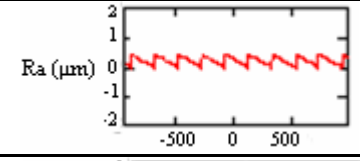
36	V= 1600 m/min fz= 0.3 mm/ rev * tooth ap= 3.5 mm r = 2.5 mm	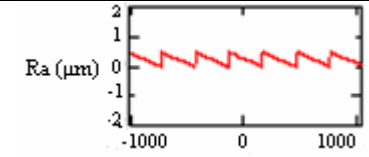

The Fourier series profile of each trial was analyzed following the schematic shown in Figure 6.5. As observed, there is an angle between each peak which is named α_i and the results of κ_2 angle for the Fourier series of each trial is presented in Table 6.5.

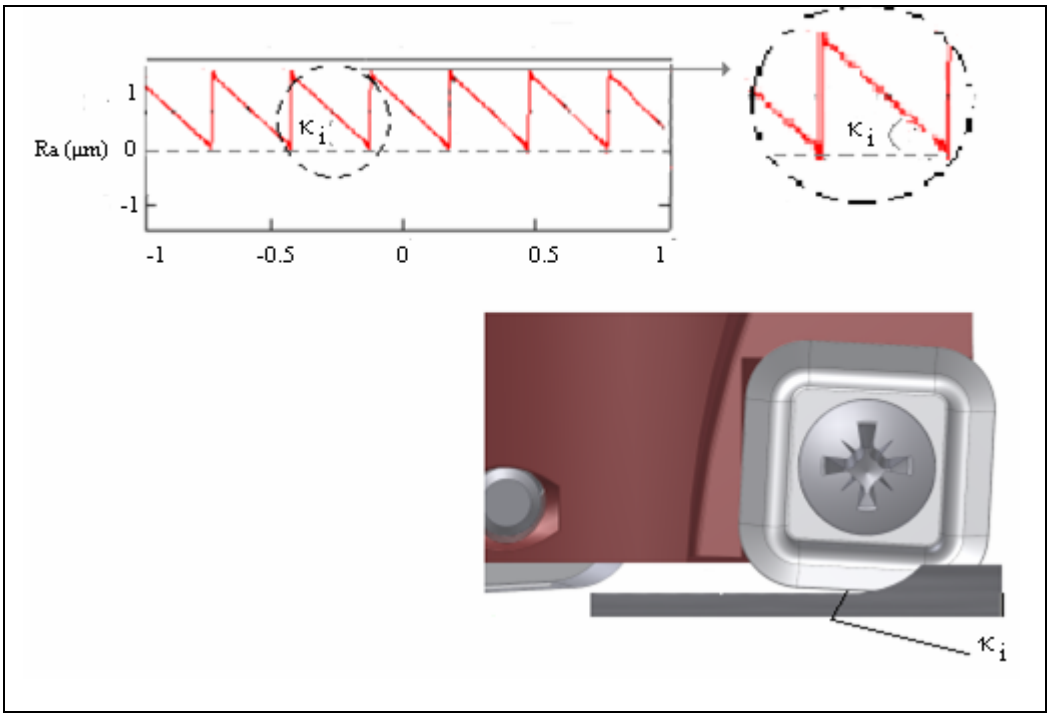

Figure 6.5- Schematic of a Fourier series and detail of (κ_i) angle

As observed when analyzing Table 6.5, the results show that since the κ_i angle is dependent of the cutting edge geometry, the values are similar for the same group of feed per tooth and tool nose radius and from this fact an average of κ_i is calculated for each of these groups and is named κ_i*.

Table 6.5- κ_i angle obtained for each trial when applying the scheme shown in Figure 6.5

	Trial	V (m/min)	fz (mm/rev*tooth)	ap (mm)	r (mm)	κ_i (^{o})
Group 1	1	600	0.1	3.0	0.8	0.40
	2	600	0.2	3.5	0.8	0.29
	4	800	0.1	3.5	0.8	0.39
	5	800	0.2	4.0	0.8	0.24
	6	800	0.3	3.0	0.8	0.13
	7	1000	0.1	4.0	0.8	0.41
	8	1000	0.2	3.5	0.8	0.24
	9	1000	0.3	3.0	0.8	0.13
Group 2	10	600	0.1	3.0	2.5	0.22
	11	600	0.2	3.5	2.5	0.12
	13	800	0.1	3.5	2.5	0.19
	14	800	0.2	4.0	2.5	0.11
	15	800	0.3	3.0	2.5	0.08
	16	1000	0.1	4.0	2.5	0.21
	17	1000	0.2	3.5	2.5	0.12
	18	1000	0.3	3.0	2.5	0.07
Group 3	19	1200	0.1	3.0	0.8	0.31
	20	1200	0.2	3.5	0.8	0.22
	21	1200	0.3	4.0	0.8	0.15
	22	1400	0.1	3.5	0.8	0.39
	23	1400	0.2	4.0	0.8	0.19
	24	1400	0.3	3.0	0.8	0.13
	26	1600	0.2	3.5	0.8	0.25
	27	1600	0.3	3.0	0.8	0.17
Group 4	28	1200	0.1	3.0	2.5	0.21
	29	1200	0.2	3.5	2.5	0.13
	30	1200	0.3	4.0	2.5	0.08
	31	1400	0.1	3.5	2.5	0.20
	32	1400	0.2	4.0	2.5	0.13
	33	1400	0.3	3.0	2.5	0.09
	34	1600	0.1	4.0	2.5	0.23
	35	1600	0.2	3.5	2.5	0.12
	36	1600	0.3	3.0	2.5	0.09

From the 33 trials, 27 were selected random for the development of the model and the other six were left for its validation and later prediction of the surface roughness.

The six trials selected for validation are: 7, 2 and 27 for specimens milled with r = 0.8 mm and fz= 0.1 mm/rev*tooth, fz = 0.2 mm/rev*tooth and fz = 0.3 mm/rev*tooth respectively and trials 16, 29 and 18 for specimens milled with r= 2.5 mm and fz=0.1 mm/rev*tooth, fz=0.2 mm/rev*tooth and fz=0.3 mm/rev*tooth, respectively.

It must be highlighted that, the α_i angle of the trials that were selected to validate the model and later to predict the surface roughness were not taken into account for the κ_i* (κ_i average) calculus.

Tables 6.6 and 6.7 show the α_i angle for each trial and κ_i* for each group of feed per tooth when face milling with r = 0.8 and r = 2.5 mm, respectively.

Table 6.6 – κ_i for each trial and κ_i* for each group of feed per tooth when face milling with r = 0.8 mm.

Trial	fz (mm/rev*tooth)	V (m/min)	ap (mm)	κ_i (^{o})	κ_i* (^{o})
1	0.1	600	3.0	0.40	
4	0.1	800	3.5	0.39	**0.38**
19	0.1	1200	3.0	0.31	
22	0.1	1400	3.5	0.39	
5	0.2	800	4.0	0.24	
8	0.2	1000	3.0	0.24	
20	0.2	1200	3.5	0.22	**0.24**
23	0.2	1400	4.0	0.19	
26	0.2	1600	3.0	0.25	
6	0.3	800	3.0	0.12	
9	0.3	1000	3.5	0.13	**0.14**
21	0.3	1200	4.0	0.15	
24	0.3	1400	3.0	0.13	

Table 6.7- The κ_i angle for each trial and κ_i* for each group of feed per tooth when face milling with r = 2.5 mm.

Trial	fz (mm/rev*tooth)	V (m/min)	ap (mm)	κ_i (^{o})	κ_i* (^{o})
10	0.1	600	3.0	0.20	
13	0.1	800	3.5	0.19	
28	0.1	1200	3.0	0.21	**0.21**
31	0.1	1400	3.5	0.20	
34	0.1	1600	4.0	0.23	
11	0.2	600	3.5	0.11	
14	0.2	800	4.0	0.11	
17	0.2	1000	3.0	0.12	**0.12**
32	0.2	1400	4.0	0.13	
35	0.2	1600	3.0	0.14	
15	0.3	800	3.0	0.08	
30	0.3	1200	4.0	0.08	**0.08**
33	0.3	1400	3.0	0.09	
36	0.3	1600	3.5	0.09	

The development of the empirical expression for surface roughness prediction based on Fourier series is obtained by using, linear multiple regressions, by using the Microsoft ^{TM} Excel software. Equation 6.17 presents the result of this expression**.**

$$Ra_P = \lambda \cdot 1000 \cdot fz \cdot tg\left(\kappa_i^*\right) \tag{6.17}$$

$$\lambda = a + b \cdot ap + c \cdot V + d \cdot ap \cdot V \tag{6.18}$$

$R^2 = 100\%$

$R^2_{adj} = 100\%$

where:

r (mm)	fz (mm/rev.tooth)	κ_i^* (°)	a	b	c	d
0.8	**0.1**	0.381	2.924	-0.00278	-0.549	0.0008
	0.2	0.238	-0.194	0.00137	0.369	-0.0004
	0.3	0.142	1.052	-0.00046	-0.089	0.0002
2.5	**0.1**	0.209	-0.42	0.453	0.014	-0.00044
	0.2	0.123	0.467	0.467	0.0004	-0.00069
	0.3	0.083	-0.01	-0.01	0.0011	-0.00031

Once the model is developed, it is ready to use for the prediction of the surface roughness under different cutting conditions and Tables 6.8 and 6.9 shows the results of the predicted surface roughness (Rap) obtained by using equation 6.17 when using r = 0.8 mm and r = 2.5 mm respectively. Also the experimental values of surface roughness (Ra) as well as the $\%RE_P$ obtained in each trial are presented**.**

Table 6.8- Experimental and predicted surface roughness obtained when using equation 6.17 for r = 0.8 mm and the $\%RE_P$.

Trial	fz (mm/rev*tooth)	V (m/min)	ap (mm)	κ_i* (°)	Ra (µm)	Rap (FS) (µm)	$\%RE_P$ (FS)
1	0.1	600	3.0	0.38	0.699	0.699	0.00
4	0.1	800	3.5	0.38	0.679	0.679	0.00
19	0.1	1200	3.0	0.38	0.548	0.548	0.00
22	0.1	1400	3.5	0.38	0.688	0.687	0.14
5	0.2	800	4.0	0.24	0.838	0.835	0.36
8	0.2	1000	3.0	0.24	0.835	0.828	0.84
20	0.2	1200	3.5	0.24	0.759	0.780	2.77
23	0.2	1400	4.0	0.24	0.668	0.661	1.05
26	0.2	1600	3.0	0.24	0.872	0.869	0.34
6	0.3	800	3.0	0.14	0.646	0.694	7.43
9	0.3	1000	3.5	0.14	0.699	0.699	0.00
21	0.3	1200	4.0	0.14	0.781	0.781	0.00
24	0.3	1400	3.0	0.14	0.694	0.694	0.00

Table 6.9- Experimental and predicted surface roughness obtained when using equation 6.17 for r = 2.5 mm and the $\%RE_P$.

Trial	fz (mm/rev*tooth)	V (m/min)	ap (mm)	κ_i* (°)	Ra (µm)	Rap (FS) (µm)	$\%RE_P$ (FS)
10	0.1	600	3.0	0.21	0.376	0.380	1.06
13	0.1	800	3.5	0.21	0.328	0.324	1.22
28	0.1	1200	3.0	0.21	0.365	0.356	2.47
31	0.1	1400	3.5	0.21	0.344	0.359	4.36
34	0.1	1600	4.0	0.21	0.408	0.402	1.47
11	0.2	600	3.5	0.12	0.399	0.393	1.50
14	0.2	800	4.0	0.12	0.368	0.372	1.09
17	0.2	1000	3.0	0.12	0.422	0.427	1.18
32	0.2	1400	4.0	0.12	0.437	0.436	0.23
35	0.2	1600	3.0	0.12	0.418	0.416	0.48
15	0.3	800	3.0	0.08	0.425	0.408	4.00
30	0.3	1200	4.0	0.08	0.415	0.415	0.00
33	0.3	1400	3.0	0.08	0.408	0.408	0.00
36	0.3	1600	3.5	0.08	0.453	0.453	0.00

Tables 6.10 and 6.11 show the results of experimental and predicted values of surface roughness as well as the $\%RE_P$ for specimens milled with r = 0.8 mm and r = 2.5 mm, respectively, using the trials selected for validation and later prediction of the surface roughness.

Table 6.10- Experimental and predicted surface roughness obtained when using the validating data for r = 0.8 mm and the $\%RE_P$.

Trial	fz (mm/rev*tooth)	V (m/min)	ap (mm)	κ_i * (^{o})	Ra (μm)	Rap (FS) (μm)	$\%RE_P$ (FS)
7	0.1	1000	4.0	0.38	0.712	0.766	7.58
2	0.2	600	3.5	0.24	1.017	0.846	16.81
27	0.3	1600	3.5	0.14	0.888	0.789	11.15

Table 6.11- Experimental and predicted surface roughness obtained when using the validating data for r = 2.5 mm and the $\%RE_P$.

Trial	fz (mm/rev*tooth)	V (m/min)	ap (mm)	κ_i * (^{o})	Ra (μm)	Rap (FS) (μm)	$\%RE_P$ (FS)
16	0.1	1000	4.0	0.21	0.365	0.308	15.62
29	0.2	1200	3.5	0.12	0.461	0.419	9.11
18	0.3	1000	3.5	0.08	0.381	0.395	3.67

As observed from Tables 6.10 and 6.11, in general by using the empirical expression shown in equation 6.17 the $\%RE_P$ is less then 17%. This result can be considered as a very good approach considering that the surface roughness is measured in μm. Also it must be highlighted that when measuring the surface roughness of each specimen in three different areas, a difference of 20% between these measurements was obtained.

6.4 Artificial Neural Networks (ANN) development (Model 2).

For the development of this model, the MATLAB 7.5 Neural Network Toolbox function was used. This software allows the creation, training and validation of different ANN; when considering the cutting parameters (cutting speed, feed per tooth, axial depth of cut and tool nose radius) as the inputs of the networks. The output of the network is the experimental surface roughness obtained when milling Al 7075-T7351 under different cutting conditions. Once the ANN is validated is ready to be used for the prediction of the surface roughness under different cutting conditions.

For this study a comparison between the Radial Base Neural Network (RBNN), the Feed Forward Neural Network (FFNN) and the Generalized Regression Neural Network (GRNN) was conducted. Different networks architectures were built considering different factors such as: combinations of number of neurons in the hidden layer; number of hidden layers, spread parameter, learning rate, etc. It must be highlighted that the best network architecture capable to predict a value of roughness as close to the experimental value is obtained by trial and error.

For each of the three studied networks, 21 trials and 6 trials were picked randomly to train and validate the network respectively. Once the network is validated is ready to use for the prediction of the surface roughness. The prediction of roughness is conducted by using the 6 trials remained from the group of 33 trials. It must be highlighted that by using different conditions (trials) for the validation of the selected network and later on for the prediction of the surface roughness, the efficiency of the network it is guaranteed since these trial are completely different from the ones used to train the network.

Figure 6.6 shows a general scheme of an architecture network.

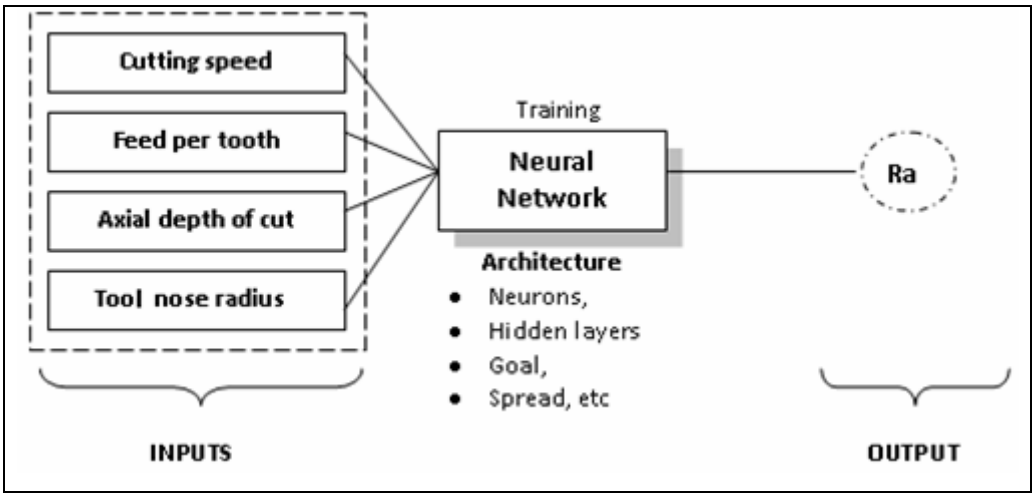

Figure 6.6- Inputs and output of a network for surface roughness prediction

Table 6.12 shows the 21 trials picked randomly to train each of the networks selected for study.

Table 6.12- Trials selected for training the network.

Trial	V (m/min)	fz (mm/rev*tooth)	ap (mm)	r (mm)	Ra (µm)
4	800	0.1	3.5	0.8	0.679
5	800	0.2	4.0	0.8	0.838
6	800	0.3	3.0	0.8	0.646
8	1000	0.2	3.0	0.8	0.835
9	1000	0.3	3.5	0.8	0.699
10	600	0.1	3.0	2.5	0.376
13	800	0.1	3.5	2.5	0.328
14	800	0.2	4.0	2.5	0.368
15	800	0.3	3.0	2.5	0.425
17	1000	0.2	3.0	2.5	0.422
19	1200	0.1	3.0	0.8	0.548
20	1200	0.2	3.5	0.8	0.759
21	1200	0.3	4.0	0.8	0.781
22	1400	0.1	3.5	0.8	0.688
24	1400	0.3	3.0	0.8	0.694
26	1600	0.2	3.0	0.8	0.872
30	1200	0.3	4.0	2.5	0.415
31	1400	0.1	3.5	2.5	0.344
32	1400	0.2	4.0	2.5	0.437
33	1400	0.3	3.0	2.5	0.408
34	1600	0.1	4.0	2.5	0.408

As previously mentioned, once the network is trained, this one is validated and later used for predicting the surface roughness. Tables 6.13 and 6.14 present the trials picked randomly for validation and prediction purposes, respectively.

Table 6.13- Trials picked randomly in order to validate the selected trained network.

Trial	V (m/min)	fz (mm/rev*tooth)	ap (mm)	r (mm)	Ra (μm)
1	600	0.1	3.0	0.8	0.699
11	600	0.2	3.5	2.5	0.399
23	1400	0.2	4.0	0.8	0.668
28	1200	0.1	3.0	2.5	0.365
35	1600	0.2	3.0	2.5	0.418
36	1600	0.3	3.5	2.5	0.453

Table 6.14- Trials selected for predicting the surface roughness once selecting the proper network.

Trial	V (m/min)	fz (mm/rev*tooth)	ap (mm)	R (mm)	Ra (μm)
2	600	0.2	3.5	0.8	1.017
7	1000	0.1	4.0	0.8	0.712
16	1000	0.1	4.0	2.5	0.365
18	1000	0.3	3.5	2.5	0.381
27	1600	0.3	3.5	0.8	0.888
29	1200	0.2	3.5	2.5	0.461

During the training and validation of the network and later prediction of the surface roughness with the selected network, the calculated output ($Ra_{x,}$ where x represents: t=trained, v=validated and p=predicted surface roughness) is compared with the target output (Ra, experimental surface roughness). The $\%RE_X$ is calculated by using equation 6.1 in order to obtain the performance assessment of the selected ANN.

The best network architecture is reached by trial and error, this was very time consuming, since each network is tried one by one. For this reason, a small program was introduced. This program allows changing of goal values, spread, hidden layers, etc; characteristic of each Neural Network and is set in order to report the architectures that reaches the smaller %EM (Error Module) of trained, validated and predicted at the same time by using a maximum of 1000 iterations. As the values of goal, spread etc, are changed, the structure of the network changes as well. This procedure is an internal procedure conducted by the MATLAB software. Figure 6.7 presents a flow chart of how the selection of the network architecture is conducted.

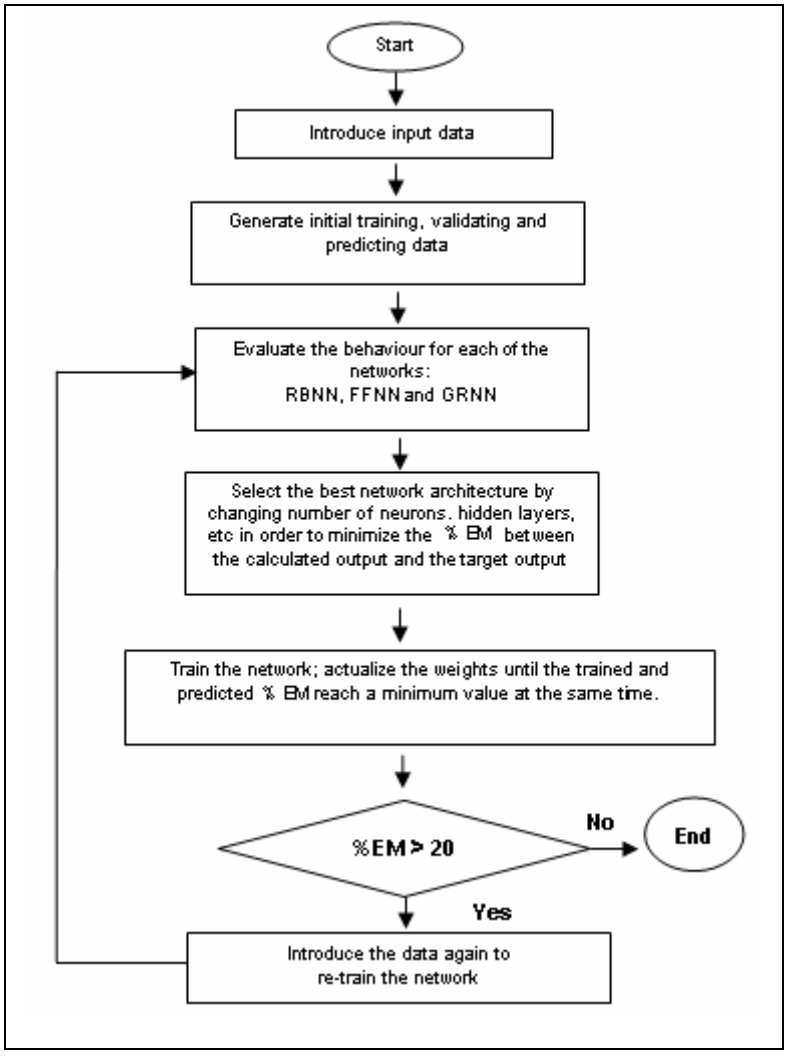

Figure 6.7- Flow chart for the selection of the network architecture

This EM (Error Module) for a group of measurements is calculated by using equation 6.2:

$$EM = \sqrt{\sum_{e=1}^{n}\left(\frac{(Y_e - T_e)}{T_e}\cdot 100\right)^2} \tag{6.2}$$

where:

Y_e: represent the values of the calculated outputs (trained, validated or predicted).
T_e: represent the experimental values.
n: represent the amount of samples: 21 for training, 6 for validating and 6 for predicting.

As observed, the selection of a network architecture was obtained when reaching a %EM≤ 20. This value of 20% was selected, since it was considered as a reasonable difference between the calculated outputs and the targets outputs, knowing that in some cases a difference of 20% was obtained between the three measurements of surface roughness conducted on the specimens after the milling process.

The developed program for the selection of the network architecture reports a table which contains the different architectures that reached the minimum $\%EM_x$ (x represents: trained, validated and predicted) at the same time. Once the best architecture is found, it is introduced into the software in order to obtain the calculated outputs. This last stage is performed, since the program only saves the last tried architecture, which is not necessarily the best architecture.

Once the network architecture is selected and validated it is ready to be used for the prediction of the target output (surface roughness in this case).

The results of the different developed models based on computational methods now follow:

6.4.1. Radial Base Neural Network (RBNN)

To start the training of this Neural Network, 4 inputs (cutting speed, feed per tooth, axial depth of cut and tool nose radius), 6 neurons in the hidden layer varying it every 4, a goal of 0.01 varying it every 0.001 and a spread parameter of 1.0 varying it every 0.02, were considered. These parameters were changed as much as was necessary until the RBNN architecture reached a minimum value of $\%EM_T$, $\%EM_V$ and $\%EM_P$ at the same time. Table 6.15 shows the table that the program reports. In this table few examples of different RBNN architectures that were tried with the purpose of reaching the minimum value of %EM between the calculated output (Ra_T, Ra_V and Rap) and the target output (Ra) at the same time.

Table 6.15- A few Radial Base Neural Network architectures (goal and spread) and %EM obtained between the calculated output (Ra_T, Ra_V and Rap) and the target output (Ra).

Network	Goal	Spread	$\%EM_T$ (RBNN)	$\%EM_V$ (RBNN)	$\%EM_P$ (RBNN)
1	0.001	1.82	2.91	28.75	39.47
2	0.002	1.82	2.91	28.75	39.47
3	0.003	1.82	2.91	28.75	39.47
4	0.003	1.88	4.20	29.37	38.88
5	0.004	1.82	2.91	28.75	39.47
6	0.004	1.88	4.20	29.37	38.88
7	0.004	1.94	5.39	30.08	38.19
8	0.005	1.82	2.91	28.75	39.47
9	**0.005**	**1.88**	**4.20**	**29.37**	**38.88**
10	0.005	1.94	5.39	30.08	38.19
11	0.006	1.82	2.91	28.75	39.47
13	0.006	1.94	5.39	30.08	38.19
14	0.007	1.82	2.91	28.75	39.47
15	0.007	1.88	4.20	29.37	38.88
16	0.007	1.94	5.39	30.08	38.19
17	0.008	1.82	2.91	28.75	39.47
18	0.008	1.88	4.20	29.37	38.88
19	0.008	1.94	5.39	30.08	38.19
20	0.009	1.82	2.91	28.75	39.47
21	0.009	1.88	4.20	29.37	38.88
22	0.009	1.94	5.39	30.08	38.19
23	0.010	1.82	2.91	28.75	39.47
24	0.010	1.88	4.20	29.37	38.88

As observed when analyzing Table 6.15, none of the tried architectures could reach a minimum value of % EM=20. The best performance was reached by architecture # 9, since the $\%EM_T$, $\%EM_V$ and $\%EM_P$ reached the smaller values when compared with the other architectures.

This architecture uses a goal of 0.005, a spread of 1.88, a number of 22 neurons in the hidden layer and as stated before 4 inputs. Figure 6.8 shows the RBNN architecture selected and used to predict the surface roughness in this study, where number 4 represents the number of inputs (cutting speed, feed per tooth, axial depth of cut and tool nose radius), number 22 the number of neurons in the hidden layer and number 1 the number of outputs (experimental surface roughness).

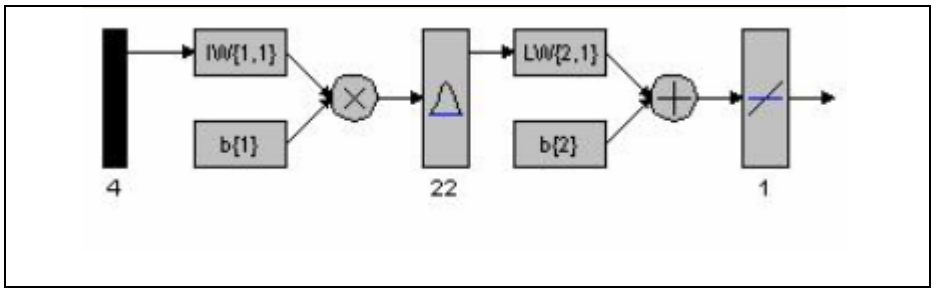

Figure 6.8- Radial Base Neural Network architecture used in this study.

Once this Neural Network architecture is selected the calculated outputs (Ra_T, Ra_V and Rap) are obtained and the %RE (relative error) between the calculated outputs (Ra_T, Ra_V and Rap) and the target output (Ra) are calculated. Tables 6.16, 6.17 and 6.18 show the respective results.

Table 6.16- Experimental and trained values of surface roughness and $\%RE_T$ obtained by using the selected RBNN architecture.

Trial	V (m/min)	fz (mm/rev*tooth)	ap (mm)	r (mm)	Ra (µm)	Ra_T (RBNN) (µm)	$\%RE_T$ (RBNN) (µm)
4	800	0.1	3.5	0.8	0.679	0.678	0.15
5	800	0.2	4.0	0.8	0.838	0.838	0.00
6	800	0.3	3.0	0.8	0.646	0.648	0.31
8	1000	0.2	3.0	0.8	0.835	0.832	0.36
9	1000	0.3	3.5	0.8	0.699	0.699	0.00
10	600	0.1	3.0	2.5	0.376	0.373	0.80
13	800	0.1	3.5	2.5	0.328	0.334	1.83
14	800	0.2	4.0	2.5	0.368	0.365	0.82
15	800	0.3	3.0	2.5	0.425	0.422	0.71
17	1000	0.2	3.0	2.5	0.422	0.428	1.42
19	1200	0.1	3.0	0.8	0.548	0.550	0.37
20	1200	0.2	3.5	0.8	0.759	0.760	0.13
21	1200	0.3	4.0	0.8	0.781	0.780	0.13
22	1400	0.1	3.5	0.8	0.688	0.688	0.00
24	1400	0.3	3.0	0.8	0.694	0.693	0.14
26	1600	0.2	3.0	0.8	0.872	0.872	0.00
30	1200	0.3	4.0	2.5	0.415	0.417	0.48
31	1400	0.1	3.5	2.5	0.344	0.334	2.91
32	1400	0.2	4.0	2.5	0.437	0.436	0.23
33	1400	0.3	3.0	2.5	0.408	0.408	0.00
34	1600	0.1	4.0	2.5	0.408	0.413	1.23

Table 6.17- Experimental and validated values of surface roughness and $\%RE_V$ obtained by using the selected RBNN architecture.

Trial	V (m/min)	fz (mm/rev*tooth)	ap (mm)	r (mm)	Ra (µm)	Ra_V (RBNN) (µm)	$\%RE_V$ (RBNN) (µm)
1	600	0.1	3.0	0.8	0.699	0.652	6.72
11	600	0.2	3.5	2.5	0.399	0.391	2.01
23	1400	0.2	4.0	0.8	0.668	0.778	16.47
28	1200	0.1	3.0	2.5	0.365	0.321	12.06
35	1600	0.2	3.0	2.5	0.418	0.500	19.62
36	1600	0.3	3.5	2.5	0.453	0.437	3.53

Table 6.18- Experimental and predicted values of surface roughness and $\%RE_P$ obtained by using the selected RBNN architecture.

Trial	V (m/min)	fz (mm/rev*tooth)	ap (mm)	r (mm)	Ra (µm)	Rap (RBNN) (µm)	$\%RE_P$ (RBNN) (µm)
2	600	0.2	3.5	0.8	1.017	0.845	16.91
7	1000	0.1	4.0	0.8	0.712	0.794	11.52
16	1000	0.1	4.0	2.5	0.365	0.377	3.29
18	1000	0.3	3.5	2.5	0.381	0.337	11.55
27	1600	0.3	3.5	0.8	0.888	0.698	21.39
29	1200	0.2	3.5	2.5	0.461	0.359	22.13

As observed from Tables 6.16, 6.17 and 6.18 the $\%RE_T$ of the trained network is much smaller when comparing it to the validated and predicted values of roughness. This result was expected since the network is trained to achieve the target output by considering the introduced inputs.

The values of the validated and predicted surface roughness were expected to be higher than the trained values, since the trials used to validate the network and later to predict the roughness were completely new for the network. Also, as observed in Table 6.18 a maximum $\%RE_P = 22.13$ was obtained between the experimental and the predicted values of roughness and this result is considered as a good approach since as previously mentioned the surface roughness is measured in µm.

In order to illustrate the results shown in the different tables, between the trained, validated and predicted values of surface roughness, graphs were developed. (Figure 6.9, 6.10 and 6.11)

Figure 6.9 show the results obtained with the experimental-trained surface roughness values.

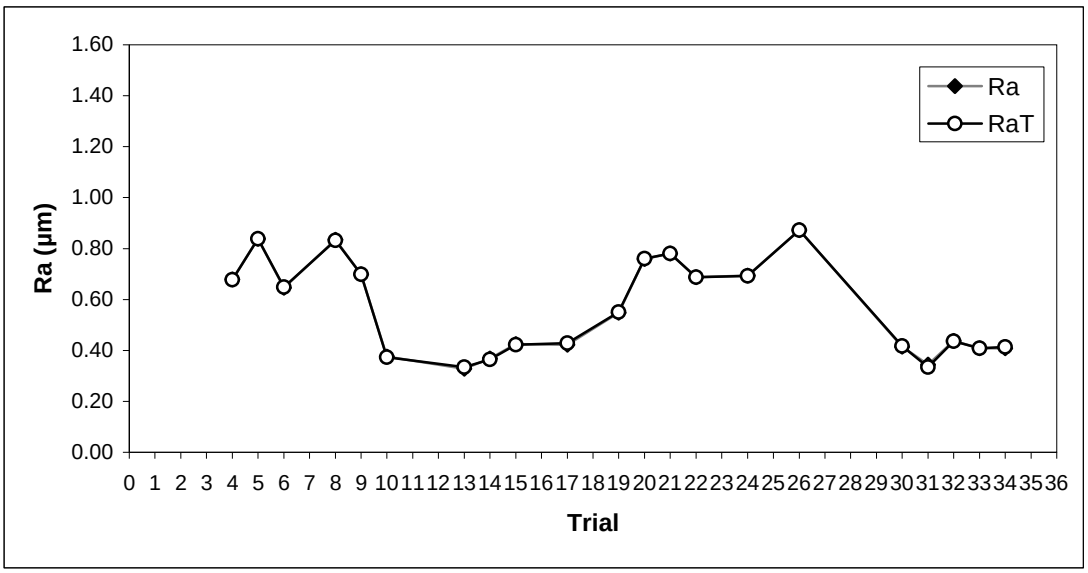

Figure 6.9- Experimental and trained values of surface roughness for different trials for the selected RBNN architecture (RaT overlaps Ra)

As observed and expected when analyzing Figure 6.9 the difference between the trained and experimental values of surface roughness is so small that the values are overlapped. This result is due to the fact that the network is trained to reach as exact as possible the target output (experimental surface roughness).

Figures 6.10 and 6.11 show the results of the experimental-validated values and the experimental-predicted values of surface roughness respectively.

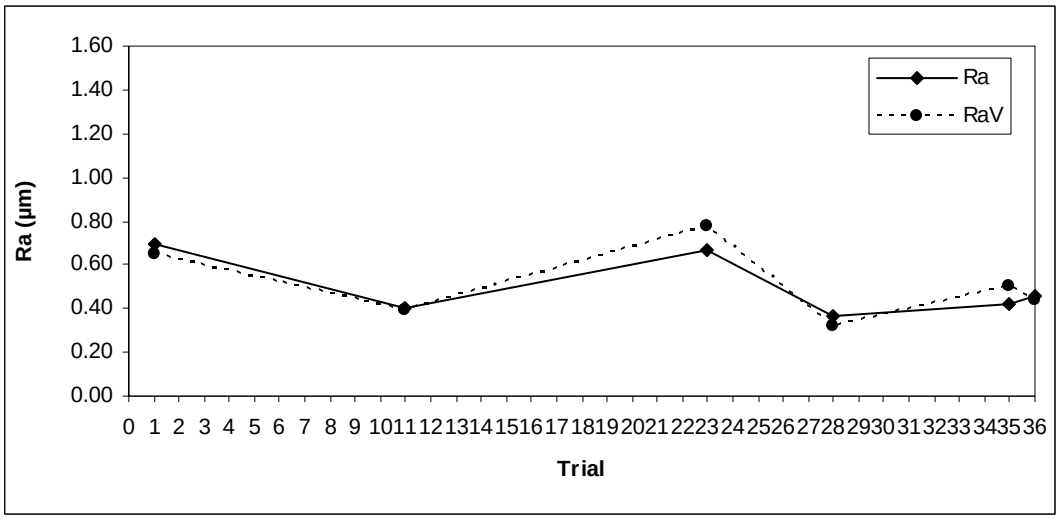

Figure 6.10- Experimental and validated values of surface roughness for different trials for the selected RBNN architecture.

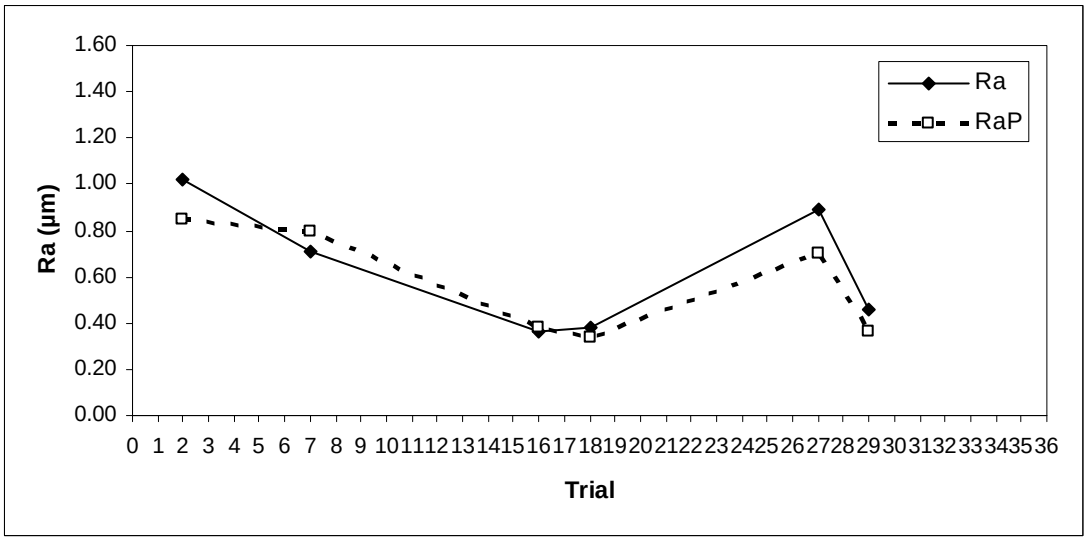

Figure 6.11- Experimental and predicted values of surface roughness for different trials for the selected RBNN architecture.

As observed when analyzing Figure 6.10 the validated graph tends to show a similarly behaviour to the experimental graph but with a slight difference between the validated and experimental values. A similar trend is observed in Figure 6.11 where the predicted and experimental values of surface roughness are presented, however in this case the gaps between the predicted and the experimental values are slightly bigger when compared to the validated values results.

6.4.2 Feed Forward Neural Network (FFNN).

For this Neural Network the same 4 inputs as were used in the RBNN, (cutting speed, feed per tooth, depth of cut and tool nose radius) were considered.

In this case, the Lavenberg-Marquardt algorithm was selected and from trial and error a maximum of two (2) hidden layers and maximum of 10 neurons were used. The activation function for the 3 layers architecture network (input layer, hidden layer and output layer) were *tansig, purelin* and the activation function for the 4 layers architecture network (input layer, hidden layer #1, hidden layer #2 and output layer) were *tansig, logsig, purelin*. Also a goal of 0.01, 100 epochs and a maximum of 1000 iterations were used. This number of iterations was used in order to reach the minimum %EM between the calculated outputs (trained, validated and predicted values of surface roughness) and the target out (experimental surface roughness) at the same time.

Table 6.19 show a few of the FFNN architectures that were tried, as well as the minimum %EM between the calculated output (Ra_T, Ra_v and Rap) and the target output (Ra).

Table 6.19- A few Feedforward Neural Networks architectures and %EM between the calculated output (Ra_T, Ra_v and Rap) and the target output (Ra).

Network	Network Architecture	Iteration	$\%EM_T$ (FFNN)	$\%EM_V$ (FFNN)	$\%EM_P$ (FFNN)
1	4-3-1	805	17.7	28.7	27.6
2	4-4-1	202	9.0	19.6	27.2
3	4-5-1	505	1.2	16.6	19,4
4	4-10-1	135	0.9	23.3	27.0
5	4-3-4-1	32	2.9	13.8	25.9
6	4-3-8-1	395	4.7	17.5	30.8
7	4-3-9-1	573	10.7	10.9	28.0
8	4-3-10-1	225	4.5	10.4	29.0
9	4-4-3-1	279	2.9	22.3	18.0
10	**4-4-4-1**	**530**	**2.5**	**17.6**	**17.6**
11	4-4-5-1	323	5.3	14.4	23.7
12	4-4-8-1	331	14.4	16.8	24.3
13	4-4-9-1	450	13.5	18.6	23.5
14	4-4-10-1	58	8.7	16.8	23.1
15	4-5-3-1	644	7.1	11.3	23.8
16	4-5-4-1	197	3.8	19.1	20.1
17	4-5-8-1	720	8.2	12.2	22.1
18	4-5-9-1	129	2.6	17.6	22.6
19	4-5-10-1	529	9.3	17.5	19.7
20	4-6-3-1	53	11.4	11.3	22.3
21	4-6-8-1	391	6.5	22.1	24.3
22	4-6-9-1	611	7.7	21.3	22.5
23	4-6-10-1	60	9.9	17.2	29.9
24	4-7-3-1	692	8.3	22.0	24.2
25	4-7-4-1	42	10.2	16.0	27.1
26	4-7-6-1	74	5.7	24.3	29.4
27	4-8-3-1	33	0.6	14.3	24.4
28	4-8-5-1	83	1.2	15.7	24.4
29	4-9-7-1	126	0.7	22.8	22.0
30	4-9-10-1	185	10.9	19.4	25.0
31	4-10-3-1	983	5.0	19.9	20.1
32	4-10-4-1	97	10.7	17.4	28.1
33	4-10-10-1	54	0.7	20.6	20.8

As observed from Table 6.19 the FFNN architecture #10, among all the architectures that were tried, is the one that reached, at the same time, the minimum % EM between the calculated output (Ra_T, Ra_v and Rap) and the target output (Ra). This architecture uses 4 inputs, 1 output, 4 neurons in hidden layer # 1, 4 neurons in hidden layer # 2 and it took 530 iterations to reach this goal.

Figure 6.12 shows the selected FFNN architecture used in this study, where as appeared in the graph, number 4 represents the number of inputs, number 4 the number of neurons in the hidden layer #1, number 4 the number of neurons in the hidden layer #2 and number 1 the number of outputs respectively. Also the activation function of each layer is observed, where:

= *tansig,* = *logsig* and = *purelin*

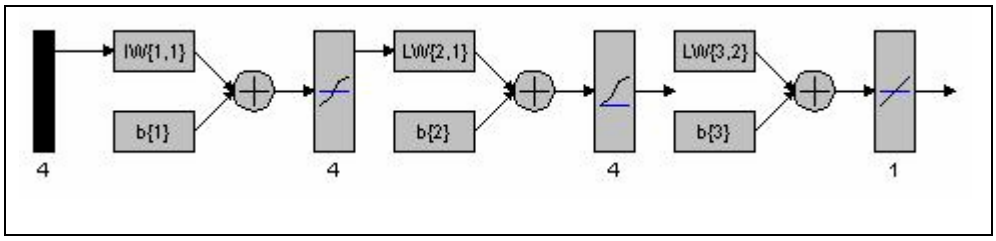

Figure 6.12- Feed Forward Neural Network architecture used in this study.

Once this FFNN architecture was selected the calculated outputs (Ra_T, Ra_v and Rap) are obtained and the %RE between the target output (Ra) and the calculated output (Ra_T, Ra_v and Rap) are presented in Tables 6.20, 6.21 and 6.22, respectively**.**

Table 6.20- Experimental and trained values of surface roughness and $\%RE_T$ obtained by using the selected FFNN architecture.

Trial	V (m/min)	fz (mm/rev*tooth)	ap (mm)	r (mm)	Ra (μm)	Ra_T (FFNN) (μm)	$\%RE_T$ (FFNN) (μm)
4	800	0.1	3.5	0.8	0.679	0.679	0.00
5	800	0.2	4.0	0.8	0.838	0.834	0.48
6	800	0.3	3.0	0.8	0.646	0.642	0.62
8	1000	0.2	3.0	0.8	0.835	0.839	0.48
9	1000	0.3	3.5	0.8	0.699	0.705	0.86
10	600	0.1	3.0	2.5	0.376	0.376	0.00
13	800	0.1	3.5	2.5	0.328	0.326	0.61
14	800	0.2	4.0	2.5	0.368	0.369	0.27
15	800	0.3	3.0	2.5	0.425	0.428	0.71
17	1000	0.2	3.0	2.5	0.422	0.421	0.24
19	1200	0.1	3.0	0.8	0.548	0.550	0.36
20	1200	0.2	3.5	0.8	0.759	0.761	0.26
21	1200	0.3	4.0	0.8	0.781	0.775	0.77
22	1400	0.1	3.5	0.8	0.688	0.689	0.15
24	1400	0.3	3.0	0.8	0.694	0.697	0.43
26	1600	0.2	3.0	0.8	0.872	0.871	0.11
30	1200	0.3	4.0	2.5	0.415	0.418	0.72
31	1400	0.1	3.5	2.5	0.344	0.347	0.87
32	1400	0.2	4.0	2.5	0.437	0.434	0.69
33	1400	0.3	3.0	2.5	0.408	0.405	0.74
34	1600	0.1	4.0	2.5	0.408	0.409	0.25

Table 6.21- Experimental and validated values of surface roughness and $\%RE_V$ obtained by using the selected FFNN architecture.

Trial	V (m/min)	fz (mm/rev*tooth)	ap (mm)	r (mm)	Ra (µm)	Ra_V (FFNN) (µm)	$\%RE_V$ (FFNN) (µm)
1	600	0.1	3.0	0.8	0.699	0.698	0.14
11	600	0.2	3.5	2.5	0.399	0.356	10.78
23	1400	0.2	4.0	0.8	0.668	0.724	8.38
28	1200	0.1	3.0	2.5	0.365	0.381	4.38
35	1600	0.2	3.0	2.5	0.418	0.418	0.00
36	1600	0.3	3.5	2.5	0.453	0.407	10.15

Table 6.22- Experimental and predicted values of surface roughness and $\%RE_P$ obtained by using the selected FFNN architecture.

Trial	V (m/min)	fz (mm/rev*tooth)	ap (mm)	r (mm)	Ra (µm)	Rap (FFNN) (µm)	$\%RE_P$ (FFNN) (µm)
2	600	0.2	3.5	0.8	1.017	0.907	10.82
7	1000	0.1	4.0	0.8	0.712	0.680	4.49
16	1000	0.1	4.0	2.5	0.365	0.367	0.55
18	1000	0.3	3.5	2.5	0.381	0.415	8.92
27	1600	0.3	3.5	0.8	0.888	0.820	7.66
29	1200	0.2	3.5	2.5	0.461	0.434	5.86

As observed from Tables 6.20, 6.21 and 6.22 the $\%RE_T$ of the selected FFNN architecture is much smaller when comparing it to the $\%RE_V$ and $\%RE_P$. This result was expected since the idea of training the network is to achieve a very good approach of the target output when considering specific inputs.

The values of the validated and predicted values of surface roughness are a little higher than the trained values, as expected, since the trials used to validate the network and later to predict the roughness were completely new for the network. Also, as observed in Table 6.22 a maximum $\%RE_P$=10.82 was obtained between the experimental and the predicted values of roughness. This result is almost 50% better than the result obtained by using the RBNN.

In order to illustrate the results shown in the previous tables, between the trained, validated and predicted values of surface roughness different graphs were developed. Figure 6.13 show the results between the trained and the experimental values of surface roughness obtained by using the selected FFNN architecture.

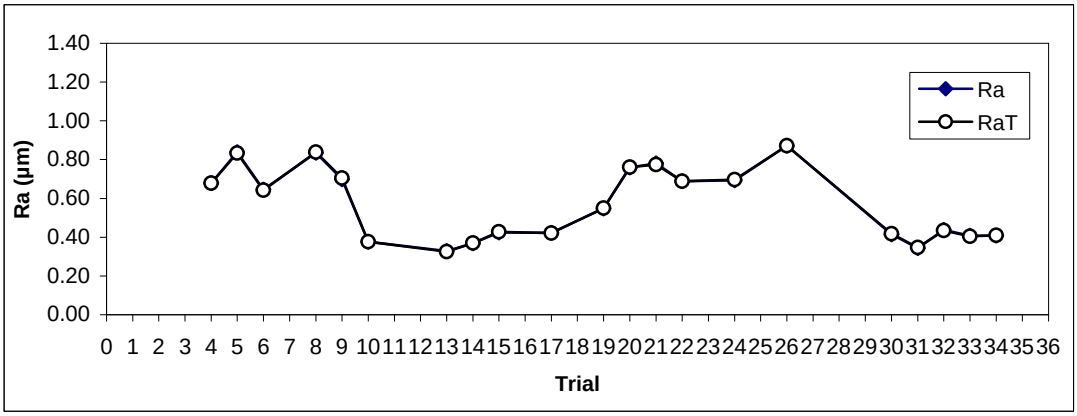

Figure 6.13- Experimental and trained values of surface roughness for different trials for the selected FFNN architecture. (RaT overlaps Ra)

As observed when analyzing Figure 6.13 the experimental values and the trained values are overlapped and this is, as previously stated, because the network is trained to reach the target out with a high accuracy.

Figures 6.14 and 6.15 show the results of the experimental-validated values and the experimental-predicted values of surface roughness respectively by using the selected FFNN architecture.

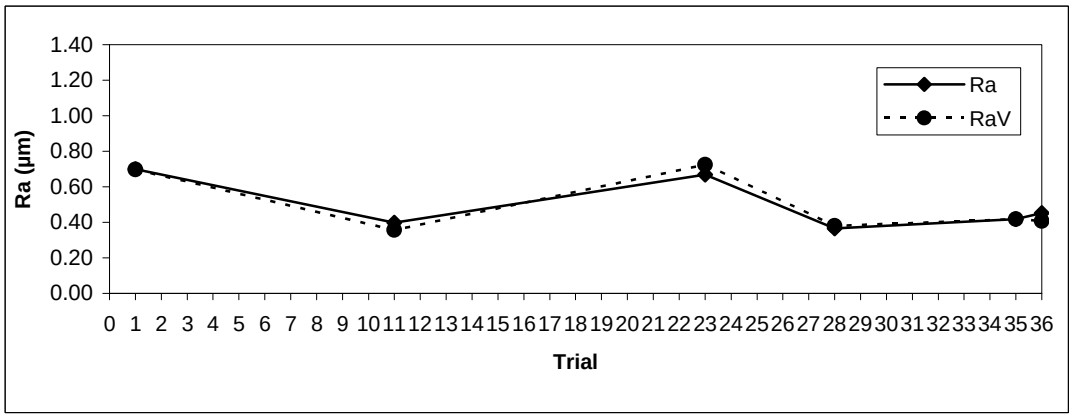

Figure 6.14- Experimental and validated values of surface roughness for different trials for the selected FFNN architecture.

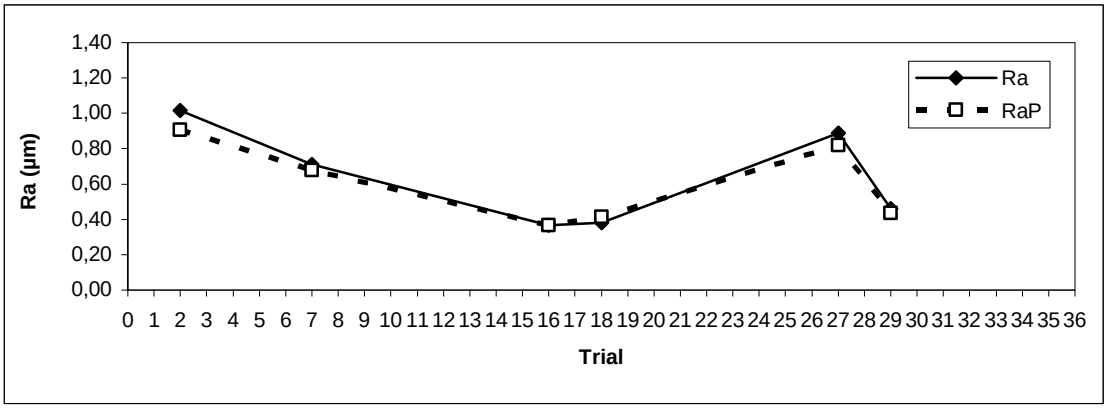

Figure 6.15- Experimental and predicted values of surface roughness for different trials for the selected FFNN architecture

Once again as observed in Figure 6.14 the validated values are closed to the experimental values and a similar behaviour was observed in Figure 6.15 where the predicted and experimental values are presented. Also the better performance of this FFNN when comparing it with the RBNN is highlighted where a reduction of almost 50% in the difference between the predicted and the experimental values was obtained, making it a 150% more effective in predicting the surface roughness.

6.4.3. Generalized Regression Neural Network. (GRNN)

To start the training of this Neural Network, 4 inputs (cutting speed, feed per tooth, axial depth of cut and tool nose radius), 2 neurons in the hidden layer and a spread parameter of 0.1 varying it every 0.01 were considered. Once again these parameters were changed until any GRNN architecture reached a minimum $\%EM_{T,}$ $\%EM_V$, $\%EM_P$ at the same time.

Table 6.23 shows a few of the GRNN architectures that were tried, as well as the minimum %EM between the calculated output (Ra_T, Ra_v and Rap) and the target output (Ra).

Table 6.23- A few GRNN architectures and %EM between the calculated outputs (Ra_T, Ra_V, Rap) and the target output (Ra).

Network	Spread	$\%EM_T$ (GRNN)	$\%EM_V$ (GRNN)	$\%EM_P$ (GRNN)
1	0.12	0.00	23.10	38.23
2	0.15	0.00	23.10	38.23
3	0.22	0.00	23.18	38.20
4	0.23	0,00	23.21	38.18
5	0.24	0.00	23.25	38.16
6	0.25	0.00	23.29	38.12
7	0.27	0.00	23.37	38.03
8	0.28	0.01	23.40	37.98
9	0.29	0.01	23.43	37.92
10	0.38	0.46	23.33	37.27
11	0.39	0.62	23.27	37.18
12	0.40	0.83	23.20	37.10
13	0.42	1.37	23.04	36.94
14	0.45	2.56	22.74	36.73
15	0.46	3.07	22.63	36.66
16	0.49	4.90	22.28	36.49
17	**0.50**	**5.60**	**22.16**	**36.44**
18	0.51	6.35	22.03	36.39
19	0.53	7.14	21.90	36.34
20	0.56	9.70	21.50	36.22
21	0.61	14.30	20.78	36.06
22	0.64	17.09	20.30	36.00
23	0.73	24.87	18.54	35.97
24	0.79	28.70	17.40	36.10
25	0.98	41.54	16.12	38.28

As observed from Table 6.23 the GRNN architecture that reached the minimum %EM between the calculated outputs (Ra_T, Ra_v and Rap) and the target output (Ra) is the architecture # 17, which uses 4 inputs, 4 neurons in hidden layer # 1, 4 neurons in hidden layer # 2, one output and a spread of 0.50.

Figure 6.16 shows the GRNN architecture selected and used in this study, where number 4 represents the number of inputs, number 22 the number of neurons in the hidden layer and number 1 the number of outputs, respectively.

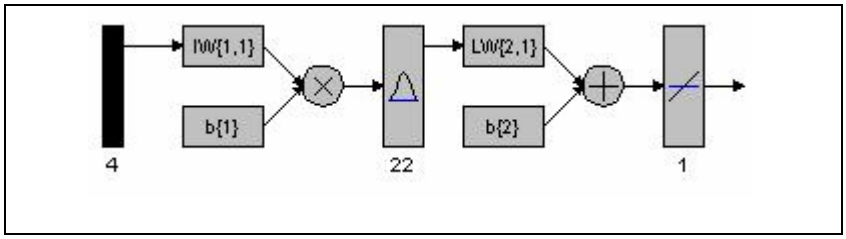

Figure 6.16- General Regression Neural Network architecture selected for this study

Once this GRNN architecture was selected the calculated outputs (Ra_T, Ra_v and Rap) were obtained and the %RE between the target output (Ra) and the calculated outputs (Ra_T, Ra_v and Rap) are calculated. The results are shown in Tables 6.24, 6.25 and 6.26, respectively.

Table 6.24- Experimental and trained values of surface roughness, and $\%RE_T$ when using the selected GRNN architecture.

Trial	V (m/min)	fz (mm/rev*tooth)	ap (mm)	r (mm)	Ra (µm)	Ra_T (GRNN) (µm)	$\%RE_T$ (GRNN) (µm)
4	800	0.1	3.5	0.8	0.679	0.680	0.15
5	800	0.2	4.0	0.8	0.838	0.836	0.24
6	800	0.3	3.0	0.8	0.646	0.656	1.55
8	1000	0.2	3.0	0.8	0.835	0.814	2.51
9	1000	0.3	3.5	0.8	0.699	0.703	0.57
10	600	0.1	3.0	2.5	0.376	0.375	0.27
13	800	0.1	3.5	2.5	0.328	0.330	0.61
14	800	0.2	4,0	2.5	0.368	0.370	0.54
15	800	0.3	3.0	2.5	0.425	0.425	0.04
17	1000	0.2	3.0	2.5	0.422	0.421	0.24
19	1200	0.1	3.0	0.8	0.548	0.569	3.83
20	1200	0.2	3.5	0.8	0.759	0.757	0.26
21	1200	0.3	4.0	0.8	0.781	0.778	0.38
22	1400	0.1	3.5	0.8	0.688	0.686	0.29
24	1400	0.3	3.0	0.8	0.694	0.701	1.01
26	1600	0.2	3.0	0.8	0.872	0.860	1.38
30	1200	0.3	4.0	2.5	0.415	0.415	0.00
31	1400	0.1	3.5	2.5	0.344	0.347	0.87
32	1400	0.2	4,0	2.5	0.437	0.434	0.69
33	1400	0.3	3.0	2.5	0.408	0.405	0.74
34	1600	0.1	4.0	2.5	0.408	0.409	0.25

Table 6.25- Experimental and validated values of surface roughness, and $\%RE_V$ when using the selected GRNN architecture.

Trial	V (m/min)	fz (mm/rev*tooth)	ap (mm)	r (mm)	Ra (µm)	Ra_V (GRNN) (µm)	$\%RE_V$ (GRNN)
1	600	0.1	3.0	0.8	0.699	0.668	4.43
11	600	0.2	3.5	2.5	0.399	0.359	10.03
23	1400	0.2	4.0	0.8	0.668	0.778	16.47
28	1200	0.1	3.0	2.5	0.365	0.377	3.29
35	1600	0.2	3.0	2.5	0.418	0.410	1.91
36	1600	0.3	3.5	2.5	0.453	0.411	9.27

Table 6.26- Experimental and predicted surface roughness, experimental surface roughness and $\%RE_P$ when using the selected GRNN architecture.

Trial	V (m/min)	fz (mm/rev*tooth)	ap (mm)	r (mm)	Ra (µm)	Rap (GRNN) (µm)	$\%RE_P$ (GRNN)
2	600	0.2	3.5	0.8	1.017	0.758	25.50
7	1000	0.1	4.0	0.8	0.712	0.750	5.33
16	1000	0.1	4.0	2.5	0.365	0.365	0.00
18	1000	0.3	3.5	2.5	0.381	0.418	9.71
27	1600	0.3	3.5	0.8	0.888	0.723	18.58
29	1200	0.2	3.5	2.5	0.461	0.394	14.53

As observed from Tables 6.24, 6.25 and 6.26 the $\%RE_T$ of the trained GRNN is much smaller when compared to the $\%RE_V$ and $\%RE_P$ values. Once again this result was expected since the training of the network achieves the target output with the minimum error possible. When analyzing Tables 6.25 and 6.26 an increase between the difference of the calculated out (validated and predicted values of roughness) and the target output (experimental values of surface roughness) is observed. Figures 6.17, 6.18 and 6.19 illustrate these results.

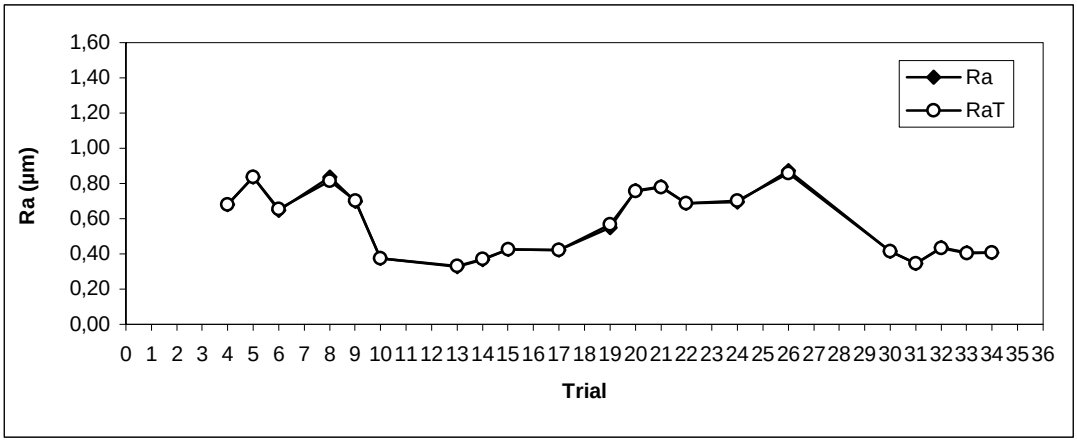

Figure 6.17- Experimental and trained values of surface roughness for different trials for the selected GRNN architecture. (RaT overlaps Ra)

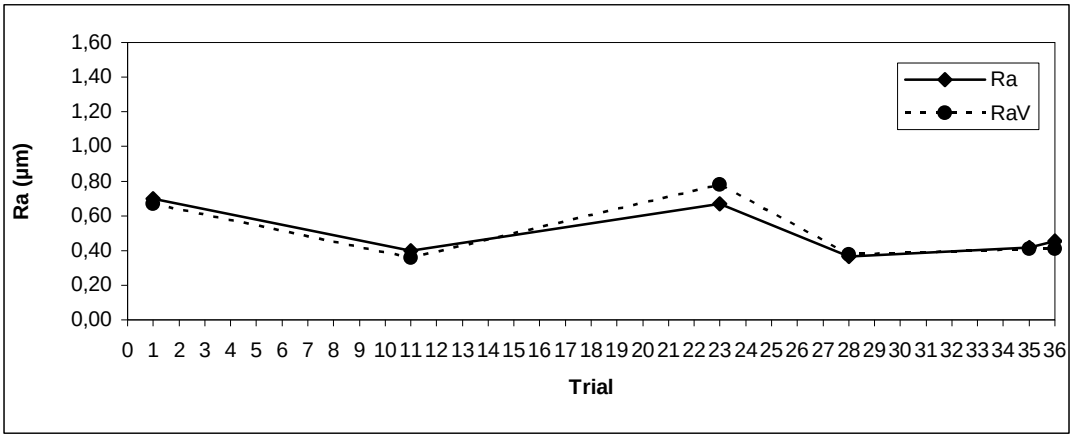

Figure 6.18- Experimental and validated values of surface roughness for different trials for the selected GRNN architecture.

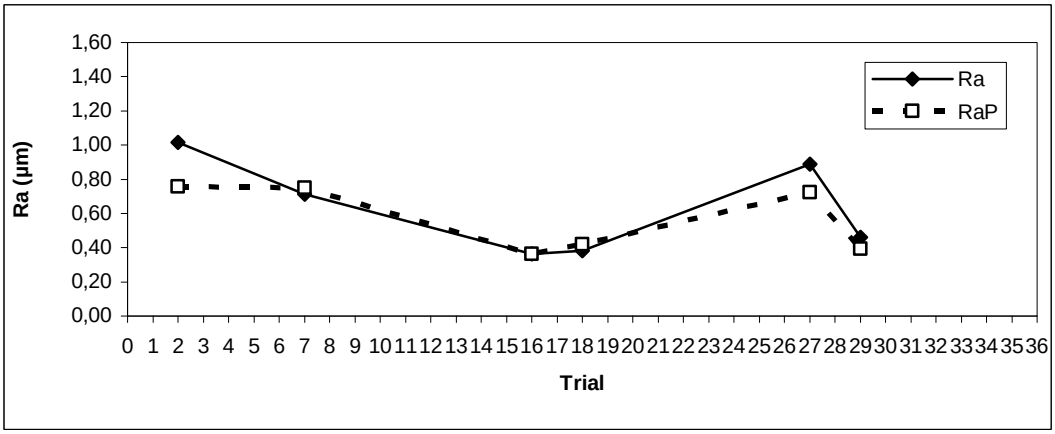

Figure 6.19- Experimental and predicted values of surface roughness for different trials for the selected GRNN architecture

As observed in Figure 6.17 no differences between the trained and the experimental values are obtained (the values are overlapped). Also, even though a slight increase between the validated and the experimental values of surface roughness is observed in Figure 6.18, this difference keeps on been smaller than the difference obtained between the predicted and the experimental values (Figure 6.19).

In this last case a maximum value of $\%RE_P$=25.50 was obtained which is almost the same result obtained when using the RBNN.

- **Evaluation of the developed ANN**

Once the different Artificial Neural Networks, RBNN, FFNN and GRNN were developed and the results of surface roughness prediction were obtained, the performance of each ANN is measured by comparing the average of the $\%RE_P$. For ease of comparison, Table 6.27 shows the minimum $\%RE_T$ and $\%RE_P$ obtained in each of the selected architecture for each studied network, and Figures 6.20 and 6.21 illustrate this result. Also, it must be highlighted that the training period of the neural networks can sometimes be time consuming. This period depends on the type of network, the training algorithms and the number of neurons employed. With regards to the RBNN and GRNN the training time was 10-60 sec. The FFNN took more time to be trained and was between 1-20 minutes. However once the network is trained the time required to predict the target output is immediate.

Table 6.27- $\%RE_T$* and $\%RE_P$* obtained from the different selected architectures networks.

Network	Architecture	$\%RE_T$*	$\%RE_P$*
RBNN	4-22-1	0.57	14.47
FFNN	4-4-4-1	0.46	6.38
GRNN	4-22-1	0.78	12.28

When comparing the average %RE (relative error) of the three selected studied architecture shown in Table 6.27, it is observed that the Feedforward Neural Network (FFNN) shows the minimum results when training the network and when predicting the values of surface roughness. In this case a $\%RE_P$=6.38 between the experimental and the predicted values of surface roughness was obtained and this value can be interpreted as a very good approach since μm is the unit used to measure the surface roughness value and also as stated before a difference of 20% was obtained between the three values of surface roughness measured in each machined specimen.

The illustration of these results is shown in Figures 6.20 and.21.

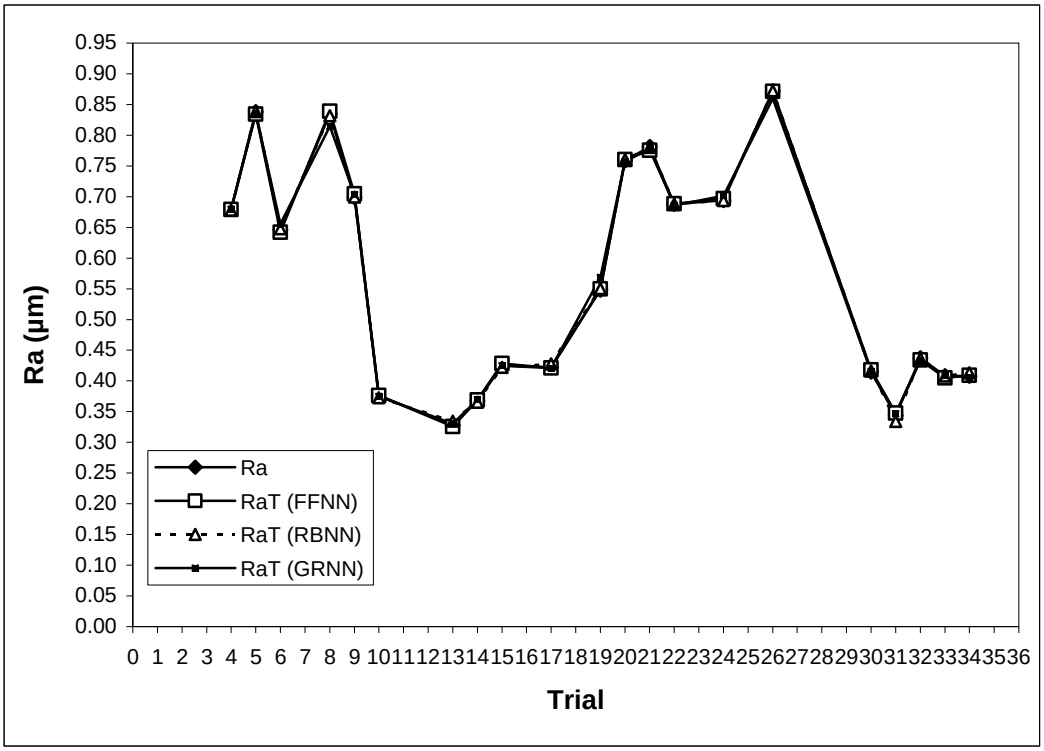

Figure 6.20- Comparison between experimental and trained values of surface roughness obtained for each selected network.

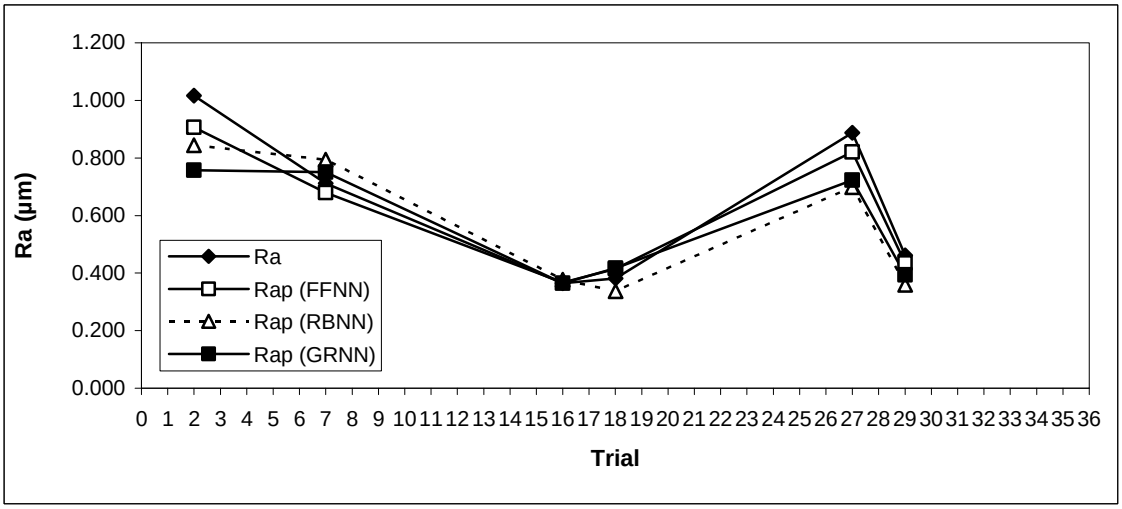

Figure 6.21- Comparison between experimental and predicted values of surface roughness obtained for each selected network.

When analyzing Figure 6.20, it is observed how all the networks were trained efficiently as they all reached the target output (experimental surface roughness) with a high accuracy (the experimental values and trained values are overlapped in all cases). When analyzing Figure 6.21 it is observed a small variation between the predicted values of roughness obtained from each of the studied networks and the experimental values of roughness; however it is observed how the predicted values of roughness obtained by using the FFNN are closer to the experimental values, giving the best result overall regarding surface roughness prediction. Despite this fact, in order to improve the $\%RE_P$*= 6.38 obtained with this FFNN that considers the tool nose radius as an input of the network, two extra FFNN will be developed but in this case one for r=0.8 mm and the other for r=2.5 mm, this means that 3 inputs are considered (cutting speed, feed per tooth and axial depth of cut) for each case.

As known, a selection of the best architecture is previously made by comparing the %EM (trained, validated and predicted) and selecting the architecture that reached the minimum %EM overall. Tables 6.28 and 6.29 presents a few FFNN architectures that were tried when using r=0.8 mm and r=2.5 mm, respectively.

Table 6.28- A few FFNN architectures and the %EM of the calculated output (Ra_T, Ra_V, Rap) and the target output (Ra) for specimens milled with r = 0.8 mm

Network	Network Architecture	Iteration	$\%EM_T$	$\%EM_V$	$\%EM_P$
1	3-3-1	341	8.5	11.6	21.6
2	3-4-1	651	6.7	7.7	11.8
3	3-5-1	481	7.2	6.9	9.8
4	**3-6-1**	**377**	**0.2**	**4.4**	**2.8**
5	3-7-1	140	0.2	8.5	11.4
6	3-8-1	242	0.2	3.7	9.3
7	3-9-1	104	0.2	9.4	13.8
8	3-10-1	379	0.2	5.5	12,7
9	3-3-3-1	405	14.6	4.4	27.7
10	3-3-4-1	109	9.6	2.7	26.3
11	3-3-5-1	971	7.5	6.9	30.9
12	3-3-6-1	263	0.2	4.9	17.8
13	3-3-7-1	3	8.2	2.6	23.7
14	3-3-8-1	15	4.8	9.8	23.6
15	3-3-9-1	61	0.2	5.3	24.3
16	3-3-10-1	183	0.2	10.3	19.7
17	3-4-3-1	177	5.1	2.5	18.8
18	3-4-4-1	864	0.2	6.1	19.6
19	3-4-5-1	350	0.8	10.7	23.9
20	3-4-6-1	59	0.1	6.2	20.9
21	3-4-7-1	67	0.3	9,4	18.2
22	3-4-8-1	72	5.0	12.6	24.7
23	3-4-9-1	395	9.4	14.8	24.2
24	3-4-10-1	200	1.8	17.5	11.4
25	3-5-3-1	766	8.3	11.0	18.3
26	3-5-4-1	41	3.2	1.8	24.0
27	3-5-5-1	31	5.4	0.1	13.7
28	3-5-6-1	67	4.9	18.7	19.5
29	3-5-7-1	5	2.3	4.4	22.7
30	3-5-8-1	217	0.2	9.9	21.7
31	3-5-9-1	108	7.7	15.8	19.9
32	3-5-10-1	29	4.1	8.6	19.5
33	3-6-3-1	286	2.3	4.5	12.1
34	3-6-4-1	401	9.9	1.8	15.6
35	3-6-5-1	33	0.2	15.0	25.0
36	3-6-6-1	9	1.2	4.3	19.1
37	3-6-7-1	369	7.7	13.2	25.0
38	3-6-8-1	120	0.5	11.4	23.0
39	3-6-9-1	107	1.8	10.2	21.3
40	3-6-10-1	2	0.1	17.7	22.5

Table 6.29- A few FFNN architectures and the %EM of the calculated output (Ra_T, Ra_V, Rap) and the target output (Ra) for specimens milled with r = 2.5 mm

Network	Network Architecture	Iteration	$\%EM_T$	$\%EM_V$	$\%EM_P$
1	3-3-1	12	3.0	5.0	12.5
2	3-4-1	200	6.9	8.8	9.8
3	3-5-1	41	3.6	8.7	9.7
4	3-6-1	270	8.9	6.6	9.1
5	3-7-1	639	7.9	2.6	10.0
6	**3-8-1**	**186**	**0.1**	**5.9**	**5.8**
7	3-9-1	268	0.2	5.9	7.6
8	3-10-1	24	7.5	5.4	9.4
9	3-3-3-1	192	3.4	1.6	13.7
10	3-3-4-1	114	3.1	7.3	13.6
11	3-3-5-1	225	8.5	7.6	13,6
12	3-3-6-1	46	10.0	3.5	13.2
13	3-3-7-1	64	4.8	7.0	13.9
14	3-3-8-1	18	3.7	9.3	13.9
15	3-3-9-1	9	8.0	4.3	13.5
16	3-3-10-1	66	5.6	4.6	13.7
17	3-4-3-1	88	2.7	6.8	10.8
18	3-4-4-1	55	6.0	6.1	12.8
19	3-4-5-1	89	0.1	2.4	12.9
20	3-4-6-1	179	6.5	7.9	7.9
21	3-4-7-1	178	5.8	6.0	12.5
22	3-4-8-1	94	9.6	6.2	13.3
23	3-4-9-1	225	0.4	8.7	11.2
24	3-4-10-1	49	8.5	6.0	10.9
25	3-5-3-1	15	7.8	7.8	13.7
26	3-5-4-1	14	3.1	3.6	14.0
27	3-5-5-1	59	9.2	4.3	13.5
28	3-5-6-1	67	4.4	3.7	11.1
29	3-5-7-1	27	0,2	8.4	10.5
30	3-5-8-1	33	8.8	6.6	12.9
31	3-5-9-1	154	7.9	5.1	12.3
32	3-5-10-1	13	3.5	2.2	9.6
33	3-6-3-1	49	3.4	3.7	10.4
34	3-6-4-1	201	3.8	3.8	12.6
35	3-6-5-1	57	0.1	3.4	10.8
36	3-6-6-1	63	0.9	3.5	13.6
37	3-6-7-1	6	0.3	1.6	8.4
38	3-6-8-1	6	6.6	9.3	13.9
39	3-6-9-1	153	0.4	9.9	11.5
40	3-6-10-1	11	0.1	9.9	8.7

When analyzing Tables 6.28 and 6.29 it is observed that the best FFNN architecture when face milling with r = 0.8 mm is architecture # 4, which used 3 inputs, 6 neurons in the hidden layer #1 and 1 output. With regard to the best FFNN architecture when face milling with r = 2.5 mm, architecture # 6 showed the best results, where 3 inputs, 8 neurons in the hidden layer and 1 output was used. These network architectures are shown in Figures 6.22 and 6.23, respectively.

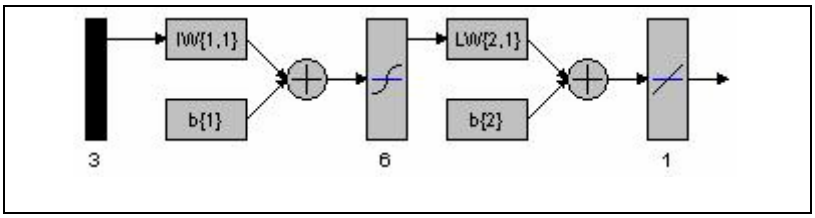

Figure 6.22- Feed Forward Neural Network architecture selected for this study when face milling with r=0.8 mm.

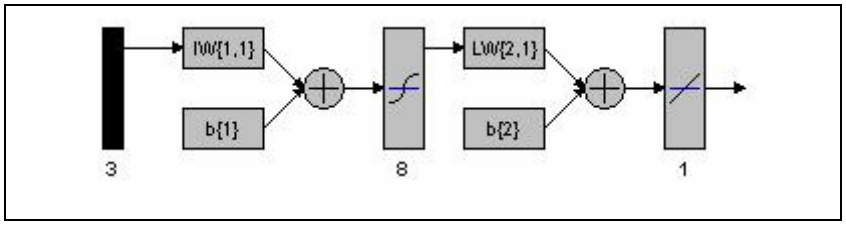

Figure 6.23- Feed Forward Neural Network architecture selected for this study when face milling with r=2.5 mm.

Once the FFNN architecture for each tool nose radius was selected, each of them were introduced in the software in order to calculate the outputs (Ra_T, Ra_V and Rap) and then %RE between the target output (Ra) and the calculated outputs. Tables 6.30, 6.31 and 6.32 present the results for the FFNN using r = 0.8 mm and Figures 6.24, 6.25 and 6.26 illustrates these results.

Table 6.30- Experimental and trained values of surface roughness, and $\%RE_T$ when using the selected FFNN for r = 0.8 mm

Trial	V (m/min)	fz (mm/rev*tooth)	ap (mm)	r (mm)	Ra (µm)	Ra_T (FFNN 0.8) (µm)	$\%RE_T$ (FFNN 0.8) (µm)
4	800	0.1	3.5	0.8	0.679	0.679	0.00
5	800	0.2	4.0	0.8	0.838	0.838	0.00
6	800	0.3	3.0	0.8	0.646	0.646	0.00
8	1000	0.2	3.0	0.8	0.835	0.834	0.12
9	1000	0.3	3.5	0.8	0.699	0.700	0.14
19	1200	0.1	3.0	0.8	0.548	0.549	0.18
20	1200	0.2	3.5	0.8	0.759	0.759	0.00
21	1200	0.3	4.0	0.8	0.781	0.781	0.00
22	1400	0.1	3.5	0.8	0.688	0.688	0.00
24	1400	0.3	3.0	0.8	0.694	0.694	0.00
26	1600	0.2	3.0	0.8	0.872	0.872	0.00

Table 6.31- Experimental and validated values of surface roughness, and $\%RE_V$ when using the selected FFNN for r = 0.8 mm

Trial	V (m/min)	fz (mm/rev*tooth)	ap (mm)	r (mm)	Ra (µm)	Ra_V (FFNN 0.8) (µm)	$\%RE_V$ (FFNN 0.8) (µm)
1	600	0.1	3.0	0.8	0.699	0.687	1.72
23	1400	0.2	4.0	0.8	0.668	0.695	4.04

Table 6.32- Experimental and predicted values of surface roughness, and $\%RE_P$ when using the selected FFNN for r = 0.8 mm

Trial	V (m/min)	fz (mm/rev*tooth)	ap (mm)	r (mm)	Ra (µm)	Rap (FFNN 0.8) (µm)	$\%RE_P$ (FFNN 0.8) (µm)
2	600	0.2	3.5	0.8	1.017	1.019	0.20
7	1000	0.1	4.0	0.8	0.712	0.707	0.70
27	1600	0.3	3.5	0.8	0.888	0.912	3.60

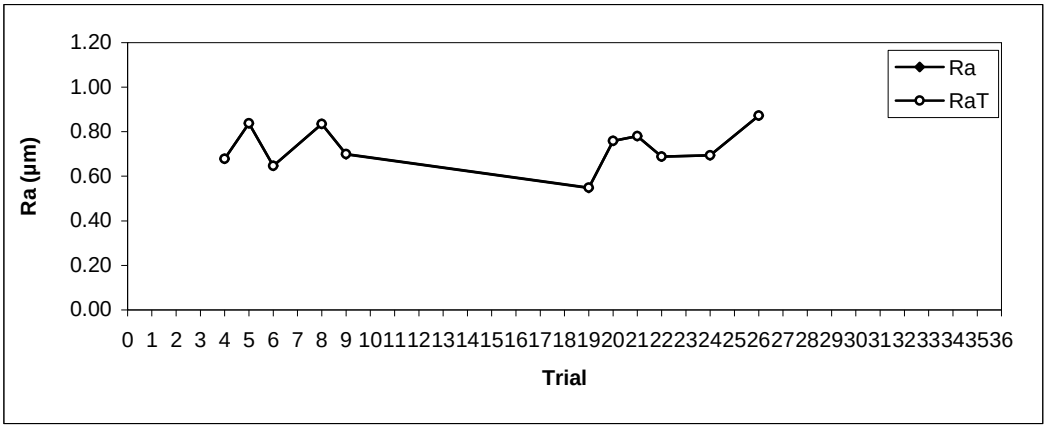

Figure 6.24- Experimental and trained values of surface roughness when using the selected FFNN architecture for r = 0.8 mm.

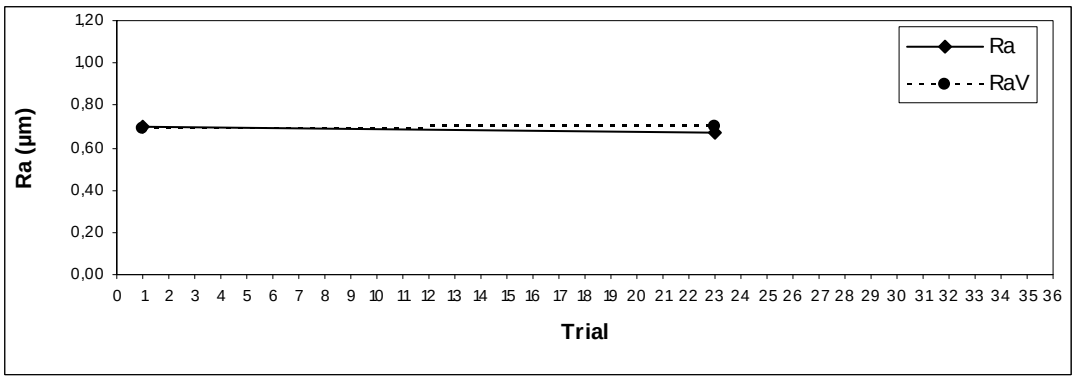

Figure 6.25- Experimental and validated values of surface roughness when using the selected FFNN architecture for r = 0.8 mm.

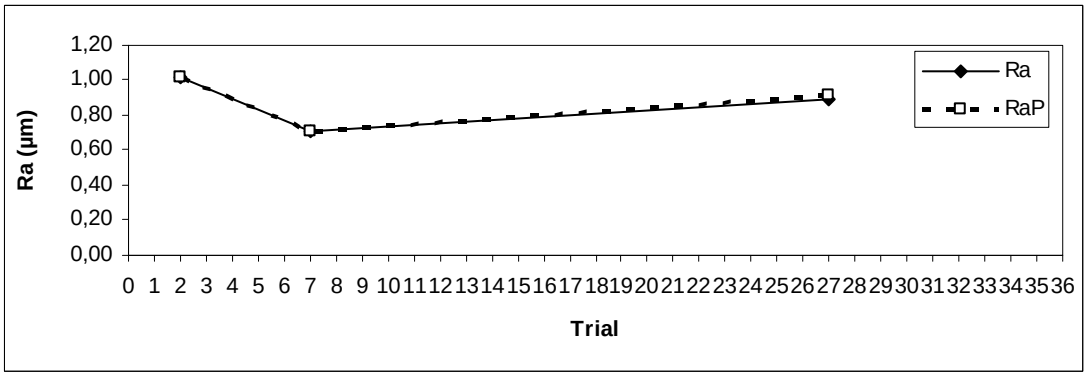

Figure 6.26- Experimental and predicted values of surface roughness when using the selected FFNN architecture for r = 0.8 mm.

As observed when analyzing the results presented in Tables 6.30, 6.31 and 6.32 which are illustrated in Figures 6.24, 6.25 and 6.26 once again the trained values are overlapped with the experimental values and in this case closer values between the validated and experimental values of roughness (Figure 6.25) and between predicted and experimental values of roughness (Figure 6.26) are obtained. This reveals that a better performance of the FFNN is obtained when developing a network for a specific value of tool nose radius, since the difference between the calculated outputs and the target output become smaller when comparing them to the results of the FFNN that uses the tool nose radius as an input of the network (Section 6.4.2).

With regard to the results obtained for the FFNN when using r=2.5 mm, Tables 6.33, 6.34 and 6.35 presents the different results between the calculated outputs (Ra_T, Ra_V, Rap) and the target output (Ra) and Figures 6.27, 6.28 and 6.29, illustrates them.

Table 6.33- Experimental and trained values of surface roughness, and $\%RE_T$ when using the selected FFNN for r = 2.5 mm

Trial	V (m/min)	fz (mm/rev*tooth)	ap (mm)	r (mm)	Ra (µm)	Ra_T (FFNN 2.5) (µm)	$\%RE_T$ (FFNN 2.5) (µm)
10	600	0.1	3.0	2.5	0.376	0.376	0.00
13	800	0.1	3.5	2.5	0.328	0.328	0.00
14	800	0.2	4.0	2.5	0.368	0.368	0.00
15	800	0.3	3.0	2.5	0.425	0.425	0.00
17	1000	0.2	3.0	2.5	0.422	0.422	0.00
30	1200	0.3	4.0	2.5	0.415	0.415	0.00
31	1400	0.1	3.5	2.5	0.344	0.344	0.00
32	1400	0.2	4.0	2.5	0.437	0.437	0.00
33	1400	0.3	3.0	2.5	0.408	0.408	0.00
34	1600	0.1	4.0	2.5	0.408	0.408	0.00

Table 6.34- Experimental and validated values of surface roughness, and $\%RE_V$ when using the selected FFNN for r = 2.5 mm

Trial	V (m/min)	fz (mm/rev*tooth)	ap (mm)	r (mm)	Ra (µm)	Ra_v (FFNN 2.5) (µm)	$\%RE_V$ (FFNN 2.5) (µm)
11	600	0.2	3.5	2.5	0.365	0.384	5.21
28	1200	0.1	3.0	2.5	0.453	0.453	0.00
35	1600	0.2	3.0	2.5	0.399	0.408	2.26
36	1600	0.3	3.5	2.5	0.418	0.422	0.96

Table 6.35- Experimental and predicted values of surface roughness, and $\%RE_P$ when using the selected FFNN for r = 2.5 mm

Trial	V (m/min)	fz (mm/rev*tooth)	ap (mm)	r (mm)	Ra (µm)	Rap (FFNN 2.5) (µm)	$\%RE_P$ (FFNN 2.5) (µm)
16	1000	0.1	4.0	2.5	0.365	0.372	1.92
18	1000	0.3	3.5	2.5	0.381	0.393	3.15
29	1200	0.2	3.5	2.5	0.461	0.440	4.56

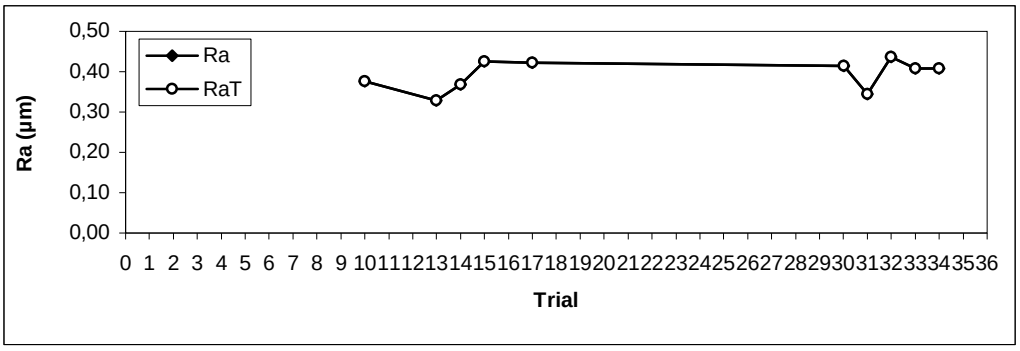

Figure 6.27- Experimental and trained values of surface roughness when using the selected FFNN architecture for r = 2.5 mm.

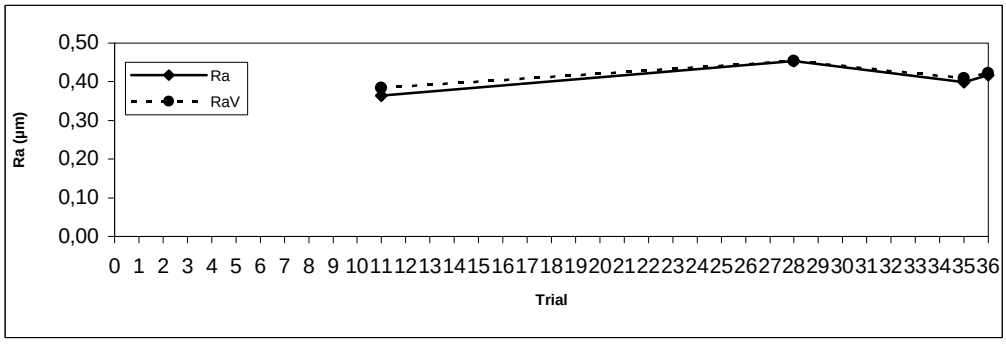

Figure 6.28- Experimental and validated values of surface roughness when using the selected FFNN architecture for r = 2.5 mm.

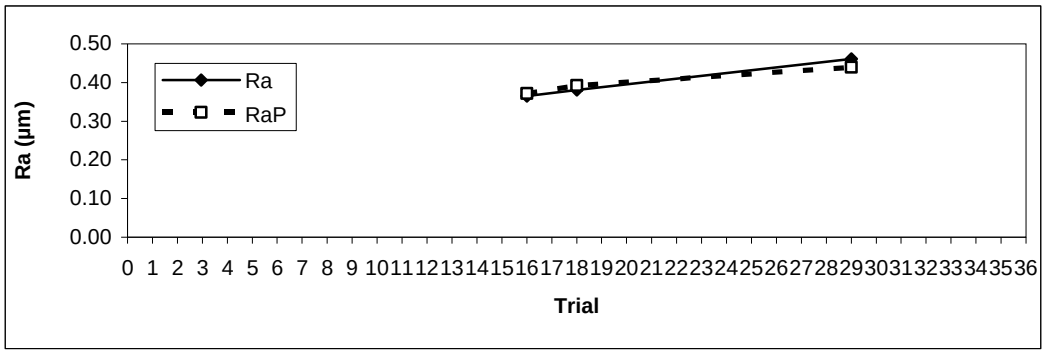

Figure 6.29- Experimental and predicted values of surface roughness when using the selected FFNN architecture for r = 2.5 mm.

When analyzing the results of FFNN for r=2.5 mm presented in Tables 6.33, 6.34 and 6.35 and illustrated in Figures 6.27, 6.28 and 6.29, it is observed that once again better results were obtained when developing a FFNN for a specific tool nose radius, since a closer value between the calculated outputs and the target output is obtained.

When comparing the results of FFNN for r=0.8 mm and for r= 2.5 mm with the FFNN architecture that considers the tool nose radius as an input, it is observed that the $\%RE_P$* for FFNN architecture that considers the tool nose radius, was reduced from 6.38% to a $\%RE_P$=1.5 and $\%RE_P$=3.21 when considering FFNN for r = 0.8 mm and FFNN for r = 2.5 mm, respectively.

Analyzing the complete study conducted with the Artificial Neural Network, it is observed that this is valuable tool for surface roughness prediction since it can reach accuracy as high as 98% especially when using FFNN architectures. This result is in agreement with previous research conducted by Tsai et al. in 1999, where an accuracy of 94% was obtained when using FFNN for the prediction of roughness during an end milling process.

6.5 Theoretical model based in geometrical analysis (Model 3)

In order to continue with the prediction of surface roughness for specimens milled with square inserts under a wet cutting condition a geometrical analysis has been proposed. In this case, a visual observation of all the machined surfaces obtained under different cutting condition was conducted.

The observations revealed that, in general, only tool marks obtained from the front cutting process were observed along the machined surface and only 2 trials out of 36 showed the back cutting mark left by the tool as it rotated along the machined surface to remove the material. Figure 6.30 show machined surfaces where the front cutting and front-back cutting of the tool trail are observed.

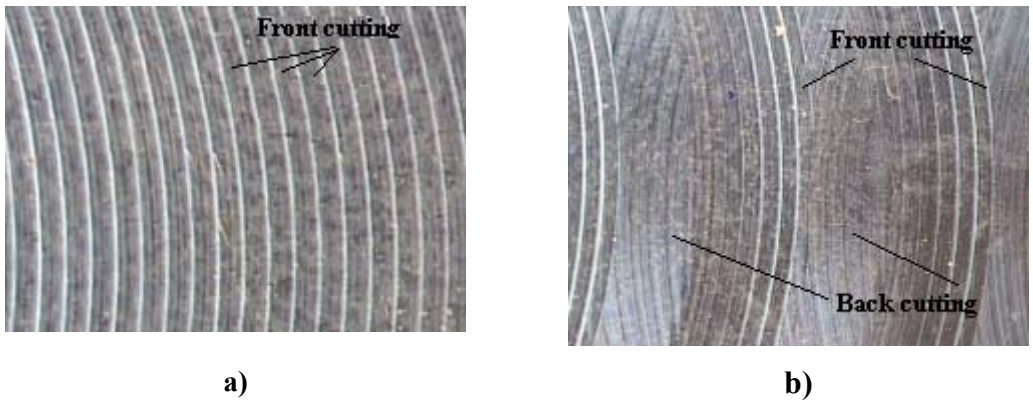

Figure 6.30- Pictures of the trail left by the tool on the Al 7075-T7351 machined surface after face milling with square inserts.
a) Front cutting and b) Front and back cutting.

This proposed model based in geometric analysis is obtained by the recreation of the tool trail left on the machined surface. In this case the tool trail is developed considering the feed per tooth, the cutting tool nose radius, angle κ_i (obtained from the Fourier series analysis, reported in section 6.3) and the tool runout errors.

From previous research (Baek, 2001 and Franco, 2004 and 2008) it was noted the influence of the tool runout variable on the surface roughness and the importance of including it for the prediction of the surface roughness.

The static tool runouts (axial deviation, εa and radial deviation, εr) are defects that consist in small discrepancies in the relative position of the different cutting teeth. These discrepancies are obtained for many reasons such as: manufacturing tolerances of the cutting tool inserts and seats, inaccuracy in the fixturing of the indexable inserts, uncertainty in the clamping force of the insert screws, imperfections in the machine tool axis movements, etc. Figure 6.31 shows a schematic of the front and back cutting and the static tool runouts and angle α_i.

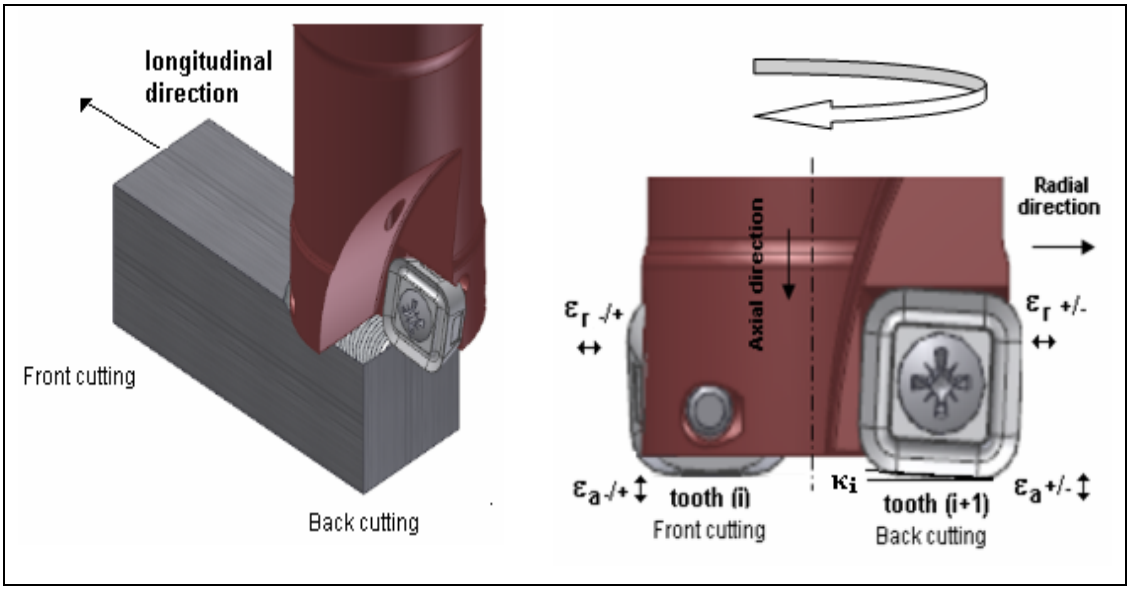

Figure 6.31- Schematic of the axial and radial deviation during rotation of the tool, where front and back cutting of tooth (i and i+1) can be observed, as well as κ_i angle and the axial and radial runout; εa and εr, respectively.

In order to know the contribution of each type of cutting (front, back and front-back cutting) on the surface roughness, three models are developed and named as followed:

- Front cutting theoretical model (F)
- Back cutting theoretical model (B)
- Front-Back cutting theoretical model (FB)

Also for the development of these models the following considerations are taken into account:

- All the models are considered as general since they can be applied to any tool diameter with "i" number of teeth.
- For each model two (2) considerations are made:
  - **"I"**. Ideal condition: no static tool runouts, (εa = ε r = 0) and $\kappa_i = \kappa_{i+1}$.
  - **"R"**. Real condition: static tool runouts, (εa ≠ 0 and εr ≠ 0) and $\kappa_i = \kappa_{i+1}$
- Since in this research a tool with two (2) teeth is employed, tooth (1) is considered the pattern with εa = εr = 0 and tooth (2) will have (εa ≠ 0 and εr ≠ 0) when considering a real condition.
- A maximum of 10 peaks (n, n+1….) is considered for the development of the 2D surface roughness profile. It must be highlighted that this number can be changed by the user and the result will be like "a zoom in or zoom out" of the 2D theoretical surface roughness profile.
- In order to generate the 2D surface roughness profile, as well as the average surface roughness value for each of the trials, an algorithm is included where random tool runout values are considered.
- Finally, small values of axial runout must be considered since this is the deviation that contributes on the surface roughness value. Figure 6.32 illustrates this fact.

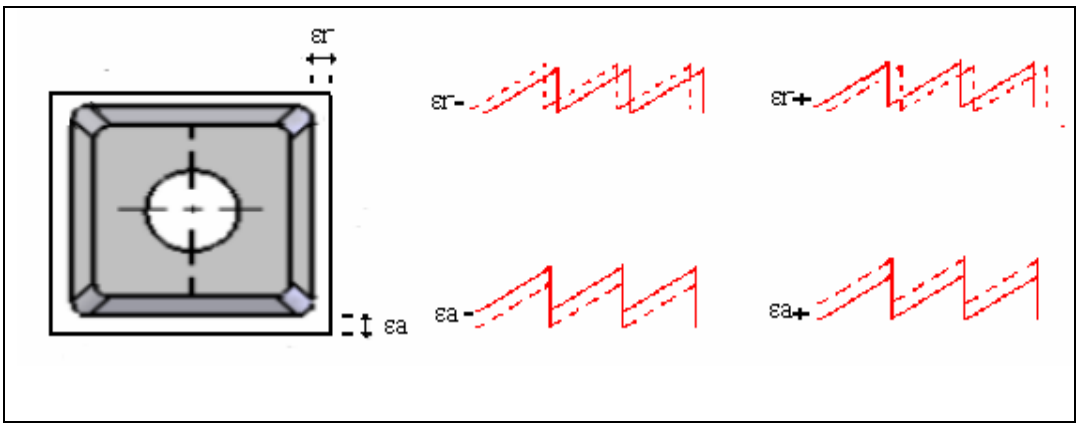

Figure 6.32- Illustration of how the 2D surface roughness profile is affected when considering "+" or "-" static tool runouts.

As observed when analyzing Figure 6.32, the axial tool deviation is the tool deviation that produces a displacement of the surface roughness profile in an "up or down" direction (depending on the sign of the deviation), affecting the deepness of the profile and consequently the value of the surface roughness. The radial tool deviation produces a small movement of the profile in a "right or left" direction (depending on the sign of the deviation).

The values of these deviations were obtained by using random numbers. In the case of the radial deviation a $\varepsilon r \leq 0.009$ mm was used since as previously stated this deviation produces a movement of the profile in a right or left direction with out affecting the value of the surface roughness. With regard to the axial deviation, this was set as $\varepsilon a \leq 0.0003$ mm and the explanation of this fact is presented later on in Table 6.42.

Once all these considerations are taken into account, the different models are developed and for all the cases, the 33 trials (left after applying the Tchebysheff's theorem) were used to predict the surface roughness value.

The development of each model is companied by an illustration of the trail left by the tool on the machined surface. This will facilitate the reader the understanding of the inclusion of the different variables in each developed model. Also as previously stated, since an ideal and a real condition is taken into account, in order to understand the importance of including the tool runout variable on the surface roughness prediction, an illustration for each case is also presented.

6.5.1 Front cutting theoretical model (F)

For the development of this model, the recreation of the tool trail is obtained by considering only the front cutting part of the inserts. Figure 6.33 and 6.34 illustrates this type of cutting under: A) an ideal condition, ($\varepsilon a = \varepsilon r = 0$) and B) a real condition, ($\varepsilon a \neq 0$ and $\varepsilon r \neq 0$). Also these figures show the parameters that are involved in the development of the 2D surface roughness profile. It is observed that the figures include the position of tooth (i) and tooth (i+1), as well as the marks left by the teeth, n and n+1. It must be highlighted that these marks depends on each tooth position and they are located as fz multiples, this means that the mark "n" is "n" times away fz (nfz).

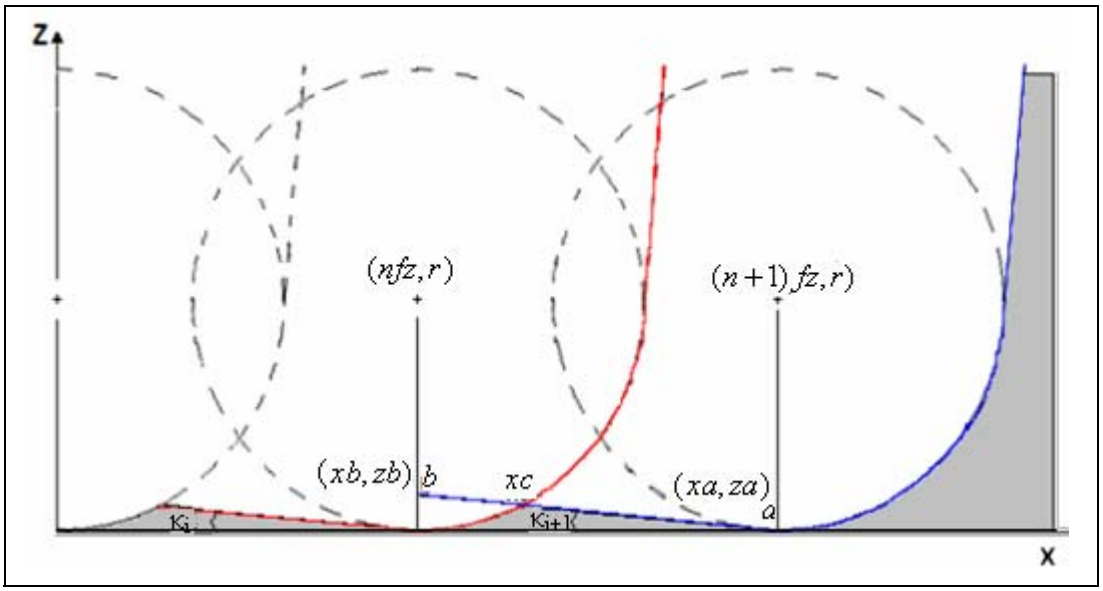

Figure 6.33- Schematic of the trail left by the cutting tool when considering front cutting and an ideal condition (εa = ε r= 0). Tooth (i) (colored solid red) and tooth (i+1) (colored solid blue). The gray area represents the 2D theoretical surface roughness profile.

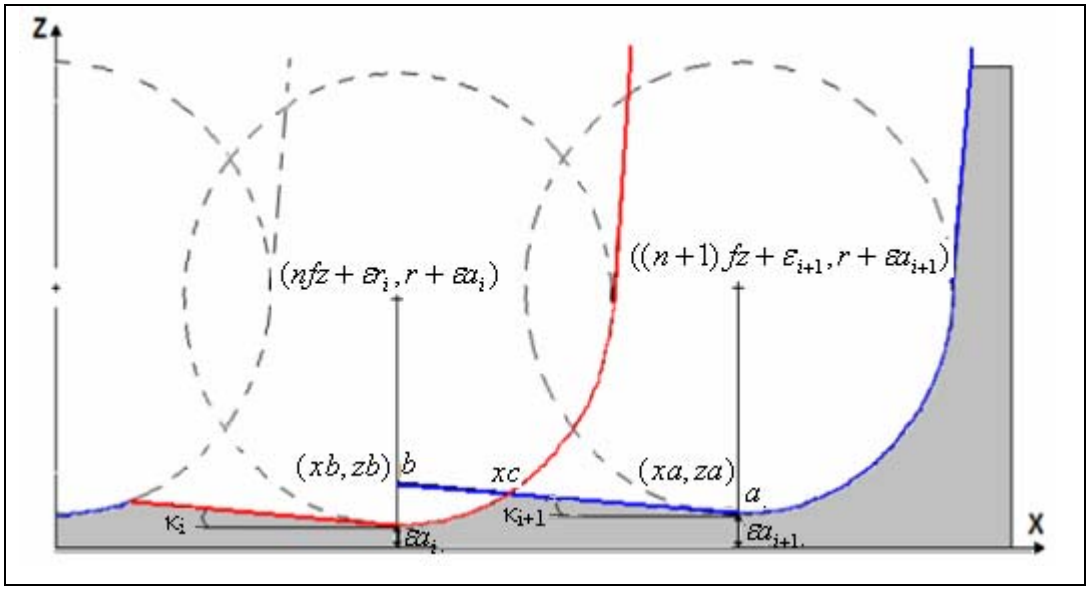

Figure 6.34- Schematic of the trail left by the cutting tool when considering front cutting and a realist condition (εa ≠ 0 and εr ≠ 0). Tooth (i) (colored solid red) and tooth (i+1) (colored solid blue). The gray area represents the surface roughness profile.

As observed when analyzing both Figures 6.33 and 6.34, when the tool moves along the cutting length, tooth (i), starts to cut (solid red line) and then tooth (i+1) (solid blue line) which is "fz" away from tooth (i), starts to cut as well. Since the inserts selected for the cutting process have a square geometry, this one is composed by two sections. The first section is delimited by a circle (tool nose radius) and the second section delimited by a line (see Chapter 5, Figure 5.2, where the geometry of the tool is illustrated).

By taking into account the intersection of the section of the circle (negative size, ($\cup$) and the section of the line; and by also considering the variables (fz and r) which are also involved in the trail left by the tool on the machined surface, the intersection point "c" is obtained. The height of this point "c" corresponds to Z_c, which also corresponds to the theoretical surface roughness value. It must be highlighted that this height (Z_c) will change depending on the static tool runouts that are considered.

Equation 6.19 presents the negative part of the square root of the circle equation, which in this case is the part of the circle that we are considering for the development of the model ($\cup$):

$$Z = Z_n - \sqrt{r^2 - \left(X - X_n\right)^2} \tag{6.19}$$

and the X_n and Z_n values are the coordinates of the centre of the circle. These coordinates corresponds to the "n" mark:

$$X_n = n \cdot fz + \varepsilon r_i \tag{6.20}$$

$$Z_n = r + \varepsilon a_i \tag{6.21}$$

or the "n+1" mark:

$$X_{n+1} = \left(n+1\right) \cdot fz + \varepsilon r_{i+1} \tag{6.22}$$

$$Z_{n+1} = r + \varepsilon a_{i+1} \tag{6.23}$$

Also **Point a** coordinates are:

$$X_a = (n+1)\cdot fz + \varepsilon r_{i+1} \tag{6.21}$$

$$Z_a = \varepsilon a_{i+1} \tag{6.22}$$

The equation of the line is reported in equation 6.23 and the equation of the slope in equation 6.24.

$$Z_L = mx + b \tag{6.23}$$

$$m = -\tan(\kappa_{i+1}) \tag{6.24}$$

When substituting equation 6.24 in equation 6.23 and considering $X=X_a$ and $Z_L=Z_a$ then the cutting point (b) with the Z axis is obtained and shown in equation 6.25.

$$b = [(n+1)\cdot fz + \varepsilon r_{i+1}]\cdot \tan(\kappa_{i+1}) + \varepsilon a_{i+1} \tag{6.25}$$

When substituting equation 6.25 and 6.24 in equation 6.23 the following is obtained:

$$Z_L = -\tan(\kappa_{i+1})\cdot[x - ((n+1)\, fz + \varepsilon r_{i+1})] + \varepsilon a_{i+1} \tag{6.26}$$

In order to obtain X_c, which is the intersection between the section of the circle and the section of the line, equation 6.19 is equated with equation 6.23, obtaining equation 6.27.

To obtain Z, which allows the generation of the 2D profile; this one is defined by equation 6.28, which as observed, is composed by two expressions, 6.28a and 6.28b.

Equation 6.28.a corresponds to the equation of the circle, which is used to calculate Z when x is bigger then X_n (eq 6.20), but smaller or equal to X_c (eq 6.27).

Equation 6.28.b corresponds to the equation of a line, which is used to calculate Z when x is bigger then X_c (eq. 6.27) but smaller than X_{n-1} (eq. 6.22)

$$X_c = \frac{-\left[m\cdot\left(b-Z_n\right)-X_n\right]+\sqrt{\left[m\cdot\left(b-Z_n\right)-X_n\right]^2-\left(m^2+1\right)\cdot\left[\left(b-Z_n\right)^2+{X_n}^2-r^2\right]}}{\left(m^2+1\right)} \tag{6.27}$$

$$Z(x,i,n)= \begin{cases} r+\varepsilon a_i-\sqrt{r^2-\left[x-\left(n\cdot fz+\varepsilon r_i\right)\right]^2} & \forall n\wedge n\cdot fz+\varepsilon r_i\le x\le X_c \quad (6.28.a) \\ -\tan\left(\kappa_{i+1}\right)\cdot\left[x-\left((n+1)\,fz+\varepsilon r_{i+1}\right)\right]+\varepsilon a_{i+1} & \forall n\wedge X_c<x\le\left(n+1\right)\cdot fz+\varepsilon r_{i+1} \quad (6.28.b) \end{cases} \tag{6.28}$$

Once the front cutting theoretical model is obtained, the predicted theoretical values of surface roughness for front cutting (RapF) were compared with the experimental surface roughness value (Ra). Table 6.36 shows the experimental and predicted values of surface roughness as well as the $\%RE_P$ when considering the front cutting for an ideal condition (εa=εr=0). Figure 6.35 illustrates this result.

Table 6.36- Experimental and predicted theoretical values of surface roughness and $\%RE_{P,}$ obtained when considering the front cutting theoretical model and an ideal condition $\varepsilon a = \varepsilon r = 0$.

Trial	κ_i (°)	Ra (µm)	RapF.I (µm)	$\%RE_P$ (F.I)
1	0.40	0.699	0.501	28.3
2	0.29	1.017	0.828	18.6
4	0.39	0.679	0.490	27.8
5	0.24	0.838	0.698	16.7
6	0.12	0.646	0.565	12.5
7	0.41	0.712	0.511	28.2
8	0.24	0.835	0.698	16.4
9	0.13	0.699	0.610	12.7
10	0.22	0.376	0.249	33.8
11	0.11	0.399	0.309	22.6
13	0.19	0.328	0.221	32.6
14	0.11	0.368	0.309	16.0
15	0.08	0.425	0.360	15.3
16	0.21	0.365	0.240	34.2
17	0.12	0.422	0.333	21.1
18	0.07	0.381	0.318	16.5
19	0.31	0.548	0.404	26.3
20	0.22	0.759	0.645	15.0
21	0.15	0.781	0.698	10.6
22	0.39	0.688	0.490	28.8
23	0.19	0.668	0.564	15.6
24	0.13	0.694	0.610	12.1
26	0.25	0.872	0.724	17.0
27	0.17	0.888	0.785	11.6
28	0.21	0.365	0.240	34.2
29	0.13	0.461	0.358	22.3
30	0.08	0.415	0.360	13.3
31	0.20	0.344	0.231	32.8
32	0.13	0.437	0.358	18.1
33	0.08	0.408	0.360	11.8
34	0.23	0.408	0.257	37.0
35	0.12	0.418	0.333	20.3
36	0.09	0.453	0.401	11.5
			$\%RE_P$* (F.I)	20.9

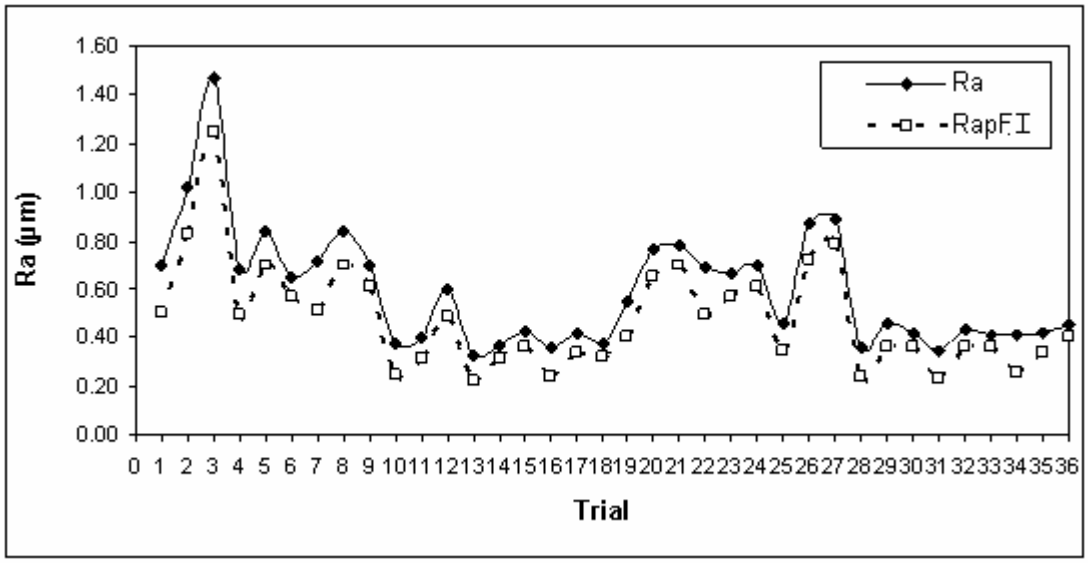

Figure 6.35- Experimental and predicted theoretical values of surface roughness when considering front cutting and an ideal condition (εa = εr = 0)

When analyzing Figure 6.35, it is observed that the predicted values obtained by using the front cutting theoretical model when considering an ideal condition, εa = εr = 0 are smaller than the experimental values (RapF.I < Ra). This result was expected since an ideal condition was considered and no workpiece imperfections and other factors that could affect the surface roughness were considered. In addition this is due to the machining process being undertaken within the elastic limits of the material. Also, in this case a $\%RE_P$* of around 21 % between the calculated output (RapF.I) and the target output (Ra) was obtained.

Table 6.37 shows the experimental and predicted values of surface roughness as well as the $\%RE_P$ (Relative Error percentage between the calculated output, (RapF.R) and the target output, (Ra)) when considering front cutting for a real condition (εa ≠ 0 and εr ≠ 0). Figure 6.36 illustrates this result.

Table 6.37- Experimental and predicted theoretical values of surface roughness and $\%RE_P$ obtained when considering the front cutting theoretical model and a real condition ($\varepsilon a \neq 0$ and $\varepsilon r \neq 0$).

Trial	κ_i (°)	εr (mm)	εa (mm)	Ra (μm)	RapF.R (μm)	$\%RE_P$ (F.R)
1	0.40	0.009	0.0002	0.699	0.686	1.9
2	0.29	0.001	0.0002	1.017	1.014	0.3
4	0.39	0.002	0.0002	0.679	0.671	1.2
5	0.24	-0.009	0.0002	0.838	0.846	1.0
6	0.12	-0.008	0.0001	0.646	0.644	0.3
7	0.41	-0.008	0.0003	0.712	0.716	0.6
8	0.24	-0.009	0.0002	0.835	0.846	1.3
9	0.13	-0.006	0.0001	0.699	0.692	1.0
10	0.22	-0.009	0.0002	0.376	0.382	1.6
11	0.11	0.001	0.0001	0.399	0.400	0.3
13	0.19	0.008	0.0001	0.328	0.361	10.1
14	0.11	-0.008	0.0001	0.368	0.384	4.3
15	0.08	-0.007	0.0001	0.425	0.443	4.2
16	0.21	-0.009	0.0002	0.365	0.375	2.7
17	0.12	-0.002	0.0001	0.422	0.419	0.7
18	0.07	-0.009	0.0001	0.381	0.401	5.2
19	0.31	-0.008	0.0002	0.548	0.539	1.6
20	0.22	0.008	0.0001	0.759	0.764	0.7
21	0.15	0.001	0.0001	0.781	0.795	1.8
22	0.39	0.005	0.0002	0.688	0.689	0.1
23	0.19	0.002	0.0001	0.668	0.662	0.9
24	0.13	-0.009	0.0001	0.694	0.685	1.3
26	0.25	-0.007	0.0002	0.872	0.879	0.8
27	0.17	0.005	0.0001	0.888	0.893	0.6
28	0.21	-0.008	0.0002	0.365	0.378	3.6
29	0.13	0.005	0.0001	0.461	0.457	0.9
30	0.08	-0.008	0.0001	0.415	0.442	6.5
31	0.20	0.009	0.0001	0.344	0.337	2.0
32	0.13	0.002	0.0001	0.437	0.451	3.2
33	0.08	-0.009	0.0001	0.408	0.441	8.1
34	0.23	-0.006	0.0002	0.408	0.398	2.5
35	0.12	-0.008	0.0001	0.418	0.408	2.4
36	0.09	-0.005	0.0001	0.453	0.486	7.3
					$\%RE_P$*(F.R)	2.4

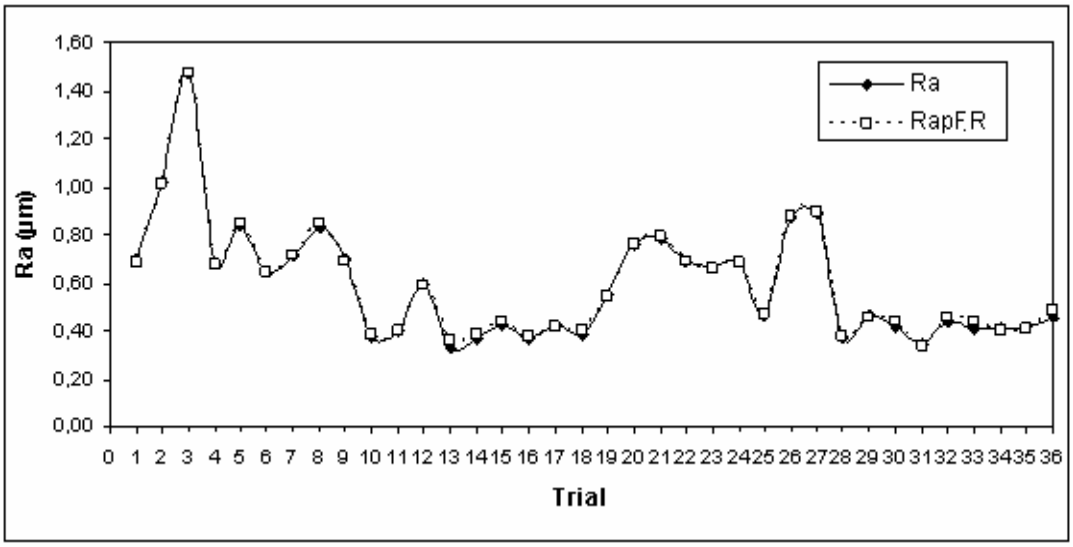

Figure 6.36- Experimental and predicted theoretical values of surface roughness considering front cutting and a real condition ($\varepsilon a \neq 0$ and $\varepsilon r \neq 0$).

When analyzing Figure 6.36, it is observed that the predicted surface roughness values get closer to the experimental surface roughness values when considering the axial and radial static tool runouts. This is a realistic assumption since the inserts are screwed to the tool holder every time a new trial is executed, producing changes in the axial and radial deviation. The results show a $\%RE_P$*= 2.4 between the calculated output (RapF.R) and the target output (Ra). This result shows the importance of considering the static tool runouts due to the excellent approach obtained between the experimental and the theoretical value of surface roughness, especially when considering that 20% between the three (3) measurements of roughness, made on the milled surface of each trial was obtained and also that µm is the unit used to measure the surface roughness.

Also the results show that a unique cutter tooth can define the surface profile of milled parts when considering the front cutting process. This result is in agreement with research made by Franco (2004).

6.5.2 Back cutting theoretical model (B)

Once the results obtained from the front cutting theoretical model were analyzed, the back cutting theoretical model was developed.

In this case, it must be highlighted that the same value of axial and radial deviation that were considered for tooth (2) but with the opposite sign from the ones used in the front cutting model are applied since the tool is rotating. (See Figure 6.31).

Since, the value of axial and radial deviation of tooth (i) must be kept constant during the front and the back cutting process, but with opposite sign, it is expected that, the same theoretical value of surface roughness will be obtained as during the front cutting process. The only difference that is obtained in this back cutting theoretical model is that, in this case, the slope of the 2D surface roughness profile is opposite when compared to the front cutting model.

In order to obtain X_c and the general expression for Z, the following equations must be applied:

$$X_c = \frac{-\left[m\cdot\left(b-Z_n\right)-X_n\right]-\sqrt{\left[m\cdot\left(b-Z_n\right)-X_n\right]^2-\left(m^2+1\right)\cdot\left[\left(b-Z_n\right)^2+{X_n}^2-r^2\right]}}{\left(m^2+1\right)} \tag{6.29}$$

$$Z\ (x,i,n) = \begin{cases} +\tan\left(\kappa_{i+1}\right)\cdot\left[x-\left(nfz+\varepsilon r_{i+1}\right)\right]-\varepsilon a_{i+1} & \forall n \wedge n\cdot fz+\varepsilon r_i \le x \le X_c \quad (6.30.a) \\ r+\varepsilon a_i-\sqrt{r^2-\left[x-\left(n\cdot fz+\varepsilon r_i\right)\right]^2} & \forall n \wedge X_c < x \le \left(n+1\right)\cdot fz+\varepsilon r_{i+1} \quad (6.30.b) \end{cases} \tag{6.30}$$

Figure 6.37 and 6.38 illustrates the 2D theoretical surface roughness profile obtained when assuming an ideal condition (εa = εr = 0) and a real condition (εa ≠ 0 and εr ≠ 0) respectively.

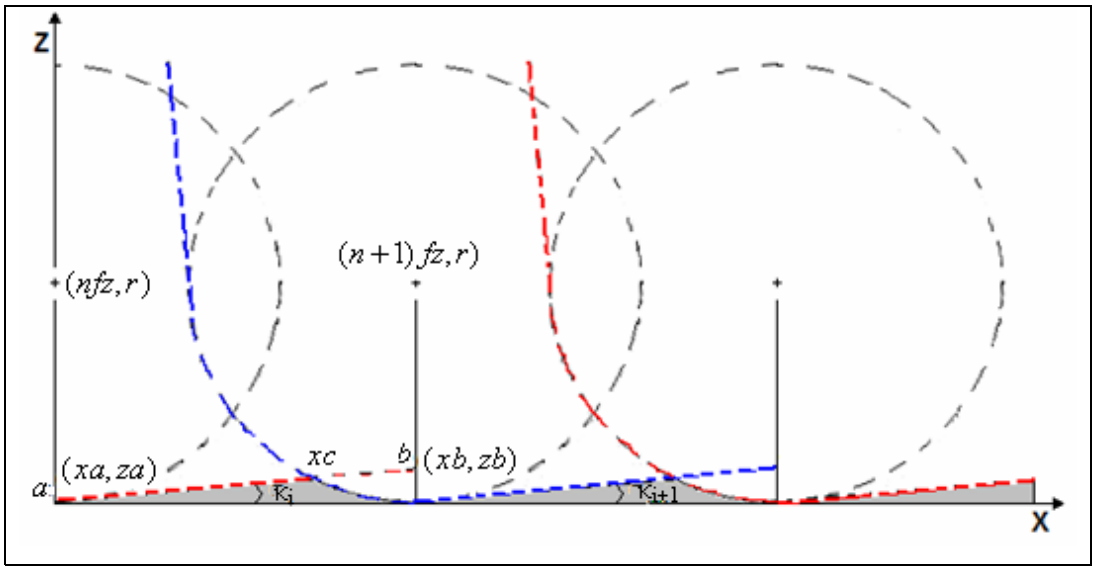

Figure 6.37- Schematic of the trail left by the cutting tool when considering back cutting and an ideal condition (εa = εr = 0). Tooth (i) (colored dashed red) and tooth (i+1) (colored dashed blue). The gray area represents the 2D theoretical surface roughness profile.

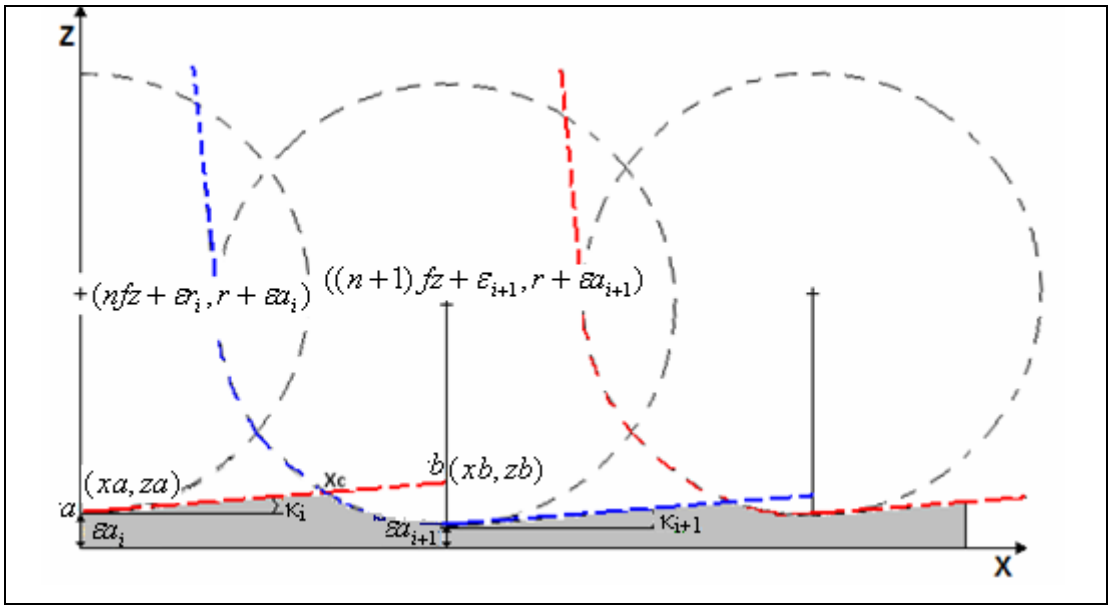

Figure 6.38- Schematic of the trail left by the cutting tool when considering back cutting and a real condition (εa ≠ 0 and εr ≠ 0). Tooth (i) (colored dashed red) and tooth (i+1) (colored dashed blue). The gray area represents the 2D theoretical surface roughness profile.

Table 6.38 shows the experimental and predicted values of surface roughness as well as the $\%RE_{P,}$ (Relative Error percentage) between the calculated output, (RapB.I) and the target output, (Ra) when considering the back cutting for an ideal condition (εa= εr = 0). Figure 6.39 illustrates this result.

Table 6.38- Experimental and predicted values of surface roughness and $\%RE_P$ obtained when considering the back cutting theoretical model and an ideal condition $\varepsilon a = \varepsilon r = 0$

Trial	κ_i (°)	Ra (µm)	RapB.I (µm)	$\%RE_P$ (B.I)
1	0.40	0.699	0.501	28.3
2	0.29	1.017	0.828	18.6
4	0.39	0.679	0.490	27.8
5	0.24	0.838	0.698	16.7
6	0.12	0.646	0.565	12.5
7	0.41	0.712	0.511	28.2
8	0.24	0.835	0.698	16.4
9	0.13	0.699	0.610	12.7
10	0.22	0.376	0.249	33.8
11	0.11	0.399	0.309	22.6
13	0.19	0.328	0.221	32.6
14	0.11	0.368	0.309	16.0
15	0.08	0.425	0.360	15.3
16	0.21	0.365	0.240	34.2
17	0.12	0.422	0.333	21.1
18	0.07	0.381	0.318	16.5
19	0.31	0.548	0.404	26.3
20	0.22	0.759	0.645	15.0
21	0.15	0.781	0.698	10.6
22	0.39	0.688	0.490	28.8
23	0.19	0.668	0.564	15.6
24	0.13	0.694	0.610	12.1
26	0.25	0.872	0.724	17.0
27	0.17	0.888	0.785	11.6
28	0.21	0.365	0.240	34.2
29	0.13	0.461	0.358	22.3
30	0.08	0.415	0.360	13.3
31	0.20	0.344	0.231	32.8
32	0.13	0.437	0.358	18.1
33	0.08	0.408	0.360	11.8
34	0.23	0.408	0.257	37.0
35	0.12	0.418	0.333	20.3
36	0.09	0.453	0.401	11.5
			$\%RE_P$* (B.I)	20.9

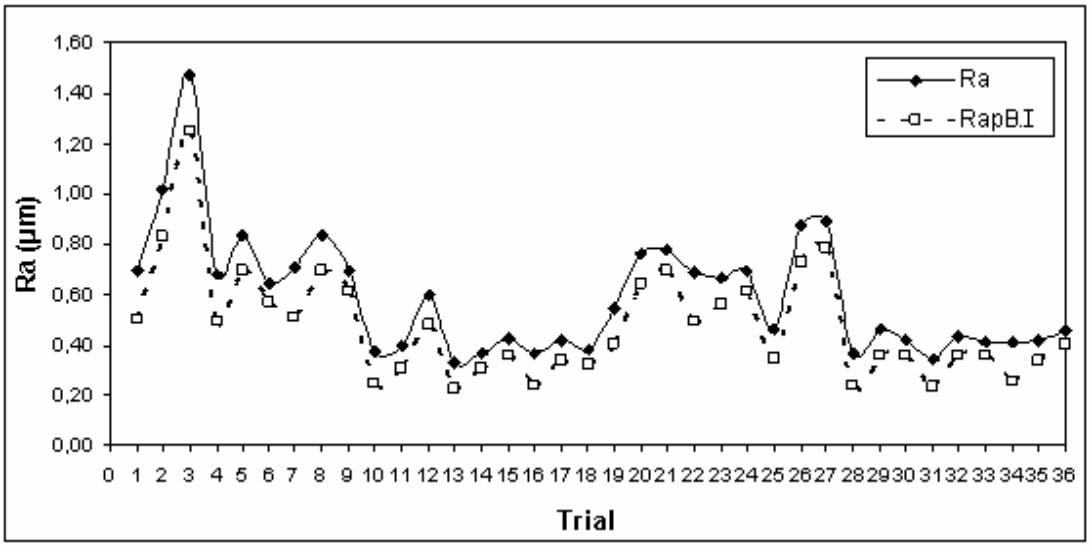

Figure 6.39- Experimental and predicted theoretical values of surface roughness when considering back cutting and an ideal condition (εa = ε r= 0)

Table 6.39 shows the experimental and predicted values of surface roughness as well as the RE_P% (Relative Error percentage between the calculated output, RapB.R and the target output, Ra) when considering the back cutting for a real condition (εa ≠ 0 and εr ≠ 0). Figure 6.40 illustrates this result.

Table 6.39- Experimental and predicted theoretical values of surface roughness and $\%RE_P$ obtained when considering the back cutting theoretical model and a real condition ($\varepsilon a \neq 0$ and $\varepsilon r \neq 0$).

Trial	κ_i (°)	εr (mm)	εa (mm)	Ra (µm)	RapB.R (µm)	$\%RE_P$ (B.R)
1	0.40	-0.009	0.0002	0.699	0.686	1.9
2	0.29	-0.001	0.0002	1.017	1.014	0.3
4	0.39	-0.002	0.0002	0.679	0.671	1.2
5	0.24	0.009	0.0002	0.838	0.846	1.0
6	0.12	0.008	0.0001	0.646	0.644	0.3
7	0.41	0.008	0.0003	0.712	0.716	0.6
8	0.24	0.009	0.0002	0.835	0.846	1.3
9	0.13	0.006	0.0001	0.699	0.692	1.0
10	0.22	0.009	0.0002	0.376	0.382	1.6
11	0.11	-0.001	0.0001	0.399	0.400	0.3
13	0.19	-0.008	0.0001	0.328	0.361	10.1
14	0.11	0.008	0.0001	0.368	0.384	4.3
15	0.08	0.007	0.0001	0.425	0.443	4.2
16	0.21	0.009	0.0002	0.365	0.375	2.7
17	0.12	0.002	0.0001	0.422	0.419	0.7
18	0.07	0.009	0.0001	0.381	0.401	5.2
19	0.31	0.008	0.0002	0.548	0.539	1.6
20	0.22	-0.008	0.0001	0.759	0.764	0.7
21	0.15	-0.001	0.0001	0.781	0.795	1.8
22	0.39	-0.005	0.0002	0.688	0.689	0.1
23	0.19	-0.002	0.0001	0.668	0.662	0.9
24	0.13	0.009	0.0001	0.694	0.685	1.3
26	0.25	0.007	0.0002	0.872	0.879	0.8
27	0.17	-0.005	0.0001	0.888	0.893	0.6
28	0.21	0.008	0.0002	0.365	0.378	3.6
29	0.13	-0.005	0.0001	0.461	0.457	0.9
30	0.08	0.008	0.0001	0.415	0.442	6.5
31	0.20	-0.009	0.0001	0.344	0.337	2.0
32	0.13	-0.002	0.0001	0.437	0.451	3.2
33	0.08	0.009	0.0001	0.408	0.441	8.1
34	0.23	0.006	0.0002	0.408	0.398	2.5
35	0.12	0.008	0.0001	0.418	0.408	2.4
36	0.09	0.005	0.0001	0.453	0.486	7.3
					$\%RE_P$*(B.R)	2.4

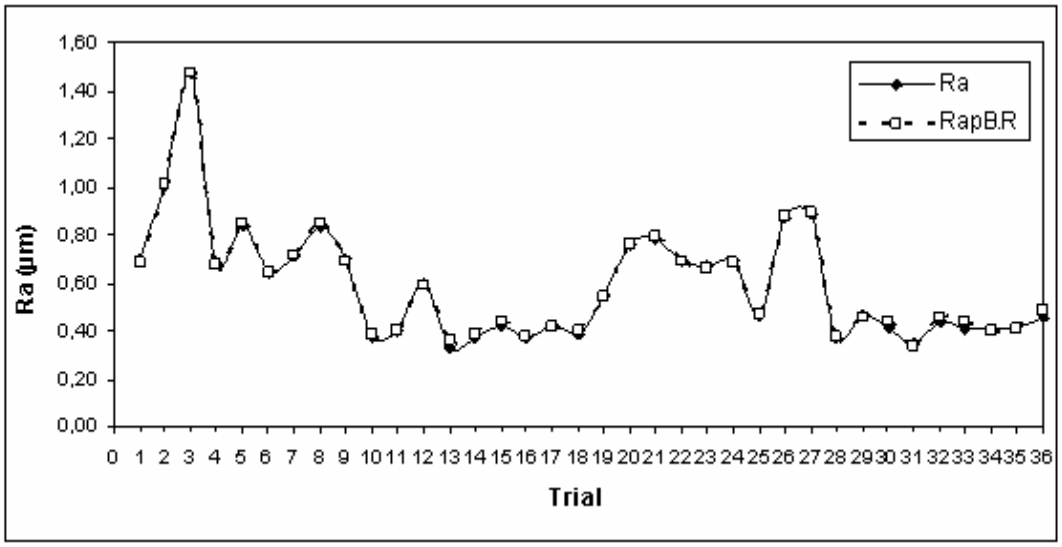

Figure 6.40- Experimental and predicted theoretical values of surface roughness considering back cutting and a real condition ($\varepsilon a \neq 0$ and $\varepsilon r \neq 0$).

As expected, the predicted theoretical surface roughness values obtained with the back cutting model are the same as obtained when considering the front cutting, since the values of axial and radial deviation of tooth (i) for each of the trials was kept constant. Also, the same $\%RE_P$*= 2.4 between the calculated output (RapB.R) and the target output (Ra) was obtained when comparing it with the front cutting theoretical predicted surface roughness values when the real case is considered.

6.5.3 Front-Back cutting theoretical model (FB)

Once individual front and back cutting models were developed, the interference between them is analyzed in order to develop the front-back cutting theoretical model; as well as knowing the contribution of each of these cutting processes on the surface roughness profile.

In this case Figures 6.41 and 6.42 illustrate the theoretical surface roughness profile obtained when considering front-back cutting process in an ideal condition and a real condition respectively.

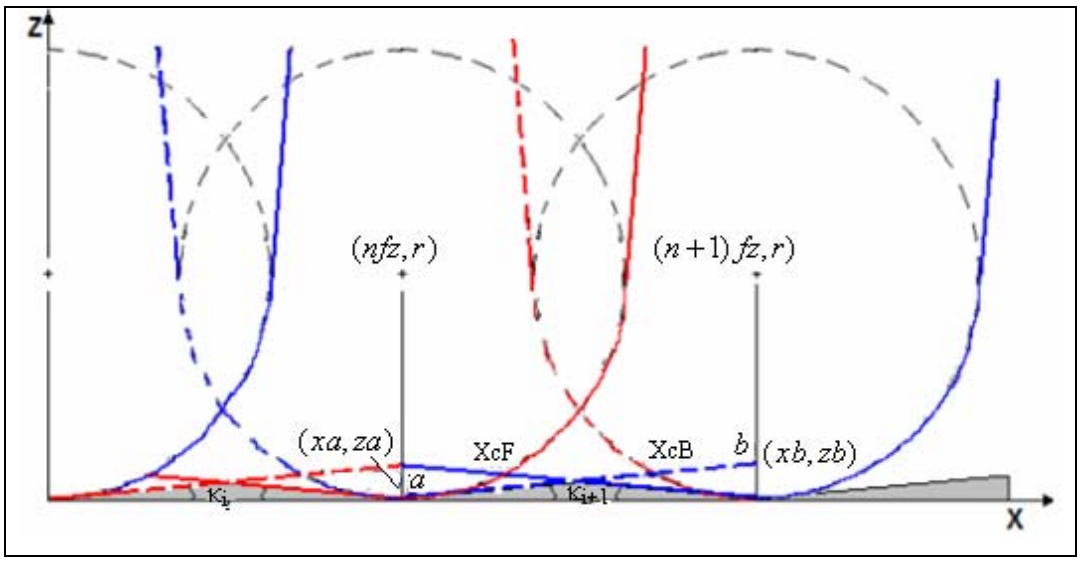

Figure 6.41- Schematic of the trail left by the cutting tool when considering Front-Back cutting and an ideal condition (εa = ε r= 0). Tooth (i) (colored in solid red for the front cutting and dashed red for the back cutting) and tooth (i+1) (colored in solid blue for the front cutting and dashed blue for the back cutting). The gray area represents the 2D theoretical surface roughness profile.

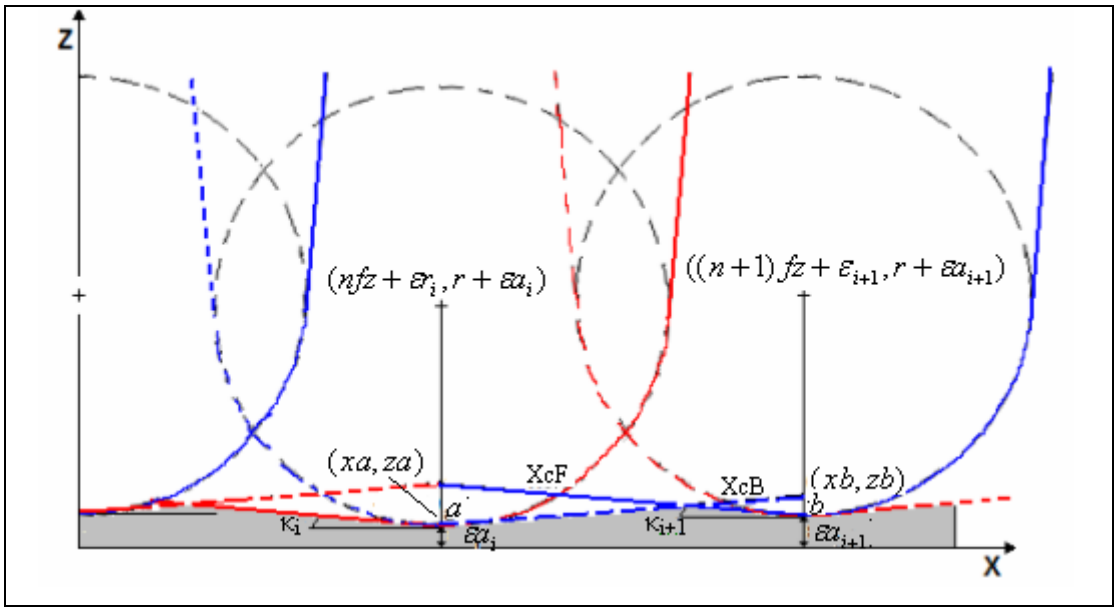

Figure 6.42- Schematic of the trail left by the cutting tool when considering Front-Back cutting and a real condition (εa ≠ 0 and εr ≠ 0). Tooth (i) (colored in solid red for the front cutting and dashed red for the back cutting) and tooth (i+1) (colored in solid blue for the front cutting and dashed blue for the back cutting). The gray area represents the 2D theoretical surface roughness profile.

In order to develop the surface roughness profile obtained when considering front-back cutting model, different considerations must be made, and in order to facilitate its understanding, Figure 6.43 illustrates different cases.

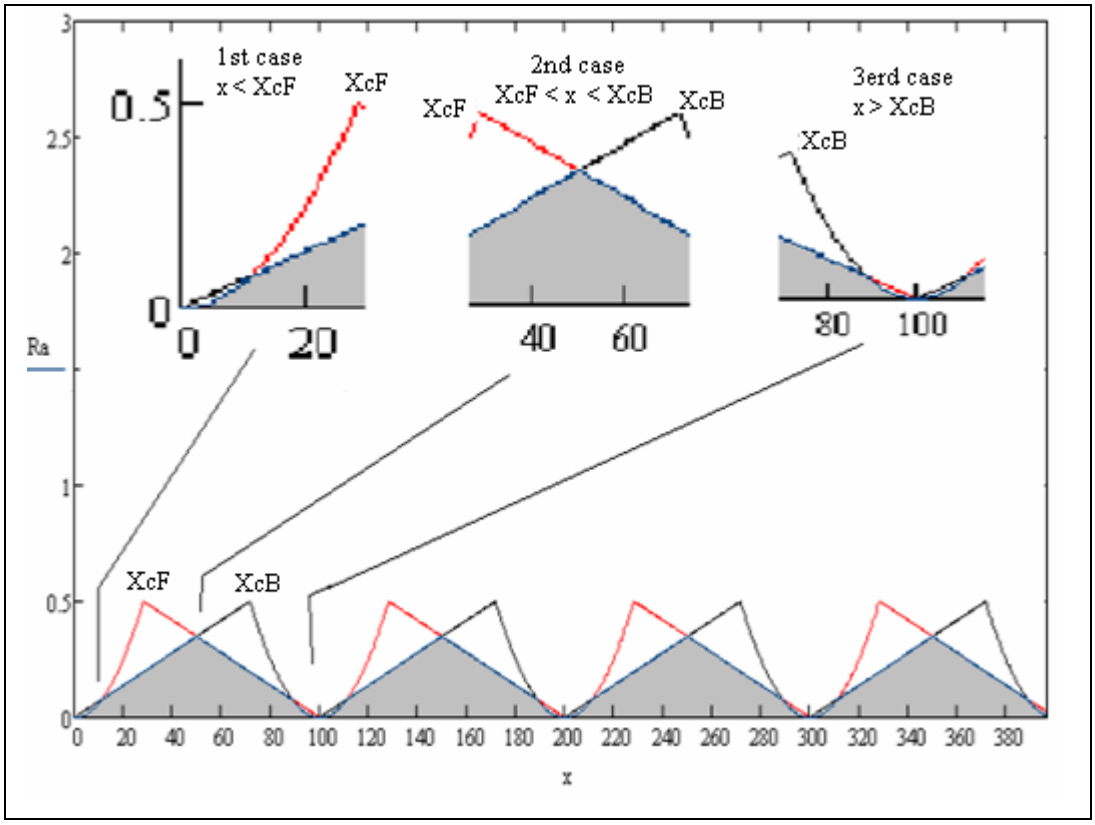

Figure 6.43- 2D theoretical surface roughness profile obtained when considering a Front-Back cutting model.

Figure 6.43 shows different cases in order to know how a 2D surface roughness profile will be obtained by considering a front and a back cutting process at the same time.

As observed the intersection points, XcF and XcB are taken as a reference for the different cases, where XcF is the intersection point obtained in the front cutting analysis and XcB the intersection point obtained in the back cutting analysis. The cases are as follows:

1st case: when considering any generic "x", if "x" is located before XcF, then "Z" of the front cutting (circle) is compared to "Z" of the back cutting (line), plotting the smaller value (circle or line).

2nd case: if "x" is located after XcF and before XcB, then "Z" of the back cutting (line) is compared with "Z" of the front cutting (line) and evaluated, plotting the smaller value or the line that belongs to the back cutting or the line that belongs to the front cutting.

3rd case: if "x" is located after XcB, the "Z" of the back cutting (circle) and the "Z" of the front cutting (line) are compared, plotting once again the smaller of these values (circle or line).

Table 6.40 shows the experimental and predicted theoretical values of surface roughness as well as the RE_P% (Relative error percentage between the calculated output, RapFB.I and the target output, Ra), when considering the front-back cutting process and an ideal condition ($\varepsilon a = \varepsilon r = 0$). Figure 6.44 illustrates this result.

Table 6.40- Experimental and predicted theoretical values of surface roughness and $\%RE_P$ obtained when considering the Front-Back cutting theoretical model and an ideal condition $\varepsilon a = \varepsilon r = 0$

Trial	κ_i (°)	Ra (µm)	RapFB.I (µm)	$\%RE_P$ (FB.I)
1	0.40	0.699	0.349	50.1
2	0.29	1.017	0.506	50.2
4	0.39	0.679	0.340	49.9
5	0.24	0.838	0.419	50.0
6	0.12	0.646	0.314	51.4
7	0.41	0.712	0.358	49.7
8	0.24	0.835	0.419	49.8
9	0.13	0.699	0.340	51.4
10	0.22	0.376	0.192	48.9
11	0.11	0.399	0.192	51.9
13	0.19	0.328	0.166	49.4
14	0.11	0.368	0.192	47.8
15	0.08	0.425	0.209	50.8
16	0.21	0.365	0.183	49.9
17	0.12	0.422	0.209	50.5
18	0.07	0.381	0.183	52.0
19	0.31	0.548	0.271	50.5
20	0.22	0.759	0.384	49.4
21	0.15	0.781	0.393	49.7
22	0.39	0.688	0.340	50.6
23	0.19	0.668	0.332	50.3
24	0.13	0.694	0.340	51.0
26	0.25	0.872	0.436	50.0
27	0.17	0.888	0.445	49.9
28	0.21	0.365	0.183	49.9
29	0.13	0.461	0.227	50.8
30	0.08	0.415	0.209	49.6
31	0.20	0.344	0.175	49.1
32	0.13	0.437	0.227	48.1
33	0.08	0.408	0.209	48.8
34	0.23	0.408	0.201	50.7
35	0.12	0.418	0.209	50.0
36	0.09	0.453	0.236	47.9
			$\%RE_P$* (FB.I)	50.0

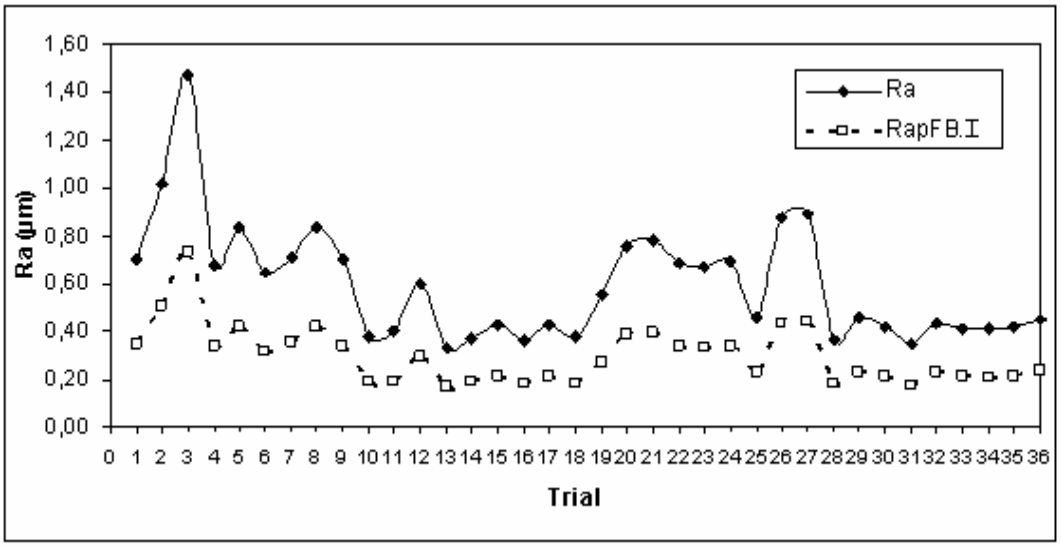

Figure 6.44- Experimental and predicted values of surface roughness when considering front-back cutting and an ideal condition ($\varepsilon a = \varepsilon r = 0$)

When analyzing Figure 6.44, it is observed that once again the predicted theoretical values of surface roughness are smaller than the experimental values (RapFB.I < Ra), although in this case the difference between them is bigger when compared to the results obtained when considering front or back cutting process individually. The results show an average error of 50 % between the experimental and the predicted values. This error is considered to be very high and is probably due to the fact that, when the back cutting is presented the tooth is removing the same amount of material that was removed when considering the front cutting but in an opposite direction, generating a sawtooth type profile, since both the front and the back cutting are considered on the development of the surface. As observed when comparing the tool trail drawn in Figure 6.41 and 6.42 this one is very different to the experimental 2D profiles obtained when milling Al 7075-T7351 and that are reported in Tables 5.5 and 5.6 in Chapter 5. From this fact it can be say that the back cutting process seems no to contribute in the removal of material during the machining operation unless there is a workpiece surface distortion or an imperfection in the tool holder alignment. This result is also supported by the analysis given in Figure 6.43.

Table 6.41 shows the experimental and predicted values of surface roughness as well as the $\%RE_P$ (Relative Error percentage between the calculated output, RapFB.R and the target output, Ra), when considering the front-back cutting process and a real condition ($\varepsilon a \neq 0$ and $\varepsilon r \neq 0$). Figure 6.45 illustrates this result.

Table 6.41- Experimental and predicted theoretical values of surface roughness and $\%RE_P$ obtained when considering the Front-Back cutting model and a real condition ($\varepsilon a \neq 0$ and $\varepsilon r \neq 0$)

Trial	κ_i (°)	εr (mm)	εa (mm)	Ra (µm)	RapFB.R (µm)	$\%RE_P$ (FB.R)
1	0.40	0.009	0.0002	0.699	0.479	31.5
2	0.29	0.001	0.0002	1.017	0.600	41.0
4	0.39	0.002	0.0002	0.679	0.445	34.5
5	0.24	-0.009	0.0002	0.838	0.497	40.7
6	0.12	-0.008	0.0001	0.646	0.353	45.4
7	0.41	-0.008	0.0003	0.712	0.479	32.7
8	0.24	-0.009	0.0002	0.835	0.497	40.5
9	0.13	-0.006	0.0001	0.699	0.381	45.5
10	0.22	-0.009	0.0002	0.376	0.273	27.4
11	0.11	0.001	0.0001	0.399	0.242	39.3
13	0.19	0.008	0.0001	0.328	0.222	32.3
14	0.11	-0.008	0.0001	0.368	0.234	36.4
15	0.08	-0.007	0.0001	0.425	0.254	40.2
16	0.21	-0.009	0.0002	0.365	0.266	27.1
17	0.12	-0.002	0.0001	0.422	0.256	39.3
18	0.07	-0.009	0.0001	0.381	0.227	40.4
19	0.31	-0.008	0.0002	0.548	0.346	36.9
20	0.22	0.008	0.0001	0.759	0.446	41.2
21	0.15	0.001	0.0001	0.781	0.440	43.7
22	0.39	0.005	0.0002	0.688	0.456	33.7
23	0.19	0.002	0.0001	0.668	0.385	42.4
24	0.13	-0.009	0.0001	0.694	0.379	45.4
26	0.25	-0.007	0.0002	0.872	0.519	40.5
27	0.17	0.005	0.0001	0.888	0.471	47.0
28	0.21	-0.008	0.0002	0.365	0.268	26.6
29	0.13	0.005	0.0001	0.461	0.281	39.0
30	0.08	-0.008	0.0001	0.415	0.252	39.3
31	0.20	0.009	0.0001	0.344	0.240	30.2
32	0.13	0.002	0.0001	0.437	0.277	36.6
33	0.08	-0.009	0.0001	0.408	0.259	36.5
34	0.23	-0.006	0.0002	0.408	0.288	29.4
35	0.12	-0.008	0.0001	0.418	0.251	40.0
36	0.09	-0.005	0.0001	0.453	0.281	38.0
					$\%RE_P$*(FB.R)	37.6

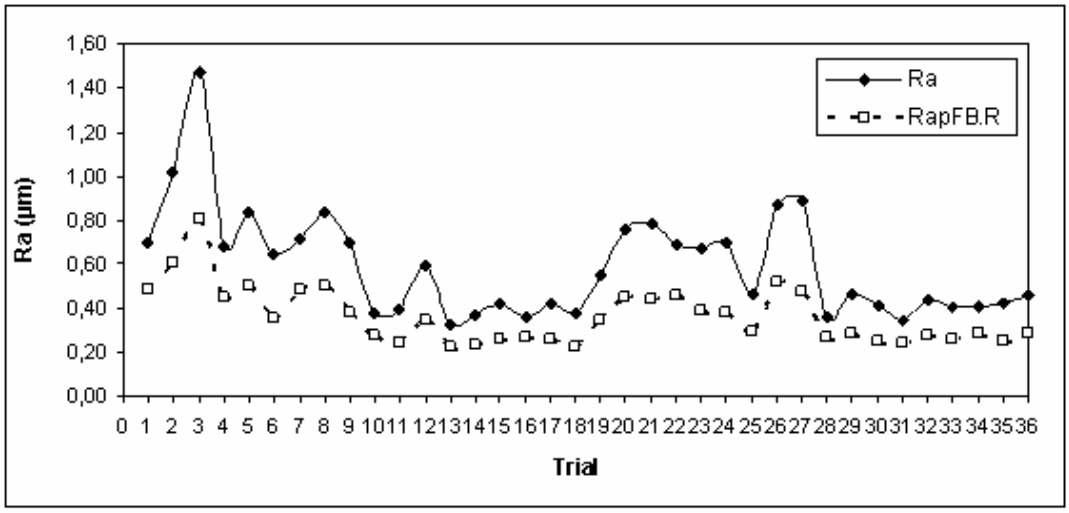

Figure 6.45- Experimental and predicted theoretical values of surface roughness considering front- back cutting and a real condition ($\varepsilon a \neq 0$ and $\varepsilon r \neq 0$).

As observed when analyzing Table 6.41 a $\%RE_P^*$=37.6 was obtained. Even though the value decreased when comparing the results of front-back cutting theoretical model considering an ideal condition, the difference between the experimental and the predicted theoretical value of surface roughness are still very high. This result was expected, since the same sawtooth type 2D surface roughness profile was also obtained.

When analyzing the three main models based on the geometrical analysis it can be concluded that apparently only the front cutting process is responsible for the surface roughness profile generation, removing all the material in this moment as stated also by Franco in 2004. With regard to the fact that in some cases the back cutting trail is observed in few of the milled surfaces, this could be attributed to possible waviness, characteristic of materials that have been laminated for the production of square bars such as the ones used for this study or to other imperfections such as the tool holder alignment, which in this case is discharged due to the vibration study conducted in Chapter 5, section 5.5.

Table 6.42 presents the possible changes on the 2D theoretical surface roughness profile obtained for a specific condition when considering the different models and different axial deviation. The idea of showing these profiles is to illustrate the fact of, why a very small axial deviation must be employed when considering a real condition.

Table 6.42- Example of 2D theoretical surface roughness profiles when considering different values of axial deviation (εa) for the three (3) theoretical models.

Model	Deviation (μm) 0.0	0.1	0.5	0.7
Front Cutting	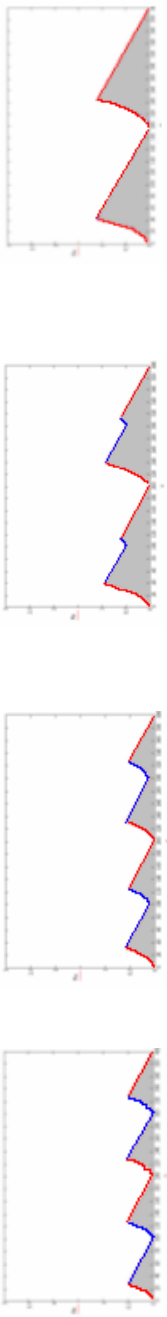			
Back Cutting	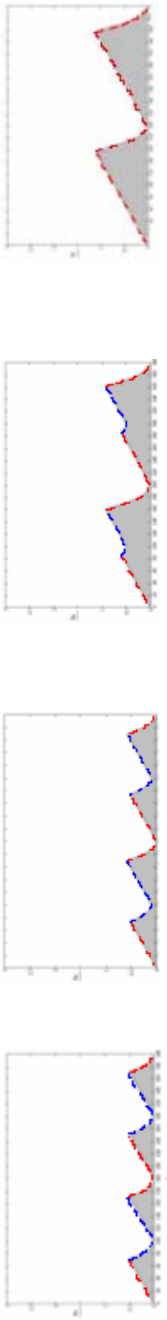			
Front-Back Cutting	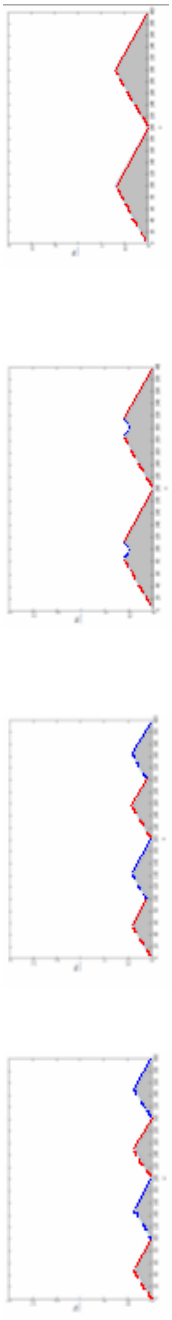			

As observed as axial deviation is increased for each of the cutting model there is a point (0.5 μm) where the tooth (i+1) does not make any contribution to the surface roughness profile generation, this is why the axial deviations is a very small value as selected for the development of the different models.

6.6 Summary and general conclusions

In this study a new contribution to knowledge is made by developing different models for surface roughness prediction when face milling with square inserts.

The models were developed based on mathematical, computational and geometric analysis. Overall the results show that the Fourier series is a very useful representation for the successful operation of the profile reconstruction process as well as for the calculation of κ_i angle which is an important variable to be considered for the recreation of the tool trail left on the machined surface.

The different ANN that were developed for the prediction of the surface roughness show that the FFNN (that considers the tool nose radius as an input) obtained the best results with a $\%RE_P^*$= 6.38 when comparing it to the RBNN and GRNN where the $\%RE_P^*$ is 14.47 and 12.28 respectively.

When considering individual FFNN for r=0.8 mm and r=2.5 mm an improvement of the $\%RE_P^*$ was obtained, from $\%RE_P^*$= 6.38 to $\%RE_P^*$ = 2.11 and $\%RE_P^*$=3.21, when considering r=0.8 mm and r=2.5 mm respectively.

With regards to the development of the theoretical models based on geometrical analysis it was observed that the static tool runouts have a very strong influence on the surface roughness and that the front cutting model that considers the real condition achieved the best results with a $\%RE_P^*$=2.40. Also it was observed that the back cutting process does not contribute on the generation of the surface profile unless a distortion of the workpiece surface or in the tool alignment is presented.

Finally it was observed the importance of considering small axial deviation for the development of the tool trail left on the machined surface.

7 SurfRough 1.0 User's Guide

7.1 Introduction

SurfRough 1.0 is a pilot computer program that has been developed in order to facilitate the prediction of surface roughness without using the equations developed in Chapter 6 for the Front cutting model. In addition, it gives reproduction of a 2D surface roughness profile, machined under different cutting conditions, when using a face milling cutting process based just in a geometric analysis. This program is expected to be a useful tool in the manufacturing field, but also for designers in the area, since by knowing different variables of the cutting process an estimate of the surface roughness resulting from the process can be obtained, without having to go through an experimental process with the corresponding cost and time implications.

This chapter is divided into two further sections:

Section 7.2: Presents an explanation of each of the fields that are involved in the SurfRough 1.0 program.

Section 7.3: Includes the summary and the general conclusions obtained from these studies.

7.2 Detailed Contents

Figure 7.1 shows a screen shot of the SurfRough 1.0 program and each of the different fields are explained as follows:

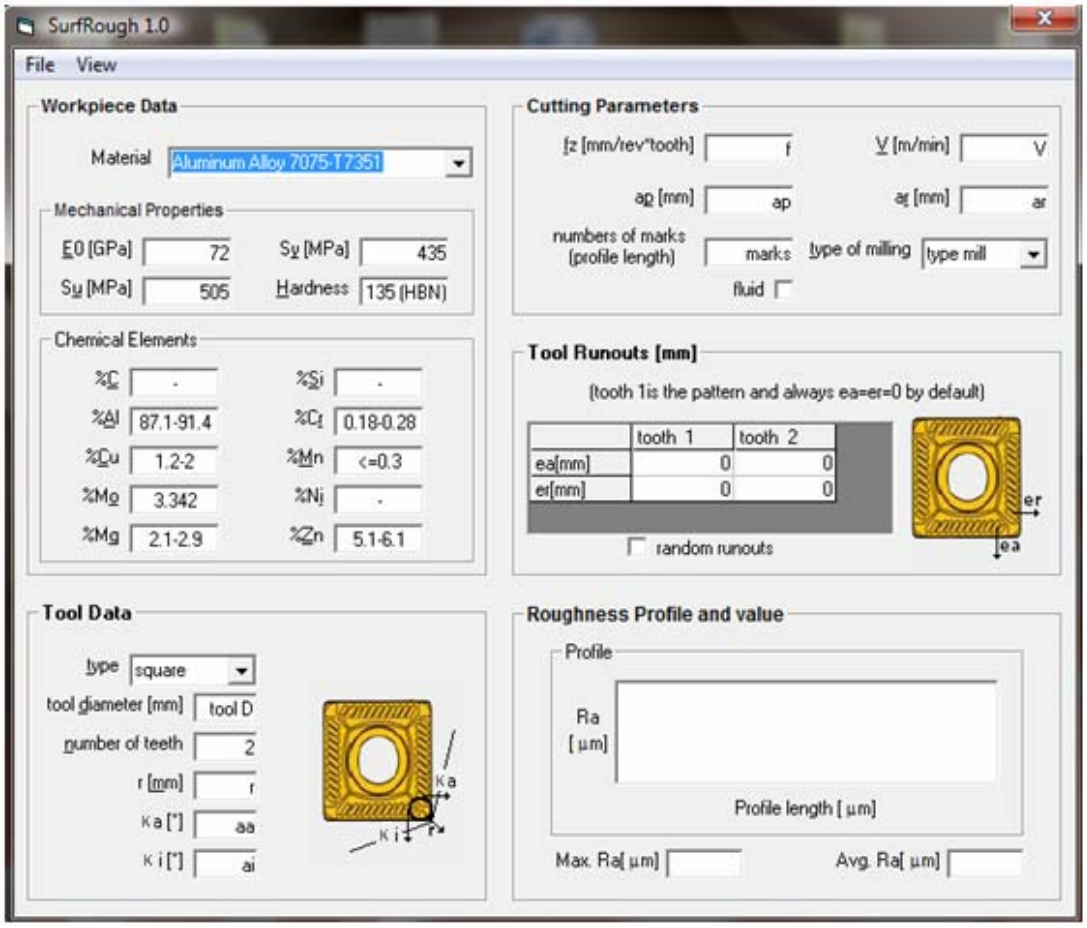

Figure 7.1- SurfRough 1.0 program screen.

7.2.1 Workpiece Database

This field "Workpiece Database" has several materials included, where their respective mechanical properties and chemical composition are presented. This is presented as an informative field and also allows the inclusion of new materials that are not included in the original database. The details are shown in Figure 7.2

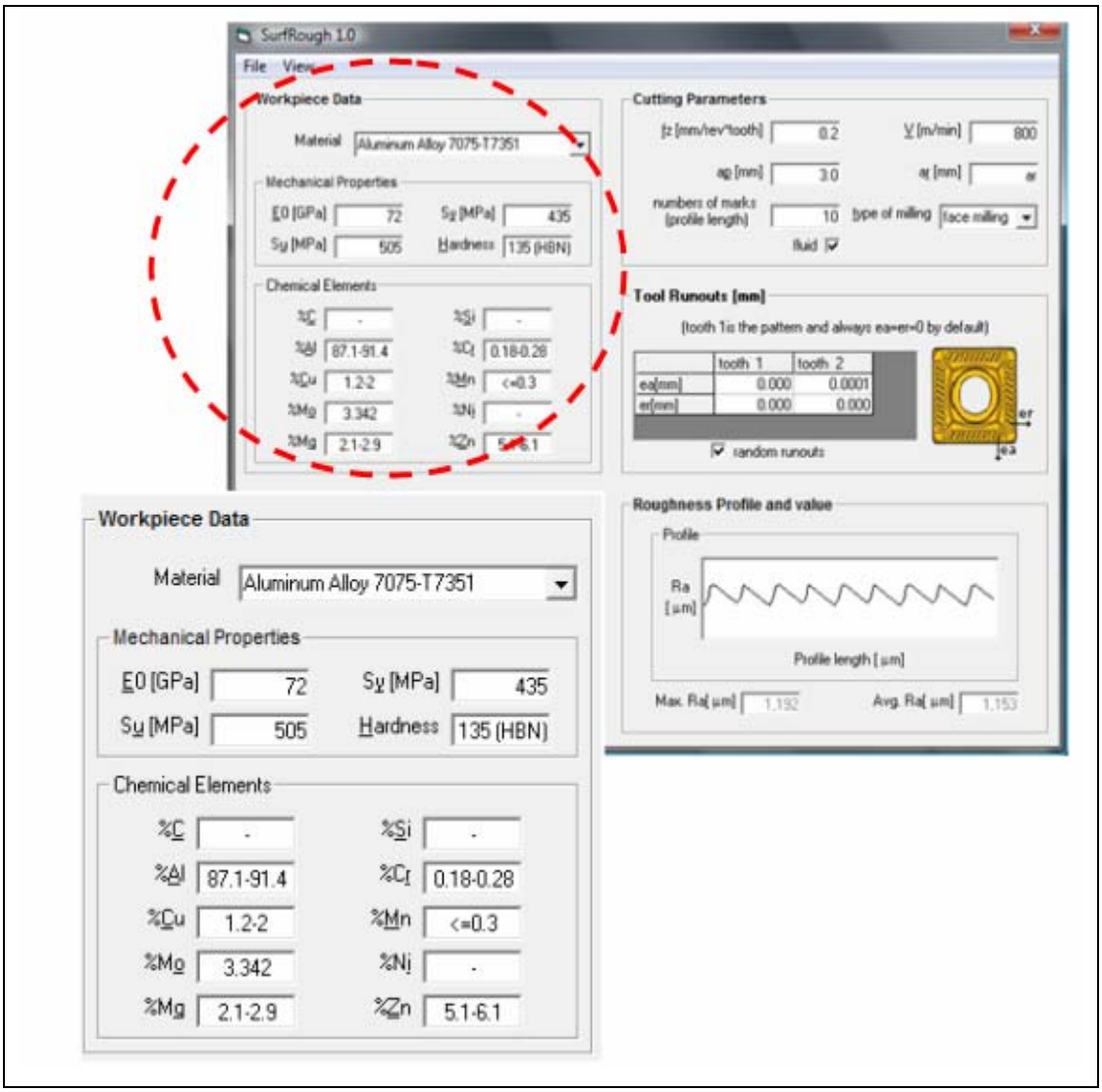

Figure 7.2- Detail of the Workpiece data field

The mechanical properties section includes: modulus of elasticity, ultimate tensile strength, yield tensile strength and hardness of each material. A wide selection of chemical elements are included, such as: %C, %Al, %Cu, %Mo, %Mg, %Si, %Cr, %Mn, %Ni and %Zn.

If a user wants to save a new material that is not in the Workpiece Database, the user must click File icon and checked the "Save Workpiece Data".

It must be noted that the material properties and the chemical composition do not affect the surface roughness profile when tool wear is not considered, such as in our case study.

7.2.2 Tool Geometry Data

The "Tool geometry data" field has several bits of information that need to be included, since they influence the surface roughness development. This information includes tool type (square, round, triangle), tool diameter, number of teeth, tool nose radius, κ_a and κ_i. Figure 7.3 show this field.

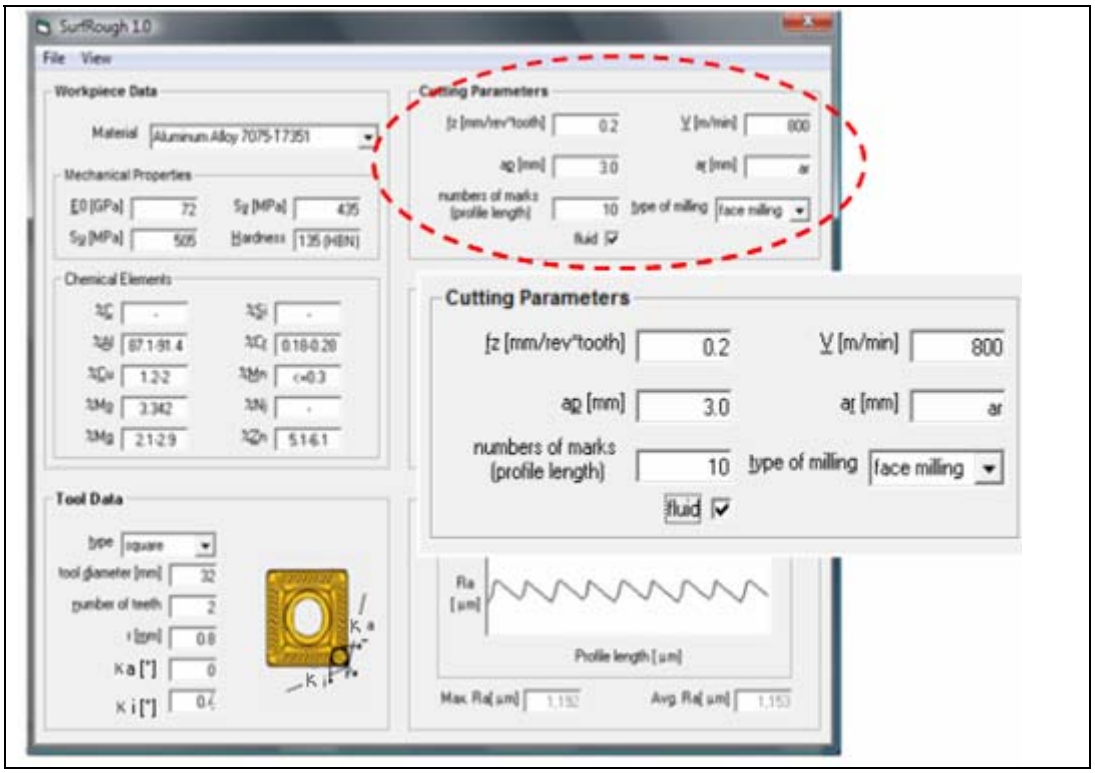

Figure 7.3- Tool Geometry Data field

- **Tool type**

When selecting this field, the user can choose an insert with a square shape or a round shape, and when selecting any of them a figure showing the selected tool will be displayed.

It must be noted that the objective of this work is the development of a theoretical model for surface roughness prediction when using square inserts. However, the surface roughness prediction for round inserts is also included, so these two are the only types of inserts that can be selected.

- **Square type**

When selecting this field, in addition to giving the information regarding, tool diameter, number of teeth and tool nose radius, the κ_i field must be filled, since the surface roughness model depends on this variable. The value of κ_i can be obtained from the results presented in Chapter 6, Section 6.3, Tables 6.6 and 6.7. Figure 7.4 show this field.

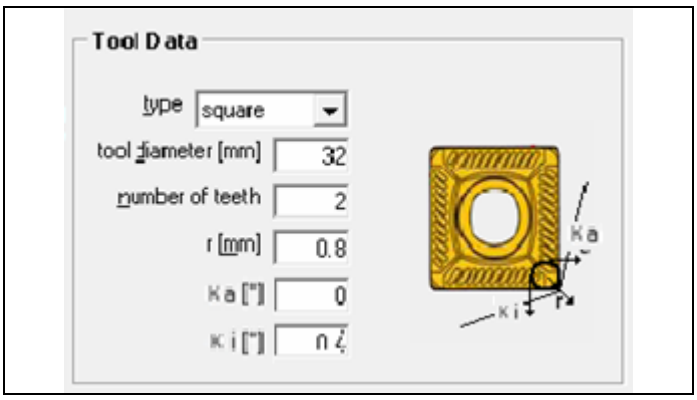

Figure 7.4- Tool Data field. Square type

- **Round type**

When selecting this field, the only information needed is: tool diameter, number of teeth and tool nose radius. In this case the κ_a and κ_i fields are blocked. The details are shown in Figure 7.5.

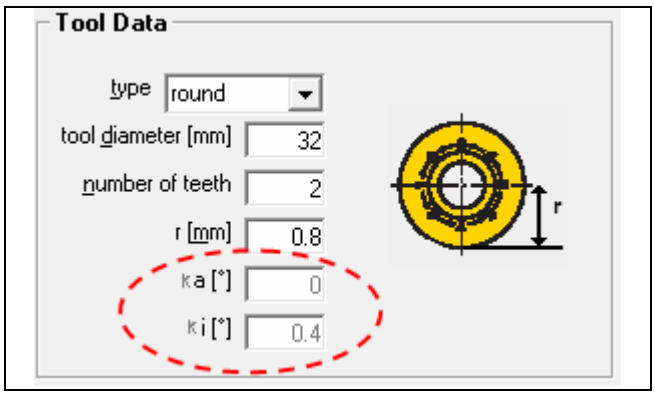

Figure7.5- Tool Data field. Round type.

7.2.3 Cutting parameters

The "Cutting parameters" field includes information such as: cutting speed, axial depth of cut, radial depth of cut, and the most important one, the feed per tooth which is mandatory to be included, since it is the variable that affects the surface roughness and the other variables are just for information purposes. Figure 7.6 show the screen of this field.

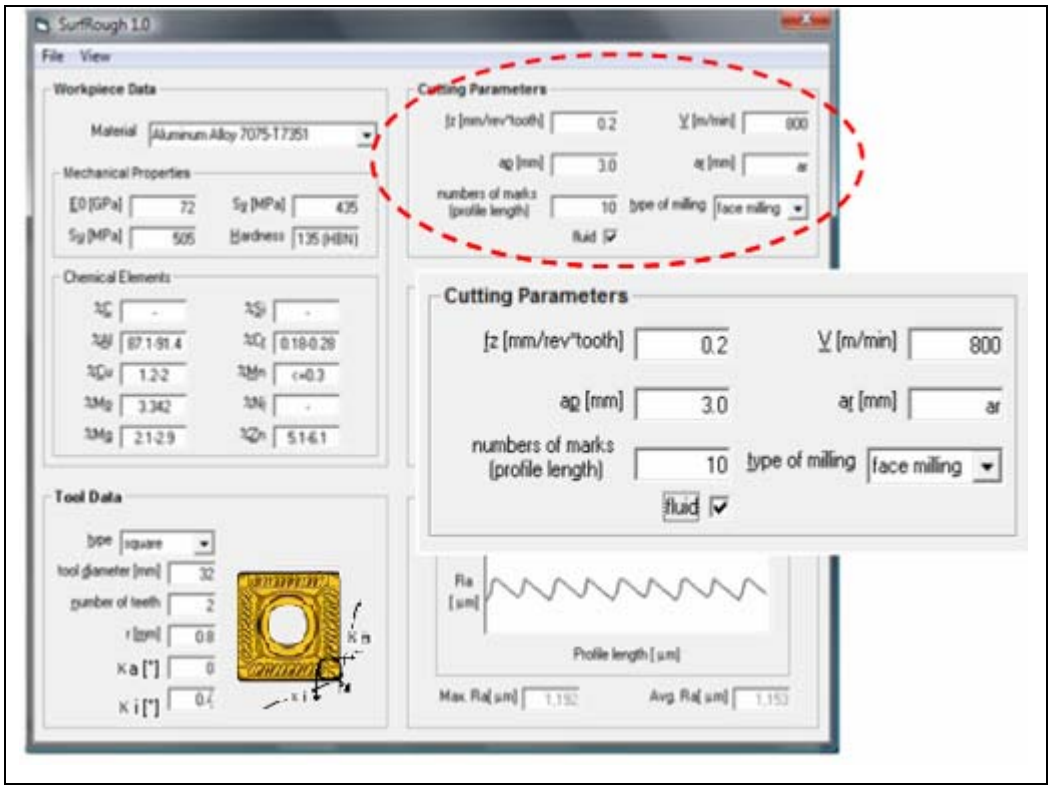

Figure 7.6- Cutting Parameters field.

As observed in Figure 7.6, this field also includes information such as: type of milling (face milling, end milling), numbers of marks (profile length) and cutting fluid used.

With regards to the type of milling, the program only allows the face milling process since it was the objective of study. The fluid box can be checked or unchecked. Finally, the number of marks (profile length) will influence in the visual presentation of the length profile that is developed. This 2D profile is shown in the bottom left of the screen. Figure 7.7 show the illustration of this field.

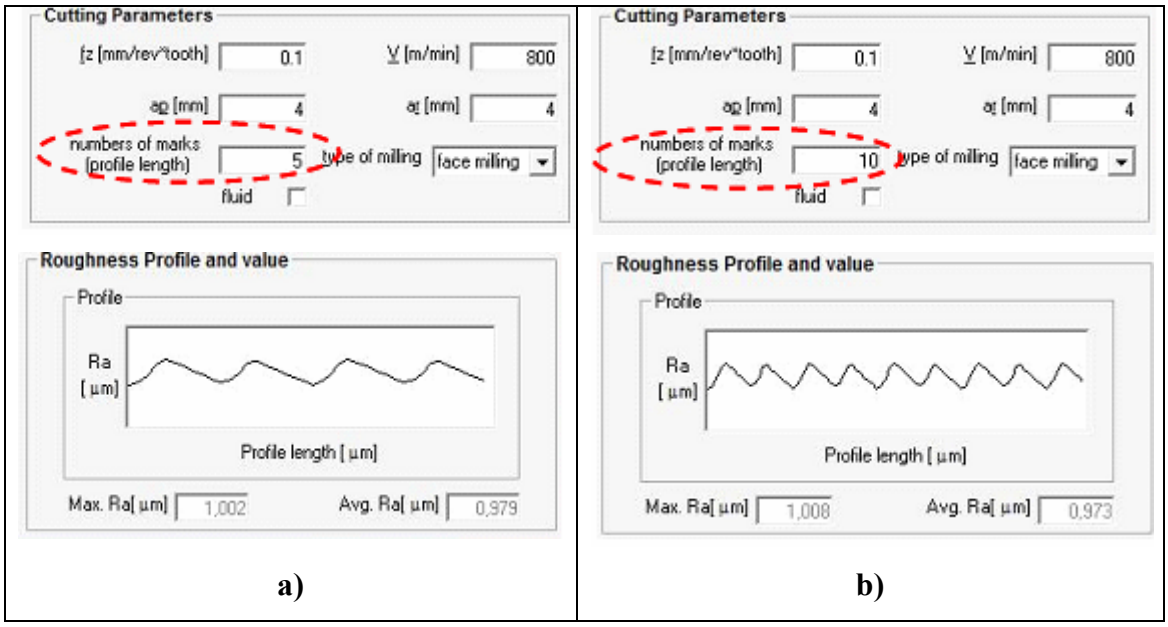

Figure 7.7- Detail of the number of marks (profile length) field.

When analyzing Figure 7.7 it is observed how a "zoom" in the surface roughness profile length is obtained by changing the number of marks in the "Cutting Parameters" field.

7.2.4 Static tool runouts

This "Static tool runouts" field is very important since analysis of work has shown that these variables affect the surface roughness. This field can be filled manually, or the random runouts box can be selected. In this last case the program will give random numbers and as previously stated in Chapter 6, Section 6.5 these random runouts are ea≤0.0003 mm (axial deviation) and er≤0.009 mm (radial deviation) and ea=er=0 for tooth 1 (by default since this tooth is the pattern). Also it must be noted, that the numbers of columns regarding the number of teeth are increased when including a number of teeth bigger than 2, in the "Tool Geometry Data" field. See Figure 7.8 and Figure 7.9 for details.

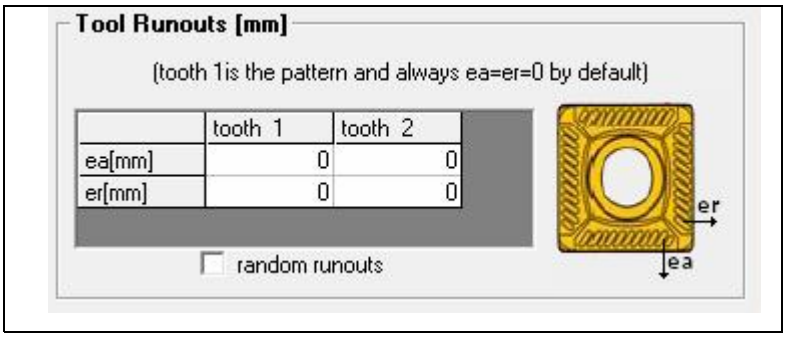

Figure 7.8- Static tool runouts field

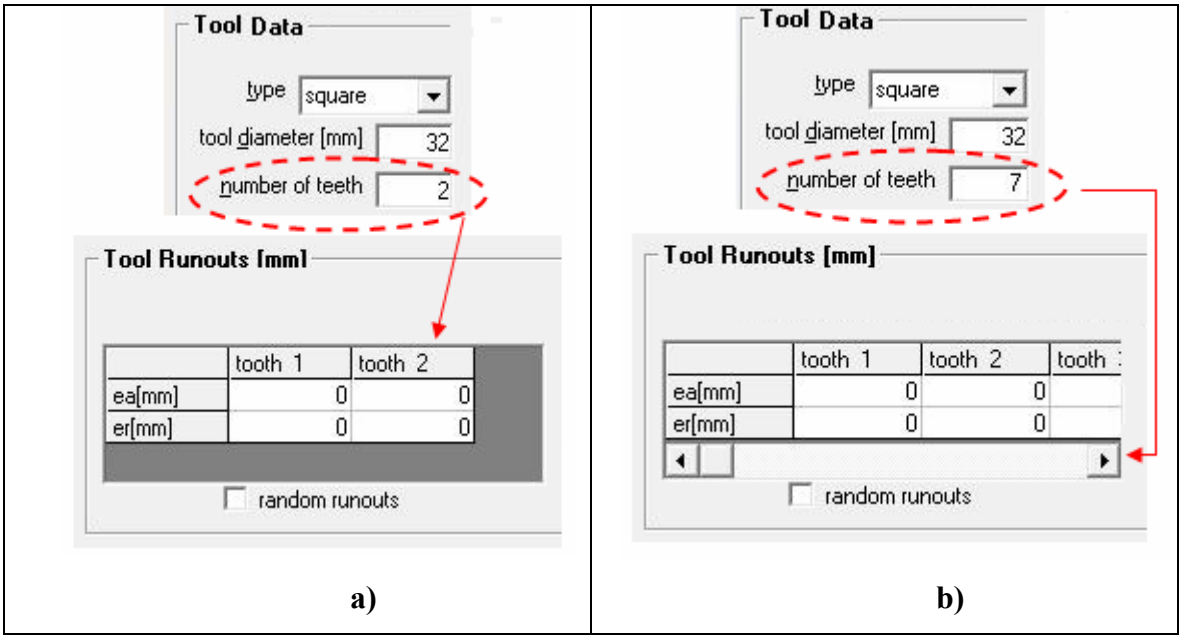

Figure 7.9- Number of teeth field.

As observed in Figure 7.9 a), the number of teeth selected is 2 and the Static tool runouts field shows only two (2) columns. In Figure 7.9 b), as the number of teeth is increased in the "Tool Geometry Data" field, the numbers of columns in the Static tool runouts columns is also increased.

7.2.5 Surface roughness value and 2D surface roughness profile

Once all the fields are filled up, the user must click the view tool box and then select the 2D Profile and the Ra value. When clicking these fields, immediately in the bottom left side of the screen, the 2D profile as well as the Surface roughness value will be displayed. Figure 7.10 show this field.

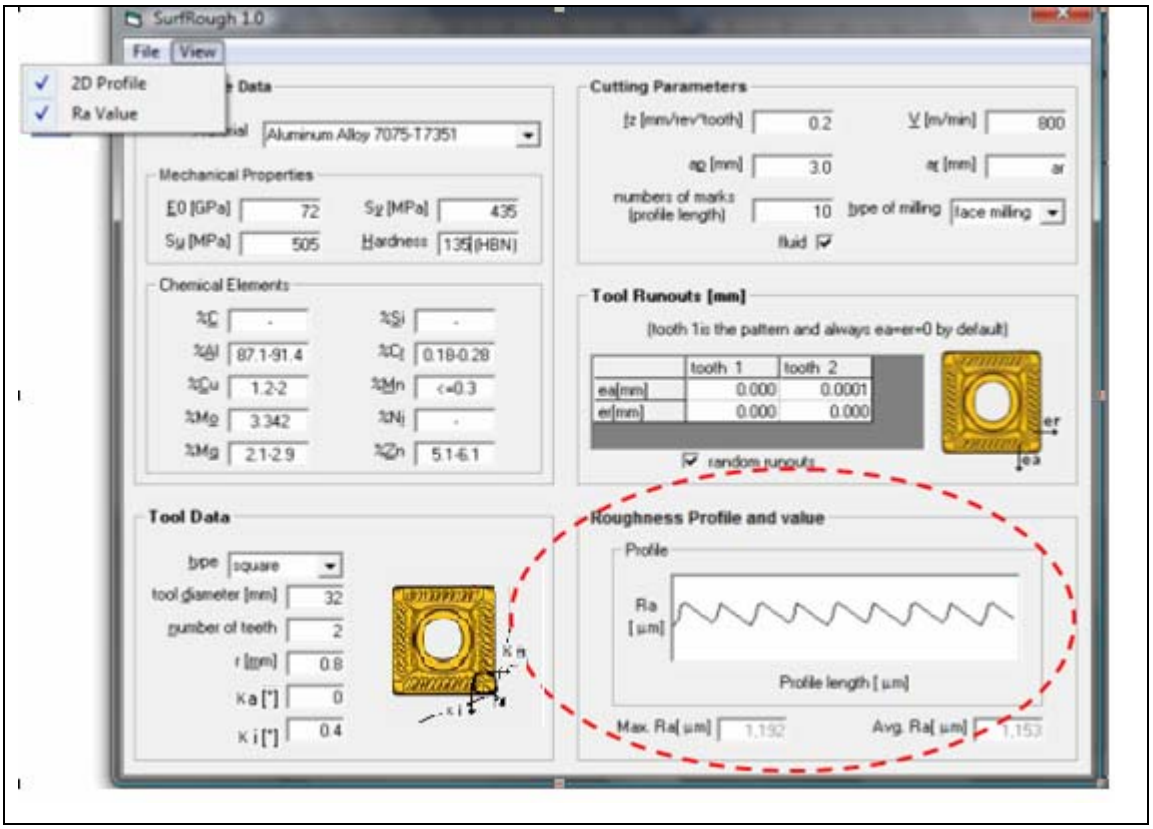

Figure 7.10- Roughness profile and surface roughness value field.

7.2.6 Saving and opening a file

Once the surface roughness 2D profile and surface roughness value are displayed, the File tool box must be clicked in order to save the file. This field also allows opening a file or exiting the program. Details are shown in Figure 7.11.

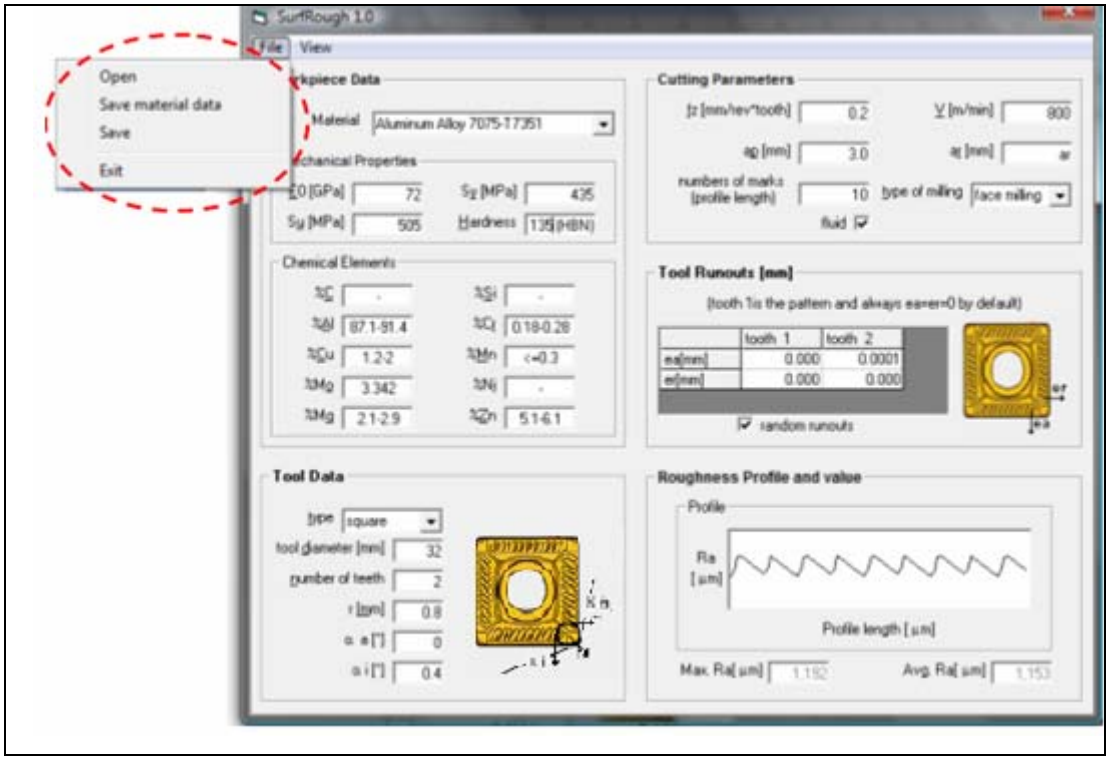

Figure 7.11- Detail of File field.

7.3 Summary and general conclusions for SurfRough 1.0 User's Guide

In this study a computational pilot program called SurfRough 1.0 was developed. The idea of developing this program is to facilitate possible users to predict the surface roughness value as well as the 2D surface roughness profile, when face milling any material with a new tool and when not considering tool wear.

Also, even though the study was conducted in relation to Al 7075-T7351 when using square inserts, the program allows the selection of round insert geometry.

It must be highlighted that the developed 2D surface roughness profile is based on the developed "Front Cutting theoretical" model that was developed from the geometric analysis (see Chapter 6, Section 6.5.1).

8 Overall results evaluation

8.1 Introduction

Once the different models were developed a comparison between them is made based on the $\%RE_P$* (Relative Error percentage average between the predicted and the experimental values of surface roughness).

In addition, a comparison between the reproductions of the 2D surface roughness profile obtained by applying the mathematical model (based on the Fourier series) and the Front cutting theoretical model is presented.

As presented in Chapter 5 the experimental values of surface roughness were obtained by milling Al 7075-T7351 using square inserts. The results represent a new contribution in knowledge since no research has been found in this material under the conditions established in this research.

This chapter is divided into three sections. The first two sections presents analysis and results and the last section the general conclusions of this study.

Section 8.2: Presents the comparison between the experimental and predicted values of surface roughness obtained by using Fourier series, Artificial Neural Networks and the Theoretical model.

Section 8.3: Presents the comparison between the 2D experimental surface roughness profiles and the 2D surface roughness profiles obtained by using the Fourier series and the Theoretical model.

Section 8.4: Includes the general conclusions obtained from the study.

Figure 8.1 shows a schematic overall description of the comparison and final selection of the model that best predicts the surface roughness.

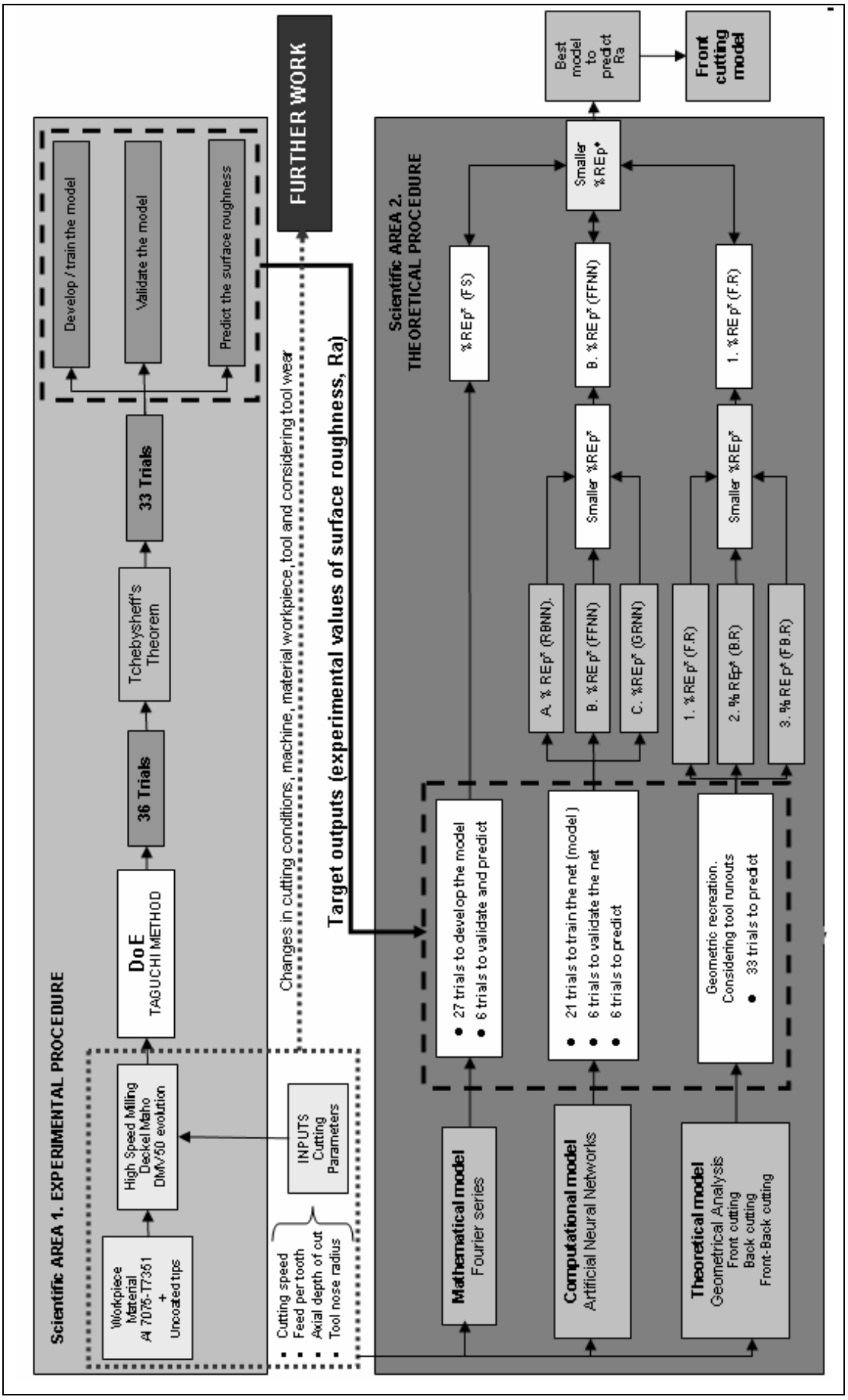

Figure 8.1- Schematic diagram for the selection of the best model to predict the surface roughness when face milling with square inserts.

When analyzing Figure 8.1 it is observed that this study seems to be divided into two main areas, however Scientific Area 1 is just included to remind the reader how the target outputs (Ra) were obtained, since this area was developed in Chapter 5. As previously mentioned 36 trials, each of them under different cutting conditions, were used to conduct the milling process on an Al 7075-T7351.

As stated in Chapter 6, once the face milling process was concluded and the values of surface roughness were obtained the Tchebysheff's theorem was applied. The results showed that only 33 trials out of 36 were inside 95% of normal distribution.

The 33 trials were divided in three different groups for the development of the model its validation and later prediction of the surface roughness.

Scientific Area 2 shows exactly the amount of trials used to develop and validate each of the models and also the amount of trials used to predict the surface roughness. As observed, the amount of trials of each group changes depending on the model that is been developed. The mathematical model based on Fourier series used 27 trials to develop the model and 6 trials to predict and validate the model at the same time. The Artificial Neural Networks employed 21 trials for the training of the network, six trials to validate the selected network and six trials to predict the values of surface roughness. Since the Theoretical model is developed based on a geometrical recreation of the tool trail left on the machined surface, the complete 33 trials were used to predict the values of roughness once the model was developed.

Once the predicted values of roughness were obtained from each of the models the $\%RE_P$ (Relative Error percentage between the predicted and experimental values of surface roughness) were obtained. Afterward the $\%RE_P$* (Relative Error percentage average) of each of the models is calculated and compared. The smaller %Rep* between all the models will be used to make the selection of the best model that predict the surface roughness when face milling with square inserts.

Also in Figure 6.1 it is observed that further work could be made if the starting conditions of the study are changed, such as: cutting speed, feed per tooth, material workpiece, tool material and geometry, milling machine, etc. and the tool wear is included in the analysis, this will represent a new contribution to knowledge.

8.2 Comparison between the experimental and predicted values of surface roughness obtained by using developed Fourier series, Artificial Neural Networks (FFNN) and the Front cutting theoretical model.

In order to select the optimal model for surface roughness prediction, the calculated output (predicted value of surface roughness) is compared with the target output (experimental surface roughness).

In order to facilitate readers understanding, a summary of all the trials that were used to predict the values of surface roughness by using each developed is model (Chapter 6) is presented in Table 8.1. This table also presents their respective experimental value of surface roughness. Table 8.2 presents their respective $\%RE_P$ between the experimental and the predicted values of surface roughness.

It must be highlighted that the predicted values of surface roughness for the ANN case, were obtained by using the FFNN for r=0.8 mm and r=2.5 mm, as stated in Chapter 6, Section 6.4 this network achieved the best performance when compared with RBNN and GRNN. In the case of the theoretical model, the predicted values of surface roughness were obtained by using the Front cutting theoretical model, as stated in Chapter 6, Section 6.5.1, this model achieved the best performance, by obtaining the minimum $\%RE_P$ between the experimental and the predicted values when comparing it with the Back and Front-Back cutting models.

Table 8.1- Experimental and predicted values of surface roughness obtained by using Fourier series model (FS), Feed Forward Artificial Neural Network model (FFNN) and the Front cutting theoretical model considering the real case (F.R).

Trial	V (m/min)	fz (mm/rev*tooth)	ap (mm)	r (mm)	Ra (µm)	Rap (FS) (µm)	Rap (FFNN) (µm)	Rap (F.R) (µm)
2	600	0.2	3.5	0.8	1.017	0.846	1.019	1.014
7	1000	0.1	4.0	0.8	0.712	0.766	0.707	0.716
16	1000	0.1	4.0	2.5	0.365	0.308	0.372	0.375
18	1000	0.3	3.0	2.5	0.381	0.395	0.393	0.401
27	1600	0.3	3.0	0.8	0.888	0.789	0.912	0.893
29	1200	0.2	3.5	2.5	0.461	0.419	0.440	0.457

Note: FFNN for r=0.8 mm and FFNN for r=2.5 were used depending on which tool nose radius was under study.

Table 8.2- $\%RE_P$ between the experimental and predicted values of surface roughness, obtained by using Fourier series model (FS), Feed Forward Neural Network model (FFNN) and the Front cutting theoretical model when considering a real case (F.R).

Trial	V (m/min)	fz (mm/rev*tooth)	ap (mm)	r (mm)	$\%RE_P$ (FS)	$\%RE_P$ (FFNN)	$\%RE_P$ (F.R)
2	600	0.2	3.5	0.8	16.81	0.20	0.3
7	1000	0.1	4.0	0.8	7.58	0.70	0.6
16	1000	0.1	4.0	2.5	15.62	1.92	2.7
18	1000	0.3	3.0	2.5	3.67	3.15	5.2
27	1600	0.3	3.0	0.8	11.15	3.60	0.6
29	1200	0.2	3.5	2.5	9.11	4.56	0.9
				$\%RE_P$*	10.65	2.36	1.72

Figure 8.2 illustrates the results of experimental and predicted values of surface roughness obtained for each of the developed models.

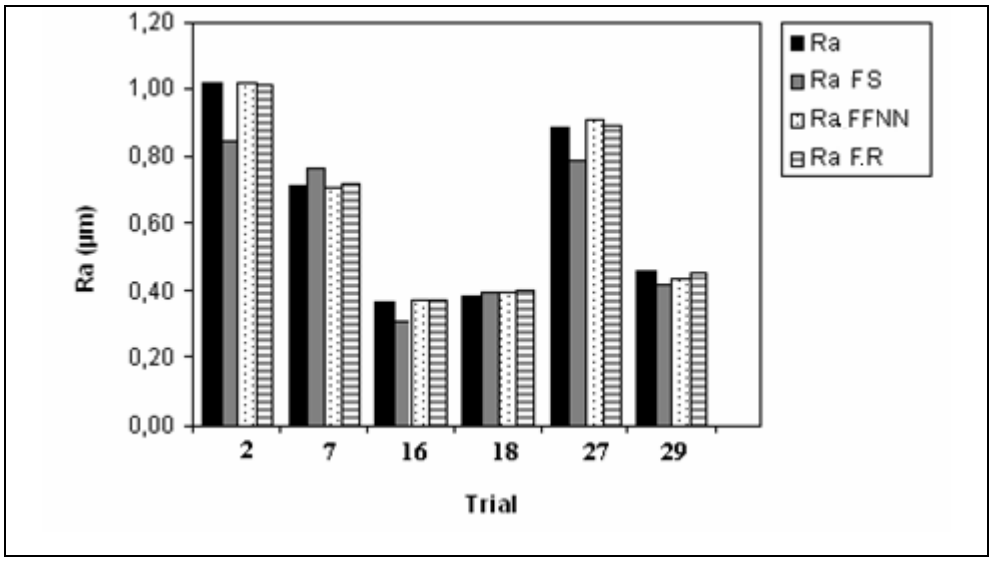

Figure 8.2- Comparison between experimental and predicted values of surface roughness obtained when applying the different developed models (Fourier series, FS; Feed Forward Neural Network, FFNN and the Front cutting theoretical model when considering a real case F.R).

When analyzing Table 8.1 and Figure 8.2 it is observed that the developed models presented a high accuracy for the prediction of surface roughness when face milling with square inserts.

The best accuracy is reached by the Front cutting theoretical model when the static tool runouts were considered. As observed this model can predict the surface roughness with an accuracy of almost 98%, followed by the FFNN with an accuracy of 97.4% and the Fourier series with an accuracy of 89.4%.

These results present a new contribution to knowledge since it gives the opportunity to select the model that best suits the necessity of the user, considering the fact that a 20% difference between the three (3) values of measured roughness was obtained in the machined specimens.

8.3 Comparison between experimental and 2D profiles obtained by using the different developed models.

The comparison of the 2D predicted profiles is made between the trials that were selected randomly for predicting the surface roughness (trials 2, 7 and 27 for r=0.8 mm and trials, 16,18 and 29 for r=2.5mm). Also it must be highlighted that this comparison is made with the Fourier series (FS) and the Front cutting theoretical model (F.R), since the FFNN model (and the other ANN developed models) only reports a value of surface roughness and not a profile.

Once the Fourier series of each trial was developed, each series is compared with the experimental 2D surface roughness profile. This comparison is shown in Table 8.3 and Table 8.4 when using r=0.8 mm and r= 2.5 mm respectively.

Table 8.3- Comparison between the experimental 2D surface roughness profile and the Fourier series 2D profile for different cutting conditions and r=0.8 mm.

Trial	Cutting parameters	Fourier series profile / Experimental surface roughness profile
2	V= 600 m/min fz= 0.2 mm/ rev * tooth ap= 3.5 mm r= 0.8 mm	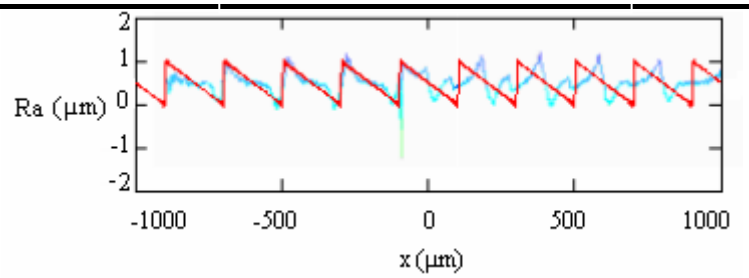
7	V= 1000 m/min fz= 0.1 mm/ rev * tooth ap= 4.0 mm r= 0.8 mm	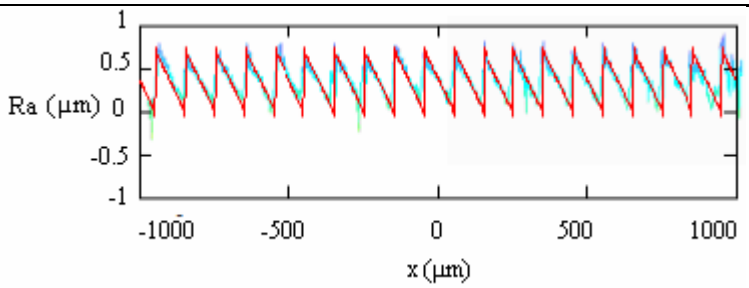
27	V= 1600 m/min fz= 0.3 mm/ rev * tooth ap= 3.5 mm r= 0.8 mm	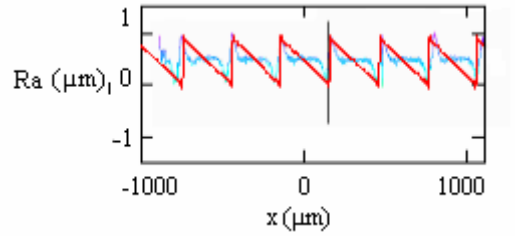

Table 8.4- Comparison between the experimental 2D surface roughness profile and the Fourier series 2D profile for different cutting conditions and r=2.5 mm.

Trial	Cutting parameters	Fourier series profile / Experimental surface roughness profile
16	V= 1000 m/min fz= 0.1 mm/ rev * tooth ap= 4.0 mm r= 2.5 mm	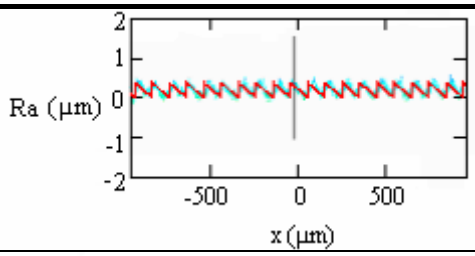
18	V= 1000 m/min fz= 0.3 mm/ rev * tooth ap= 3.5 mm r= 2.5 mm	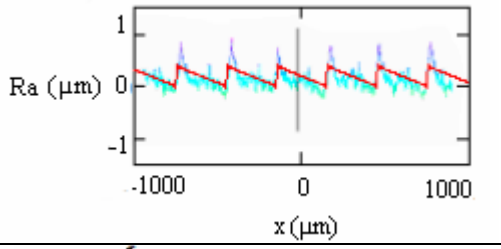
29	V= 1200 m/min fz= 0.2 mm/ rev * tooth ap= 3.5 mm r= 2.5 mm	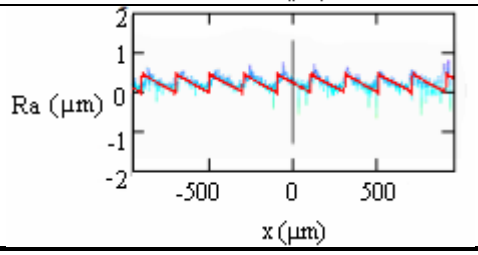

As observed, each Fourier series matches very well with the experimental 2D surface roughness profile obtained from each specimen milled under a set of cutting conditions. Also, as observed in Table 8.3, trial 2, the experimental surface roughness profile shows front and back cutting. As previously stated in Chapter 6, only a few milled surfaces presented the back cutting marks on some parts of their surface, and when developing and analyzing the different theoretical models, it was observed that a unique cutter tooth can define the surface profile of milled parts when considering the front cutting process. So the appearance of this back cutting can be attributed to waviness in the machined piece. In this case, misalignment of the tool is not considered due to the fact that the CNC HSM machine used to conduct the experiment did not show any irregularity when conducting the vibration studies reported in Chapter 5.

The comparison between the 2D predicted profile obtained by using the front cutting theoretical model when considering static tool runouts, and the experimental 2D profile obtained after face milling the AL 7075-T7351 with square inserts are reported in Table 8.5 and Table 8.6 for r=0.8 mm and r=2.5 mm respectively.

Table 8.5- Comparison between the experimental 2D surface roughness profile and the Front cutting 2D theoretical profile for different cutting conditions and r=0.8 mm

Trial	**Cutting parameters**	Front cutting theoretical model Experimental surface roughness profile
2	V= 600 m/min fz= 0.2 mm/ rev * tooth ap= 3.5 mm r= 0.8 mm	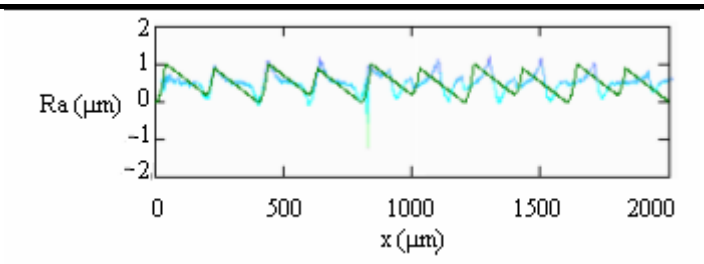
7	V= 1000 m/min fz= 0.1 mm/ rev * tooth ap= 4.0 mm r= 0.8 mm	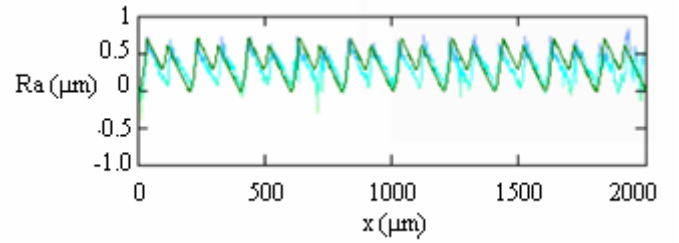
27	V= 1600 m/min fz= 0.3 mm/ rev * tooth ap= 3.5 mm r= 0.8 mm	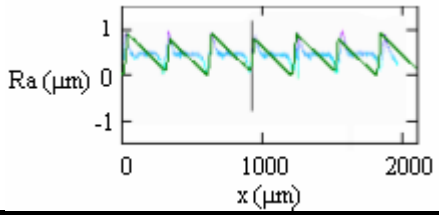

Table 8.6- Comparison between the experimental 2D surface roughness profile and the Front cutting 2D theoretical profile for different cutting conditions and r=2.5 mm

Trial	Cutting parameters	Front cutting theoretical model Experimental surface roughness profile
16	V= 1000 m/min fz= 0.1 mm/ rev * tooth ap= 4.0 mm r= 2.5 mm	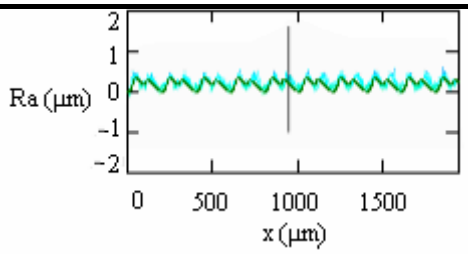
18	V= 1000 m/min fz= 0.3 mm/ rev * tooth ap= 3.5 mm r= 2.5 mm	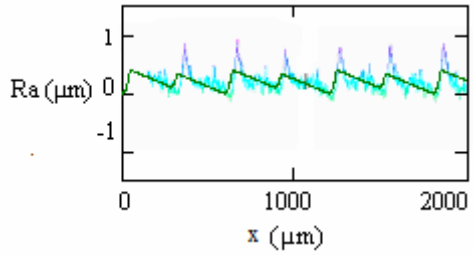
29	V= 1200 m/min fz= 0.2 mm/ rev * tooth ap= 3.5 mm r= 2.5 mm	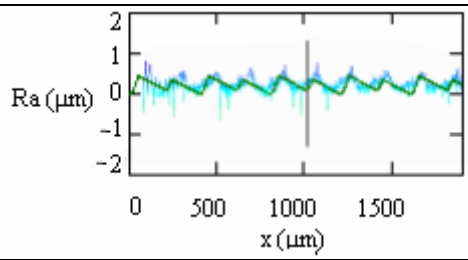

Once again, as observed in Table 8.5 and Table 8.6 the 2D Front cutting theoretical profile matches very well with the experimental 2D surface roughness profile.

Table 8.7 and Table 8.8 presents the 2D surface roughness profiles obtained from experiments, Fourier series and Front cutting theoretical model. In order to observe in detail, the behaviour of each model when using r=0.8 mm and r=2.5 mm respectively.

Table 8.7- Comparison between experimental 2D surface roughness profile, Fourier series 2D profile and Front cutting 2D theoretical model profile for different cutting conditions and r=0.8 mm.

Trial	Cutting parameters	Front cutting theoretical model profile Fourier series profile Experimental surface roughness profile
2	V= 600 m/min fz= 0.2 mm/ rev * tooth ap= 3.5 mm r= 0.8 mm	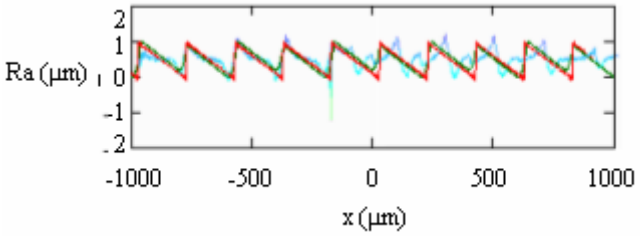
7	V= 1000 m/min fz= 0.1 mm/ rev * tooth ap= 4.0 mm r= 0.8 mm	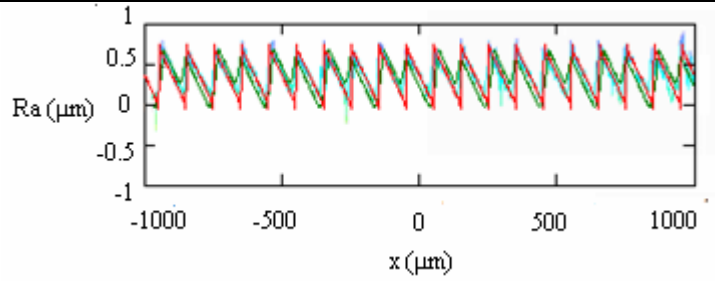
27	V= 1600 m/min fz= 0.3 mm/ rev * tooth ap= 3.5 mm r= 0.8 mm	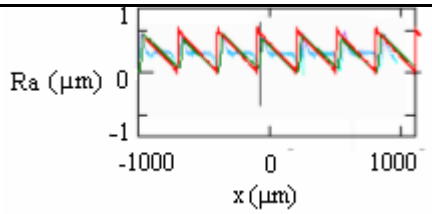

Table 8.8- Comparison between experimental 2D surface roughness profile, Fourier series 2D profile and Front cutting theoretical model 2D profile for different cutting conditions and r=2.5 mm.

Trial	Cutting parameters	Front cutting theoretical model profile Fourier series profile Experimental surface roughness profile
16	V= 1000 m/min fz= 0.1 mm/ rev * tooth ap= 4.0 mm r= 2.5 mm	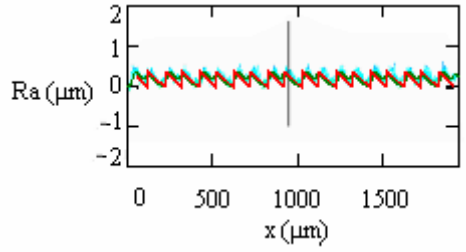
18	V= 1000 m/min fz= 0.3 mm/ rev * tooth ap= 3.5 mm r= 2.5 mm	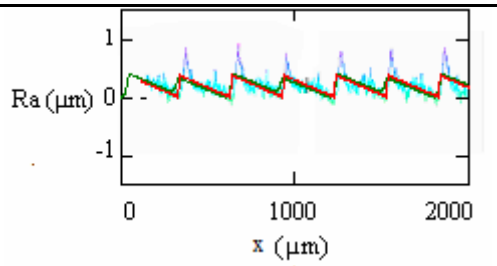
29	V= 1200 m/min fz= 0.2 mm/ rev * tooth ap= 3.5 mm r= 2.5 mm	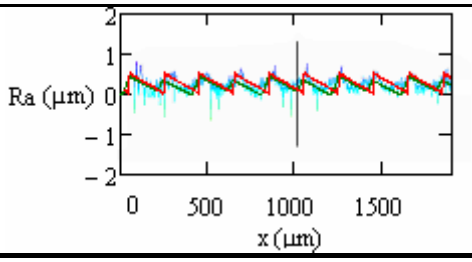

As observed from Table 8.7 and Table 8.8, in general, the Front cutting theoretical profile matches very well with the Fourier series profile and the experimental profile. This is a very good result, since it verifies how the surface roughness is affected especially by the feed per tooth and the tool nose radius.

The idea of reproducing a 2D surface roughness profile represents a new contribution to knowledge when face milling with square inserts. It also represents a useful tool for people in the area, since not only the prediction of a surface roughness value can be obtained, but also a good approach of the surface roughness profile.

8.4 Summary and general conclusions of this study

A new contribution to knowledge is made, showing that the three developed models give enough accuracy to predict the surface roughness when face milling with square inserts.

Also the possibility of reproducing the 2D surface roughness profile by using either the mathematical model based on the Fourier series, or the Front cutting model when considering static tool runouts is presented.

Finally the overall results showed that the Front cutting theoretical model which considers the static tool runouts has the highest accuracy (98%) followed by the FFNN (97.4%) and the Fourier series (89.4%).

9 General conclusions and further work

9.1. Conclusions and novelty justification

The following conclusions are drawn from this research.

- The three developed models make a new and valuable contribution to the metalworking industry by predicting the surface roughness when HSM with square inserts with an accuracy of 98 % for the theoretical front cutting model, 97 % for the FFNN and 90 % for the Fourier series.
- The front cutting theoretical model based on a geometric analysis can be extended for the use of similar combinations of workpiece material – tool material.
- The predicting time of a surface roughness value is provided immediately when using any of the developed models, however the training time of the Neural Networks where 1-20 minutes.
- FFNN achieved a better accuracy for surface roughness prediction when compared with the RBNN and GRNN; however, they took more time to train the network.
- The research has shown that 2D surface roughness profiles and 3D surface topography can be used to identify the presence of tool wear and possible vibrations affecting the machined surface.
- Under the selected cutting conditions, it was observed that in general, the surface microhardness did not vary more then 12% due to work hardening when compared with the original surface (not machined).
- It was corroborated that an increase in cutting speed and tool nose radius produced a smother surface.
- It was substantiated that an increase in the feed per tooth produced a rougher surface roughness.
- The Pareto ANOVA diagram results show a strong influence of the tool nose radius on surface roughness, with almost 70% of contribution, followed by the cutting speed and the feed per tooth (with almost 15% each). The axial depth of cut seems to have a negligible influence on the surface roughness since a value larger than the tool nose radius was used.
- The FFT graphs are useful tools to identify any equipment problem when conducting a machining process.

- An improvement of 900% in tool life was achieved when using low values of cutting parameters.
- An increase of 350% of the material removal is obtained when using high values of cutting parameters.
- An increase of 25% of the tool wear produced an increase of 30% in the surface roughness.

9.2 Further work

Regarding further work, the theoretical front cutting model could be improved by including tool wear. This future work would require a large amount of additional experimental work, which will also provide the opportunity of further validation of the model.

Also, the theoretical frontm cutting model could be improved by including the vibration parameter.

References

Abou-El-Hossein, K.A; Yahya, Z. "High Speed End Milling of AISI 304 Stainless Steels Using New Geometrically Developed Carbide Inserts". *Journal of Materials Processing Technology* . Vol. 162-163, pp. 596-602, 2005.

Arizmendi, M; Campa, F.J; Fernández, J; López de Lacalle L.N; Gil, A, Bilbao, E; Veiga, F and Lamikiz, A. "Model for Surface Topography Prediction in Peripheral Milling Considering Tool Vibration". *CIRP Annals-Manufacturing Technology* . Vol. 58, pp. 93-96, 2009.

Aslan, E. "Experimental Investigation of Cutting Tool Performance in High Speed Cutting of Hardened X210Cr12 Cold-Work Tool Steel (62 HRc)". *Materials and Design*. Vol. 26, pp. 21-57, 2005.

American Society of Testing Material. "Standard Practice for Preparation of Metallographic Specimens". ASTM E 3.

American Society of Testing Material. "Standard Test Method for Microindentation Hardness of Materials". ASTM E384.

American Society of Testing Material. "Standard Practice for Microetching Metals and Alloys" ASTM E407-99.

Axinte, D.A and Dewes, R.C. "Surface Integrity of Hot Work Tool Steel after High Milling Experimental Data and Empirical Models". *Journal of Materials Processing Technology* . Vol.127, pp.325-335, 2002.

Babur, O and Mahmut B. "The Statistical Modelling of Surface Roughness in High-Speed Flat End Milling". *International Journal of Machine Tools & Manufacture*. Vol. 46, pp. 1395–1402, 2006.

Balkrishna, R and Shin, Y. "Analysis on High-Speed Face-Milling of 7075-T6 Aluminium Using Carbide and Diamond Cutters". *International Journal of Machine Tools & Manufacture*. Vol. 41, pp. 1763–1781, 2001.

Baek, D; Ko, T and Kim, H. "Optimization of Feed Rate in a Face Milling Operation using a Surface Roughness Model". *International Journal of Machine Tools and Manufacture.* Vol. 41, No. 3, pp. 451-462, 2001.

Black, S; Chiles, V; Lissaman, A.J and Martin, S.J. "Principles of Engineering manufacture". Butterworth-Heinemann. UK, 1996, pp-237-240

Bolton, W. "Mathematics for Engineers. Fourier Series". *Langman Scientific & Technical.* England, pp. 1-5, 1995.

Boothroyd, G. "Fundamentos del Corte de Metales y de las Máquinas Herramientas". *McGraw-Hill. Latinoamericana*. Mexico. pp. 127-142. 1989.

Bouzakis, K.D; Hadjiyiannis, S; Skordaris, G; Mirisidis, I; Michailidis, N; Koptsis,D. "Milling Performance of Coated Inserts with Variable Coating Thickness on Their Rake and Flank". *Annals of the CIRP*. Vol. 53/1, pp. 81-84, 2004.

Bouzakis, K.D; Skordaris, G; Mirisidis, I; Mesomeris, G; Michailidis, N; Pavlidou, E; Erkens, G. "Micro-Blasting of PVD Films, an Effective Way to Increase the Cutting Performance of Coated Cemented Carbide Tools". *Annals of CIRP*. Vol. 54/1, pp. 95-98, 2005.

Braghini, A; Diniz, E and Filho, F. "Tool Wear and Tool Life in End Milling of 15-5 PH Stainless Steel under Different Cooling and Lubrication Conditions*".International Journal of Advanced Manufacturing Technology*. Vol. 43. No.7-8, pp. 756-764, 2009.

Bracewell R. "The Fourier Transform and its applicattions". Mc. Graw Hill. USA, 1999

Canavos, G. "Probabilidad y Estadística. Aplicaciones y Métodos". México. 1988

Calamaz, M; Limido, J; Nouari, M; Espinosa, C; Coupard, D; Salaun, M; Girot, F and Chieragatti, R ."Toward a Better Understanding of Tool Wear Effect through a Comparison between Experiments and SPH Numerical Modelling of Machining Hard Materials". *International Journal of refractory Metals & Hard Metals.* Vol 27. No. 3, pp. 595-604, 2009.

Campbell, C; Bendersky, L;, Boettinger, W and Ivester, R. "Microstructural Characterization of Al-7075-T651 Chips and Workpieces Produced by High-Speed Machining". *Materials Science and Engineering A-Structural Materials Properties Microstructure and Processing*. Vol. 430. Issue: 1-2, pp. 15-26, 2006.

Che-Haron. "Tool Life and Surface Integrity in Turning Titanium Alloy". *Journal of Material Processing Technology*. Vol. 118, pp. 231-237, 2001.

Childs, T.H.C; Sekiya, K; Tesuka, R; Yamane, Y; Dornfeld, D; Lee, D.E; Min, S and Wright, P.K. "Surface Finishes from Turning and Facing with Round Nosed Tools". *CIRP Annals. Manufacturing Technology*. Vol. 57, pp. 89-92, 2008.

Choundhury, S.K and Srinivas, P. "Tool Wear Prediction in Turning". *Journal of Materials Processing Technology*. Vol.153-154, pp. 276-280, 2004.

Chunzehg, D and Minjie, W. "Some Metallurgical Aspects of Chips Formed in High Speed Machining of High Strength Low Alloy Steel". *Scripta Materialia*. Vol. 52, pp. 1001-1004, 2005.

Corduan, N; Himbert, T; Poulachon, G; Dessoly, M; Lambertin, M; Vigneau,J; Payoux, B. "Wear Mechanisms of New Tool Materials for Ti-6Al-4V High Performance Machining". *Annals of the CIRP*. Vol. 52/1. pp. 73-76, 2003.

Dabade, U.A; Joshi, SS and Ramakrishan. "Analysis of Surface Roughness and Chip Cross-Sectional Area While machining with Self Propelled Round Insert Milling Cutter". *Journal of Materials Processing Technology*. Vol. 132, pp. 305-312, 2003.

Datsko J. "Material Properties and Manufacturing Processes". *John Wiley and Sons, Inc*.USA. pp. 352-474, 1966.

de Oliveira, A and Diniz, E. "Tool Life and Tool Wear in the Semi-Finish Milling of Inclined Surfaces". *Journal of Materials Processing Technology.* Vol. 209. No.14. pp. 5448-5455, 2009.

Derakhshan E and Akbari A. "Experimental Investigation on the Effect of Workpiece Hardness and Cutting Speed on Surface Roughness in Hard Turning with CBN Tools". *Proceedings of the World Congress on Engineering*. Vol II. London, U.K. 2009.

D'Errico, G.E; Gugliemi, E; Rutelli, G. "A Study of Coatings for End Mills in High Speed Metal Cutting". *Journal of Materials Processing Technology.* Vol. 92-93, pp. 251-256, 1999.

DeGarmo, P; Black, T and Kosher R. "Materials and Processes in Manufacturing". *Macmillan Publishing Company*. 7th Edition. USA, pp. 516-547; 651-671, 1988.

Dhar, N.R; Kamruzzaman, M and Ahmed, M. *"Effect of Minimum Quantity Lubrication (MQL) on Tool Wear and Surface Roughness in Turning AISI-4340 Steel*". Journal of Materials Processing Technology 172, pp. 299–304, 2006.

Dilipak, H; Gueldas, A and Gezgin, Akin. "An Investigation of the Number of Inserts Effect on the Machining Time and Metal Removal Rate During the Milling of AISI D3 Steel at High Cutting Speeds". *Journal of Mechanical Engineering* . Vol. 55 .No. 7-8, pp. 438-443, 2009.

Diniz, A.E and Filho, J.C. "Influence of the Relative Positions of Tool and Workpiece on Tool Life, Tool Wear and Surface Finish in the Face Milling Process". *Wear*. Vol. 232 (1), pp 67-75, 1999.

Dolinsek, S; Sustarsic, B and Kopac, J. "Wear Mechanisms of Cutting Tools in High Speed Cutting Processes". *Wear.* Vol. 250, pp. 349-356, 2001.

Doyle, L; Keyser, C; Leach, J; Schrader, G and Singer M. "Manufacturing Processes & Materials for Engineers"**.** *Prentice Hall*. 3rd Edition. USA, pp. 110-113; 632-647, 1985.

Elbestawi, M.A; Chen, L; Becze, C.E and El-Wardany, T.. "High-Speed Milling of Dies and Molds inTheir Hardened State". *Annals of the CIRP*. Vol. 46/1, pp. 57-62. 1997.

Edwards and Endean,. "Materials in Action. Manufacturing with Materials". *The Open University.* UK, pp. 233-272, 1990.

Fang, N. "Characteristic Variations of Chip Morphology and Cutting Forces in Flat Milling with Flat faced and Grooved Tool Inserts". *JSME International Journal. Series A.*Vol 46. No 3, pp. 230-236, 2003.

Franco, P; Estrems, M and Faura, F. "Influence of radial and Axial Runouts on Surface Roughness in Face Milling With Round Insert Cutting Tool*". International Journal of Machine Tool and Manufacturing.*Vol. 44, pp.1555-1565, 2004.

Franco, P; Estrems, M and Faura F. "A Study of back Cutting Surface Finish Form Tool Errors and Machine Tool Deviations During Face Milling".*International Journal of Machine Tool and Manufacturing*. Vol. 48, pp.112-123, 2008.

Freund, J and Simon, G. "Fundamental Statistics". *Prentice-Hall*. México, D.F., pp.2-13, 379-416, 1994.

Gatto, A and Iuliano L. "Advanced Coated Ceramic Tools for Machining Superalloys". *Inst. Journal .Mach. Tools Manufact*. Vol. 37, No. 5, pp. 591- 605, 2003.

Ghani, J.A; Choudhury, I.A and Hassan, H. "Application of Taguchi Method in the Optimization of End Milling Parameter". *Journal of Material Processing Technology*. Vol. 145, pp. 84-92, 2004.

Ginting, A and Nouari, M. "Surface Integrity of Dry Machined Titanium Alloys". *International Journal of Machine Tools & Manufacture.* Vol.49. 3-4. pp. 325-332, 2

Gopalsamy, B; Mondal, B and Ghosh, S. "Taguchi Method and ANOVA: An Approach for Process Parameters o

Groover, M. "Fundamentals of Modern Manufacturing Materials Processes & Systems". *John Wiley & Sons.* 2nd Edition, USA, 2002.

Guo, Y and Yen, W. "FEM Study on Mechanisms of Discontinuous Chip Formation in Hard Machining". *Journal of Material Process and Technology*. pp. 55–156:1350–6. 2004.

Harvey. "Neural Network Principles". *Prentice Hall.* International editions. USA, 1994.

ISO Standard. 8688-1. Tool Life testing In Milling. Part 1. Face Milling. 1989

http://ve.kalipedia.com/kalipediamedia/geografia/med (Accessed 22/10/2009)

http://steel.keytometals.com/Articles/Art104.htm (Accessed 03/03/2010)

Jesuthanam, C.P; Kumanan, S and Asokam, P. "Surface Roughness Prediction Using Hybrid Neural Networks". *Machining Science and Technology.* Vol. 11, pp.271-286, 2007.

Kalpakjian, S. "Manufacturing Processes for Engineering Materials and Technology". Vol. 157-158, pp. 543-552, 2003.

Kim Jeong-Du and Kang Youn-Hee. "High Speed Machining of Aluminium Using Diamond End Mills". *International Journal of Machining Tool and Manufacturing*. Vol 37. No.8, pp. 1155-1165, 1997.

Kishawy, H.A, Dumitrescu, M, Ng, E.G, Elbestawi, M.A. "Effect of Coolant Strategy on Tool Performance, Chip Morphology and Surface Quality during High Speed Machining of A356 Aluminium Alloy". *International Journal of Machine Tools & Manufacture.* Vol. 45, pp. 219-227, 2005.

Kishawy, H.A; Kannan, S and Balasinski, M. "Analytical Modelling of Tool Wear Progression during Turning Particulate Reinforced Metal Matrix Composites". *Annals of the CIRP.* Vol. 54/1., pp. 55-58, 2005.

Kopac. J. "Influence of Cutting Material and Coating on Tool Quality and Tool Life". *Journal of Materials Processing Technology*. Vol. 78, pp. 95-103, 1998.

Korkut, I; Mustafa K, Ibahim C and Ulvi S. "Determination of Optimum Cutting Parameters during Machining of AISI 304 Austenitic Stainless Steel". *Materials and Design*. Vol. 25, pp. 303-305, 2004

Koshy, P; Dewes, R.C; Aspinwall D.K. "High Speed End Milling of Hardened AISI D2 Tool Steel (58 HRc)". *Journal of Material Processing Technology.* Vol.127, pp. 266-273, 2002.

Lin, S.Y; Cheng, S.H and Chang, C.K. "Construction of a Surface Roughness Prediction Model for High Speed Machining". *Journal of Mechanical Science and Technology.* Vol. 21, pp.1622-1629, 2007.

Lin, TS. "Reliability and Failure of face Milling Tools When Cutting Stainless Steels*".* *Journal of Materials Processing Technology* . Vol. 79, pp. 41-46, 1998.

Lin, TS. "Experimental Design and performance Analysis of TiN-Coated Carbide Tool in Face Milling Stainless Steel". *Journal of Materials Processing Technology.* Vol 127, pp. 1-7, 2002.

Lindberg, R. "Processes and Materials of Manufacture". *Prentice Hall*. 4th Edition, pp 42-48; 305-326, 1983.

Lipson, C. "Statistical Design and Analysis of Engineering Experiments". *McGraw Hill.* New York, USA, pp.194-197, 1973.

Liu, Z.Q; Zhang, A; Whang, Z and Wan, Y. "Wear Patterns and Mechanisms of Cutting Tools in High –Speed Face Milling". *Journal of Material Processing and Technology*. Vol. 129, pp. 222-226, 2002.

Mansour A, Abdalla, H ."*Surface Roughness Model for End Milling: a Semi-Free Cutting Carbon Case Hardening Steel (EN 32) in dry Condition"*. Journal of materials processing technology. 124, 2002, pp 183-191

Mativenga, P.T and Hon, K.K.B. "A Study of Cutting Forces and Surface Finish in High Speed Machining of ASI H13 Tool Steel Using Carbide Tools with TiAlN Based Coatings" *Proc. IMech. Part B: J. Engineering Manufacture*. Vol. 217, pp. 143-151, 2003.

Mativenga, P and Hon, K. "Wear and Cutting Forces in High-Speed Machining of H13 Using Physical Vapour Deposition Coated Carbide Tool". *Proc. IMech. Part B: J. Engineering Manufacture.* Vol. 219, pp 191-199, 2005.

Medicus, K; Daves, M; Dutterer, B; Evans, C and Fielder, R. "Tool Wear and Surface Finish in HSM of Aluminium Bronze". *Machining Science and Technology*. Vol 5(2), pp. 255-268, 2001.

Metals Handbook. ASM. "*Metallography and Microstructures"***.** Vol 09. USA, 1972

Mitchell, J. "Introduction to Machinery Analysis and Monitoring". 2nd Edition. *Pennwell Books.* USA, pp 6-24-521, 1993.

Molinari, A; Nouari, M. "Modelling of Tool Wear by Diffusion in Metal Cutting". *Wear*. Vol. 252, pp. 135-149, 2002.

Montgomery, D.C. "Design, Analyses of Experiments". 3erd Edition. *John Whiley & Sons*, 1997.

Myung, C; Jeong, S and Kwang, H. "Fractal Dimension Analysis of Machined Surface Depending on Coated Tool Wear". *Surface Coatings Technology*. Vol 193. pp. 259-265, 2005.

Ng, E; Lee, W; Sharman, A; Dewes, R and Aspinwall, D.K. "High Speed Ball Nose End Milling of Inconel 718*"***.** *Annals of the CIRP*. Vol 49/1, pp. 41-46, 2000.

Ning, M; Rahman, Y and Wong. "Investigation of Chip Formation in High Speed End Milling". *Journal of Materials Processing Technology*. Vol. 113, pp 360-367, 2001.

Oktema, H; Erzurumlu, T and Erzincanli, F. "Prediction of Minimum Surface Roughness in End Milling Mold Parts Using Neural Network and Genetic Algorithm". *Materials and Design*. Vol. 27, pp. 735-744, 2005.

Petropoulos, G. "The Effect of Feed Rate and Tool Nose Radius on the Roughness of Oblique Finished Turned Surfaces". *Wear* . Vol. 23, pp. 299-310, 1973.

Poulachon, G; Bandyopadhyay, B; Jawahir, I; Pheulpin, S and Seguin, E. "The Influence of the Microstructure of Hardened Tool Steel Workpiece on the Wear of

PCBN Cutting Tool". *International Journal of Machine Tools & Manufacture*. Vol. 43, pp. 139-144, 2003.

Poulachon, G; Albert, A; Schluraff, M and Jawahir, I. "An Experimental Investigation of Work Material Micrsostructure Effects on White Layer Formation in PcBN Hard Turning". *International Journal of Machine Tool and Manufacturing*. Vol. 45, pp. 211-218, 2005.

Rashad, R and El-Hosïny, T. "Machinability of 7116 Structural Aluminium Alloy". *Material and Manufacturing Process*. Vol 21, pp. 23-27, 2006.

Rashed, F and Mahmoud, T. "Prediction of Wear Behaviour of A356/SiCp MMCs using Neural Nnetworks". *Tribology International*. Vol. 42. No. 5, pp. 642-648, 2009.

Ravindra, D and Pattern, J. "Improving the Surface Roughness of a CVD Coated Silicon Carbide Disk by Performing Ductile Regime Single Point Diamond Turning". *Proceedings of the ASME International Manufacturing Science and Engineering Conference.* Vol 1, pp. 155-161, 2008.

Sai, W. "An Investigation of Tool Wear in High Speed Turning of AISI 4340". *International Journal of Advance Manufacturing Technology*. Vol. 26, pp, 330-334, 2005.

Saï K and Bouzid W. "Roughness Modelling in Up Face Milling". *International Journal of Advance Manufacturing Technology.* Vol. 26, pp. 324-329, 2005.

Sahin Y. "Comparison of Tool Life between Ceramic and Cubic Boron Nitride (CBN) Cutting Tools When Machining Hardened Steels". *Journal of Materials Processing Technology*. Vol. 209. No. 7, pp. 3478-3489, 2009.

Sandvik Coromant. "Modern Metal Cutting".Tofters Tryckeri AB. Sweden, 1994

S_eref A, Eyup B, Aykut K, Osman Y. "Experimental Observation of Tool Wear, Cutting Forces and Chip Morphology in Face Milling of Cobalt Based Super-Alloy with Physical Vapour Deposition Coated and Uncoated Tool". *Materials and Design*. Vol. 28, pp. 1880–1888a, 2007.

Shaw, M. "Metal Cutting Principles". Oxford *Series of Advanced Manufacturing 3*. 1991.

Shimada, S; Tanaka, H; Higuchi, M; Yamaguchi, T; Honda, S and Obata, K. "Thermo-Chemical Wear Mechanism of Diamond Tool in Machining of Ferrous Metals". *Annals of CIRP*. Vol 53/1, pp 57-60, 2004.

Shouckry, A.S. "Zones and Boundaries between Different Types of Chip". *Wear*. Vol. 69, pp. 345-353, 1981.

Siller, H; Vila, C; Rodriguez, C and Abellan, J. "Study of Face Milling of Hardened AISI D3 Steel with a Special Design of Carbide Tools". *International Journal of Advanced Manufacturing Technology.* Vol. 40. No. 1-2,. pp.12-25, 2009.

Sokovic, M; Kopac, J; Dobrzanski, L and Adamiak, M. "Wear of PVD-Coated Solid Carbide End Mills in Dry High-Speed Cutting". *Journal of Material Processing and Technology.* Vol. 157-158, pp. 422-426, 2004.

Steen, L. "The Science of Patterns". *Science*. Vol. 240, pp 616, 1988.

Stout, K and Blunt, L. "Three Dimensional Surface Topography". *Penton Press*. 2nd edition, UK, 2000.

Surmann, T and Biermann, E. The Effect of Tool Vibrations on the Flank Surface Created by Peripheral Milling". *CIRP Annals-Manufacturing Technology*. Vol. 57. 1, pp. 375-378, 2008.

Tay, F; Sikdar, S and Manan, M. "Topography of the Flank Wear Surface". *Journal of Materials Processing Technology*. Vol. 120, pp. 243-248, 2002.

Tsai, Y; Chenb, J and Louc, S. "An in-process Surface Recognition System Based on Neural Networks in end Milling Cutting Operations".*International Journal of Machine Tools & Manufacture.* Vol. 39, pp. 583–605, 1999.

Toh. C.K. "Surface Topography Analysis When High-Speed Rough Milling Hardened Steel". *Materials and Manufacturing Process*. Vol 18. No 6, pp. 849-862, 2003.

Toh, C.K. "Tool Life and Tool Wear During High-Speed Rough Milling Using Alternative Cutter Path Strategies". Proc. Instn. Mech. Engrs. Part B: J. Engineering Manufacture. Vol. 217, pp. 1295-1304, 2003.

Toh, C.K. and Kanno, S. "Surface Integrity Effects on Turned 6061 and 6061-T6 Aluminium Alloys". *Journal of Materials Science*. 39. pp 3497-3500, 2004.

Toh, C.K. "Design, Evaluation and Optimisation of Cutter Path Strategies when High Speed Machining Hardened Mould and Die Materials". *Materials and Design.* Vol. 26, pp. 517-533, 2005.

Trent, E.M. "Metal Cutting". Third Edition. *Butterworth-Heinemann Ltd*. 1991

Vivancos, J; Luis, C; Costa, L and Ortiz, J. "Optimal Machining Parameters Selection in HSM of Hardened Steels for Injection Moulds". *Journal of Materials Processing Technology.* Vol. 155-156, pp. 1505-1512, 2004.

Wang, Z.G; Rahman, M and Wong, Y. "Tool Wear Characteristics of Binderless CBN Tools used in High-Speed Milling of Titanium Alloys". *Wear*. Vol. 258, pp. 752-758, 2005.

Wang, M and Chang, H. "Experimental Study of Surface Roughness in Slot End Milling Al 2014-T6.". *International Journal of Machine Tools & Manufacture.* Vol. 44, pp. 51-57, 2004.

Weinert, K; Inasaki, I; Sutherland, J and Wakabayashi, T. "Dry Machining and Minimum Quantity Lubrication". *CIRP Annals*. Vol. 53/2. 2004.

www.case-europe.com/industries/industry/AdvancedmanufacturingMachinery,15.aspx. (Accessed 22/10/2009)

www.ilo.org/public/english/dialogue/sector/techmeet/tmte2000/tmter4.htm (Accessed 22/10/2009)

www.quakerchem.com/knowledge/skill_builders/no10_machineability_ratings.pdf (Acc. 03/03/2010)
www.alcoa.com/mill_products/catalog/pdf/alloy7075techsheet.pdf
(Acc. 03/03/2010)

www.marfas.com/mechanical.html (Acc. 03/03/2010)

www.gordonengland.co.uk/hardness/vickers.htm (Acc. 04/03/2010)

Xavior, A and Adithan, M. "Determining the Influence of Cutting Fluids on Tool Wear and Surface Roughness During Turning of AISI 304 Austenitic Stainless Steel". *Journal of Materials Processing Technology*. Vol. 209, No.2, pp. 900-909, 2009.

Appendices

- **Appendix A. Calculus example**

- **S/N ratio for Tool life for a specific trial.**

(larger-the-best)

$$S/Nratio = -10 \cdot \log\left(\frac{1}{T_1^2}\right) \quad (1)$$

from Table 4.5 (Chapter 4. Section 4.2.1)

T_1= 4.2 sec, for trial1.

$$S/Nratio = -10 \cdot \log\left(\frac{1}{(4.2)^2}\right) = 12.46$$

S/N_{ratio} for T_1 for trial 1 is 12.46 dB

- **S/N ratio for Tool life for each of the cutting parameters.**

(larger-the-best)

$$S/N_{ratio}\ T_1 = \frac{[S/N\ T_1(\text{trial 1}) + S/N\ T_1(\text{trial 2}) + S/N\ T_1(\text{trial 3})]}{3} \quad (2)$$

from Table 4.6 (Chapter 4. Section 4.4.1.1)

Trial	V (m/min)	S/N_{ratio} for T_1
1	800	12.46
2	800	6.69
3	800	2.80

$$S/NratioT_1 = \left[\frac{12.46 + 6.69 + 2.80}{3}\right] = 7.32$$

S/N_{ratio} for T_1 for V= 800 m/min is 7.32 dB

- S/N ratio for Material Removal Rate for a specific trial

(larger-the-best)

$$S/Nratio = -10 \cdot \log\left(\frac{1}{MRR_1^2}\right) \quad (3)$$

from Table 4.7 (Chapter 4. Section 4.4.1.2)

MRR_1= 70.71 cm^3/min, for trial1.

$$S/Nratio = -10 \cdot \log\left(\frac{1}{(70.71)^2}\right) = 36.99$$

S/N_{ratio} for MRR_1 for trial 1 is 12.46 dB

- S/N ratio for Material Removal Rate for each of the cutting parameters.

(larger-the-best)

$$S/N_{ratio}\ T_1 = \frac{[S/N\ MRR_1(\text{trial 1}) + S/N\ MRR_1(\text{trial 4}) + S/N\ MRR_1(\text{trial 7})]}{3} \quad (4)$$

from Table 4.7 (Chapter 4. Section 4.4.1.2)

Trial	fz (mm/rev*tooth)	S/N_{ratio} for T_1
1	0.1	36.99
4	0.1	41.50
7	0.1	44.91

$$S/NratioT_1 = \left[\frac{36.99 + 41.50 + 44.91}{3}\right] = 41.13$$

S/N_{ratio} for MRR_1 for fz= 0.1 mm/rev*tooth is 41.13 dB

- S/N ratio for Tool wear for a specific trial

(smaller-the-best)

$$S/Nratio = -10 \cdot \log(VB_1)^2 \quad (5)$$

from Table 4.10 (Chapter 4. Section 4.4.1.3)

VB_1= 0.08 mm, for trial 6.

$$S/Nratio = -10 \cdot \log(0.08)^2 = 21.93$$

S/N_{ratio} for VB_1 for trial 6 is 21.93 dB

- S/N ratio for Tool wear for each of the cutting parameters.

(larger-the-best)

$$S/N_{ratio}\ T_1 = \frac{[S/N\ VB_1(\text{trial 4}) + S/N\ VB_1(\text{trial 5}) + S/N\ VB_1(\text{trial 6})]}{3} \quad (6)$$

from Table 4.7 (Chapter 4. Section 4.4.1.2)

Trial	V (m/min)	S/N_{ratio} for T_1
4	900	26.02
5	900	24.44
6	900	21.93

$$S/NratioT_1 = \left[\frac{26.02 + 24.44 + 21.93}{3}\right] = 24.13$$

S/N_{ratio} for VB_1 for V= 900 m/min is 24.13 dB

- **Predicted tool wear obtained by using equation 4.1**

Equation 4.1 $$V_{BP} = 10^{-8.62} \cdot V^{2.79} \cdot fz^{0.28} \cdot ap^{0.04} \cdot t^{0.42}$$

For trial 1: V=800 m/min
fz=0.1 mm/rev*tooth
ap=1.0 mm
t=0.06 min

then $$V_{BP} = 10^{-8.62} \cdot 800^{2.79} \cdot 0.1^{0.28} \cdot 1.0^{0.04} \cdot 0.06^{0.42} = 0.047$$

- **Relative Error Percentage**

Equation 4.2 $$\%RE = \left| \frac{V_B - V_{BP}}{V_B} \right| * 100$$

$$\%RE = \left| \frac{0.04 - 0.047}{0.04} \right| * 100 = 17.5$$

- **Pareto ANOVA Calculus**

- Surface roughness addition for each tool nose radius level

Addition of all the Ra values obtained when cutting with r=0.8 mm (level 1) and r=2.5 mm (level 2)

Trial	r (mm)	Ra (µm)	Sum
1	0.8	0.695	
2	0.8	1.017	
3	0.8	1.472	
4	0.8	0.679	
5	0.8	0.838	
6	0.8	0.646	
7	0.8	0.412	
8	0.8	0.835	
9	0.8	0.699	**13.65**
19	0.8	0.548	
20	0.8	0.759	
21	0.8	0.781	
22	0.8	0.688	
23	0.8	0.668	
24	0.8	0.694	
25	0.8	0.461	
26	0.8	0.872	
27	0.8	0.888	
10	2.5	0.376	
11	2.5	0.399	
12	2.5	0.596	
13	2.5	0.328	
14	2.5	0.368	
15	2.5	0.425	
16	2.5	0.365	
17	2.5	0.422	
18	2.5	0.381	**7.37**
28	2.5	0.365	
29	2.5	0.461	
30	2.5	0.415	
31	2.5	0.344	
32	2.5	0.437	
33	2.5	0.408	
34	2.5	0.408	
35	2.5	0.418	
36	2.5	0.453	

- Surface roughness addition for each cutting speed level

Addition of all the Ra values obtained when cutting with V=600 m/min (level 1) V= 800 m/min (level 2), V=1000 m/min (level 3), V=1200 m/min (level 4), V=1400 m/min (level 5) and V= 1600 m/min (level 6).

Trial	V (m/min)	Ra (µm)	Sum
1	600	0.695	
2	600	1.017	
3	600	1.472	4.56
10	600	0.376	
11	600	0.399	
12	600	0.596	
4	800	0.679	
5	800	0.838	
6	800	0.646	**3.28**
13	800	0.328	
14	800	0.368	
15	800	0.425	
7	1000	0.412	
8	1000	0.835	
9	1000	0.699	3.11
16	1000	0.365	
17	1000	0.422	
18	1000	0.381	
19	1200	0.548	
20	1200	0.759	
21	1200	0.781	3.33
28	1200	0.365	
29	1200	0.461	
30	1200	0.415	
22	1400	0.688	
23	1400	0.668	
24	1400	0.694	**3.239**
31	1400	0.344	
32	1400	0.437	
33	1400	0.408	
25	1600	0.461	
26	1600	0.872	
27	1600	0.888	3.5
34	1600	0.408	
35	1600	0.418	
36	1600	0.453	

- Surface roughness addition for each feed per tooth level

Addition of all the Ra values obtained when cutting with fz=0.1 mm/rev*tooth (level 1) fz=0.2 mm/rev*tooth (level 2), fz=0.3 mm/rev*tooth (level 3).

Trial	fz (mm/rev*tooth)	Ra (µm)	Sum
1	0.1	0.695	
4	0.1	0.679	
7	0.1	0.412	
10	0.1	0.376	
13	0.1	0.328	
16	0.1	0.365	**5.67**
19	0.1	0.548	
22	0.1	0.688	
25	0.1	0.461	
28	0.1	0.365	
31	0.1	0.344	
34	0.1	0.408	
2	0.2	1.017	
5	0.2	0.838	
8	0.2	0.835	
11	0.2	0.399	
14	0.2	0.368	
17	0.2	0.422	**7.49**
20	0.2	0.759	
23	0.2	0.668	
26	0.2	0.872	
29	0.2	0.461	
32	0.2	0.437	
35	0.2	0.418	
3	0.3	1.472	
6	0.3	0.646	
9	0.3	0.699	
12	0.3	0.596	
15	0.3	0.425	
18	0.3	0.381	**7.86**
21	0.3	0.781	
24	0.3	0.694	
27	0.3	0.888	
30	0.3	0.415	
33	0.3	0.408	
36	0.3	0.453	

- Surface roughness additions for each axial depth of cut level

Addition of all the Ra values obtained when cutting with ap= 3.0 mm (level 1) ap=3.5 mm (level 2), ap=4.0 mm (level 3).

Trial	ap (mm)	Ra (µm)	Sum
1	3.0	0.695	
6	3.0	0.646	
8	3.0	0.835	
10	3.0	0.376	
15	3.0	0.425	
17	3.0	0.422	**6.704**
19	3.0	0.548	
24	3.0	0.694	
26	3.0	0.872	
28	3.0	0.365	
33	3.0	0.408	
35	3.0	0.418	
2	3.5	1.017	
4	3.5	0.679	
9	3.5	0.699	
11	3.5	0.399	
13	3.5	0.328	
18	3.5	0.381	**7.096**
20	3.5	0.759	
22	3.5	0.688	
27	3.5	0.888	
29	3.5	0.461	
31	3.5	0.344	
36	3.5	0.453	
3	4.0	1.472	
5	4.0	0.838	
7	4.0	0.412	
12	4.0	0.596	
14	4.0	0.368	
16	4.0	0.365	**7.221**
21	4.0	0.781	
23	4.0	0.668	
25	4.0	0.461	
30	4.0	0.415	
32	4.0	0.437	
34	4.0	0.408	

- Square differences addition (TG) for each cutting parameter

- For the tool nose radius

$$TG(r) = (13.65 - 7.37)^2 = 39.44$$

- For the cutting speed

$$TG(V) = \left[(4.56-3.28)^2 + (3.28-3.11)^2 + (3.11-3.33)^2 + (3.33-3.24)^2 + (3.24-3.5)^2 + (3.5-4.56)^2\right] +$$

$$+ \left[(3.28-3.33)^2 + (3.28-3.24)^2 + (3.28-3.5)^2 + (3.11-4.56)^2 + (3.11-3.24)^2 + (3.11-3.5)^2\right] +$$

$$+ \left[(3.33-4.56)^2 + (3.33-3.5)^2 + (3.24-4.56)^2\right] = 8.31$$

- For the feed per tooth

$$TG(fz) = \left[(5.67-7.49)^2 + (7.49-7.86)^2 + (7.86-5.67)^2\right] = 8.25$$

- For the axial depth of cut

$$TG(ap) = \left[(6.704-7.096)^2 + (7.096-7.22)^2 + (7.22-6.704)^2\right] = 0.44$$

- Total of the square difference addition (TT)

$$TT = TG(r) + TG(V) + TG(f_z) + TG + (a_p)$$

Then

$$TT = 39.44 + 8.31 + 8.24 + 0.44 = 56.43$$

- Contribution ratio (%)

$$Contribution\ ratio = \frac{TG(X)}{TT}$$

X= r, V, fz, ap

Cutting parameter	r	V	fz	ap
Contribution ratio (%)	69.8	14.72	14.7	0.78
Cumulative contribution (%)	69.8	84.52	99.22	100

- **Appendix B**

Table 1.- Experimental surface roughness and average roughness for each specimen cut under different cutting conditions

Trial	V(m/min)	fz(mm/rev*tooth)	ap (mm)	r(mm)	Ra1 (um)	Ra2 (um)	Ra3 (um)	Ra (um)
1	600	0.1	3.0	0.8	0.636	0.612	0.687	0.695
2	600	0.2	3.5	0.8	0.893	0.998	1.160	1.017
3	600	0.3	4.0	0.8	1.483	1.366	1.567	1.472
4	800	0.1	3.5	0.8	0.688	0.645	0.704	0.679
5	800	0.2	4.0	0.8	0.826	0.840	0.848	0.838
6	800	0.3	3.0	0.8	0.625	0.646	0.667	0.646
7	1000	0.1	4.0	0.8	0.698	0.720	0.718	0.412
8	1000	0.2	3.0	0.8	0.842	0.823	0.840	0.835
9	1000	0.3	3.5	0.8	0.689	0.702	0.706	0.699
10	600	0.1	3.0	2.5	0.362	0.311	0.365	0.376
11	600	0.2	3.5	2.5	0.379	0.419	0.389	0.399
12	600	0.3	4.0	2.5	0.494	0.424	0.481	0.596
13	800	0.1	3.5	2.5	0.308	0.330	0.330	0.328
14	800	0.2	4.0	2.5	0.329	0.389	0.386	0.368
15	800	0.3	3.0	2.5	0.371	0.483	0.420	0.425
16	1000	0.1	4.0	2.5	0.316	0.326	0.454	0.365
17	1000	0.2	3.0	2.5	0.393	0.450	0.422	0.422
18	1000	0.3	3.5	2.5	0.382	0.371	0.389	0.381
19	1200	0.1	3.0	0.8	0.510	0.535	0.599	0.548
20	1200	0.2	3.5	0.8	0.691	0.732	0.854	0.759
21	1200	0.3	4.0	0.8	0.807	0.714	0.822	0.781
22	1400	0.1	3.5	0.8	0.516	0.522	0.608	0.688
23	1400	0.2	4.0	0.8	0.722	0.665	0.617	0.668
24	1400	0.3	3.0	0.8	0.785	0.695	0.602	0.694
25	1600	0.1	4.0	0.8	0.432	0.488	0.463	0.461
26	1600	0.2	3.0	0.8	0.912	0.845	0.859	0.872
27	1600	0.3	3.5	0.8	0.886	0.748	1.030	0.888
28	1200	0.1	3.0	2.5	0.361	0.370	0.364	0.365
29	1200	0.2	3.5	2.5	0.434	0.461	0.488	0.461
30	1200	0.3	4.0	2.5	0.410	0.470	0.415	0.415
31	1400	0.1	3.5	2.5	0.335	0.375	0.322	0.344
32	1400	0.2	4.0	2.5	0.460	0.454	0.397	0.437
33	1400	0.3	3.0	2.5	0.412	0.440	0.372	0.408
34	1600	0.1	4.0	2.5	0.331	0.432	0.461	0.408
35	1600	0.2	3.0	2.5	0.444	0.473	0.337	0.418
36	1600	0.3	3.5	2.5	0.422	0.441	0.496	0.453

Table 2- 2D surface roughness profile of a few AL 7075-T7351specimens face milled under different cutting conditions and r = 0.8 mm

TRIAL	Cutting parameters	Surface roughness Ra, profile
1	V= 600 m/min fz= 0.1 mm/ rev x tooth ap= 3.0 mm	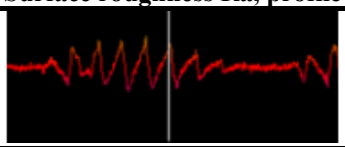
3	V= 600 m/min fz= 0.3 mm/ rev x tooth ap= 4.0 mm	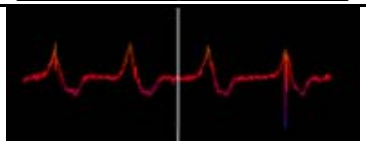
4	V= 800 m/min fz= 0.1 mm/ rev x tooth ap= 3.5 mm	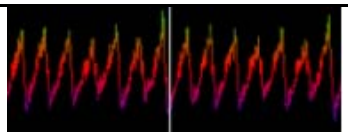
5	V= 800 m/min fz= 0.2 mm/ rev x tooth ap= 4.0 mm	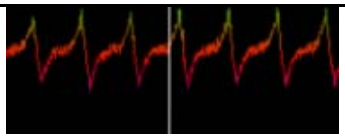
8	V= 1000 m/min fz= 0.2 mm/ rev x tooth ap= 3.0 mm	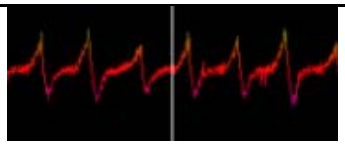
19	V= 1200 m/min fz= 0.1 mm/ rev x tooth ap= 3.0 mm	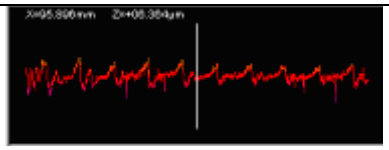
20	V= 1200 m/min fz= 0.2 mm/ rev x tooth ap= 3.5 mm	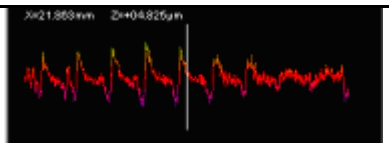
22	V= 1400 m/min fz= 0.1 mm/ rev x tooth ap= 3.5 mm	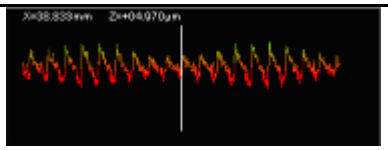
25	V= 1600 m/min fz= 0.1 mm/ rev x tooth ap= 4.0 mm	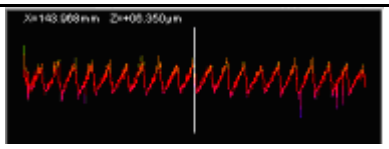
26	V= 1600 m/min fz= 0.2 mm/ rev x tooth ap= 3.0 mm	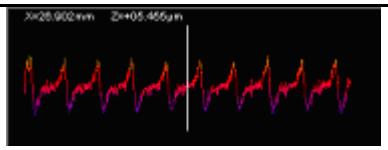

Table 3- 2D surface roughness profile of a few AL 7075-T7351specimens face milled under different cutting conditions and r = 2.5 mm

TRIAL	Cutting parameters	Surface roughness Ra, profile
11	V= 600 m/min fz= 0.2 mm/ rev x tooth ap= 3.5 mm	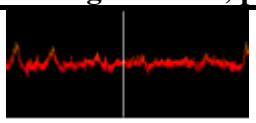
12	V= 600 m/min fz= 0.3 mm/ rev x tooth ap= 4.0 mm	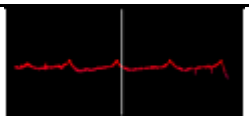
14	V= 800 m/min fz= 0.2 mm/ rev x tooth ap= 4.0 mm	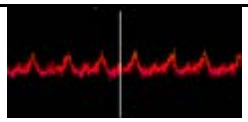
17	V= 1000 m/min fz= 0.2 mm/ rev x tooth ap= 3.0 mm	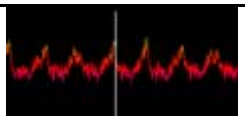
18	V= 1000 m/min fz= 0.3 mm/ rev x tooth ap= 3.5 mm	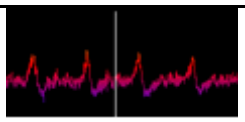
29	V= 1200 m/min fz= 0.2 mm/ rev x tooth ap= 3.5 mm	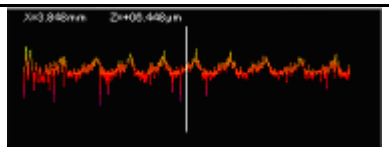
30	V= 1200 m/min fz= 0.3 mm/ rev x tooth ap= 4.0 mm	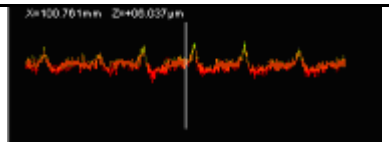
32	V= 1400 m/min fz= 0.2 mm/ rev x tooth ap= 4.0 mm	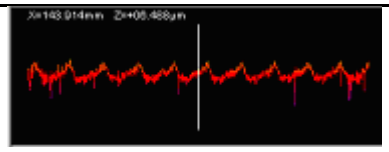
33	V= 1400 m/min fz= 0.3 mm/ rev x tooth ap= 3.0 mm	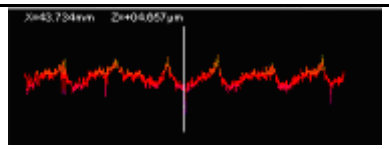
36	V= 1600 m/min fz= 0.3 mm/ rev x tooth ap= 3.5 mm	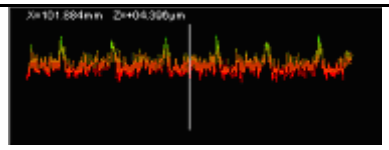

Table 4- Surface topography of a few AL 7075-T7351specimens face milled under different cutting conditions and r = 0.8 mm

Trial	Surface topography	Trial	Surface topography
1 **V=600 m/min,** **fz=0.1 mm/rev*tooth,** **ap=3.0 mm**	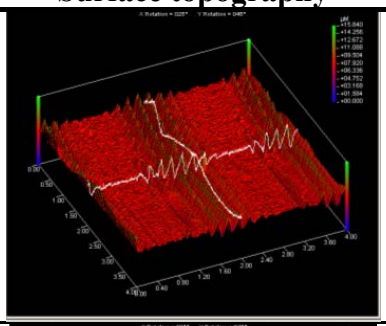	**3** **V=600 m/min,** **fz=0.3 mm/rev*tooth,** **ap=4.0 mm**	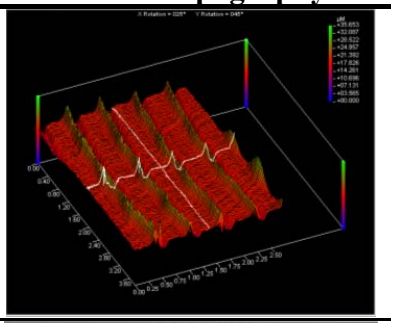
4 **V=800 m/min,** **fz=0.1 mm/rev*tooth,** **ap=3.5 mm**	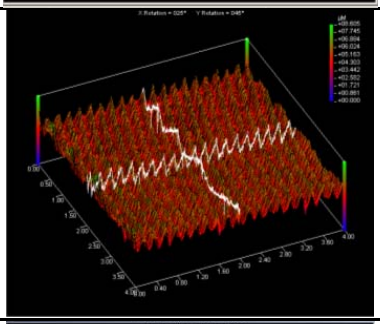	**5** **V=800 m/min,** **fz=0.2 mm/rev*tooth,** **ap=4.0 mm**	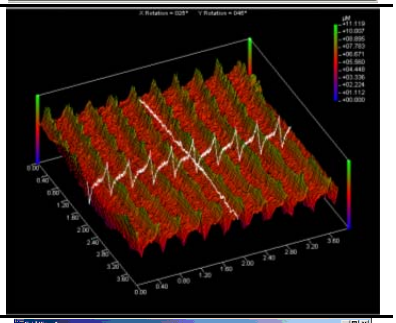
8 **V=1000 m/min,** **fz=0.2 mm/rev*tooth,** **ap=3.0 mm**	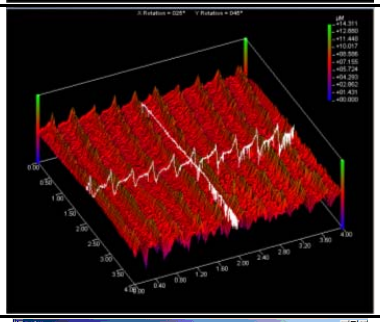	**19** **V=1200 m/min,** **fz=0.1 mm/rev*tooth,** **ap=3.0 mm**	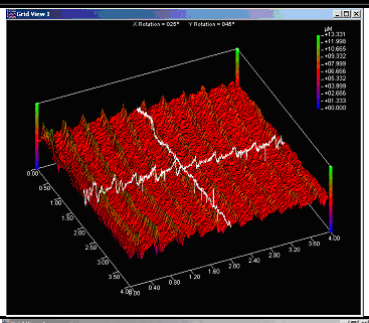
20 **V=1200 m/min,** **fz=0.2 mm/rev*tooth,** **ap=3.5 mm**	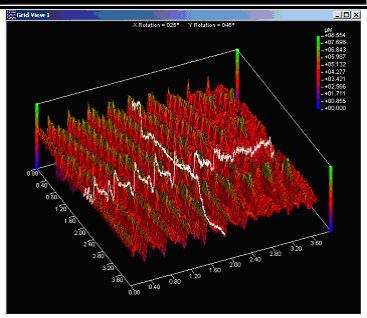	**22** **V=1400 m/min,** **fz=0.1 mm/rev*tooth,** **ap=3.5 mm**	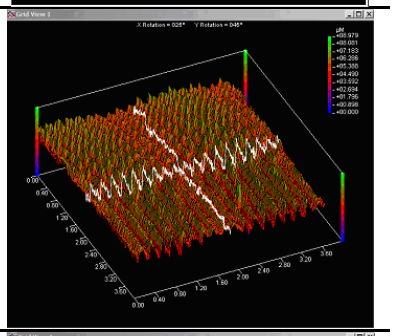
25 **V=1600 m/min,** **fz=0.1 mm/rev*tooth,** **ap=4.0 mm**	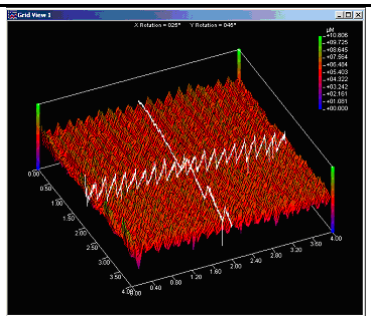	**26** **V=1600 m/min,** **fz=0.2 mm/rev*tooth,** **ap=3.0 mm**	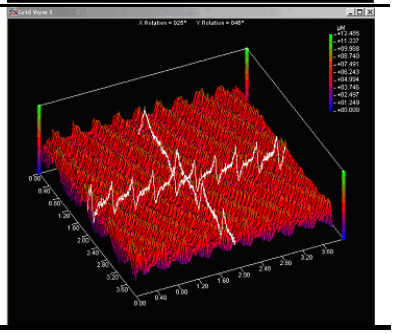

Table 5- Surface topography of a few AL 7075-T7351specimens face milled under different cutting conditions and r = 2.5 mm

Trial	Surface topography	Trial	Surface topography
19 V=1200 m/min, fz=0.1 mm/rev*tooth, ap=3.0 mm	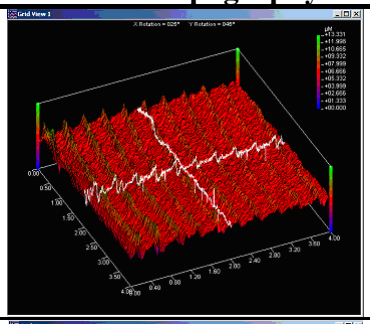	**24** V=1400 m/min, fz=0.3 mm/rev*tooth, ap=3.0 mm	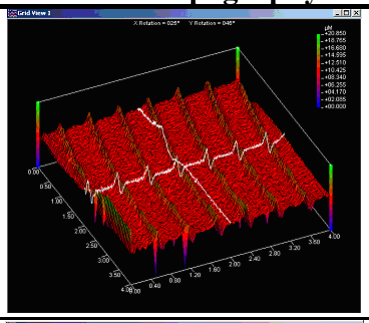
20 V=1200 m/min, fz=0.2 mm/rev*tooth, ap=3.5 mm	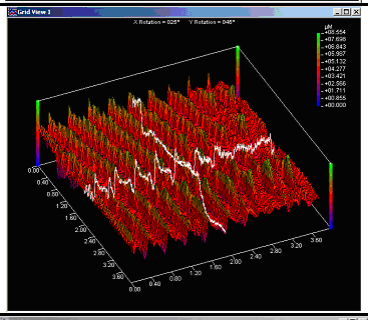	**25** V=1600 m/min, fz=0.1 mm/rev*tooth, ap=4.0 mm	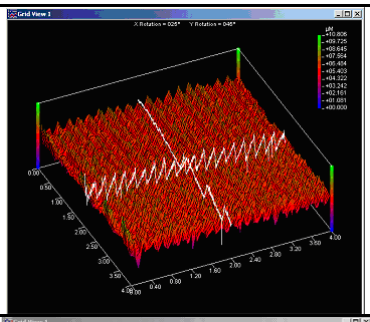
21 V=1200 m/min, fz=0.3 mm/rev*tooth, ap=4.0 mm	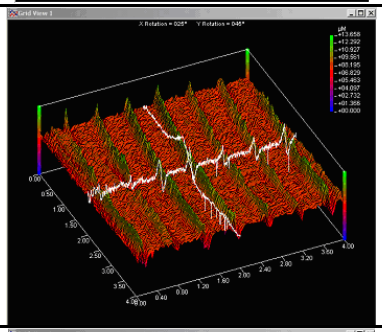	**26** V=1600 m/min, fz=0.2 mm/rev*tooth, ap=3.0 mm	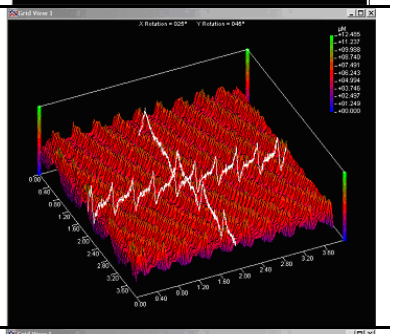
22 V=1400 m/min, fz=0.1 mm/rev*tooth, ap=3.5 mm	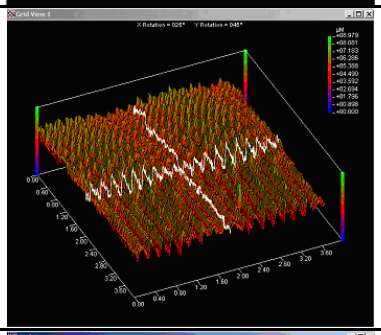	**27** V=1600 m/min, fz=0.3 mm/rev*tooth, ap=3.5 mm	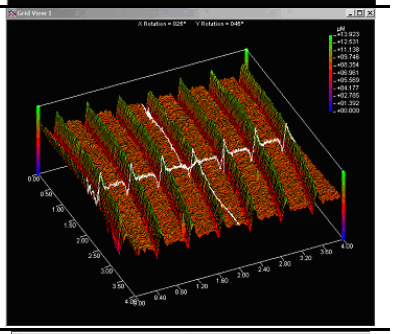
23 V=1400 m/min, fz=0.2 mm/rev*tooth, ap=4.0 mm	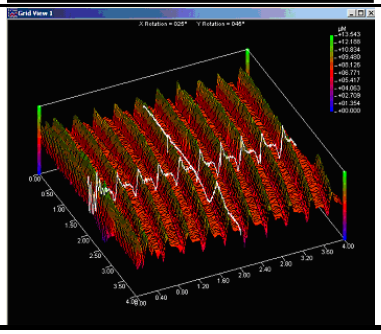	**36** V=1600 m/min, fz=0.3 mm/rev*tooth, ap=3.5 mm	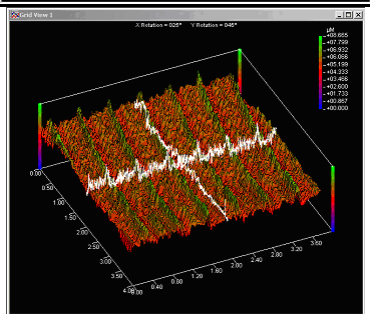

Table 6- Microstructure of a few AL 7075-T7351specimens face milled under different cutting conditions and r = 0.8 mm

TRIAL	Cutting parameters	Surface microstructure (30µm)	Surface microstructure (20 µm)
1	V= 600 m/min fz= 0.1 mm/ rev x tooth ap= 3.0 mm	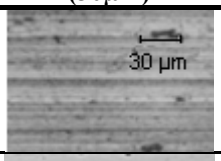	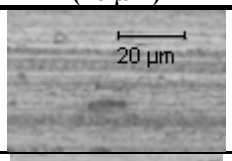
3	V= 600 m/min fz= 0.3 mm/ rev x tooth ap= 4.0 mm	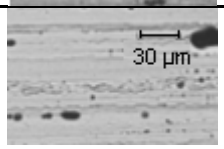	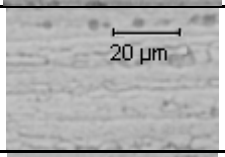
4	V= 800 m/min fz= 0.1 mm/ rev x tooth ap= 3.5 mm	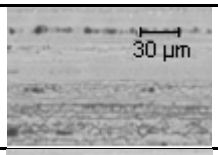	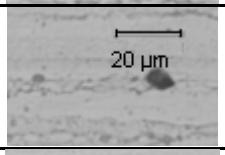
5	V= 800 m/min fz= 0.2 mm/ rev x tooth ap= 4.0 mm	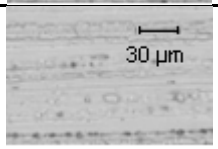	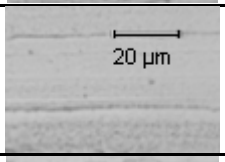
8	V= 1000 m/min fz= 0.2 mm/ rev x tooth ap= 3.0 mm	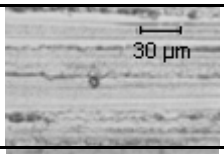	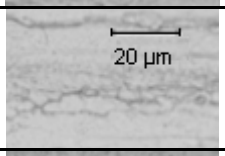
19	V= 1200 m/min fz= 0.1 mm/ rev x tooth ap= 3.0 mm	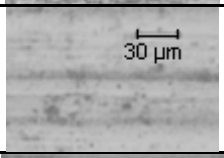	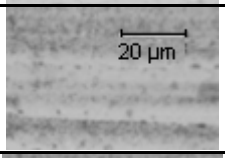
20	V= 1200 m/min fz= 0.2 mm/ rev x tooth ap= 3.5 mm	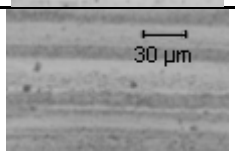	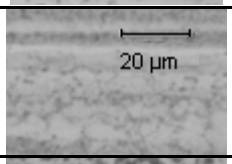
22	V= 1400 m/min fz= 0.1 mm/ rev x tooth ap= 3.5 mm	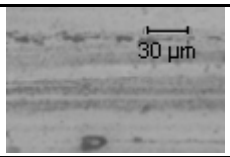	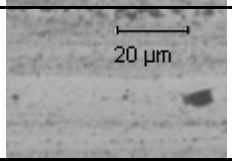
25	V= 1600 m/min fz= 0.1 mm/ rev x tooth ap= 4.0 mm	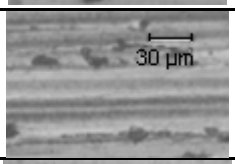	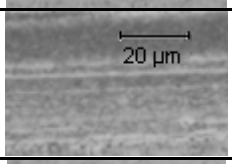
26	V= 1600 m/min fz= 0.2 mm/ rev x tooth ap= 3.0 mm	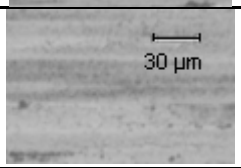	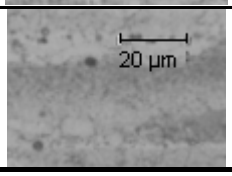

Table 7- Microstructure of a few AL 7075-T7351specimens face milled under different cutting conditions and r =2.5 mm

TRIAL	Cutting parameters	Surface microstructure (30µm)	Surface microstructure (20 µm)
11	V= 600 m/min fz= 0.2 mm/ rev x tooth ap= 3.5 mm	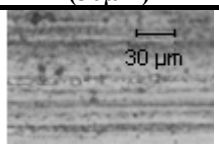	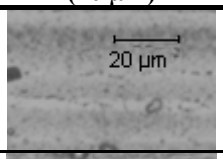
12	V= 600 m/min fz= 0.3 mm/ rev x tooth ap= 4.0 mm	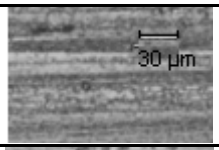	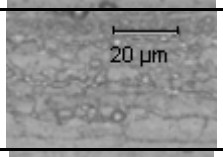
14	V= 800 m/min fz= 0.2 mm/ rev x tooth ap= 4.0 mm	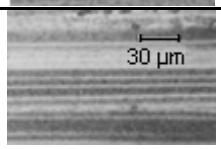	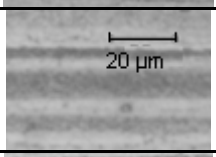
17	V= 1000 m/min fz= 0.2 mm/ rev x tooth ap= 3.0 mm	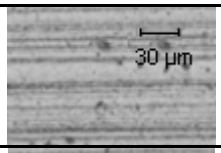	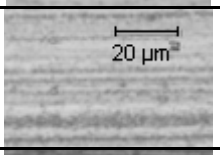
18	V= 1000 m/min fz= 0.3 mm/ rev x tooth ap= 3.5 mm	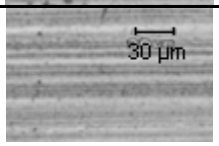	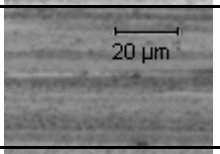
29	V= 1200 m/min fz= 0.2 mm/ rev x tooth ap= 3.5 mm	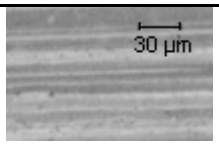	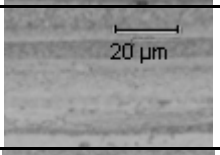
30	V= 1200 m/min fz= 0.3 mm/ rev x tooth ap= 4.0 mm	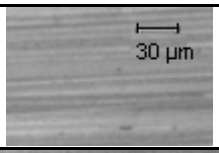	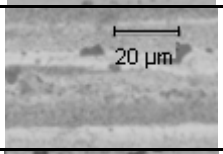
32	V= 1400 m/min fz= 0.2 mm/ rev x tooth ap= 4.0 mm	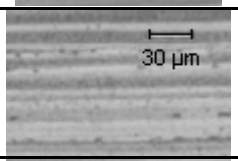	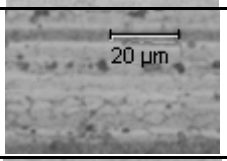
33	V= 1400 m/min fz= 0.3 mm/ rev x tooth ap= 3.0 mm	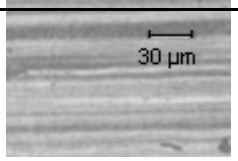	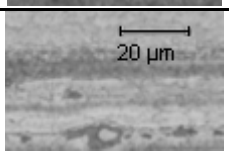
36	V= 1600 m/min fz= 0.3 mm/ rev x tooth ap= 3.5 mm	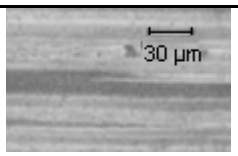	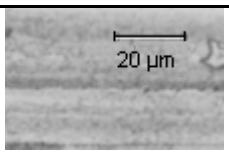

Table 8- Chip morphology of a few AL 7075-T7351 specimens face milled under different cutting conditions and r =0.8 mm

Trial	Cutting parameter	Cw (mm)	Ct (mm)	Cross-sectional area (mm^2)	9X magnifier 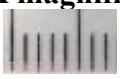
1	V= 600 m/min fz= 0.1 mm/rev*tooth ap= 3.0 mm	3.0	0.1	0.300	
3	V= 600 m/min fz= 0.3 mm/rev*tooth ap= 4.0 mm	4.0	0.32	1.280	
4	V= 800 m/min fz= 0.1 mm/ rev*tooth ap= 3.5 mm	3.5	0.15	0.525	
5	V= 800 m/min fz= 0.2 mm/rev*tooth ap= 4.0 mm	3.9	0.21	0.819	
8	V= 1000 m/min fz= 0.2 mm/rev*tooth ap= 3.0 mm	3.0	0.22	0.660	
19	V= 1200 m/min fz= 0.1 mm/rev*tooth ap= 3.0 mm	3.1	0.11	0.341	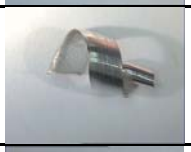
20	V= 1200 m/min fz= 0.2 mm/rev*tooth ap= 3.5 mm	3.4	0.2	0.680	
22	V= 1400 m/min fz= 0.1 mm/ rev*tooth ap= 3.5 mm	3.6	0.12	0.432	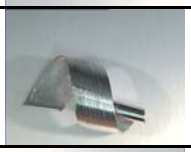
25	V= 1600 m/min fz= 0.1 mm/rev*tooth ap= 4.0 mm	4.0	0.12	0.480	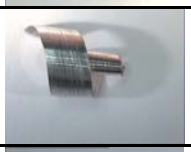
26	V= 1600 m/min fz= 0.2 mm/rev*tooth ap= 3.0 mm	2.9	0.21	0.609	

Table 9- Chip morphology of a few AL 7075-T7351 specimens face milled under different cutting conditions and r =2.5 mm

Trial	Cutting parameter	Cw (mm)	Ct (mm)	Cross-sectional area (mm^2)	9X magnifier 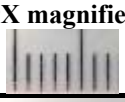
11	V= 600 m/min fz= 0.2 mm/rev*tooth ap= 3.5 mm	3.5	0.2	0.700	
12	V= 600 m/min fz= 0.3 mm/rev*tooth ap= 4.0 mm	4.0	0.45	1.800	
14	V= 800 m/min fz= 0.2 mm/rev*tooth ap= 4.0 mm	4.0	0.17	0.680	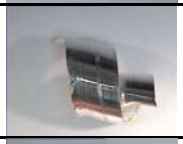
17	V= 1000 m/min fz= 0.2 m/rev*tooth ap= 3.0 mm	3.0	0.3	0.900	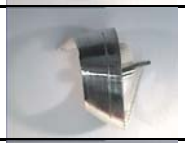
18	V= 1000 m/min fz= 0.3 mm/rev*tooth ap= 3.5 mm	3.5	0.35	1.225	
29	V= 1200 m/min fz= 0.2 mm/rev*tooth ap= 3.5 mm	3.5	0.19	0.665	
30	V= 1200 m/min fz= 0.3 mm/rev*tooth ap= 4.0 mm	4.1	0.3	1.230	
32	V= 1400 m/min fz= 0.2 mm/rev*tooth ap= 4.0 mm	4.0	0.2	0.800	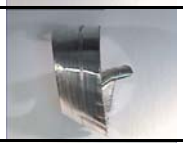
33	V= 1400 m/min fz= 0.3 mm/rev*tooth ap= 3.0 mm	3.2	0.29	0.928	
36	V= 1600 m/min fz= 0.3 mm/rev*tooth ap= 3.5 mm	3.4	0.29	0.986